COLLECTIVE NUCLEAR STRUCTURE STUDIES IN THE OSMIUM NUCLEI

by

Richard F. Casten
B. S. , College of the Holy Cross, 1963
M. S. , Yale University , 1964

A Dissertation Presented to the Faculty of the
Graduate School of Yale University in
Candidacy for the Degree of
Doctor of Philosophy
1967

To my father, my mother,

and to Jo-Ann

ABSTRACT

Collective nuclear structure studies on the four even-even isotopes of osmium, $Os^{186, 188, 190, 192}$ have been pursued using Coulomb excitation induced by O^{16} ions with incident energies between 42 and 80 MeV obtained from the Yale MP Tandem Van de Graaff accelerator. The osmium isotopes span the important transition region from highly deformed to nearly spherical nuclei located at the high mass extremity of the rare earth region of collectivity and they have therefore long been the center of much theoretical and experimental interest. The deexcitation radiation has been observed singly, in coincidence with O^{16} ions backscattered from the target, and in coincidence with other γ-rays representing the $2^+ \rightarrow 0^+$ and $4^+ \rightarrow 2^+$ transitions in each isotope. In $Os^{186, 188, 190}$ all levels through the 6^+ state of the ground state rotational band as well as the $2^{+\prime}$ and $4^{+\prime}$ levels of the so-called γ-vibrational band have been excited. In Os^{188} an additional 0^+ level at 1086 kev was observed while in Os^{192} all known states except the unnatural parity 3^+ level were detected. Furthermore, in Os^{188}, Os^{190}, and Os^{192} new states at 780, 840, and 855 kev, respectively, are tentatively proposed with J^π assignments of 2^+ or 3^- ascribed as likely and not inconsistent with any of our measurements.

The main emphasis has been on the extraction of absolute reduced transition probabilities (B(E2) values). These have been obtained, for the excitation of all states previously known, by both model-dependent and model-independent analyses. The results have been compared with several macroscopic and microscopic nuclear models, with particular attention to that of Kumar and Baranger. The latter has proved the most complete and successful of any in predicting both absolute B(E2) values and the variations of these with neutron number in the osmium isotopes. The trend toward the spherical or vibrational limit in Os^{192} is calculated to be somewhat sharper than is observed experimentally. Suggestions are made for possible improvements in the pairing-plus-quadrupole model of these authors. An interpretation of the osmium isotopes as typified by shallow potential minima for moderately prolate deformations (and slightly axially asymmetric equilibrium configurations in $Os^{190, 192}$) and by extreme softness to vibrations in both β and γ emerges from this comparison and is actually confirmed by both the successes and failures of the other models with which comparisons are made. Discussion is also made of the possible existence and implications of finite excited state quadrupole moments predicted in osmium by Kumar and Baranger and in other spherical nuclei by other authors. Finally, suggestions for future experimental tests of the theoretical calculations in this transition region are offered.

ACKNOWLEDGEMENTS

It is a great pleasure to acknowledge my appreciation to Dr. J. S. Greenberg and to Prof. D. A. Bromley who supervised the research performed here. I would like to thank Dr. Greenberg for his advice and participation in all phases of this work and for the guidance in the data analysis provided by his probing questions and suggestions. I am very deeply indebted to Prof. Bromley not only for making available the facilities of the A. W. Wright Nuclear Structure Laboratory of Yale University but also especially for numerous invaluable discussions concerning this work and for his generous support and counsel in so many matters.

I am indebted to Dr. K. Kumar for discussions concerning his calculations and for communication of certain results of those calculations prior to their publication.

I am grateful to Dr. G. A. Burginyon for his extensive cooperation and advice in the collection and analysis of the data presented herein, for his help with the computer programs and for innumerable discussions concerning many facets of this work. Thanks are also extended to S. Sie for help in the later phases of data acquisition. I would like to thank the entire faculty of the Nuclear Structure Laboratory, as well as my fellow graduate students there, for the many interesting discussions dealing with all aspects of nuclear physics. I would also like to express my appreciation to the entire operating and support staffs of the accelerator for their continual assistance and ready cooperation during the course of these measurements and during the preparation of this final manuscript.

I would like to thank my wife, Jo-Ann, for her constant encouragement and, in particular, for typing the various drafts and the final manuscript of this thesis.

No aspect of this work would have been even remotely possible were it not for the singularly unfailing lifelong support, encouragement, guidance and stimulation of my father to whom I can in no way express sufficient gratitude and appreciation. The inspiration and example he has provided will never be forgotten.

I am indebted to the Danforth Foundation for its abiding interest in all aspects of my graduate education and for its grants which supported that education in particularly tangible fashion.

Finally, I would like to thank the United States Atomic Energy Commission for financial support of this research.

TABLE OF CONTENTS

I. ORIENTATION

There is as yet no exact mathematical technique for the complete calculation of the properties of a many-body quantum mechanical system. Except for its lightest representatives, the atomic nucleus in general constitutes such a system. In addition, even if such a mathematical apparatus were available, the nuclear (or nucleon-nucleon) force is only very imperfectly known. In order to make progress in the elucidation of nuclear structure one must therefore make certain mathematical and physical assumptions and approximations. The recent history of nuclear structure physics has consisted largely of a succession of such nuclear models and has been characterized by a steadily improving accord between them and the experimental facts which encourage and test them.

Broadly speaking, there are two striking features revealed by the data of nuclear physics: the nearly independent motion of the nucleons in the nucleus and the strong correlations among the motions of many nucleons resulting in apparently collective behaviour. These two seemingly contradictory aspects have given rise to two general models of nuclear structure, the shell model and the collective model. Both of these, of course, have many variants.

The earliest collective models were "phenomenological" in that they postulated, without derivation, that the nucleus possessed certain gross properties implied by the data. Thus, for example, in order to explain certain features of the data recognizable as similar to those of a rotating symmetric, quantum mechanical top, the nucleus was consequently assumed to be deformed and to rotate. No accounting was made as to why this should be so.

The seemingly contradictory nature of the two models and the "macroscopic" nature of the collective model were disconcerting and led to attempts to derive the collective model itself from a more basic or "microscopic" viewpoint. In particular, many attempts were made to obtain "collectivity" from a shell model approach with residual interactions included[1-10]. As will be noted in the following pages, such microscopic models have had impressive successes although much remains to be done.

Of course, the shell model itself is, in a sense, phenomenological and

attempts have also been made to reproduce some of its features by starting with even more basic ideas, on the nuclear force, derived from nucleon-nucleon scattering data[11]. It should be remembered, however, that science must remain phenomenological at some level. The most that can be hoped for is that that level can be continually pushed back so that the phenomenological starting point may become, in time, as "fundamental" as possible.

In their basic forms the macroscopic models of collective motion are simplified accounts of nuclear structure which apply with accuracy only to those nuclei which closely approximate the extreme limiting cases envisioned. Thus the rotational model is quite satisfactory for highly and permanently deformed nuclei relatively far from closed shells, whereas collective excitations in spherical nuclei are often best described by the simple harmonic oscillator model. More sophisticated models often attempt to incorporate deviations from the extremes by treating the sources of these deviations as small perturbations on the basic model structure. One of the interesting tests of these models and of the degree to which nuclei behave according to their simplified pictures is therefore in those regions of transition in which the nuclear properties vary between the limiting cases through an intermediate stage characterized by large deviations from either extreme.

Generally, the macroscopic models have one or more free parameters whose values must be determined separately for each nucleus to which the model is applied. The hope is that, as one spans a region of the periodic table, these parameters will exhibit a smooth variation. The microscopic models, on the other hand, have the advantage that they seek to fit the properties of nuclei in an entire region with a single set of parameters. The parameters may vary somewhat from nucleus to nucleus but the variation should, ideally, be predicted and determined by the model itself. Since an entire region must be serviced by one parameter set, the most sensitive areas in which to test these microscopic models are, again, those in which one finds the greatest variations of nuclear properties.

The purpose of this thesis is to provide a test of certain macroscopic and microscopic collective nuclear models in one of these particularly sensitive areas of the periodic table. The region chosen is that spanned by the even-even isotopes of osmium. These are found at the high A end of the rare earth region of collec-

tivity. This transitional zone is the only one known[12] in which the variation between highly deformed and nearly spherical nuclei occurs gradually over a significant span of nuclear species. Phenomenologically speaking, the nuclei $Os^{186, 188}$ are fairly well approximated by the rotational model. The incipient trend in these two nuclei toward the vibrational limit emerges much more clearly in Os^{190}. Finally, by Os^{192}, the vibrational extreme is definitely being approached although strong remnants of rotational structure are also intermingled. The complementary transition zone at the low A end of this collective region is spanned much more abruptly[25, 117].

Among the properties of the nucleus some of the most sensitive to the details of the nuclear wave functions are transition rates. Even small admixtures of other states into the wave function for a given level may drastically alter the matrix elements involving this state and therefore its excitation and deexcitation probabilities. On the other hand, properties such as its energy may be only slightly affected. Therefore the principal stress in this thesis has been on the accurate measurement of the various reduced matrix elements (essentially "B(E2) values") interconnecting the several low-lying collective states in $Os^{186, 188, 190, 192}$.

The results reported here improve and expand the existing data on each of the four nuclei. However, the primary interest that this work hopes to engender is in any additional light it may shed on the detailed structure of the osmium transition region, viewed as a whole, and in any consequent insight gleaned into the more general problems of collective nuclear motion and its basis in the behaviour of the individual nucleons and in their mutual interactions.

The results obtained here are compared to the predictions of several models. The specific emphasis has been on the comparison with microscopic calculations and in particular with the recent work of Kumar and Baranger[13]. Certain recent successes[14] of their theory have raised hopes that a more comprehensive understanding of collective behaviour may now be within reach. The results of the work reported here have more thoroughly tested many of the predictions of the Kumar and Baranger calculations and some comments are made as to possible directions of improvement in their model. As an overall conclusion, it may be said that the hopes initially raised for that model have not now been diminished and that it has,

in several ways, proved considerably proficient in its treatment of a difficult region. It will be of interest to test it further in certain specific ways mentioned in Chapter VII and especially to compare its predictions, when they become available[121], with data obtained previously[25, 27, 117, 118] on the structure of the light end of the rare earth region.

II. THEORETICAL CONSIDERATIONS

A. Macroscopic Models

Despite the impressive successes of the nuclear shell model it has long been noted that, in its simpler forms, it could not account for such experimental facts as extremely large nuclear quadrupole moments, enhanced E2 transition rates, and certain features of energy level and spin and parity systematics. The need was recognized for the introduction, somehow, of collective effects involving many nucleons. Phenomenological or macroscopic models were developed to include these effects[15-22] and, through the agency of the assumed cooperative or correlated motions, quadrupole moments and transition probabilities much larger than the single particle estimates were obtained. It was also found, for example, that the often observed energy level relation, $E_J \propto J\,(J+1)$[17, 20], where J is the angular momentum, could be derived on the assumption of a deformed nuclear shape with its consequent rotations. Early successes of these simple models led the way to many refinements involving, for example, the inclusion of previously neglected effects[29, 31] (e.g., the rotation-vibration interaction) in the form of perturbations on the basic model structure.

Although a more microscopic understanding of collective motion is now emerging and although the phenomenological models have certain obvious shortcomings (see Chapter I), their past and present value in correlating vast amounts of data is undisputed. Furthermore, they still provide a valuable physical picture and conceptual framework in terms of which it is often extremely convenient to think. Finally, in their more sophisticated present-day forms they are still frequently quantitatively accurate and useful[25, 27].

The following several pages will briefly summarize the basic ideas behind some of these models. Extensive detail is unnecessary since many excellent (often classic) articles and review articles on this subject abound in the literature[15-20].

The model of Bohr and Mottelson[15] pictures a competition between long and short range forces near the nuclear surface that can result in vibrations about a spherical equilibrium shape or in a permanently deformed structure capable of

undergoing rotational motions. In the model the nuclear surface is expressed by the familiar result (relative to space fixed axes):

$$R = R_o \left[1 + \sum_{\lambda \mu} \alpha_{\lambda \mu} (t) \; Y_{\lambda \mu} (\theta, \varphi) \right] \qquad \text{II-1}$$

where R_o is the equilibrium spherical radius and $\alpha_{\lambda \mu}(t)$ expresses the deviation of multipole order $\lambda\mu$ from sphericity. $Y_{\lambda \mu} (\theta, \varphi)$ is the usual spherical harmonic. For nuclei with spherical equilibrium shape, oscillations about that shape correspond to the (assumed small) variations in time of the $\alpha_{\lambda \mu}(t)$'s.

Expansion of the kinetic and potential energies about the equilibrium shape leads to a lowest order Hamiltonian for these collective excitations analagous to that of a simple harmonic oscillator:

$$H = T + V = \frac{1}{2} \sum_{\lambda, \mu} B_\lambda \left| \dot{\alpha}_{\lambda \mu} \right|^2 + \frac{1}{2} \sum_{\lambda, \mu} C_\lambda \left| \alpha_{\lambda \mu} \right|^2 \qquad \text{II-2}$$

with the frequency of oscillation being given by: $\omega_\lambda = \sqrt{C_\lambda / B_\lambda}$. In eq. 2 (equations are referred to by Arabic numerals in the chapter in which they occur, by their full designation elsewhere), C_λ and B_λ may be likened to the restoring force and effective mass constants of a simple harmonic oscillator although they are best determined quantitatively by fitting the empirical data. $\lambda = 0$ represents density oscillations while $\lambda = 1$ corresponds to translational modes of excitation of the entire nucleus. $\lambda = 2$, therefore, characterizes the lowest order of interest, that corresponding to quadrupole oscillations. Henceforth, we usually specialize to this case although the more general treatment is analogous. The energy levels associated with the oscillator model are equally spaced and are given by[21]

$$E = \hbar \omega \, (N + 5/2) \qquad \text{II-3}$$

where N is the number of quadrupole phonons involved in the excitation. The ground state of an even-even nucleus has N = 0 and a J^π assignment of 0^+. The first quadrupole vibration produces a 2^+ state. The next excitation (N = 2) is obtained by

coupling two quadrupole phonons together and the result is a degenerate triplet of states of spin and parity: 0^+, 2^+, 4^+. An N = 3 excitation is also possible. It is fivefold degenerate with levels of spins 0, 2, 3, 4, 6. (This latter statement may be trivially shown using the technique of Young tableaux[21]). In practice the degeneracy of these multiple phonon states is broken by residual interactions. Scharff-Goldhaber and Weneser[22] have considered the breaking of the degeneracy via coupling to particle states and have also reproduced the experimental energy ratio $E_{2^{+\prime}}/E_{2^+} \cong 2.2$. (A prime (') on a state label indicates the second lowest occurrence of a state of the indicated spin and parity). Anharmonic terms in the potential have also been included[23] and in fact their presence is actually indicated by results of microscopic calculations using the higher random phase approximation[24].

Transition matrix elements involving the electric quadrupole operator may be easily calculated and are given by[21]

$$\sum |< N-1 \mid M(E2, \mu) \mid N >|^2 = 5\left(\frac{3 Z e R_0}{4\pi}\right)^2 \frac{\hbar N}{2\sqrt{BC}} \qquad \text{II-4}$$

where Z is the atomic number. Thus an important feature of the model is the prediction that

$$\frac{B(E2: 2^{+\prime} \rightarrow 2^+)}{B(E2: 2^{+\prime} \rightarrow 0^+)} = 2 \quad . \qquad \text{II-5}$$

(See Section B of this chapter for a definition of the quantities $B(E2: J_i \rightarrow J_f)$). Finally, since the quadrupole operator is a one phonon creation or destruction operator the transition $2^{+\prime} \rightarrow 0^+$ is forbidden: that is, in the ideal case,

$$\frac{B(E2: 2^{+\prime} \rightarrow 0^+)}{B(E2: 2^{+\prime} \rightarrow 2^+)} = 0 \quad . \qquad \text{II-6}$$

By the same argument, transitions between the $0^{+\prime}$, $2^{+\prime}$, 4^+ states of the N = 2 triplet are likewise forbidden.

In many situations the above model is inadequate since the nucleus is permanently deformed. In this case it is best to specify the nuclear orientation

in a body-fixed system. This is done by defining quantities a_ν by:

$$a_\nu = \sum_\mu \alpha_{2\mu} D^2_{\mu\nu} (\Theta, \Phi, \Psi) \qquad \text{II-7}$$

where Θ, Φ, Ψ are the Eulerian angles relating the body-fixed and space-fixed axes and where $D^2_{\mu\nu}$ is the usual rotation matrix. Since $a_2 = a_{-2}$ and $a_1 = a_{-1} = 0$ there are only five independent degrees of freedom and these are specified by a_2, a_0 and the three Eulerian angles. It is customary to write a_2, a_0 in terms of two new parameters, β and γ:

$$\begin{aligned} a_0 &= \beta \cos \gamma \\ a_2 &= \frac{1}{\sqrt{2}} \beta \sin \gamma \end{aligned} \qquad \text{II-8}$$

β is related to the degree of deformation of the nuclear surface (note that $\Sigma_\mu \left| \alpha_{\lambda\mu} \right|^2 = \sum_\nu \left| a_\nu \right|^2 = \beta^2$ and so $V = \frac{1}{2} C \beta^2$) while γ determines the degree of departure from axial symmetry[20]. With these variables the kinetic energy may be separated into rotational and vibrational parts and is written

$$T = \frac{1}{2} B (\dot\beta^2 + \beta^2 \dot\gamma^2) + \sum_i \frac{J_i^2}{2I_i} \qquad \text{II-9}$$

where I_i is the moment of inertia about the i^{th} axis. Transforming the above classically-oriented description into the operator formalism of quantum mechanics yields an expression for the complete nuclear Hamiltonian[26]:

$$\begin{aligned} H &= H_\beta + H_\gamma + H_{rot} + V \\ &= -\frac{\hbar^2}{2B} \left[\frac{1}{\beta^4} \frac{\partial}{\partial\beta} \left(\beta^4 \frac{\partial}{\partial\beta} \right) + \frac{1}{\beta^2} \frac{1}{\sin 3\gamma} \frac{\partial}{\partial\gamma} \left(\sin 3\gamma \frac{\partial}{\partial\gamma} \right) \right] \\ &\quad + \left[\frac{\hbar^2}{4I_1} + \frac{\hbar^2}{4I_2} \right] \left[J(J+1) - K^2 \right] + \frac{\hbar^2}{2I_3} K^2 + \left[\frac{\hbar^2}{2I_1} - \frac{\hbar^2}{2I_2} \right] \left[J_1^2 - J_2^2 \right] + V \end{aligned} \qquad \text{II-10}$$

where K is the component of angular momentum along the nuclear symmetry axis and V is the potential energy. In general, $V = V(\beta, \gamma)$ but often one assumes a

form $V = \frac{1}{2} C\beta^2$ although this is probably not adequate[9, 23]. The term in $(J_1^2 - J_2^2)$ has non-zero matrix elements only between states differing by ± 2 in their component, K, of angular momentum along the nuclear symmetry axis and is usually neglected or treated as a perturbation. In the adiabatic approximation and provided $V = V(\beta)$, the wave function may be written in antisymmetrized form as:[20]

$$\psi = f_J(\beta) \sum_{K=0}^{J}{}' g_K(\gamma) \mid JMK\rangle$$

where $$\mid JMK\rangle = \left[\frac{2J+1}{16\pi^2(1+\delta_{KO})}\right]^{\frac{1}{2}} \left[D^J_{MK} + (-1)^J D^J_{M-K} \right] \qquad \text{II-11}$$

From eq. 11 it is apparent that, for $K = 0$, only even J are allowed while, for $K \neq 0$, J may be odd. In all cases $J \geq K$ and the symbol $\sum'$ denotes even values for K.

In this model the nucleus may simply rotate about an axis perpendicular to the axis of symmetry. It may also undergo axially symmetric or asymmetric shape oscillations in, respectively, β and γ, with rotations superposed on these vibrational excitations. The excited rotational "bands" thus formed are characterized by $K = 0$, $J = 0^+, 2^+, 4^+ \ldots$ for the "β band" and $K = 2$, $J = 2^+, 3^+, 4^+ \ldots$ for the "γ band". In all these cases:

$$E_J = \frac{\hbar^2}{2I}\left[J(J+1) - K^2 \right] . \qquad \text{II-12}$$

The model described above has many other ramifications. In particular, since the rotational and vibrational parts of the wave functions are known and separable it is possible, therefore, to evaluate relative transition probabilities for both interband and intraband transitions. One obtains, for example, the following important results[21]:

$$B(E2: J_i K \rightarrow J_f K) = e^2 Q_o^2 \, \langle J_i 2KO \mid J_f K\rangle \qquad \text{II-13}$$

and

$$\frac{B(E2: J_1 \rightarrow J_2)}{B(E2: J_3 \rightarrow J_4)} = \frac{\langle J_1 2KO \mid J_2 K\rangle^2}{\langle J_3 2KO \mid J_4 K\rangle^2} \qquad \text{II-14}$$

for transitions within a band where Q_o is the intrinsic quadrupole moment and the right-hand sides contain the usual Clebsch-Gordan coefficients.

For interband transitions one obtains, similarly[21],

$$\frac{B(E2: J_i K_i \rightarrow J_f K_f)}{B(E2: J_i K_i \rightarrow J_f' K_f)} = \frac{\langle J_i K_i 2, K_f - K_i \mid J_f K_f \rangle^2}{\langle J_i K_i 2, K_f - K_i \mid J_f' K_f \rangle^2} \qquad \text{II-15}$$

Of course, in practice, this simple model is rarely obeyed accurately. We have, for example, neglected mixing between K = 0 and K = 2 bands and the effects of the Coriolis force[17] and its antipairing properties[10]. We have also employed the adiabatic approximation in which collective frequencies are assumed small compared to those for independent particle excitations. Although corrections to energy levels, spins and parities due to these approximations may not be large, strong dynamic effects can occur since even small admixtures of wave functions may drastically alter transition matrix elements and intensities.

One specific correction to the model described above is particularly important to include. It was cited above and involves the calculation of the effects, on energy levels and transition probabilities, of the mixing of β and γ band wave functions into the ground state band[29, 30, 120]. These effects may be included within the framework of the model, via first order perturbation theory, since the mixing arises from terms in the Hamiltonian originally present (see eq. 10) but subsequently neglected. One may easily show[25, 27] that the correction terms to the ground state rotational band energies are of the form:

$$\Delta E_J^{\beta} = -\epsilon_{\beta}^2 \hbar \omega_{\beta} J^2 (J+1)^2$$

and

$$\Delta E_J^{\gamma} = -\epsilon_{\gamma}^2 \hbar \omega_{\gamma} \left[J^2 (J+1)^2 - 2J(J+1) \right] \qquad \text{II-16}$$

where ϵ_{β} and ϵ_{γ} are defined below. Thus eq. 12, for the ground state band, becomes

$$E_J = AJ(J+1) + BJ^2 (J+1)^2 \qquad \text{II-17}$$

where $A = \hbar/2I'$, I' being a renormalized moment of inertia, and where B is given by the sum of the coefficients of the terms in $J^2 (J+1)^2$ in eq. 16. An equation for the energy levels of the type given by eq. 17 is gratifying because the experimental results in nuclei not too far removed from the rotational limit, often require

exactly such an expression. The B(E2) values for transitions between bands are also strongly affected by the mixing and deviate from the Alaga relations[28] relevant to pure bands. The amount of deviation is expressed through parameters z_β and z_γ which in turn are related to the ϵ_β and ϵ_γ of eq. 16 via the equations

$$z_\beta = 2\epsilon_\beta\alpha_\beta \; ; \quad z_\gamma = \epsilon_\gamma\alpha_\gamma\sqrt{24} \qquad \text{II-18}$$

where all quantities are defined and discussed in references 25 and 27. From one absolute transition probability and an interband branching ratio z_γ and α_γ (and z_β and α_β) may be determined empirically and thus eqs. 18 may be solved for ϵ_γ (and ϵ_β) and the coefficient B in eq. 17 determined. It turns out[25, 27] that the contributions to B obtained in this way are not sufficient to explain the experimental deviations from the J(J + 1) law. But, even this failure is enlightening for it indicates that other important aspects of the collective nuclear motion are being neglected. Marshalek[9] has recalculated B on a microscopic model and found other large contributions to B than those considered above. His results are in much better accord with experiment. Much more detailed treatments of these rotation-vibration interactions in the macroscopic model are provided in references 25, 27, 117, 120 and 29-31 where numerical and analytic results necessary for the application of the theory to specific cases (as is done in Chapter VI of this thesis) are derived and tabulated.

Thus far we have considered only the case in which the equilibrium value of $\gamma = 0$, that is, axially symmetric nuclei. This restriction is not essential and, in fact, Davydov and co-workers[32-35] have calculated the effects of permitting non-zero equilibrium values of γ. In their early calculations[32] β and γ were kept fixed at their equilibrium values but this adiabatic approximation was later dropped[34] (although actual numerical results for the case of variable γ have not yet become available).

Very briefly, the model in its later, more general form[34] considers the Hamiltonian for β vibrations and for rotations in an axially asymmetric nucleus to be given by

$$H = \frac{\hbar^2}{2B}\left[\frac{1}{\beta^3}\frac{\partial}{\partial\beta}\left(\beta^3\frac{\partial}{\partial\beta}\right) - \sum_\lambda \frac{J_\lambda^2}{4\beta^2\sin^2(\gamma - \frac{2}{3}\pi\lambda)}\right] \qquad \text{II-19}$$

It will be noted that this is essentially the same as eq. 10 provided one neglects mixing terms and γ vibrations and assumes for the three moments of inertia the values

$$I_\lambda = 4 B \beta^2 \sin^2 (\gamma - \tfrac{2}{3} \pi \lambda) \qquad \text{II-20}$$

appropriate to the hydrodynamic model. The essential difference is that γ is not set equal to zero. The rest of the model calculations consist simply of solving the Schrodinger equation with this Hamiltonian for the wave functions and rotational energy levels. Transition probabilities and branching ratios are then easily obtained since the wave functions are known. Davydov[32-35] and Davidson and Davidson[36] tabulate many of the numerical results.

All of the predictions of the model are determined for a given nucleus once two parameters, γ and μ, are specified. These are determined empirically from the ratios: E_{4^+}/E_{2^+} and E_{2^+}'/E_{2^+}. γ is the usual asymmetry parameter ($0^\circ \leq \gamma \leq 30^\circ$) while μ is a measure of the "stiffness" against β vibrations. For $\mu<1/3$ coupling between rotations and β vibrations is small (adiabatic limit) while for $\mu \geq 1/3$ the nucleus is "soft". For small μ the expression obtained for the rotational energies contains a term of the same form as one suggested by Mallman and Kerman[37] on empirical grounds.

The main result of the model is that one obtains a set of rotational energy levels comprised of the levels usually associated with the ground state band plus a second group that decreases rapidly in energy (from $E \rightarrow \infty$) as γ increases from 0 to $\pi/6$. This second set of levels has spins of 2, 3, 4.... and is the analogue of the γ-vibrational band states in the axially symmetric model. A crucial difference is that, in the latter model, the γ-band states are rotations based on vibrational excitations, that is, their structure is significantly different from the ground state, while in the Davydov calculations there are no essential differences among any of the rotational levels. It would seem, therefore, that an experimental decision between these two models could result in considerable physical insight into the structure of the low-lying states in collective nuclei. Unfortunately, it has been pointed out[38] that results of the Davydov model with finite γ are essentially identical to those of the Bohr-Mottelson model, with zero equilibrium value of γ

but with $\gamma_{rms} = \gamma_{Davydov}$, in all predictions concerned with measureable quantities involving only low-lying states with K = 0 or 2. The two models do reach different conclusions concerning K = 4 bands[39] but these are infrequently observed and hard to study. However, the models also differ in their results for the relative matrix elements to the 2^+ and $2^{+'}$ states via beta decay from the neighboring odd-odd nuclei[39]. Recently, Yamazaki et al[39] have considered data pertaining to the decay of $Re^{186, 188}$ into the final nuclei $Os^{186, 188}$. Despite the early successes of the Davydov calculations as applied to the osmium nuclei[40], they have concluded that the axially symmetric Bohr-Mottelson picture is to be favored over the Davydov model in these isotopes. There is a further discussion of the quantitative application of the Davydov model to the osmium isotopes in Chapter VI of this thesis.

There are numerous other calculations along the lines of the phenomenological models. Those of Mallman and Kerman[37] and of Faessler et al.[41] are noteworthy examples. We cannot go into all of these here but refer the reader to the literature.

Without the aid of parameters specifically fitted to each nucleus, most of the phenomenological approaches can predict only relative transition rates or, at best, admittedly crude limits on absolute ones (e. g. , hydrodynamic model estimates). On the other hand, one of the most impressive features of the microscopic theories to be discussed below is their calculation of absolute B(E2) values. Since these latter are precisely what were measured in the experiments performed here, and since they provide an extremely sensitive test of calculated wave functions, we now turn out main attention to these microscopic models.

B. Microscopic Models

In this section we outline a particular form of microscopic theory of collective motion. It borrows heavily from formalisms developed in the treatment of electron gases[124] and in the BCS theory of superconductivity[43]. The approach described here was largely initiated by a suggestion of Bohr, Mottelson and Pines[42] that the energy gap in the spectra of even-even nuclei could be derived with the use of a pairing force. A formalism for the calculation of the effects of a pairing-plus-quadrupole residual interaction was developed and applied to the nuclear problem by many authors[1-10]. These calculations were executed both with and without the adiabatic approximation.

The literature on the subject is considerable and the mathematical details can become quite involved. The conceptual structure and formalism, however, in a sense is not difficult although questions related to its validity and justification are often quite subtle. These latter will not be dealt with here in any detail nor will a generally complete treatment be offered. The main emphasis will be placed upon an indication of the manner in which collective excitations can be obtained by the introduction of coherent superpositions of simpler excitations. To do this, we sketch a simplified version of this sort of approach and refer the reader, for greater detail concerning the formalism, to articles by Belyaev[1] and by M. Baranger[5], and to the excellent treatment given by Lane[44]. The latter not only elucidates the formalism in a clear and systematic manner but also provides an historical guide to the development and applications of the theory. The treatment below is based largely on these three references.

The development to be given is not intended to disparage other attempts to derive collective effects from a microscopic basis. Important developments along these lines, to cite but three, are the Hartree-Fock calculations of Kelson[46] and of Kelson and Levinson[45], the surface delta force model of Moszkowski[47] and the derivations of nuclear deformation and rotational band structure through the use of the SU_3 symmetry group[48].

In the analysis that follows it is convenient to use the language of second quantization. It is assumed that no extensive discussion of the notation and concepts

of creation or destruction operators or of their commutation relations is necessary. Let H be an independent particle Hamiltonian. Suppose that we can find a set of operators O_r such that

$$[H, O_r] = \sum_s M_{rs} O_s \quad . \qquad \text{II-21}$$

If we define another set of operators, O_α^+, by

$$O_\alpha^+ = \sum_r x_{\alpha r} O_r , \qquad \text{II-22}$$

then it follows that

$$[H, O_\alpha^+] = \omega_\alpha O_\alpha^+ . \qquad \text{II-23}$$

The vectors $\bar{x}_\alpha$ and energies ω_α are given by the matrix equation:

$$\tilde{M} \bar{x}_\alpha = \omega_\alpha \bar{x}_\alpha \qquad \text{II-24}$$

where M is the matrix whose elements are M_{rs}. Now, if eq. 22 is true, then for any eigenstate ψ of H (of energy E), there is another eigenstate ψ_α of energy E_α given by

$$\psi_\alpha = O_\alpha^+ \psi \qquad \text{II-25}$$

where $$E_\alpha - E = \omega_\alpha .$$

In particular, if ψ_o is the nuclear ground state defined by

$$O_\alpha \psi_o \equiv 0, \qquad \text{II-26}$$

then excited states of energy $E_\alpha = E_o + \omega_\alpha$ are found by operating on ψ_o with O_α^+.

The justification of the so-called linear approximation of eq. 21 is discussed in reference 44 and involves the assumption that the operators O_α^+, O_α satisfy Boson commutation relations even though they are constructed from pairs of Fermion creation and destruction operators. This "quasi-boson" approximation is reasonable provided the number of particles in a shell is much less than the number of states in that shell.

We must now consider the nature of the set of operators O_r in eq. 21. Several approximations are possible. To consider these, let us define A_i^+ to be

an operator that creates a particle in the orbit p_i and a hole in orbit h_i. A_i is the corresponding particle-hole destruction operator. Then, following Lane[44], we can have, in set notation:

$$\{ O_r \} \equiv \{ A_i^+ \} \qquad \text{II-27a}$$

$$\{ O_r \} \equiv \{ A_i^+ \} + \{ A_i \} \qquad \text{II-27b}$$

or,

$$\{ O_r \} \equiv \{ A_i^+ \} + \{ A_i \} \quad + \text{higher terms of order } A_i A_i^+ . \qquad \text{II-27c}$$

Eq. 27a is known as the Tamm-Dancoff or TD approximation. In this case eq. 21 becomes:

$$[H, A_i^+] = \sum_j M_{ij} A_j^+ \qquad \text{II-28}$$

It is easy to show from this that

$$M_{ij} = \langle j | H | i \rangle - \langle O | H | O \rangle \delta_{ij} - \sum_{n \neq O} \langle O | A_j A_i^+ | n \rangle \langle n | H | O \rangle \qquad \text{II-29}$$

where $|O\rangle$ is the unperturbed ground state defined by $A_i | O \rangle \equiv 0$. Note, however, that the condition $O_\alpha \psi = \sum_r x_{\alpha r} A_r \psi_o = 0$ implies that ψ_o also satisfies $A_i \psi_o \equiv 0$: that is, ψ_o, too, is an unperturbed ground state, a pure shell model state. Thus the nuclear ground state in this approximation is "uncorrelated" and hence has no "collectivity" built into it. Now, the excited states are formed from the ground state not by a single excitation, but by a linear combination of one-particle-one hole excitations. This enables one to obtain the desired collective enhancements for matrix elements between excited states. However, the lack of correlations in the ground state results in insufficient enhancement in matrix elements involving this state[44]. Thus the approximation of eq. 27a is inadequate for many purposes and we turn to the model corresponding to eq. 27b. This is called the random phase approximation (RPA), while eq. 27c is often referred to as the higher RPA or HRPA.

In the RPA, eq. 21 becomes (analagous equation exists for $[H, A_i \cdot]$):

$$[H, A_i^+] = \sum_j (M_{ij} A_i^+ + M'_{ij} A_j) \qquad \text{II-30}$$

Again, we can easily show that M_{ij} is given by eq. 29 while

$$M'_{ij} = \langle ij | H | O \rangle \qquad \text{II-31}$$

The physical interpretation of this and the other approximations in terms of "forward- and backward-going graphs" is well-known[49]. Suffice it to say here that since, in the RPA,

$$O_\alpha^+ = \sum_r \left(x_{\alpha r} A_r^+ + y_{\alpha r} A_r \right), \qquad \text{II-32}$$

the condition $O_\alpha \psi_o = 0$ is easily shown to imply that

$$\psi_o = \left[\chi_o + \sum_{ij} \chi_{ij} A_i^+ A_j^+ + \sum_{ijkl} \chi_{ijkl} A_i^+ A_j^+ A_k^+ A_l^+ + \ldots . \right] | 0 \rangle \qquad \text{II-33}$$

where the χ's are the amplitudes for different excited particle - hole configurations in ψ_o and are determinable from the condition $O_\alpha \psi_o = 0$. Thus it is apparent that ψ_o, the ground state, is not unperturbed in this case but is "correlated" or collective in nature in that it is a coherent superposition of many configurations. Excited states ψ_α are given by:

$$\psi_\alpha = O_\alpha^+ \psi_o = \left[\sum_i \chi_i^\alpha A_i^+ + \sum_{ijk} \chi_{ijk}^\alpha A_i^+ A_j^+ A_k^+ + \ldots . \right] | 0 \rangle \qquad \text{II-34}$$

The eigenvalue matrix equations for ω_α are:

$$\begin{aligned} M \bar{x}_\alpha - M' \bar{y}_\alpha &= \omega_\alpha \bar{x}_\alpha \\ \text{and} \qquad M' \bar{x}_\alpha - M \bar{y}_\alpha &= \omega_\alpha \bar{y}_\alpha . \end{aligned} \qquad \text{II-35}$$

Justification of the RPA is difficult and perhaps best approached via time-dependent Hartree-Fock theory. In the latter, the matrix equations (eqs. 35) are also obtained[2, 49] provided one performs a linearization in the time-dependent density matrix. In this case, however, the linearization finds its own justification in that, without it, the coupled differential equations for the elements of the density matrix are non-linear and hence would not result in the correct time dependence

(harmonic or sum of harmonc components) for the calculated wave functions.

A crucial feature of the RPA is that all states consist of linear combinations of one particle-one hole states since O^+_α is basically a sum of one particle-hole creation and destruction operators. The validity of this is not always transparent but the limitation may be avoided by using instead the HRPA of eq. 27c in which the third term in $\{ O_r \}$ can create or destroy two particle-hole excitations. We shall not go into detail on the HRPA since its treatment is similar to the previous cases considered although the mathematical details are more complex. As will be seen in Chapter VI, the use of the HRPA in the treatment of nearly spherical nuclei may be necessitated by the need to account for apparent anharmonicities and possible finite excited state quadrupole moments.

Now that the basic formalism is developed the calculation of ground and excited states is reduced to the evaluation of the elements of the matrix M (see eqs. 29, 31). Once this is done the eigenvalues ω_α and the expansion coefficients $x_{\alpha r}$ and/or $y_{\alpha r}$ may be obtained by solving eqs. 24. Thus the operator O^+_α is determined and from this the structure of ground and excited states is calculable. Once this is done the problem is fully determined and any desired quantities, such as transition rates (or B(E2) values), may also be calculated. In considering the nature of the nuclear matrix elements occurring in each M_{ij}, Lane[44] discusses what he calls "schematic" models, that is, model assumptions concerning the quantities $< i | V | j >$ and $< ij | V | 0 >$ that enter in the matrix elements of the Hamiltonian H. For example, assume that all matrix elements are of the form:

$$< i | V | j > = c\, D_i\, D_j \qquad \text{II-36}$$

where c is a constant. Inserting this value into eqs. 29 and 31 and solving the matrix equations 35, easily leads to the following result for the energy ω_α in the RPA, of the first excited collective state:

$$\sum_k c\, D_k^2 \left(\frac{1}{\omega_\alpha - \Delta\epsilon_k} - \frac{1}{\omega_\alpha + \Delta\epsilon_k} \right) = 1 \qquad \text{II-37}$$

where $\Delta\epsilon_k$ is the particle-hole energy corresponding to the creation operator A^+_k.

Eq. 37 shows that the excited state energies are obtained by the solution of a dispersion relation in ω_α. The same type of result is obtained in the TD approximation and with certain more complicated schematic forms for the matrix elements.

The assumption of eq. 36 and similar schematic approximations are equivalent to adoption of a multipole force for the residual interaction. Thus, for example, a quadrupole interaction is frequently used to simulate the lower order terms in a multipole expansion of the nuclear force.

The discussion above has not specifically introduced the pairing force. However, the entire approach can be carried over nearly unchanged to this latter situation provided one considers the operators A_i^+ and A_i as creation and destruction operators of quasi-particles rather than of particle-hole excitations. That is, the above formalism allows one to consider the generation of collective states (and non-collective excitations as well) that arise with the introduction of a multipole force as the residual interaction between independent shell model particle states. However, when pairing forces are introduced, the shell model particles are no longer independent, or, alternatively, the quadrupole force is not the full residual interaction. The schematic form of the matrix elements (eq. 36) then no longer remains simple and the advantages of the method are lost. However, if a canonical transformation from interacting particles to new, approximately independent, entities, called quasi-particles, is made, then the matrix elements again assume the simple schematic form when the quadrupole force is introduced with H now taken as the Hamiltonian for nearly independent quasi-particles.

We now consider in some detail this treatment of the pairing force. In the discussion below the interactions between neutrons and protons are neglected. A partial justification of this approximation is that neutrons and protons are filling different major shells and so little mixing will occur. Again, the notation of second quantization will be used. Defining $c^+_{\nu+}$ and $c_{\nu+}$ as the creation and destruction operators for the single particle shell model state $|\ \nu, +m>$ we can introduce the pairing force by writing the nuclear Hamiltonian as[6]:

$$H_o = H_{sp} + H_{pair} = \sum_\nu \epsilon_\nu (c^+_{\nu+} c_{\nu+} + c^+_{\nu-} c_{\nu-}) - \frac{G}{2} \sum_{\nu,\omega} (c^+_{\nu+} c^+_{\nu-} c_{\omega-} c_{\omega+}) \quad \text{II-38}$$

where the first term, H_{sp}, is the single particle Hamiltonian, and ϵ_ν is the eigenvalue of the (degenerate, time reversed) single particle states ν^+ and ν^-. H_{pair} is the pairing force Hamiltonian and G measures the strength of the pairing interaction. This latter is defined, in the j-j coupling scheme, as an attractive force acting only between pairs of particles, of the same j and opposite projection quantum numbers $\pm m$, coupled to total angular momentum $J = 0$. The matrix elements of the pairing force between such two-particle states are defined to be independent of j (and m) and to have the constant value, -G.

The reason for the introduction of the pairing force is that it is easy to handle analytically and that it mocks up the effects of the short range components of the nuclear force, that is, the higher order multipoles in an expansion of that force. The behaviour of heavy nuclei is viewed as due to a competition between the short range pairing force and the long range quadrupole interaction. In an unfilled shell with N particles the total pairing force is proportional to N/2 while the long range forces are proportional to N(N-1). Thus, as the number of nucleons, N, in a shell is increased, the long range interaction tends to dominate over the pairing force, leading to the well-known (quadrupole) deformations of the nuclear surface and the consequent rotational spectra. Near closed shells, however, the pairing force may dominate and produce spherical nuclei.

It is not intended that this composite pairing-plus-quadrupole residual interaction, or the nuclear models based upon it, be exact replicas of the actual nuclear situation. It is hoped, however, that this interaction, dealt with realistically, effectively approximates at least a significant portion of the real residual nuclear force.

To transform the problem from one concerned with interacting particles (second term of eq. 38) to independent quasi-particles, we define creaction and destruction operators for these quasi-particles by the canonical transformation of Bogoliubov and Valatin[50]:

$$\alpha_\nu^+ = U_\nu c_{\nu^+}^+ - V_\nu c_{\nu^-}; \quad \beta_\nu^+ = U_\nu c_{\nu^-}^+ + V_\nu c_{\nu^+} \qquad \text{II-39}$$

where

$$U_\nu^2 + V_\nu^2 = 1 \qquad \text{II-40}$$

The destruction operators α_ν, β_ν are analogously defined. Physically, U_ν and V_ν represent, respectively, the probability that the shell model orbit ν is empty or filled.

The meaning of the new operators and of the quasi-particles they create can be seen by considering a level ν well below the Fermi surface. Then $V_\nu \cong 1$, $U_\nu \cong 0$ and, for example, $\beta_\nu^+ \cong c_{\nu+}$; i.e., β_ν^+ destroys a particle in the $|\nu,+m>$ state. Above the Fermi level, $U_\nu \cong 1$, $V_\nu \cong 0$ and $\beta_\nu^+ \cong c_{\nu-}^+$ creates a particle in the $|\nu,-m>$ state. For intermediate levels β_ν^+ is a linear combination of particle and hole creation operators. The inverse of eqs. 39 is the transformation

$$c_{\nu+} = U_\nu \alpha_\nu + V_\nu \beta_\nu^+$$
$$c_{\nu-} = U_\nu \beta_\nu - V_\nu \alpha_\nu^+ \qquad \text{II-41}$$

Unfortunately, the transformation to quasi-particles does not conserve the number of particles. To correct for this we introduce a Lagrangian multiplier λ, the "chemical potential", to serve as a constraint that the expectation value of the number of particles in the ground state is N. Thus the Hamiltonian H_o becomes:

$$H' = H_o - \lambda N = H_o - 2\lambda \sum_\nu V_\nu^2 \qquad \text{II-42}$$

Substitution of eqs. 41 into eq. 42 for H' is straightforward and leads to the expression

$$H' = U + H_{11} + H_{20} + H_{int} \qquad \text{II-43}$$

where H_{20} consists of terms containing factors of the form $\alpha_\nu^+ \beta_{\nu'}^+$ and therefore represents interactions between quasi-particles. These are assumed absent and so we set

$$H_{20} = 0. \qquad \text{II-44}$$

(H_{int} represents even higher order interactions and is also neglected). Thus, only U and H_{11} survive and are given by:

$$U = \sum_\nu (\epsilon_\nu - \lambda) 2 V_\nu^2 - G_\nu \sum_{\nu\nu'} U_\nu V_\nu U_{\nu'} V_{\nu'} \qquad \text{II-45}$$

and

$$H_{11} = \sum_{\nu} \{ (\epsilon_\nu - \lambda)(U_\nu^2 - V_\nu^2) + G \sum_{\nu'} U_{\nu'} V_{\nu'} (2 U_\nu V_\nu) \} \times \{ \alpha_\nu^+ \alpha_\nu + \beta_\nu^+ \beta_\nu \} . \qquad \text{II-46}$$

Defining the gap parameter Δ as

$$\Delta = G \sum_{\nu} U_\nu V_\nu \qquad \text{II-47}$$

and the quasi-particle energy E_ν by

$$E_\nu = \sqrt{(\epsilon_\nu - \lambda)^2 + \Delta^2} \quad , \qquad \text{II-48}$$

and substituting these into U and H_{11}, we get for H' :

$$H' = \sum_{\nu} (\epsilon_\nu - \lambda) 2V_\nu^2 - \frac{\Delta^2}{G} + \sum_{\nu} E_\nu (\alpha_\nu^+ \alpha_\nu + \beta_\nu^+ \beta_\nu). \qquad \text{II-49}$$

From the conditions specified by eqs. 40 and 44 one determines that

$$U_\nu^2 = \frac{1}{2}\left[1 + \frac{\epsilon_\nu - \lambda}{\sqrt{(\epsilon_\nu - \lambda)^2 + \Delta^2}}\right] \; ; \; V_\nu^2 = \frac{1}{2}\left[1 - \frac{\epsilon_\nu - \lambda}{\sqrt{(\epsilon_\nu - \lambda)^2 + \Delta^2}}\right] \qquad \text{II-50}$$

Eqs. 50 show that the occupation probabilities of levels ν do not fall off sharply to zero at the Fermi level but trail off gradually over an energy range of the order of 2Δ.

The ground state of the nucleus contains no quasi-particles and so the energy of this state, $H = H' + \lambda N$, is given by:

$$H = \sum_{\nu} \epsilon_\nu 2 V_\nu^2 - \frac{\Delta^2}{G} \quad . \qquad \text{II-51}$$

In even-even nuclei the simplest intrinsic excitation corresponds to the breaking of a pair of particles, that is, to the creation of two quasi-particles. Consequently the minimum energy for such an excitation (see eq. 48) is 2Δ, thus accounting for the energy gap in even-even nuclei. (Actually, the gap can be somewhat less than 2Δ due to the effects of "blocking" in which changes in the U_ν's and V_ν's in

an excited state due to the presence of quasi-particle excitations leads to a reduced, effective gap, $\Delta_{eff.}$). There is no gap implied in the excitations of odd nuclei since their ground states already contain one quasi-particle.

There are two unknowns as yet: Δ and λ. However, if we know the single particle shell model energies, ϵ_ν, and the pairing force parameter, G, then the "number equation",

$$N = 2 \sum_\nu V_\nu^2 \ , \qquad \text{II-52}$$

and the "gap equation" (resulting from substitution of eqs. 50 into eq. 47),

$$\frac{G}{2} \sum_\nu \frac{1}{\sqrt{(\epsilon_\nu - \lambda)^2 + \Delta^2}} = 1 \ , \qquad \text{II-53}$$

are sufficient to determine both these unknowns. Finally, for completeness, the ground state wave function is given by

$$\psi_o = \prod_\nu \left[U_\nu + V_\nu c_{\nu^+} c_{\nu^-}^+ \right] | \ 0 > \qquad \text{II-54}$$

and excited state wave functions are obtained by operating on ψ_o with linear combinations of quasi-particle crea tion and/or destruction operators.

As can be seen from the above analysis, the only parameter, aside from the single particle energies ϵ_ν, is the pairing force strength, G. G can be determined empirically from the observed energy gap in even-even nuclei (but one must beware of blocking effects) or from the odd-even mass difference. Once G is so determined the nuclear problem in this model is solved. Excited state energies and wave functions are known and transition rates involving matrix elements of known operators may be calculated.

So far we have considered only intrinsic excitations. Collective states may also be obtained and their properties can be calculated in two ways. Both methods involve the introduction of the long-range quadrupole force. The first, and more general, is to follow the formalism of the TD or RPA approximations described earlier, defining the matrix elements $< i | V | j >$ by

$$< i | V | j > = c \, \bar{Q} \cdot \bar{Q} \qquad \text{II-55}$$

That is, the full Hamiltonian H is taken to be

$$H_{tot} = H_{sp} + H_{pair} + H_{Q\text{-}Q} = H_{ind} + H_{Q\text{-}Q}. \qquad \text{II-56}$$

$H_{sp} + H_{pair} = H_{ind}$, the Hamiltonian for independent entities (quasi-particles), is to be substituted for H in the RPA analysis.

There have been many calculations of this type in the last few years. Lane[44] gives numerous references to the important calculations by Thouless, Valatin, Sawicki, Fallieros, Goswami, Pal and many others on closed shell nuclei and on studies of the validity and relative merits of the TD, RPA and HRPA approximations. Yoshida[51] has considered the implications of the microscopic theory in stripping and pickup reactions while Cohen and Price[51] have experimentally measured the quantities U_ν and V_ν in the tin isotopes using the (d, p) and (d, t) reactions. More relevant to the subject of this thesis are the early calculations of M. Baranger[5], Arvieu and Veneroni[52], Marumori[53] and Tamura and Udagawa[7]. Numerical calculations specifically related to this thesis on the β and γ vibrational states, including calculations of E2 transition probabilities involving these states, have been performed by Bès and coworkers[6, 54] and by Marshalek and Rasmussen[8]. Marshalek[9] (among others[9]), using a slightly different approach, has calculated in detail the values of the coefficient B in eq. 17. He discusses the various contributions to B from mixing of β and γ bands into the ground state band, from centrifugal stretching, from the tendency of the Coriolis force to reduce the strength of the pairing interaction (Coriolis antipairing effect or CAP) and from the influence of the Coriolis force on the independent quasi-particle motions themselves. Faessler, Greiner and Sheline[10] discuss the CAP effects on the moment of inertia and on vibrational energies as well. They also estimate the effects of blocking on the vibrational band moments of inertia.

The second method of calculating collective effects avoids the RPA formalism (but is a limiting case of it) and considers the pairing-plus-quadrupole force in the adiabatic approximation. Among the important early calculations of this type are those of Belyaev[1], Kisslinger and Sorensen[2], Griffin and Rich[3], Nilsson and Prior[3],

and Gallagher and Soloviev[4]. In the work of these authors the pairing formalism was used as described above. However, the quadrupole force was generally included earlier in the calculations by letting the single particle energy levels ϵ_ν be those of particles in a quadrupole deformed Nilsson potential. Alternatively the quadrupole force can be included specifically as a term, $-\mu Q$, in the Hamiltonian. In this latter case, the procedure is to solve for the Lagrangian multiplier, μ, by enforcing the self-consistency constraint that the nuclear density distribution be the same as the potential distribution. Mathematically this condition is expressed as:

$$< \psi (Q) | \; Q_{op} | \psi (Q) > = Q \qquad \text{II-57}$$

where Q_{op} is the quadrupole operator and Q the nuclear quadrupole moment.

Proceeding along these lines Belyaev[1] was able to calculate the nuclear deformation and quadrupole moments as a function of the number of particles outside closed shells. He was the first to explain the sudden onset of deformation after a shell closure as opposed to its gradual development. Bès[6] showed, in the adiabatic approximation that collective excitation energies are much lower than the quasi-particle energy gap Δ, that the microscopic Hamiltonian could be written in the familiar collective form:

$$H = W_o + \frac{1}{2} CQ^2 + \frac{1}{2} B\dot{Q}^2 . \qquad \text{II-58}$$

He calculated C byconsidering the variation of nuclear energy with small changes in the deformation and B from the "cranking model"[55]. Once B and C are determined, it is easy to obtain the collective energy $E_{coll} = \hbar \omega_{coll} = \hbar \sqrt{C/B}$. In particular, Bès calculates both the energy and B(E2) values associated with the γ band. Kisslinger and Sorensen[7] had previously calculated in a similar manner the energies of the lowest collective 2^+ states in single closed shell nuclei.

One of the greatest successes of the adiabatic model was the calculation of moments of inertia of deformed nuclei[1, 3]. The phenomenological model had been notoriously unable[20] to calculate moments of inertia that compared favorably to experimental results. The microscopic calculations used the same cranking formula as the macroscopic theories, but the energies and wave functions inserted into that formula were those of the quasi-particles. Written in terms of the single

particle wave functions the result is

$$I = 2\hbar^2 \sum_{\nu\nu'} \frac{<\nu|J|\nu'>}{E_\nu + E_{\nu'}} \left(U_\nu V_{\nu'} - V_\nu U_{\nu'}\right)^2 \quad . \qquad \text{II-59}$$

The last factor in the numerator and the large quasi-particle energies in the denominator both serve to reduce I below the macroscopic estimates, bringing it into excellent accord with experimental results for almost all nuclei in regions of deformation.

Before closing the discussion of the various microscopic theories it is important to mention specifically that of Kumar and Baranger[13]. Recent measurements[56] of large spectroscopic quadrupole moments in nuclei heretofore considered spherical have cast some doubt on previous versions of the so-called vibrational model. These versions have generally predicted for these nuclei that Q = 0. The calculations of Kumar and Baranger[13], however, have not only obtained large quadrupole moments but also have not thereby sacrificed agreement with the other experimentally observed features of nearly spherical nuclei[14, 22]. Other aspects of the model worth noting are that it bridges the gap between microscopic and macroscopic models, that the macroscopic elements of the calculations are generalized and, finally, that no approximations of small or uncoupled oscillations in β and γ are assumed. The authors obtain wave functions and nuclear potentials which, if correct, will modify our concepts of collective nuclei and of their equilibrium structures.

For these reasons, then, their theory has been of considerable interest of late and thus far the results are encouraging. Numerical calculations to date have centered chiefly in the Os-Pt region and in Chapter VI of this thesis the relevant predictions are compared in detail with the experimental results on osmium. For now, a brief outline of the model will suffice.

Kumar and Baranger begin with Bohr's complete collective Hamiltonian except that they generalize it by replacing the three moments of inertia, the three vibrational inertial parameters, B, and the potential energy by seven arbitrary functions of β and γ. The generalized form resulting is

$$\begin{aligned} H_{KB} = {} & \frac{1}{2}\left[I_1(\beta,\gamma)\omega_1^2 + I_2(\beta,\gamma)\omega_2^2 + I_3(\beta,\gamma)\omega_3^2 \right] \\ & + \frac{1}{2}\left[B_{\beta\beta}(\beta,\gamma)\dot{\beta}^2 + B_{\beta\gamma}(\beta,\gamma)\dot{\beta}\dot{\gamma} + B_{\gamma\gamma}(\beta,\gamma)\dot{\gamma}^2 \right] \\ & + V(\beta,\gamma) \quad . \end{aligned} \qquad \text{II-60}$$

They treat this not so much as a specific model Hamiltonian than as the most general form for H to second order in the velocities. This is related to a generalized adiabatic assumption.

Next, they calculate the seven functions from a microscopic pairing-plus-quadrupole model. They do this by applying techniques related to the RPA approach described earlier but couched more nearly in terms of a self-consistent time-dependent Hartree-Fock analysis. The parameters entering into these calculations are the single particle energies ϵ_ν, the proton and neutron pairing force strengths G_p and G_n, the strength of the quadrupole force χ, an effective charge and an additional constant reflecting contributions from the core nucleons. All these parameters are determined empirically. The effective number of single particle levels to be included is obtained by comparison of quadrupole force matrix elements with those of "realistic" forces. The result is a reduction by a certain factor of contributions from the second unfilled shell. In some of their earlier calculations Kumar and Baranger also evaluated χ itself by a similar general normalization of quadrupole and "realistic" force matrix elements. When the several parameters are determined no free variables are left and the theory proceeds unambiguously to a prediction of the properties of the entire region $50 \leq Z \leq 82$ and $82 \leq N \leq 126$.

Once these seven functions are calculated the model calculations are reduced to solving the Schrodinger equation with the Hamiltonian, H_{KB}. Previous macroscopic treatments of the collective Hamiltonian have usually assumed, initially, the separation of rotations, β and γ vibrations. Rotation-vibration interactions are sometimes approximately included later as perturbations. Among the reasons for this common approximation are the extreme mathematical difficulties involved in avoiding it. Kumar and Baranger, however, have overcome these and in fact solve the problem exactly with no assumptions concerning separability. A computer code involving a large β-γ mesh is used in which the seven functions are evaluated at each point of the mesh.

The result of these calculations are wave functions, energy levels and static and dynamic transition moments for the lowest seven states (all of spin $J \leq 4$). In the osmium nuclei the theory correctly predicts the gradual trend from rotational to spherical nuclear character as one proceeds from Os^{186} to Os^{192}.

The potential for $Os^{186, 188}$ corresponds to a deformed prolate shape. For $Os^{190, 192}$ a slightly asymmetric but very shallow well is indicated. In these latter nuclei, in fact, zero point motion in the ground state is actually sufficient to enable the nucleus to oscillate back and forth through many shapes. Large quadrupole moments result since even the more "vibrational" nuclei, $Os^{190, 192}$, oscillate about a slightly deformed potential minimum but, as the authors point out[13], other properties, such as energy levels, can approximate the vibrational model since the nucleus in its zero point motion spends much of its time near the spherical shape.

In addition to predicting the finite quadrupole moments of 2^+ states and the transition toward the vibrational limit near Os^{192}, the model has also proved extremely successful in its predictions for the $B(E2:0^+ \rightarrow 2^+)$ values relevant to the excitation of the first 2^+ states[13, 57, 58]. It is likewise nearly in accord with experimental results on the g factors for these states[13].

One of the chief results of this thesis is a more thorough comparison, with this model, of experimental results on the higher lying $2^{+\prime}$, $4^{+\prime}$, and $0^{+\prime}$ states. In Chapter VI, some of the actual numerical results of Kumar and Baranger are tabulated and a detailed discussion is presented of the comparisons of these with our experimental measurements.

C. Coulomb Excitation Theory

The nuclear excitations observed in this work were produced by the time-dependent electromagnetic interaction of the incident projectiles with the target nucleus in the process known as Coulomb excitation. This excitation mechanism was adopted because, on the scale of energies indicated here, the electromagnetic interaction is well understood[59] and can be handled conveniently mathematically. It has the advantage that the incident projectiles, with energies well below the Coulomb barrier, never actually penetrate the nucleus itself. Thus the analysis of the data is nearly free of uncertainties due to our lack of detailed knowledge of the forces abounding within the nuclear confines.

There are three principal approaches to the analysis of the excitation mechanism and each will be discussed below. First, it is approrpriate to note that the excitation cross sections may be calculated either semi-classically or in a full quantum mechanical manner. In the former the electromagnetic interaction is treated quantum mechanically as that between two poin t charges but the projectile is assumed to follow the classical hyperbolic Rutherford orbit. The rigorous quantum mechanical treatment describes the particles by Coulomb wave functions and employs a Hamiltonian consisting of four terms: ones for the projectile, the target nucleus, the radiation field and for the point charge interaction. One solves the problem by expanding the vector potential $\overline{A}$ in multipole components and taking matrix elements between initial and final states of the system. The excitation occurs via the exchange of virtual photons. A fuller discussion of these points and a derivation of the quantum mechanical results is found in reference 60, hereafter often referred to as ABHMW.

The strength of the Coulomb interaction is characterized by the Sommerfeld parameter η given by:

$$\eta = \frac{Z_1 Z_2 e^2}{\hbar v}$$

where Z_1, Z_2 are the charges of the projectile and target nucleus, respectively, and v is the velocity of the incident projectile. If $\eta \gg 1$ the interaction can be described by the semi-classical approach in which a classical trajectory is assumed

and in which the energy loss of the projectile due to the excitation is small compared to its incident energy. In all cases considered in this thesis, $\eta \gg 1$ (typically $\eta \cong 40$), and so we need not consider the quantum mechanical case further.

Under the assumption that the Rutherford orbit for the projectile is unperturbed by the excitation induced, the differential cross section for excitation of level f in the target nucleus is[60]:

$$d\sigma_f = P_f d\sigma_R. \qquad \text{II-61}$$

In eq. 61, $d\sigma_R = \frac{1}{4}a^2 \sin^{-4}(\theta/2)\, d\Omega$, the Rutherford cross section for scattering into solid angle $d\Omega$ at the asymptotic scattering angle θ, and $a = (Z_1 Z_2 e^2)/(m_o v^2)$ is one half the distance of closest approach. P_f is the probability that level f was excited in the collision. By summing over final and averaging over initial magnetic substates P_f may be written in terms of the amplitudes b_{if} for a transition from initial state i to final state f:

$$P = \frac{1}{2J_i + 1} \sum_{M_i M_f} |b_{if}|^2 . \qquad \text{II-62}$$

Thus the evaluation of the Coulomb excitation cross section in any situation is reduced to evaluation of the amplitudes b_{if}.

We can write the Schrodinger equation for the actual nuclear wave functions as[61]:

$$i\hbar\dot{\psi} = \left[H_o + H_E(t) \right] \psi$$

where H_o is the Hamiltonian for the free nucleus and $H_E(t)$ is that for the electromagnetic interaction. $H_E(t)$ is obtained by expanding the Coulomb interaction potential

$$\varphi(\bar{r}, t) = \frac{Z_1 e}{|\bar{r} - \bar{r}_{proj}(t)|} - \frac{Z_1 e}{\bar{r}_{proj}(t)} \qquad \text{II-64}$$

in multipole components and is given by[60]

$$H_E(t) = \sum_{\lambda, \mu} \frac{4\pi Z_1 e}{2\lambda + 1} r_{proj}^{-\lambda - 1} Y_{\lambda \mu}\left[\theta(t), \varphi(t)\right] M^*(E\lambda, \mu). \qquad \text{II-65}$$

In eq. 65, $\theta(t)$, $\varphi(t)$ specify the time dependence of the angular position of the incident projectile and M is the nuclear multipole moment given by

$$M(E\lambda, u) = \int r^{\lambda} Y_{\lambda\mu}(\theta, \varphi)\, \rho(\bar{r})\, d\bar{r}, \qquad \text{II-66}$$

$\rho(\bar{r})$being the nuclear charge density.

Now, expanding ψ in terms of the wave functions ψ_s (satisfying $H_o\psi_s = E_s\psi_s$) of the free nucleus we have

$$\psi = \sum_s a_s(t)\, \psi_s e^{-iE_s t/\hbar} \qquad \text{II-67}$$

Then, substituting eq. 67 into eq. 63, we get

$$\dot{a}_f(t) = \frac{1}{i\hbar} \sum_s \langle f | H_E(t) | s \rangle \exp\left[i (E_f - E_s)\, t/\hbar \right] a_s(t) \qquad \text{II-68}$$

The labels f and s here refer to all relevant quantum numbers.

If we seek the probability for excitation of state f from an initially unpolarized ground state, the amplitudes $a_{fm}(t)$ (explicitly labeling for a moment the magnetic substates) are the same as the quantities b_{if} and so one simply has to solve eqs. 68 for them, and substitute the results into eqs. 62 and 61. Unfortunately, the different amplitudes a_{fm} are interrelated through eqs. 68 by a (possibly infinite) set of coupled differential equations and their solution, even for a few nuclear states, requires considerable use of modern high speed digital computers. Only recently have the appropriate computers and the complicated computer code[61] for the solution of eqs. 68 been available. We shall return to this approach later.

Let us consider now, though, the case in which the probability of excitation is very small. If a_i is the amplitude for the ground state component of ψ_n, then $|a_i|^2 \cong 1$ and $|a_j|^2 \ll 1$ for $i \neq j$. In this case the sum in eq. 68 reduces to one term and we have the usual first order perturbation theory result:

$$a_f = \frac{1}{i\hbar} \int_{-\infty}^{+\infty} \langle f | H_E(t) | i \rangle e^{i\omega t}\, dt \qquad \text{II-69}$$

where $\omega = (E_f - E_i)/\hbar$. Substituting $H_E(t)$ from eq. 65, changing coordinates to the focal system of the hyperbolic orbit, and regrouping terms in eq. 69, one is able to separate the nuclear information and the orbital information. The latter, for

the fully known Rutherford orbit, is completely calculable. One thus obtains[60]

$$a_f \equiv b_{if} = \frac{4\pi Z_1 e}{i\hbar} \sum_{\lambda\mu} \frac{1}{2\lambda+1} S_{E\lambda,\mu} < f \mid M(E\lambda, \mu) \mid i > \qquad \text{II-70}$$

where the $S_{E\lambda,\mu}$ are orbital integrals defined and evaluated in ABHMW. The cross section for electric excitation of state f is given by eq. 61 using eqs. 62 and 70:

$$d\sigma_f(E\lambda) = \left(\frac{Z_1 e}{\hbar v}\right)^2 a^{-2\lambda+2} B(E\lambda: J_i \rightarrow J_f)\, df_{E\lambda}(\theta, \xi). \qquad \text{II-71}$$

$df_{E\lambda}(\theta, \xi)$ is defined in ABHMW and is closely related to the orbital integrals $S_{E\lambda,\mu}$. The so-called adiabaticity parameter $\xi = (a\Delta E)/(\hbar v) = (Z_1 Z_2 e^2 \Delta E)/(\hbar v\, 2E)$ where E is the projectile energy and ΔE the excitation energy of the final state in the target nucleus. The important quantity $B(E\lambda: J_i \rightarrow J_f)$ is defined by:

$$B(E\lambda: J_i \rightarrow J_f) = \frac{1}{2J_i+1} \left| < J_i \| M(E\lambda) \| J_f > \right|^2 \qquad \text{II-72}$$

in terms of the reduced matrix elements for an electric transition of multipole order $E\lambda$. There has been some confusion in the literature relating to the use of B(E2) values for excitation and deexcitation. If J_i in eq. 72 is always taken as the initial state no ambiguity should arise. Equating $d\sigma_f(E2)$, as given by eq. 71, to the experimental cross section allows one to solve for the only unknown, the nuclear quadrupole transition matrix element (or, equivalently, the $B(E2: J_i \rightarrow J_f)$ value).

Although the use of perturbation theory is limited to low excitation probabilities it is revealing to look at the behaviour of $d\sigma(E\lambda)$ as a function of several parameters. Some physical insight may be gained by noting that $\xi = (a/v)/(\hbar/\Delta E)$ is approximately the ratio of collision time to nuclear period and thus is a measure of the adiabaticity of the collision process. If ξ is large the nucleus has time to adjust adiabatically to the incident projectile and excitation is unlikely. On the other hand, if ξ is small, the " sudden approximation " applies and excitation probabilities can be large. Thus it is not surprising that the functions $df_{E\lambda}$ or $f_{E\lambda}$ (integral of $df_{E\lambda}$ over all angles) decrease exponentially with ξ for large $\xi (\xi \gtrsim 4)$. This is illustrated in Fig. II-1 which gives $f_{E\lambda}$ for several values of λ.

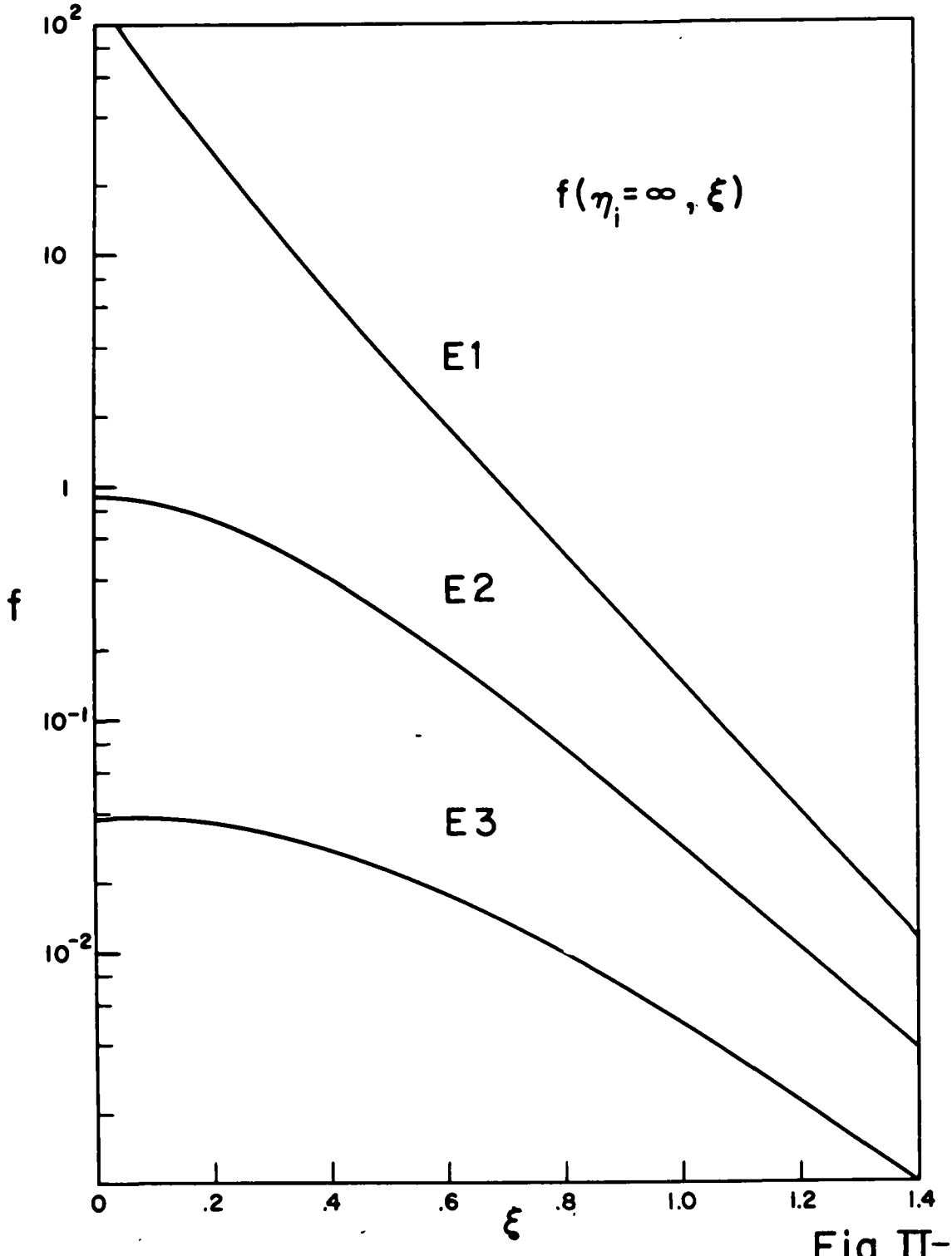

Fig. II-1

Immediately, then, we see two important features of the Coulomb excitation process. The excitation probabilities are greatly enhanced by increased projectile energy and decrease rapidly as nuclear excitation energy is increased. (In practice, a common upper limit for excitation is usually about 1.5 MeV). The former feature is further strengthened because higher projectile energies in addition imply closer distances of approach and consequently greater interaction strengths. (For E2 transitions, for example, $d\sigma/df \propto E$). We note next that, for a given value of ξ, the excitation cross section is proportional to $Z_1^2 (A_1/Z_1)^{2\lambda/3}$ which, for $\lambda = 2$, is $Z_1^2 (A_1/Z_1)^{4/3}$. Thus excitation cross sections increase with the mass and charge of the projectile and the advantages often obtained by using heavy ions become obvious. For projectiles with the same Z_1/A_1 (e.g., He^4, O^{16}, S^{32}) acceleration to energies proportional to Z_1 results in excitation cross sections proportional to Z_1^2. Finally, the cross section in first order perturbation theory is proportional to the square of a nuclear matrix element. This explains the preferential Coulomb excitation of collectively enhanced levels which is one of the most striking and useful features of this excitation mechanism.

Since E2 transitions so predominate in the osmium nuclei over other multipolarities we now limit ourselves to their consideration. Many states (e.g., 4^+, 0^+ levels) cannot be reached, however, by direct E2 transitions from the ground state. To calculate the excitation probabilities for these one may resort to higher order perturbation theory. The general features of the Coulomb excitation process (dependence on excitation and projectile energies, on projectile mass and charge, and dependence on and proportionality to nuclear matrix elements) remain and are generally enhanced. Thus in second order perturbation theory, for small ξ, $d\sigma_{E2}$ is approximately proportional to E^4. In fact, the higher the order of the excitation required to reach a state the stronger is the energy dependence of the cross section. This is indeed, in principal, a means of establishing or confirming the spins of certain states if their excitation is observed at several different bombarding energies.

The excitation of 2^+ states other than the first excited state may also be achieved through double E2 excitation via the first 2^+ state. Thus the cross section for such an excitation is

$$d\sigma_{2^+}' = d\sigma_{2^+}^{(1)}{}' + d\sigma_{2^+}^{(2)}{}' + d\sigma_{2^+}^{(1,2)}{}' \qquad \text{II-73}$$

where $d\sigma^{(1,2)}$ represents the interference between the first and second order cross sections, $d\sigma^{(1)}$ and $d\sigma^{(2)}$. Expressions for $d\sigma^{(2)}$ and $d\sigma^{(1,2)}$ are given in ABHMW and their evaluation is facilitated using tabulations performed by Douglas[62].

Consider now the case in which the excitation probability is large. Then the entire perturbation expansion is questionable. In this situation a final level is often attained only after multiple transitions through many states via repeated emission and absorption of virtual photons. Consequently, the excitation probability is no longer simply related to the nuclear matrix elements and the extraction of the latter becomes more difficult. In order to calculate the cross sections one must somehow have knowledge of all the matrix elements connecting all states involved in the excitations. Two recourses are possible.

First, one may fall back upon a nuclear model which expresses many nuclear matrix elements in terms of one or two or in terms of other known parameters. The cross sections may then be calculated but, of course, one can no longer extract matrix elements from the results. This approach is useful, however, in determining the extent to which the nucleus is structured according to the model used.

The second recourse is to fit the experimental data by varying a full set of matrix elements until theoretical and experimental excitation probabilities agree as a function of projectile energy. The computational difficulties involved in this approach (namely, solving a coupled set of differential equations of the form of eqs. 68) have recently been overcome[61]. This method of attack is described in detail after some further comments on the model-dependent approach.

There have been several of these model dependent "multiple Coulomb excitation" theories developed in recent years[63-65]. Most are based on the rotational model. Alder and Winther[63] have, for example, considered the excitation of the members of a pure rotational band. In their analysis the perturbation expansion is avoided in the sudden approximation ($\xi = 0$ for all states) which neglects the energy differences between band members. Actually, these authors expand their solution in a power series in ξ and calculate and tabulate the first order correction term also.

More specifically, using rotational model wave functions they express the excitation probabilities P_J (q) for the various band members as a function of the parameter q, defined by:

$$q = \frac{Z_1 e^2 Q_o}{4\hbar v a^2} = \sqrt{\frac{45}{16}} \left[P_{0 \rightarrow 2} (\theta = 180^o) \right]^{1/2} \qquad \text{II-74}$$

where Q_o is the intrinsic quadrupole moment of the band and $P_{0 \rightarrow 2}$ is the first order perturbation theory excitation probability for the first 2^+ state. Typical values of q in these experiments were somewhat less than 2.0.

Since large errors due to finite ξ can result even after first order correction terms in ξ are added to the excitation probabilities, Alder and co-workers[64] have modified their theory so as to calculate directly the excitation probabilities, $P_J(q, \xi)$, for finite (even large) ξ. The technique used is a diagonalization procedure involving the five lowest band members. The results are tabulated in reference 64.

In these multiple Coulomb excitation theories an approximation often used is the so-called $\mu = 0$ approximation in which all initial, final and intermediate levels are populated only in their M = 0 substates. For zero-spin projectile and target this occurs rigorously for projectiles scattered through 180^o [66]. For angles close to 180^o (usually for $\theta > 155^o$) the approximation is quite accurate. In the present experiments, the minimum angle was $\theta_{cm} = 158^o$ and for this angle the errors involved in using the $\mu = 0$ approximation are less than 5%. However, the effective errors are much less since the experimental and theoretical cross sections are weighted averages over many scattering angles. Thus the contributions, in the theoretical integrals of the cross sections, from those (smaller) angles for which errors are greater than 3%, are a small fraction of the total. Overall errors thus resulting from the $\mu = 0$ approximation are always less than 3%, and generally considerably under this limit.

The $\mu = 0$ approximation, however, far surpasses, in its usefulness, its calculational convenience in this model-dependent theory. Since it corresponds, not to a feature of the model, but to the actual physical absence of non-zero magnetic substate excitations, it is valuable in almost all Coulomb excitation calculations. In particular, in the model-independent Winther and de Boer[61]

computer code (see below) it can result in reduction of computer costs by factors of 3-5. Furthermore, in this approximation the angular distributions of the deexcitation gamma rays become independent of excitation mechanism[56] and hence of the route by which the final state is reached. This in turn results in two related advantages, one of convenience and one more fundamental. The convenience is that one now does not need to apply a different angular distribution correction to the experimental numbers for each proposed set of matrix elements (i.e., of excitation routes and probabilities). The more fundamental advantage occurs with states for which two prominent excitation routes are possible (e.g., 2^+, states). The matrix elements for the two routes may be unambiguously assigned, in this approximation, if the absolute excitation probability of the state and its deexcitation branching ratio are known. If, on the other hand, the angular distribution were a strong function of excitation route, then two experimental numbers would not be sufficient to fully determine the excitation process, and unambiguous matrix elements would not be obtainable. As in the model-dependent calculations, the overall errors involved in using the $\mu = 0$ approximation in the Winther and de Boer program are always less than 3% and, except for the excitation of 6^+ and 4^+, states, closer to 1% (See Table VI-9). Furthermore, of course, the direction of the error is known and consequently a partial correction can be made, reducing the error even further.

Returning for a moment to the model-dependent calculations, we note one important characteristic. The relative excitation probabilities for the different band members oscillate as a function of q, and hence as a function or projectile energy ($q \propto E^{3/2}$). Fig. II-2 illustrates this for the ground state band. The oscillations are seen to occur for values of q greater than about 2.0 and so were not observable in the present experiments. However, if a sulfur beam of energies from 100-150 MeV were used, the range of q covered would be $1.7 < q < 3.2$. In this case the relative 2^+ state excitation probability would be seen to "turn over" relative to the 4^+ state excitation. This oscillatory feature can be used to further test the degree to which the nucleus obeys the rotational model, especially for the higher-lying band members.

So far we have considered only the multiple excitation of the ground state band. Lutken and Winther[65], however, have dealt with the excitation of excited

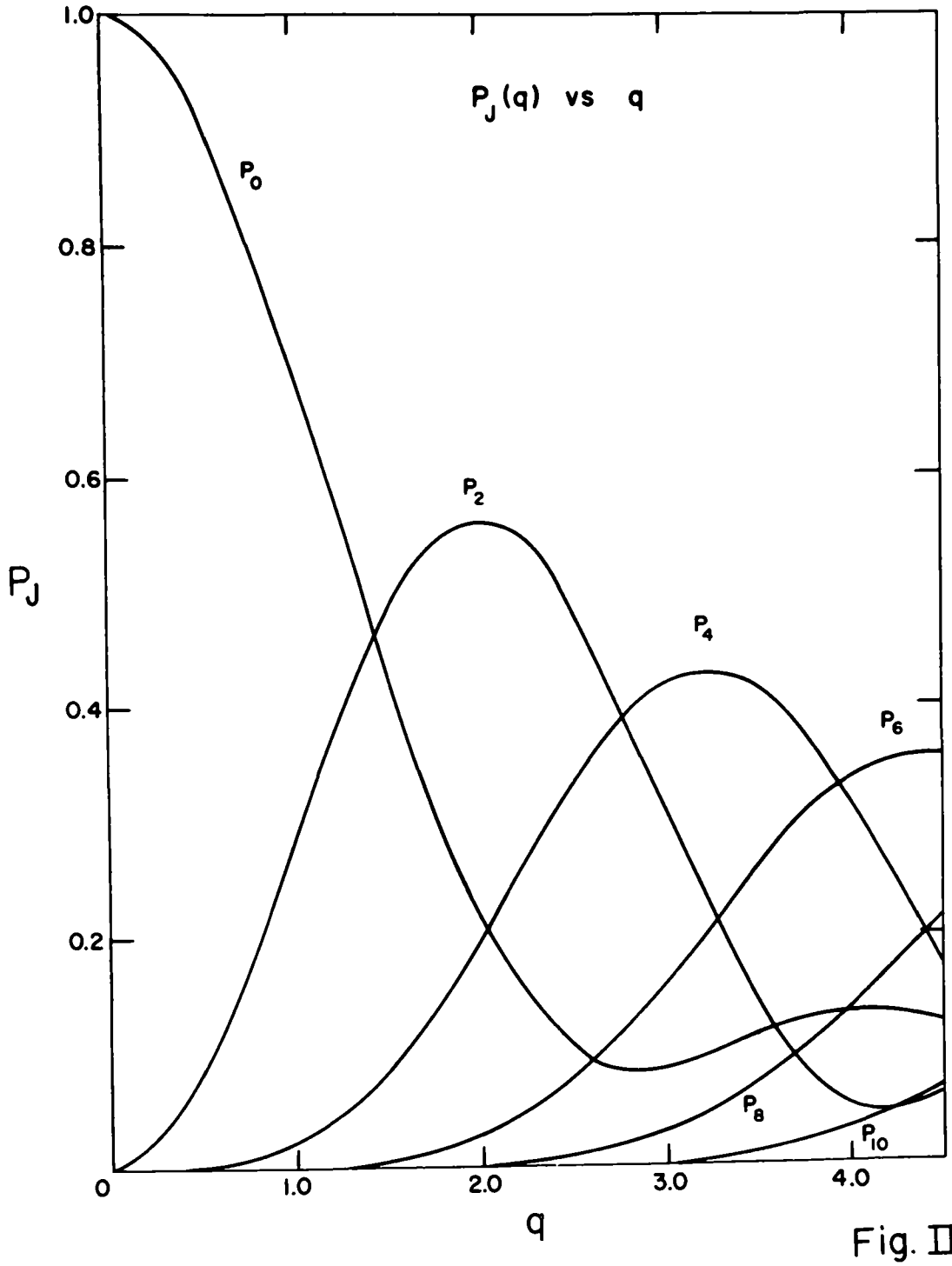

Fig. II-2

vibrational bands. Assuming the rotational model and taking the band members as degenerate (i.e., $\xi = 0$ within a band but not between bands) these authors show that the excitation probability for a given state in the final band can be written as the first order perturbation theory excitation probability to the first 2^+ state of the band times a factor $B^{\lambda\mu}_{J_f K}(q(\theta))$ which effectively redistributes the population of the band among the various states. $q(\theta)$ is defined in a manner similar to eq. 74 except that $P_{0\to 2}(\theta)$ replaces $P_{0\to 2}(180^\circ)$. In the $\mu = 0$ approximation, $B^{\lambda\mu}_{J_f K}(q(\theta))$ is independent of μ and so, for large scattering angles, a good approximation is:

$$P_{J_f K} = \left[\chi^2(\theta, \xi)\right]^2 \left| B^2_{J_f K}(q(\theta)) \right|^2 \qquad \text{II-75}$$

where $\chi(\theta, \xi) = q(\theta)/1.6771$. For the K = 2 bands populated in these studies

$$d\sigma_{J_f} = d\sigma_{2^+} \left| B^2_{J_f 2}(q(\theta)) \right|^2 \qquad \text{II-76}$$

where $d\sigma_{2^+}$ is the first order perturbation theory cross section for the excitation $0^+ (E2)\, 2^+$. Because of the structure of eq. 76 one can extract the nuclear quantity $B(E2{:}0^+ \to 2^+)$ from the calculations using the model. The quantities $B(q(\theta))$ are given in reference 65 and, for a K = 2 band, are illustrated in Fig. II-3. This figure, like Fig. II-2, shows that the excitation probabilities for various final states have different energy dependencies, the excitation of the more circuitously populated states generally requiring higher energy projectiles. Thus another features of these model-dependent calculations is that they provide a means of testing for the spins of states suspected of being members of a rotational band. (Often these states are only weakly excited and a full measurement of the angular distribution of the deexcitation gamma rays is an impractical means of establishing the spin).

Further details on these calculations are provided in references 63-65, 25, and 27 where definitions of terms, derivations, and tabulations of useful functions are provided in greater abundance than here.

The model-dependent approaches, by their very nature, need to assume most of the matrix elements required in the calculations and therefore do not provide them as output. A method of analysis that does not suffer from this disadvantage will now be described.

RELATIVE EXCITATION PROBABILITIES of
SOME GAMMA (K=2) BAND MEMBERS

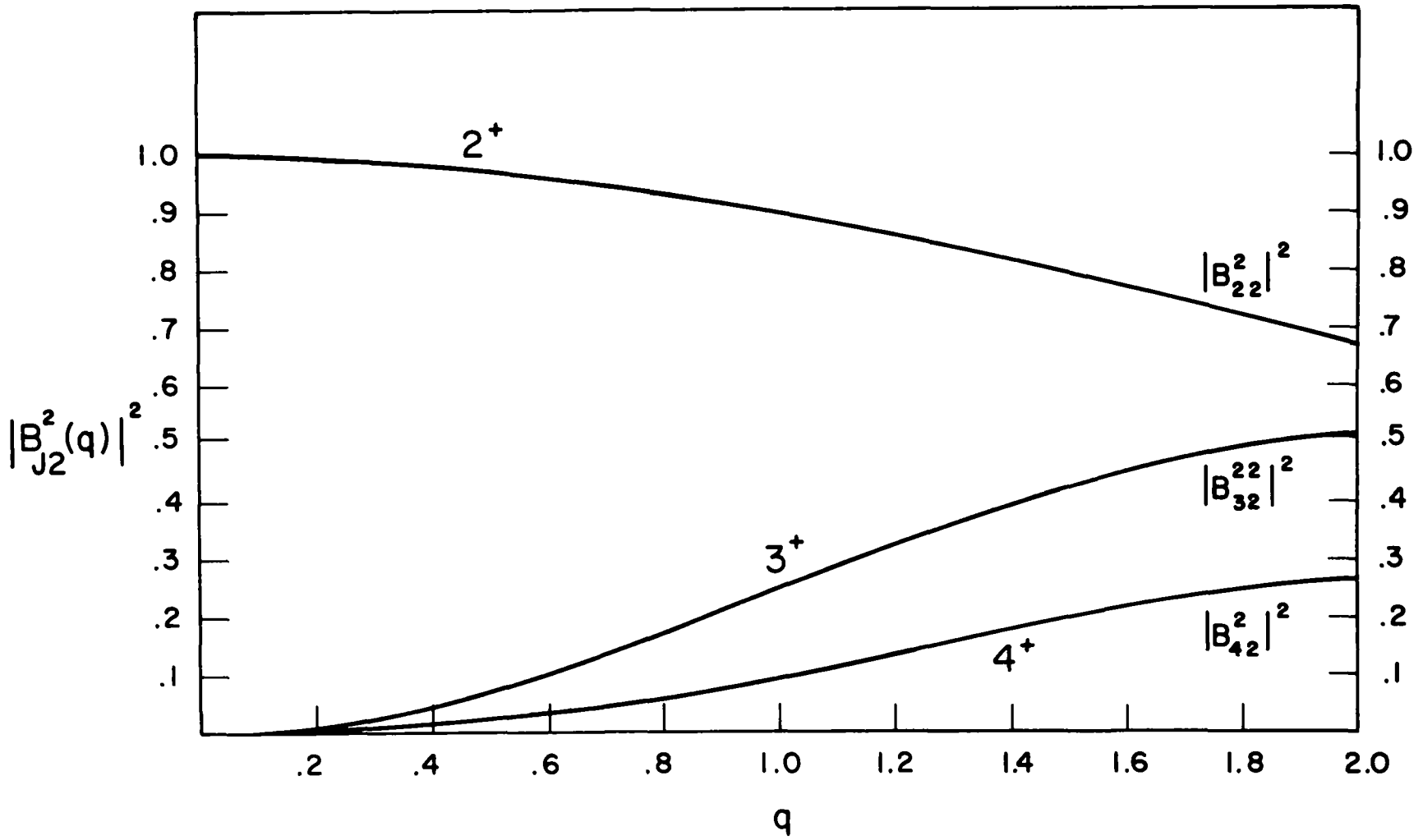

Fig. II-3

We recall that the most exact and rigorous way of calculating the Coulomb excitation cross sections is to solve the coupled equations (eqs. 68) for the time-dependent excitation amplitudes. In principle this set of equations is infinite but in practice many states are not involved in the excitation mechanism and may be neglected. The numerical solution of eqs. 68 has recently been rendered conveniently feasible by the use of a computer code developed by A. Winther and J. de Boer[61]. (A similar computer calculations has been developed by I. Berson[67]). The Winther and de Boer code solves up to ten coupled equations of the form of eqs. 68 (with up to 90 magnetic substates involved) for the excitation amplitudes a_f and from these calculates Coulomb excitation probabilities and cross sections. The calculations are done in the semi-classical approximation but include symmetrization of the classical orbits (see below) and are limited to E2 excitation processes.

After a change of variables from t to w, defined by

$$t = a/v \, (\epsilon \sinh \omega + \omega) \qquad \text{II-77}$$

where $\epsilon = 1/\sin(\theta/2)$, the integration of the transformed eqs. 68 is initiated by use of the Runge-Kutta-Gill[68] procedure. The results of this are the amplitudes and derivatives of all the a_f at the initial point in the orbit and at three successive consecutive points. These numbers then form the basis for the use of the more efficient Adams-Moulton predictor-corrector formulas[69] which obtain the values of the a_f at all successive steps in the projectile orbit. The code provides an accuracy control which determines the range of integration and the degree to which the sum of all excitation probabilities, $\Sigma_{i=0}^{N} P_i$, is allowed to deviate from unity. The program prints out results for the final excitation probabilities, laboratory and center of mass cross sections and also for coefficients used in the calculation of the angular distributions of the deexcitation gamma rays. The user can select the number of substates to be included in the calculations. For use in the analysis of the experiments performed here the program has been abbreviated and modified so as to form a subprogram in a code which performs thick target integrations of the theoretical cross sections. This modification is discussed in Section V-E and in Appendix II, where a listing is also given.

Before closing this chapter one general comment is appropriate. In all

the above discussions the energy loss of the projectile in the collision is neglected (recall the use of only a single, asymptotic, v). This is consistent with the semi-classical approximation. Without complicating matters, however, a significant improvement in these calculations (whether of the perturbation theory, model-dependent or independent types) may be obtained by " symmetrization"[61]. This is done by replacing $\xi = (Z_1 Z_2 e^2)/\hbar v$ by

$$\xi_{sym} = \frac{Z_1 Z_2 e^2}{\hbar} \left(\frac{1}{v_f} - \frac{1}{v_i} \right) \quad . \qquad \text{II-78}$$

This symmetrization procedure has been incorporated into all analyses performed in this study.

III. EXPERIMENTAL CONSIDERATIONS

A. Methods of Measurement

In order to investigate the nuclear structure of the osmium isotopes several types of experiments were performed although all used Coulomb excitation as the basic tool. After a brief outline in this section of the various species of measurement, the rest of this chapter will concern itself with a description of the experimental apparatus used.

There were three principal modes of experimental determination of nuclear information employed in these studies. In each, measurement of gamma (hereafter γ) ray spectra was the central feature. Such spectra were recorded:

1) singly in both NaI(Tl) scintillation crystals and Ge(Li) solid state detectors. (These measurements are henceforth referred to as "γ-singles" or "direct" spectra.),

2) in coincidence with γ-rays representing specific nuclear transitions in the isotopes studied (hereafter called "γ-γ" measurements),

3) in coincidence with particles of the incident beam backscattered from the target nuclei into an annular particle detector (hereafter "γ-particle" measurements).

The second approach is extremely useful for analysis of complex decay schemes and was used primarily for that purpose. Additionally, though, it revealed certain transitions that were masked in the direct and γ-particle coincidence spectra by other, stronger, γ-ray transitions degenerate with them.

The first approach is useful for obtaining branching ratios and, in the case of the Ge(Li) detector, provides γ-ray resolution far surpassing that obtainable with the NaI(Tl) crystals. Thus it also serves a valuable function in elucidating the existence and nature of composite peaks in the other γ-ray spectra.

The third method has proved by far the most valuable and has been the source of most of the quantitative results obtained. In principal, any of the three methods can be used to extract absolute nuclear transition probabilities. However, for the following reasons, the γ-particle coincidence measurements proved the most fruitful source of such information.

1) Gaps in the response of the particle detector on a millisecond time scale due to bias reduction caused by electrons emitted from the bombarded target introduced an additional source of error of about 10% into the other methods that was avoidable in the γ-particle experiments.

2) Thick target data analysis is complicated in methods (1) and (2) by the fact that integrations, over all angles and over all energies $E \leq E_{O^{16}_{inc}}$, of theoretical yields must be performed. The energy integration is merely an inconvenience but the angular one involves the foregoing of the $\mu = 0$ approximation (see Section II-C). In method (3) the angular integration is eliminated (one mean scattering angle is an excellent approximation) and a relatively high cutoff on the energy integrations is possible (see below). Data analysis is thereby rendered easier, more accurate and less expensive as well.

3) Perhaps the principal disadvantage of methods (1) and (2) is that the relative population of certain states reached by high order excitation mechanisms is reduced relative to their population in method (3) in which γ-rays are recorded in coincidence with backscattered particles whose hyperbolic Rutherford orbits corresponded to closer distances of approach to the nuclear surface and consequently to greater interaction strengths. Thus method (3) is invaluable in studying many high-lying, weakly-excited states.

4) Ambient and nuclear-reaction-induced backgrounds of γ-rays are relatively considerably higher in methods (1) and (2) than in method (3). Again, weakly excited states are thus more easily observable with the latter technique.

Measurements of γ-ray spectra in coincidence with the $2^+ \rightarrow 0^+$ and $4^+ \rightarrow 2^+$ transitions were separately recorded, at an incident O^{16} energy of 70.30 MeV, on $Os^{186, 188, 190, 192}$. It should be noted that, due to a near-degeneracy of the $4^+ \rightarrow 2^+$ and $2^{+\prime} \rightarrow 2^+$ γ-ray transitions in Os^{190}, one of the γ-γ coincidence spectra obtained from this nucleus actually consisted of coincidences with both of these transitions, not solely the $4^+ \rightarrow 2^+$ deexcitations.

Direct and γ-particle coincidence spectra were taken on some or all of the nuclei, on either (or both, in some cases) thick or thin targets at the following incident O^{16} laboratory energies (in MeV): 42.00, 48.26, 62.10, 70.30, 80.00. In these measurements the γ-ray counters were placed about 6.5 cm. from the

target and at 55^{o} to the beam direction. The latter condition served to reduce the effects of anisotropies in the γ-ray angular distributions since it corresponds to the zero of the Legendre polynomial, $P_2(\cos \theta_{\gamma}^{-})$. (See Section V-A.) The particle detector position varied somewhat from run to run but always subtended, at the target, approximately 14^{o} in the laboratory within the angular range 156^{o}-175^{o}. It was typically about 2.5 cm. from the target.

In the γ-particle runs, γ radiation due to nuclear reactions was eliminated by designating a cutoff energy, E_{min}, on the backscattered particles and by demanding that the recorded γ-rays be in coincidence with particles above that cutoff energy. This eliminates coincidences with lighter particles such as protons or alpha particles emitted in compound nuclear decay since they are generally of relatively low energy and, at any rate, can only deposit energies $E \leq E_{min}$ in the detector. It also eliminates coincidences with O^{16} ions backscattered from light target contaminants since these too have lower energy. Fig. III-1[123] illustrates a particle spectrum resulting from the bombardment of a thick samarium target with 49 MeV O^{16} ions and shows the use of the cutoff energy to discriminate against products stemming from the reaction of the O^{16} ions with a light target contaminant such as aluminum.

In addition to the above measurements, angular distributions of the deexcitation gamma radiation from the stronger transitions have been recorded in both γ-singles and γ-particle modes on $Os^{188, 192}$ at incident O^{16} energies of 48.26 and 70.30 MeV and on Os^{186} at an incident energy of 70.30 MeV. Measurements at three angles, to the incident beam, 0^{o}, 55^{o} and 90^{o}, were performed and the results have been compared with theoretical distributions. (See Chapter V.)

Further details of the experimental apparatus are contained in the succeeding sections of this chapter.

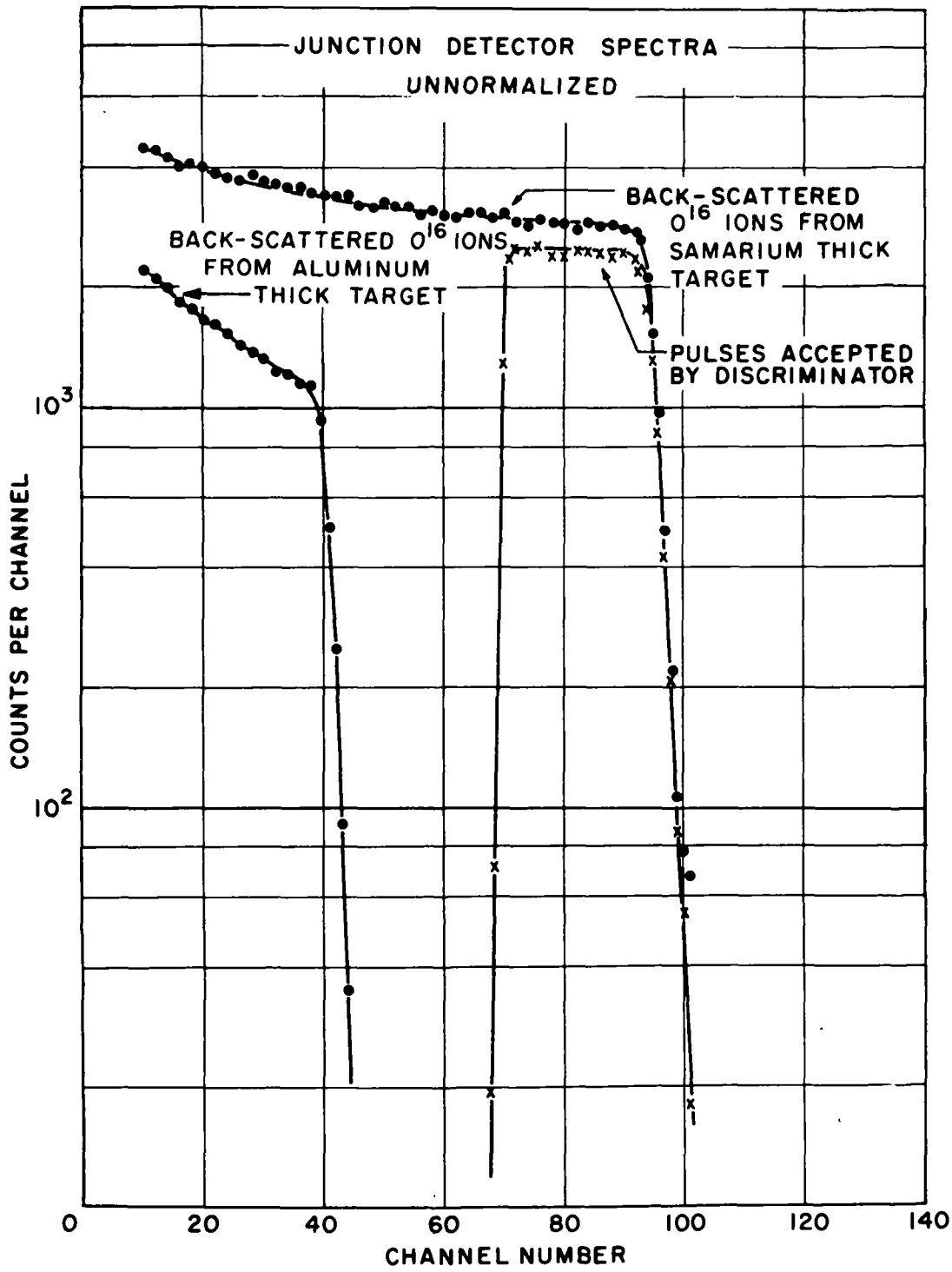
JUNCTION DETECTOR SPECTRA
UNNORMALIZED
BACK-SCATTERED O16 IONS FROM SAMARIUM THICK TARGET
BACK-SCATTERED O16 IONS FROM ALUMINUM THICK TARGET
PULSES ACCEPTED BY DISCRIMINATOR
COUNTS PER CHANNEL
10³
10²
0
20
40
60
80
100
120
140
CHANNEL NUMBER

Fig. III-1

B. Accelerator

The beams used in the experiments described herein were provided by the "Emperor" MP Tandem Van de Graaff accelerator at the A. W. Wright Nuclear Structure Laboratory of Yale University. The accelerator is, in many respects, a standard tandem Van de Graaf with positively charged central terminal and negative ion injection with the higher energy end at ground potential. However, obtainable voltages exceed 11 MeV on the central terminal and proton beams of over 5 μa on target have been obtained at energies exceeding 22 MeV. Oxygen beams used in these experiments were obtained with energies up to 80 MeV. (Previous Coulomb excitation studies on the osmium isotopes[70, 71] have generally been limited to O^{16} projectile energies of less than 49 MeV. As can be seen in the data presented herein (see Chapter IV), at such energies only the lowest three excited states are observed. The higher O^{16} energy available here has enabled us to excite about twice as many states with sufficient frequency to be able to extract B(E2) values for their excitation and thus to considerably extend the knowledge of absolute transition probabilities in the transitional osmium nuclei.)

The continuously variable projectile energy is stabilized via feedback to the corona points of an electrical signal from the image slits of the 90^{o} analyzing magnet. Using an NMR probe associated with that magnet one is able to obtain momentum analyzed beams stable in energy to less than one part in 10^{4}. At the time of this writing, proton, deuteron, alpha particle, He^{3}, carbon, oxygen, sulfur, argon, and iodine beams have been accelerated successfully. The main features of the installation are schematically shown in Fig. III-2. Below, some additional aspects of the accelerator are briefly discussed.

There are two ion sources: a duoplasmatron and a diode ion source. The latter has been used (in related experiments) to accelerate S^{32} ions obtained from a gas mixture containing H_2S. The former supplied the oxygen ions for these measurements. The O^{16} is introduced into this source in the form of a mixture of CO_2 and H_2 and is ionized in a high density plasma discharge initiated by electrons emitted from a heated filament and subsequently spiralled in a magnetic field. These O^{16} ions pass through a charge exchange canal and those that emerge in the 1^{-}

TWO STAGE TANDEM ACCELERATOR

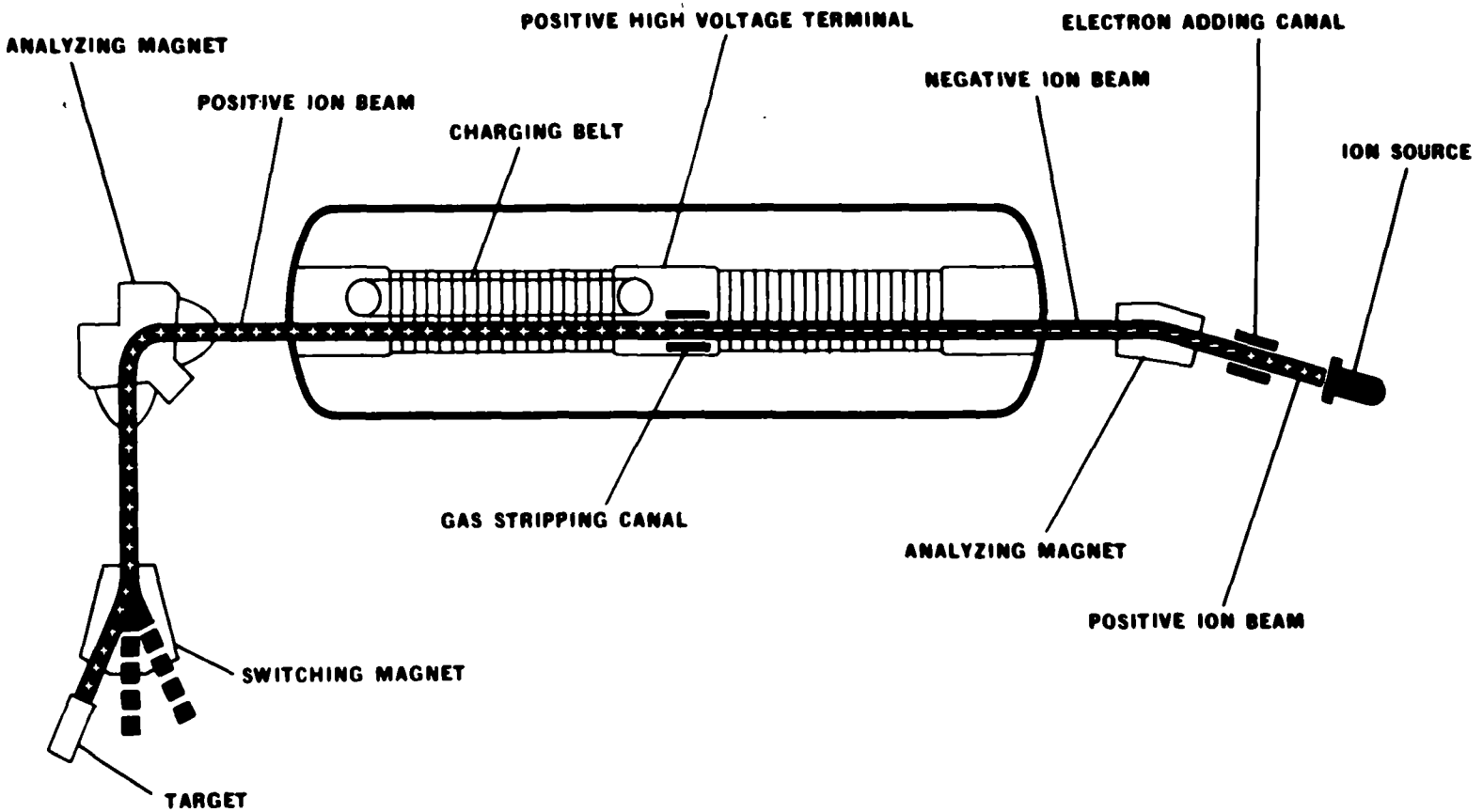

Fig.III-2

charge state are magnetically selected, focussed, and injected into the main acceleration tube. Because of the O^{16} in the initial gas mixture, filament life is limited and a compromise must be struck between filament life and beam current requirements. A 2% (approximately) mixture of CO_2 in H_2 was found to be a suitable one.

Inside the accelerator proper the negative ions are attracted toward the central terminal, at which point they pass through a "stripper" gas rendering them positively charged. The ions are then repelled from the central terminal, emerge from the higher energy end of the "tank" and are electrostatically steered and magnetically focussed. An analyzing magnet bends those ions in the selected charge state through 90^{o} and precisely defines their energy. The beam is then focussed once more, bent into the appropriate experimental "leg" by a "switching" magnet, magnetically focussed twice more and finally allowed to enter the region of the scattering chamber.

The O^{16} ions used in these experiments varied in energy from 42-80 MeV and in charge state from 5^{+} to 7^{+}. Terminal voltages ranged from 7-10 Mv. Beam currents were purposely kept low to avoid overloading particle and γ-ray counters and generally were in the 10-20 na region although on occasion several hundred nanoamperes were recorded on target. The beam spot on target was defined, by collimating slits, to slightly better than 1 mm. by 1 mm. With the rectangular slits set at .015" on each side, however, very little beam actually struck the slits.

One final feature of the installation is the use of commercially-obtained Ultec ion pumps on all beam legs instead of oil diffusion pumps. This results in very little contamination of system and targets from condensation of pump oil vapors. Typical pressures throughout the system were in the 10^{-7} to 10^{-6} mm. Hg range.

The accelerator functioned reliably during these experiments and data acquisition rates were very satisfying. A typical γ-backscattered particle coincidence experiment yielding 2-3 x 10^{5} counts in the largest γ-ray peak and 20-40 x 10^{3} counts in other main peaks required only 2.5 to 5 hours. Filament lifetime in the ion source varied from 15 to 30 hours and thus several coincidence spectra could easily be procured in consecutive runs under identical experimental conditions. Through advantageous, such a circumstance was not actually a necessity due to the excellent reproducibility of beam conditions, and thus of data, over a span of many months.

C. Scattering Chamber and Particle and Gamma Ray Detection Apparatus

The target chamber and associated apparatus are illustrated in Fig. III-3. A final quadrupole focusing magnet (not indicated in the figure) served to bring the beam to a focus at the target located about 8' away. Inserted between the quadrupole and the target chamber was a slit system consisting of two rectangular Ta slits the size of which was continuously and independently variable via sets of four micrometer depth gauges. The first slit was the beam defining collimator. The second, or antiscattering slit, was about 2' closer to the target and generally set .005" wider in each dimension than the first. To prevent radiation from the slits from entering the γ-ray detectors a wall of machined lead bricks, fitted around a narrowed section of beam tube, was placed between the slits and the detectors.

Two very similar scattering chambers were employed in these measurements. In each one the target under bombardment was suspended from the top flange while the lower flange contained the support and alignment assembly for the annular surface barrier detector used to record particles backscattered from the target. This flange was itself supported by a slotted stainless steel rod which slipped into a cylindrical hole and keyway in the main aluminum support table.

The two chambers differed only in the basic cylindrical body. (The same top and bottom flanges fit into each body.) The only difference between them is that one (illustrated in Fig. III-3) was used with thin targets and so had a flared outlet through which the unscattered incident beam could pass into an insulated Faraday cup. The other chamber, used with thick targets, needed no such outlet. With this latter chamber γ-ray detection at 0° was feasible. Beam integration with this chamber, though not necessary, could be easily (albeit crudely, in an absolute sense) achieved since the targets were electrically insulated, with teflon spacers, from the rest of the chamber.

The scattering chamber and support table were so designed that replacement of one chamber with the other required only a few moments and no realignment of targets or detectors. The vertical positioning of the entire chamber was obtained by a screw adjustment on the vertical support rod for the bottom flange. The

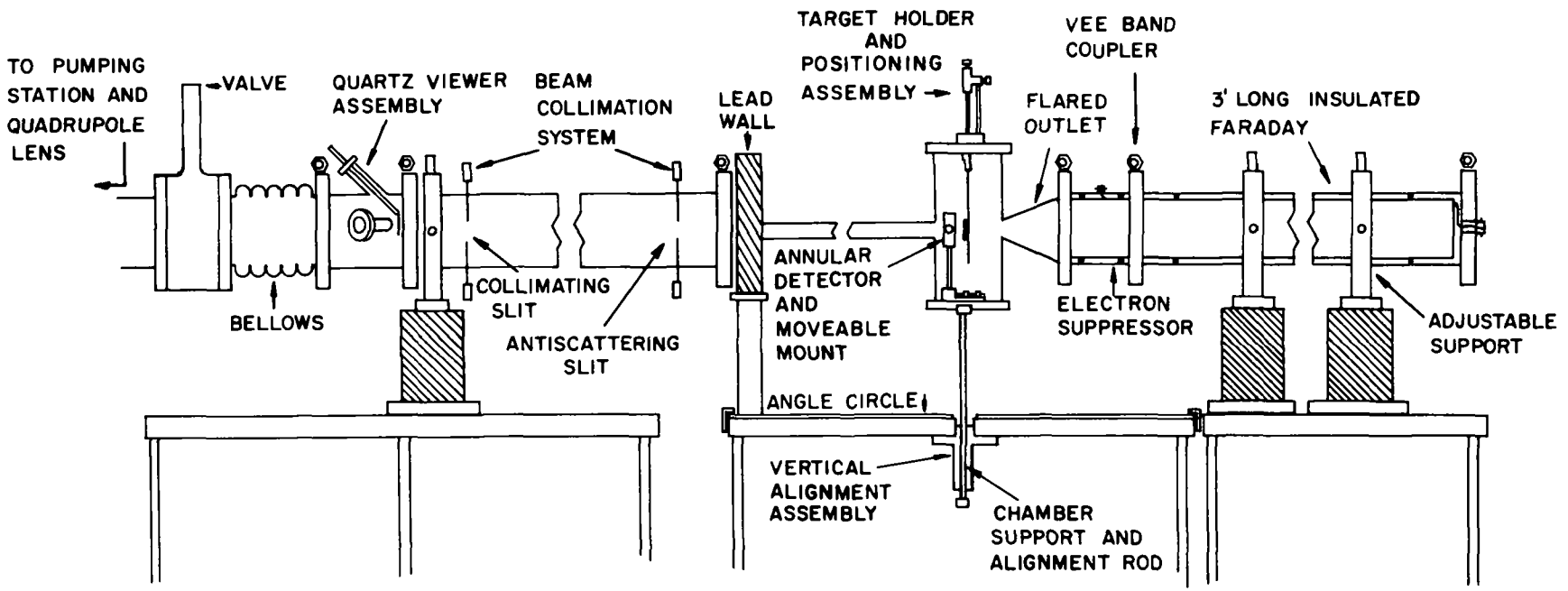

SIDE VIEW OF SLIT SYSTEM AND SCATTERING CHAMBER

ALL COMPONENTS EXCEPT CHAMBER WERE LINED WITH TANTALUM AND/OR LEAD FIG. III-3

particle detector itself was mounted in a sliding assembly on the lower flange and could be continuously moved in all directions, although not from outside the chamber. Thus one could select specific backscattering angles and solid angles with considerable freedom. The particle detector could also be positioned (roughly) at any desired forward angle by rotating the lower flange relative to the beam direction. The annular surface barrier detectors used were supplied by ORTEC and had central holes of 4 and 5 mm. diameter with sensitive regions extending from about 3 to 8.5 mm. in the radial direction. They were generally biased at 50 volts and drew from 0.2 to 3.0 μa reverse current (through 2 MΩ) depending on the prior duration of their exposure to the scattered beam.

Up to four targets, suspended from the top flange, could be moved into position in front of the beam from outside the chamber, in the standard configuration, by the vertical movement of a notched stainless steel rod. This rod was actually continuously positionable, and in addition, was provided with a fine adjustment screw, so that any position of any target could be exposed to the beam and so that, by using non-standard clamps, more than four targets could be inserted at once. This latter feature often proved valuable when one wished to bombard not only all four Os targets in turn but a gold target for calibration purposes as well.

The γ-ray detectors were 3 x 3 in. thallium activated NaI scintillation detectors mounted in protective graded Pb, Cu and Sn shielding and supported in "Y" shaped vertically positionable aluminum holders. A top view of the apparatus, shown in Fig. III-4, shows these detectors in place. The detector assemblies could be placed at distances from the target varying from about 2.5 inches to about 2 feet and could be concentrically rotated to any desired angle (except extreme backward, and, in the case of the thin target chamber, extreme forward angles) as marked on an inscribed angle circle fastened to the main aluminum table. These scintillation counters were optically coupled to Dumont 6363 photomultipliers and yielded about 9% energy resolution.

In addition a 7.7 cm^3 planar lithium drifted Ge γ-ray detector and Dewar assembly was mounted on the table and could be manually rotated to most angles. In certain direct spectra taken with this counter, maximization of counting rate was of primary importance and, for such purposes, an extension piece was made

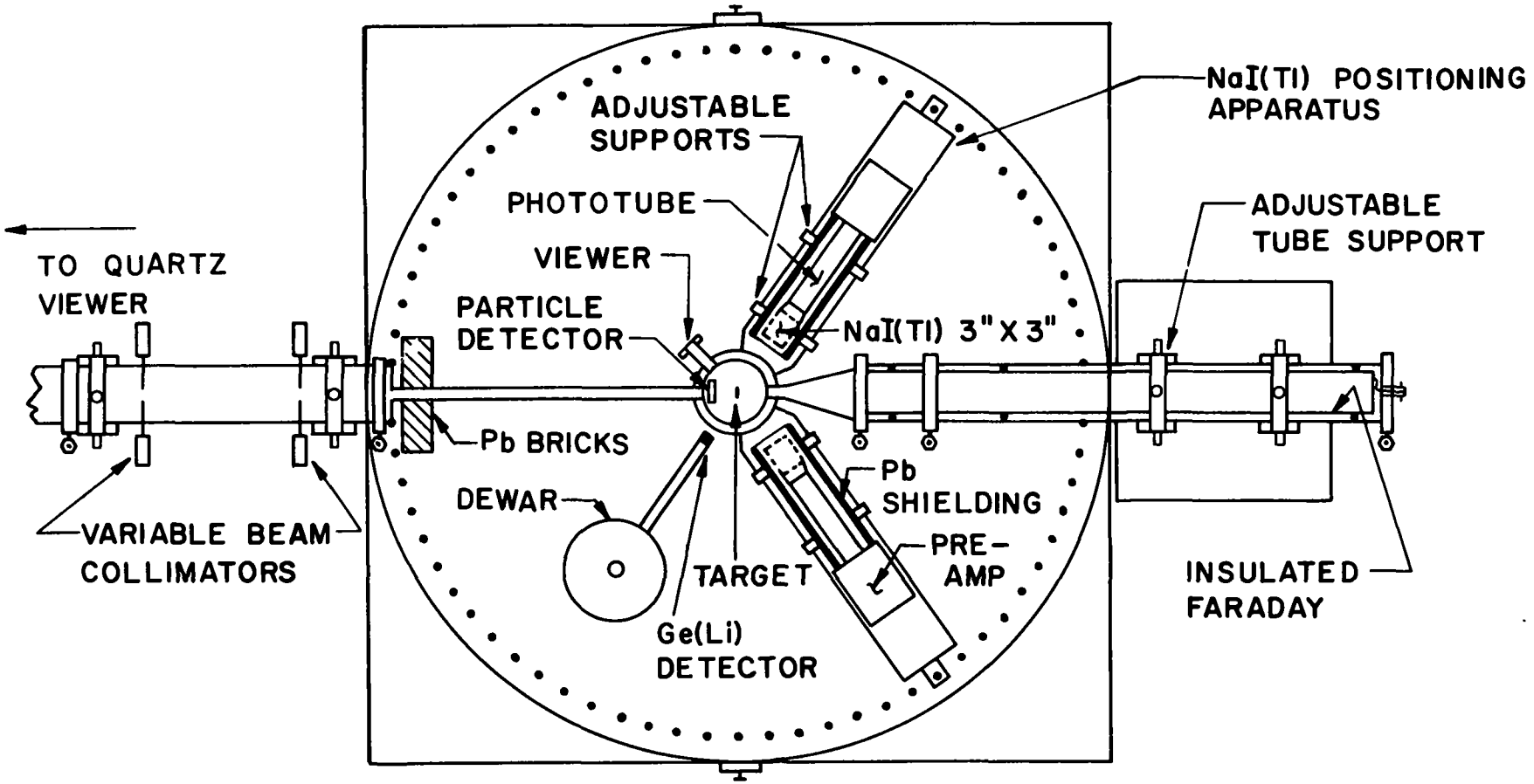

TOP VIEW OF SCATTERING CHAMBER AND ANGLE CIRCLE

Fig. III-4

with which the targets could be placed within an inch of the Ge detector face. Resolution with this detector was about 6 kev on the Na^{22} 511 kev γ-radiation.

D. Targets

The targets required in a Coulomb excitation experiment on heavy nuclei should be as free as possible from contaminants. For low Z nuclei the incident beam is well over the Coulomb barrier and profuse quantities of γ-rays, protons, neutrons and alpha particles are produced from nuclear reactions involving the decay of highly excited compound systems. Thus one must contend with high background radiation which reduces peak-to-valley ratios in the γ-ray spectra. Such radiation also tends to flood the detectors, forcing one to reduced beam intensities, hence higher relative ambient backgrounds and lower data acquisition rates. High Z contaminants are also undesirable since they are themselves Coulomb excited and such effects must be disentangled from the Coulomb excitation of the target proper.

For these reasons one would like to use clean, thin or thick, self-supporting, isotopically enriched targets. In the case of osmium such targets are extremely difficult to produce[70]. Prior to this work, the only evaporated thin Os targets produced were fabricated by J. de Boer et al.[70] However, these were $< 1\ \mu g/cm^2$ thick, were not self-supporting, and were only marginally usable for Coulomb excitation of the lowest lying, most frequently excited, states. Data acquisition rates were exceedingly low in coincidence measurements and, since surface-to-volume ratios were high, contaminant background radiation was a serious factor. Thicker Os targets have been produced in a sintering process by McGowan and Stelson[71, 91]. These, however, were not isotopically enriched and disentanglement of composite peaks made data analysis difficult. It is partially because of these target problems that B(E2) values for the osmium nuclei were only known for the excitation of the first three states and, even then, with quoted errors of 30-40% and frequent disagreement among different observers of factors of 2-4[70, 71].

A considerable effort was therefore expended on the production of more satisfactory targets. Fortunately, these efforts proved quite successful and extremely clean thick and thin self-supporting isotopically enriched targets have been fabricated. The thick targets are made by a process somewhat similar to the sintering technique of McGowan and Stelson[71]. The thin targets are made via

evaporation of osmium powder onto a glass substrate with subsequent floatation and recovery of the thin films in the form of self-supporting targets. The procedures for making these targets, as well as a discussion of certain problems inherent in the production of osmium foils, are discussed in detail in Appendix 1.

Suffice it to say here that the targets have proved very satisfactory. Consequently data acquisition rates were high and data analysis considerably facilitated. The very weak 6^+ and $4^{+'}$ states are observed even in the γ-γ coincidence data, for example. Most of the data has, in practice, been taken on the thick targets since they proved the cleaner, easier to fabricate and less expensive of the two types and resulted in higher counting rates as well. The specific type of target used in each run is labelled on the relevant spectrum in the next chapter by the words "thick" or "thin". These two descriptions designate thicknesses of $.0029 \pm .0002$" and 500-1000 $\mu g/cm^2$, respectively.

E. Electronics

The electronics consists principally of a standard fast-slow coincidence system with variable logic options. The details given below may be complemented by the discussion of a similar system in reference 25. The description here corresponds mainly to the γ-particle mode of operation. The γ-γ mode is very similar except that the particle signals are replaced by γ-ray pulses from a second NaI(Tl) detector. The γ-singles mode is nearly trivial and will not be dealt with further. A block diagram of the electronics setup in the γ-particle mode is presented in Fig. III-5.

In essence, the electronics determines whether or not a detected particle and γ-ray were in time coincidence (resolving time $\cong$ 40 ns) and, if so, allows the linear γ-ray pulse to be recorded in the memory of a multichannel analyzer (hereafter MCA). Additional requirements on the particle energy are also demanded. Some specific details are considered now.

For "fast-side" timing purposes γ-ray signalsfrom the NaI(Tl) detector were taken from the anode of a DuMont 6363 photomultiplier tube to which the scintillation crystal was optically coupled. These signals were successively amplified and 1-ma limited several times and then passed through a 100 mv discriminator set so as to just eliminate the noise pulses. The fast particle pulses from an ORTEC Model 260 time pickoff unit were fed directly into an identical discriminator unit. True and accidental coincidences were then obtained (the latter by inserting a delay of $\cong$ 100 ns) and used to open linear gates on the "slow-side". The coincidence resolving time of about 40 ns resulted in nearly 100% coincidence efficiency for all but the lowest energy γ-rays. The linear signals, preamplified, amplified and passed through the opened linear gates were then fed into the direct input of an MCA which in turn was also "prompt-gated" by the true coincidence signal itself since the linear gates had been opened by both true and accidental coincidences.

In addition, one wants (See Section III-A) to record only those γ-particle coincidences in which the backscattered particles were above a certain energy, E_{min}. Consequently the linear particle signals were allowed to pass through a single channel analyzer whose baseline was set to correspond to the desired energy

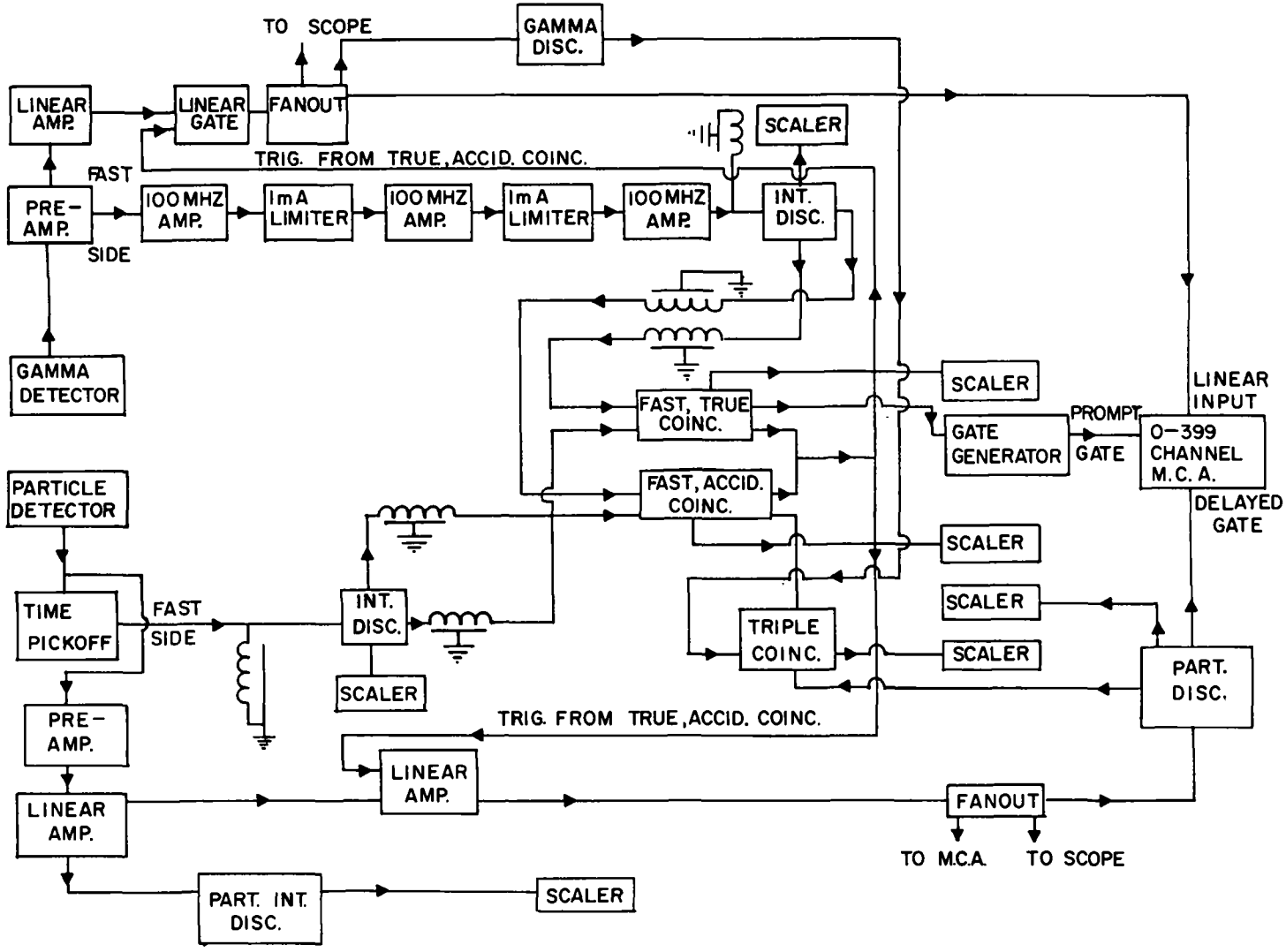

SCHEMATIC DIAGRAM of ELECTRONICS in GAMMA-PARTICLE COINCIDENCE MODE FIG. III — 5

deposited in the surface barrier particle detector. The output of this analyzer was fed into the "delayed gate" of the MCA.

Accidental coincidences were recorded on scaling circuits as the output of a logic network which demanded a threefold coincidence among the signals from the fast accidental coincidence unit, the particles above the cutoff energy and the γ-rays of energy in the same range as those recorded in the (calibrated) MCA.

Various quantities were scaled, including especially the total number of particles backscattered with energies above the cutoff and the total number of backscattered particles above that cutoff in coincidence with γ-rays.

As stated above, the γ-γ mode of operation is similar except that the fast coincidence demanded is that between two γ-rays, one from each of two NaI(Tl) detectors. The second set of γ-ray pulses replaces, logically, the particle pulses in the γ-particle mode. An additional slow coincidence requirement here is that the γ-rays recorded in the MCA must actually be in coincidence with γ-rays from the other detector which correspond to a specific transition in the target nucleus, e.g., the $2^+ \rightarrow 0^+$ or $4^+ \rightarrow 2^+$ deexcitation transitions. This requirement is met by passing the γ-ray signals from the "gating" detector through a single channel analyzer window set on the desired photopeak. The output of this analyzer opens a gate for the linear γ-ray signals.

IV. DATA PRESENTATION AND DECAY SCHEMES

A. Orientation

In this chapter most of the data taken on the four even-even isotopes, $Os^{186, 188, 190, 192}$, will be displayed and discussed. Each isotope will be considered in turn and, along with the data presentation, partial decay schemes will be shown. Despite the slight duplication resulting, it is convenient to display all four decay schemes in one figure in this introductory section. This will allow us to point out here in more detail the unity and general systematics of the osmium region and to better orient the reader to the discussions of the following sections.

In Fig. IV-1 are shown partial decay schemes for the four Os isotopes. Except for the 3^+ levels which are dotted and shown for continuity, all levels and transitions seen in this figure have been observed in the experiments performed here. In addition, several new transitions, not shown in the figure, have been observed and are discussed in the appropriate sections of this chapter.

As can be seen, all four isotopes exhibit at least incipient rotational bands based on the ground state and on the K = 2 γ-vibrational state. The band structure is actually quite well developed in $Os^{186, 188, 190}$ and higher-lying members of these bands are known[72, 73]. (In Os^{192}, however, the decay scheme of Fig. IV-1 shows all known levels[72, 76].) The transitional nature of the osmium isotopes is clear from the decay schemes alone which indicate that, as one proceeds from Os^{186} to Os^{192}, one passes from a highly and permanently deformed nucleus, quite closely approximated in many respects by the rotational model, to a nucleus, Os^{192}, which tends much more toward the vibrational limit but which still retains certain definite vestiges of rotational structure.

More specifically and quantitatively, it will be noticed that the first excited state energies gradually increase from Os^{186} to Os^{192} indicating (recall eq. II-12) that the moment of inertia, and hence the deformation, is gradually decreasing as the spherical limit is approached. In the rotational model the ratio of energies, E_{4^+}/E_{2^+}, in the ground state band, is 3.33, while in the vibrational model the 4^+ level is a two phonon excitation at twice the energy of the one phonon first excited 2^+ state. In practice, in vibrational nuclei, $E_{4^+}/E_{2^+} \cong 2.2$ and such a ratio can be obtained

PARTIAL DECAY SCHEMES
Os ISOTOPES

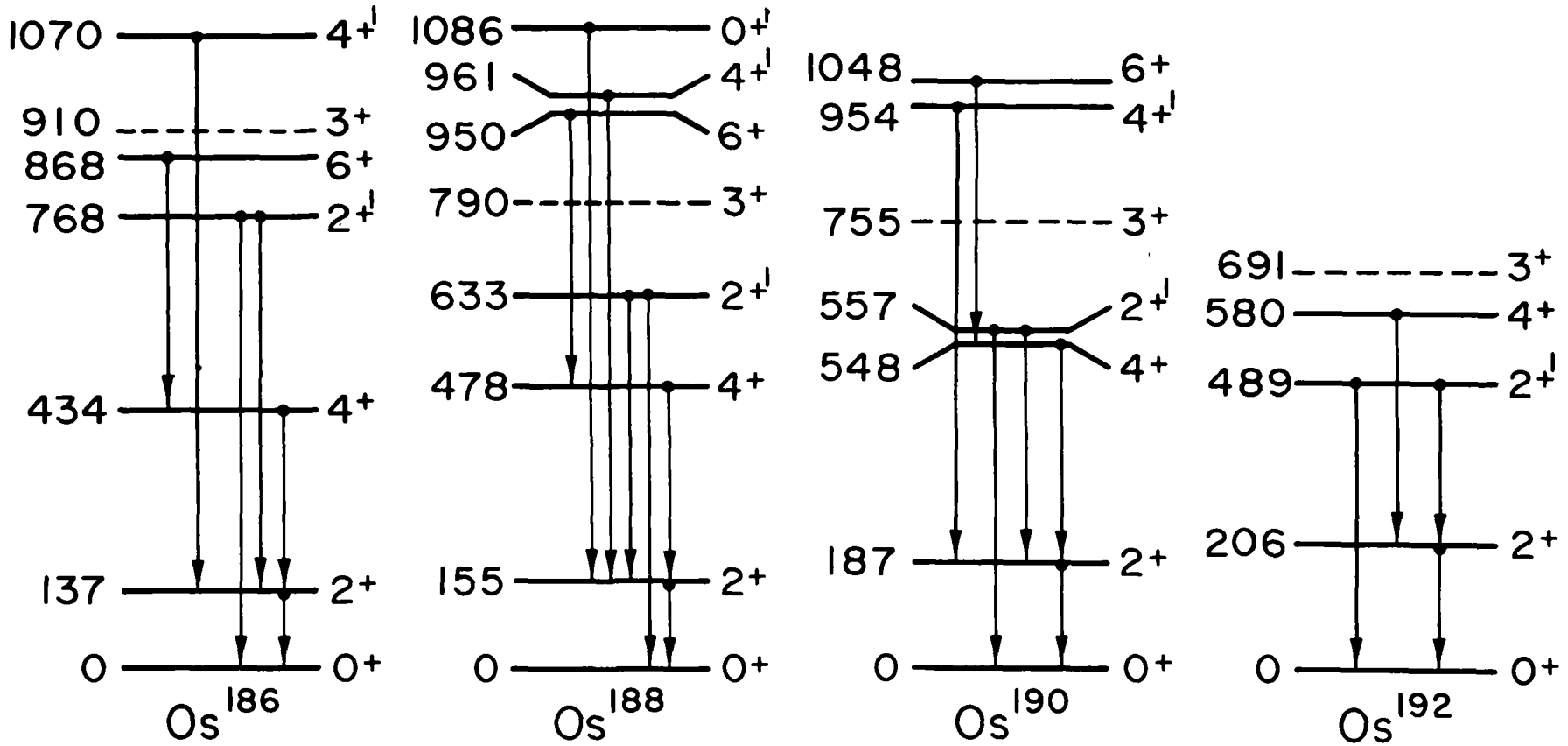

Fig. IV-1

theoretically by considering degeneracy-breaking residual interactions[22] (see Section II-A). For Os^{186} we have $E_4^+/E_2^+ = 3.17$, which is quite close to 3.33, while in Os^{192}, $E_4^+/E_2^+ = 2.82$, which is much closer to the vibrational result. Furthermore, as will be seen in Chapter VI, the branching ratio $B(E2:2^{+'} \rightarrow 2^+)/B(E2:2^{+'} \rightarrow 0^+)$ determined in these experiments is 2.67 in Os^{186} and 11.76 in Os^{192}. The rotational model result is 1.43 and the ratio is infinite in the vibrational model (see eq. II-6). Once again the trend is confirmed.

It will be noted, however, that the transition is gradual and actually not completed by Os^{192} whose structure, phenomenologically speaking, is probably a complicated mixture of rotational and vibrational motions in a shallow potential well. It is, in fact, for this reason of a gradual transition that the osmium region is of interest. It offers a sensitive testing ground for the various nuclear models[73] which must seek to reproduce the experimental results. The low A end of the rare earth region is typified by a much sharper transition region near the closed shell corresponding to neutron number N= 82[25, 117]. A truly successful theory of nuclear structure must be able to reproduce both these sharp and gradual transition regions at the two ends of the rare earth island of collectivity.

(In order to avoid repetition of explanations and to systematize the data presentation some general notes on the spectra that follow are collected here.

First, all the spectra shown below consist entirely of raw unaveraged data. Subtraction of accidental coincidences and contaminant γ-rays amounts to no more than a 3% correction except in the γ-γ spectra and as noted next for Os^{186}. The one exception to the above rule is in the γ-particle coincidence spectra for Os^{186}. Due to the large percentages of several contaminants in the Os^{186} spectra the latter actually give a misleading impression as to the nuclear information they contain. Thus, in the Os^{186} spectra used for most of the quantitative analysis (namely, the γ-particle spectra), the contaminant γ-rays have been removed. This can be done quite unambiguously since the main contaminants are the other osmium isotopes studied and data on them has been taken under identical experimental conditions. This exception is indicated on the appropriate spectra.

Secondly, in all NaI(Tl) spectra shown, the energies of those photopeaks corresponding to transitions in the nucleus being studied are given in kev above

the photopeak. It may be assumed by the reader that (except for the similarly labelled 511 kev annihilation radiation peak) peaks without such labels are due to contaminants, Compton edges, backscatter or sum peaks. Composite peaks due predominantly to one transition are labelled with the energy of that transition. Those roughly evenly split between two transitions are given two energy labels (see Os^{190} spectra). In Os^{186} the labels correspond to the spectra with contaminants subtracted. In the Ge(Li) singles spectra, on the other hand, the energies of all significant transitions are inserted above their respective photopeaks.

The Ge(Li) energies are obtained from calibrations performed with known sources: accuracies are $\pm$ 2 kev. The energy labels in the NaI(Tl) spectra are based on these spectra and their associated calibrations, on the transition energies found from the Ge(Li) data and on the results of previous decay studies on these nuclei.

Thirdly, unless specifically indicated to the contrary, the mean angle of the γ-ray detector to the beam direction was 55° and the detector-target distance was either 6.4 cm. (thick target runs) or 6.6 cm. (thin target runs). Fourthly, the absorbers listed are only those specifically placed between target and detector and do not include absorption in the target, target holders, chamber walls and detector mount and window. In the thick target runs the major absorbers were actually the target and its mount and in the thin target runs a .005" Ta sheet also lined the inside chamber walls to prevent nuclear reactions. Fifthly, the particle detector in the γ-particle measurements always subtended, at the target, 12°-14° in the center of mass between the angles 158.6° and 176.0°. The ranges of angles specific to the various runs differed occasionally by 2°-3° but this variation has negligible effect ($\leq$ 1%) on excitation probabilities (See Table VI-9).

Finally, it should be explained that all the γ-particle and γ-γ coincidence spectra taken are reproduced in the following pages. Only certain selected spectra, however, of the singles data (taken with either NaI(Tl) or Ge(Li) are shown. These are intended to be either typical samples of the data taken on a given isotope or are reproduced in order to illustrate a particular point. However, for each nucleus, at least one NaI(Tl) and one Ge(Li) singles spectrum are included.)

B. Os^{186}

In terms of obtaining quantitative information, the spectra of Os^{186} are, in practice, the most difficult to analyze. The reason is simply that separated isotopes of Os^{186} are available only in enrichments of 61.5%[77]. (See Table IV-1 for the percent isotopic content of each target.) $Os^{188, 190, 192}$ each contribute about 9% contamination and, consequently, the γ-ray spectra are heavily deluged with spurious structure. If measurements under identical conditions are performed on all four isotopes, the results from the data on $Os^{188, 190, 192}$ can be used, in conjunction with their known abundances in the Os^{186} targets, to remove the effects of these isotopes from the Os^{186} spectra. This has been done in detail in all the Os^{186} data used for quantitative analysis.

The properties of the decay scheme and certain branching ratios in Os^{186} have been extensively studied by observation of the decay of Ir^{186} and Re^{186} [72-75]. Many more levels, at higher energies, are known than were observed in these experiments[78]. (α, xn) reaction studies[79, 80] have revealed some of the higher-lying members of the ground state rotational band. The spins and parities of all the low-lying states (see Fig. IV-2) have previously been determined by the above decay studies, by work involving γ-γ directional correlations[75, 81] and by general energy level systematics in this region[12]. As noted below, our γ-γ and γ-particle measurements also attest to these assignments. In addition, the measured γ-ray angular distributions (see Section V-A) in Os^{186}, as well as in $Os^{188, 192}$, provide confirmatory evidence for the consistency of the spin and parity designations of the 2^+, 4^+, and $2^{+'}$ levels and of the transitions involving these states.

Due to the previous unavailability and present costly nature of enriched Os^{186} target material, very little Coulomb excitation work has been done on this nucleus. Prior to this work, in fact, only the $B(E2; 0^+ \rightarrow 2^+)$ value was known for this isotope from such studies[82]; also, the same B(E2) value was known from lifetime measurements.[83-86] Concurrently and independently of the work performed here, Milner et al.[58] have, however, studied the three lowest-lying states in Os^{186} via Coulomb excitation and have obtained results in good accord with those quoted here for these states. Our work, however, featured bombardment at higher O^{16} energies than

TABLE IV-1. ISOTOPIC CONTENT OF THE OSMIUM TARGETS BY PERCENT

Target \ Contributing isotope	Os^{186}	Os^{187}	Os^{188}	Os^{189}	Os^{190}	Os^{192}
Os^{186}	61.5	3.3	9.46	7.18	8.75	9.77
Os^{188}	0.5	0.5	87.7	6.2	3.8	2.5
Os^{190}	0.05	0.05	0.54	1.41	95.46	2.6
Os^{192}	0.01	0.01	0.19	0.37	0.77	98.68

was feasible in the work of the above-mentioned authors and consequently the 6^+ and $4^{+'}$ levels have also been observed and quantitative information relative to their excitation obtained.

The decay scheme of Fig. IV-2 shows the levels excited and the transitions observed in this study. Singles spectra were taken with both NaI(Tl) and Ge(Li) detectors at bombarding energies of 48.26, 62.10 and 70.30 MeV and samples are shown in Figs. IV-3 and IV-4. A weak 511 kev line is observed in these spectra due to annihilation radiation. The other transitions can be identified by comparison of their indicated energies with those in the decay scheme of Fig. IV-2. The results of the γ-γ coincidence measurements further verify these assignments (see below).

The γ-γ coincidence measurements were performed at 70.30 MeV. Spectra were taken of coincidences with the 137 kev transition ($2^+ \rightarrow 0^+$) and the 297 kev transition ($4^+ \rightarrow 2^+$). Narrow gates were set on these peaks to avoid as much as possible admission into the coincidence spectra of γ-rays in coincidence with transitions of similar energy in the other osmium isotope target contaminants. The results are shown in Figs. IV-5 and IV-6. Although the spectra are shown without prior subtraction of accidentals, it is clearly seen that the 768 kev transition is absent in both spectra indicating it is probably a direct deexcitation to the ground state. A $2^{+'}$ state is known at 768 kev. These facts, plus the intensity of the transition and its energy dependence as seen in the γ-particle data, identify it as the cross-over route by which the $2^{+'}$ state decays. The cascade route from the $2^{+'} \rightarrow 2^+$ state results in emission of γ-rays of energy 768 - 137 = 631 kev. This assignment for the 631 kev transition is confirmed by the γ-γ data which shows that the 631 kev transition is in coincidence with the $2^+ \rightarrow 0^+$ one but not with the $4^+ \rightarrow 2^+$ deexcitation. The Os^{186} targets turned out to be the least clean of any and hence backgrounds in the singles and γ-γ spectra are correspondingly higher. Thus the weak $4^{+'} \rightarrow 2^+$ transition at 933 kev, seen in the γ-particle spectra, is not discernable above the backgrounds in the spectrum of coincidences with the $2^+ \rightarrow 0^+$ γ-rays. From the energy of the transition and by comparison with the decay properties of the neighboring Os isotopes little doubt is left, however, as to the nature of this transition. Similar comments pertaining to target purity apply to the 434 kev transition, which, nevertheless, is, albeit weakly, observable in both γ-γ coincidence spectra, thus

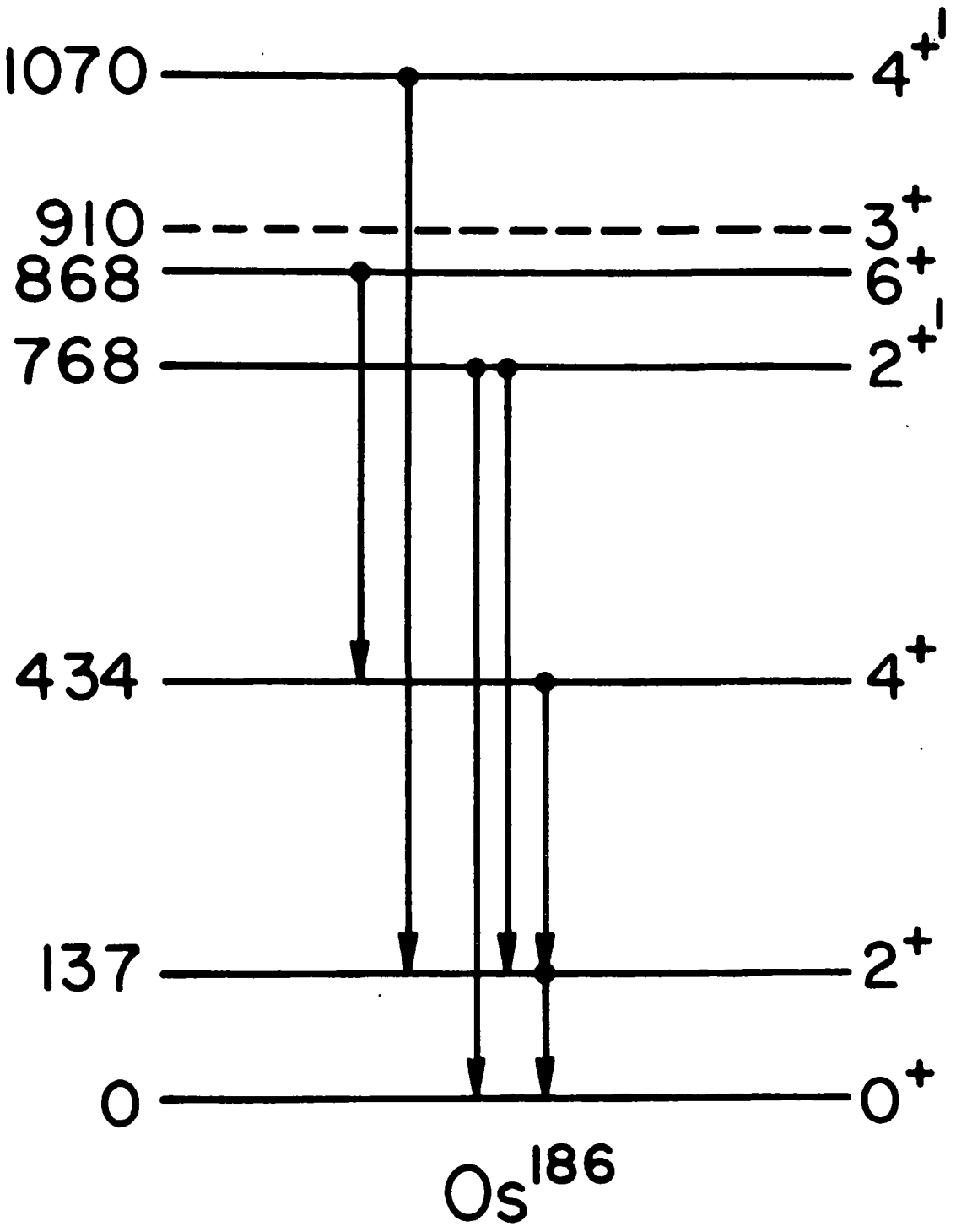

Fig. IV-2

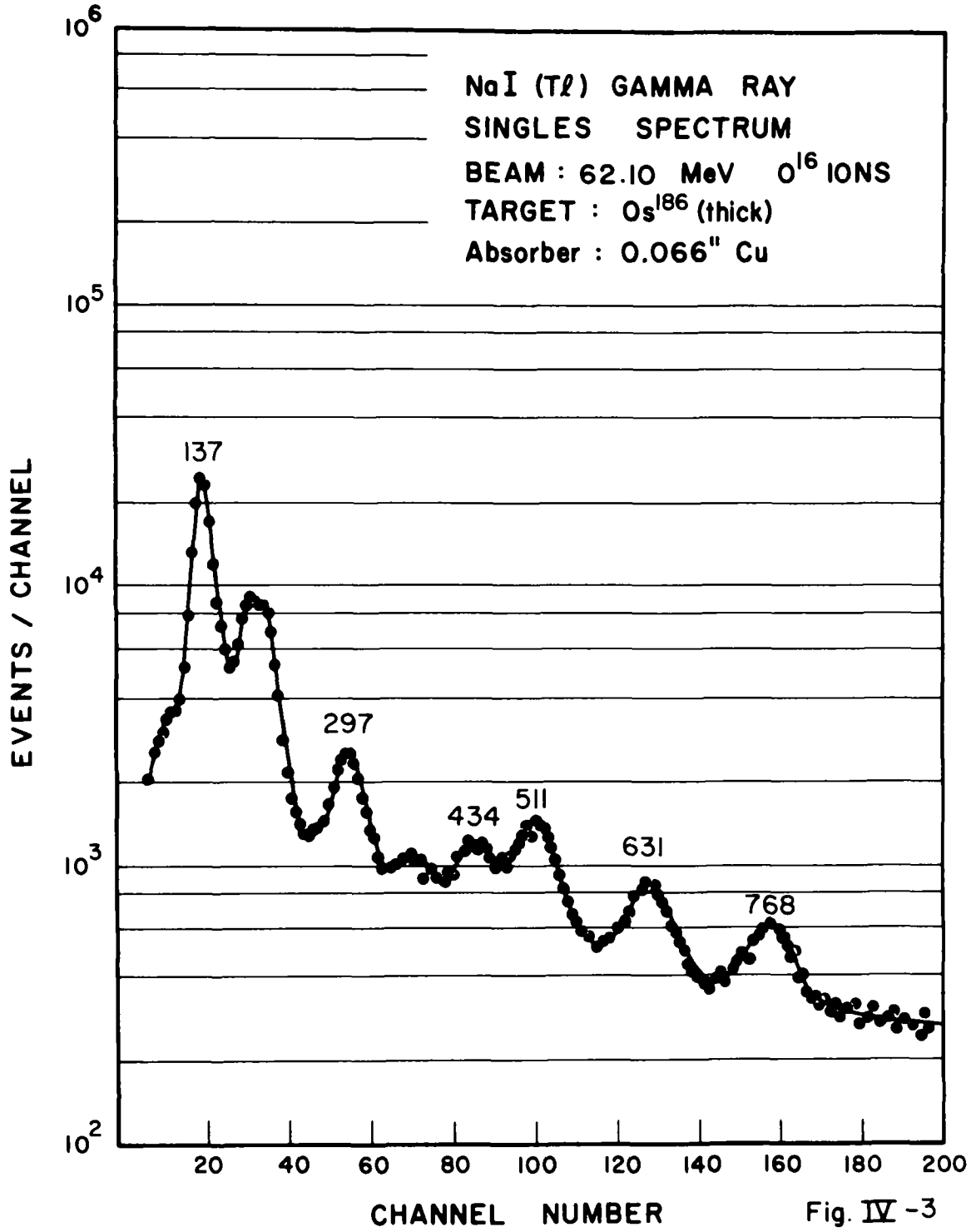
NaI (Tℓ) GAMMA RAY
SINGLES SPECTRUM
BEAM : 62.10 MeV O16 IONS
TARGET : Os186 (thick)
Absorber : 0.066" Cu
EVENTS / CHANNEL
CHANNEL NUMBER
137
297
434
511
631
768

Fig. IV -3

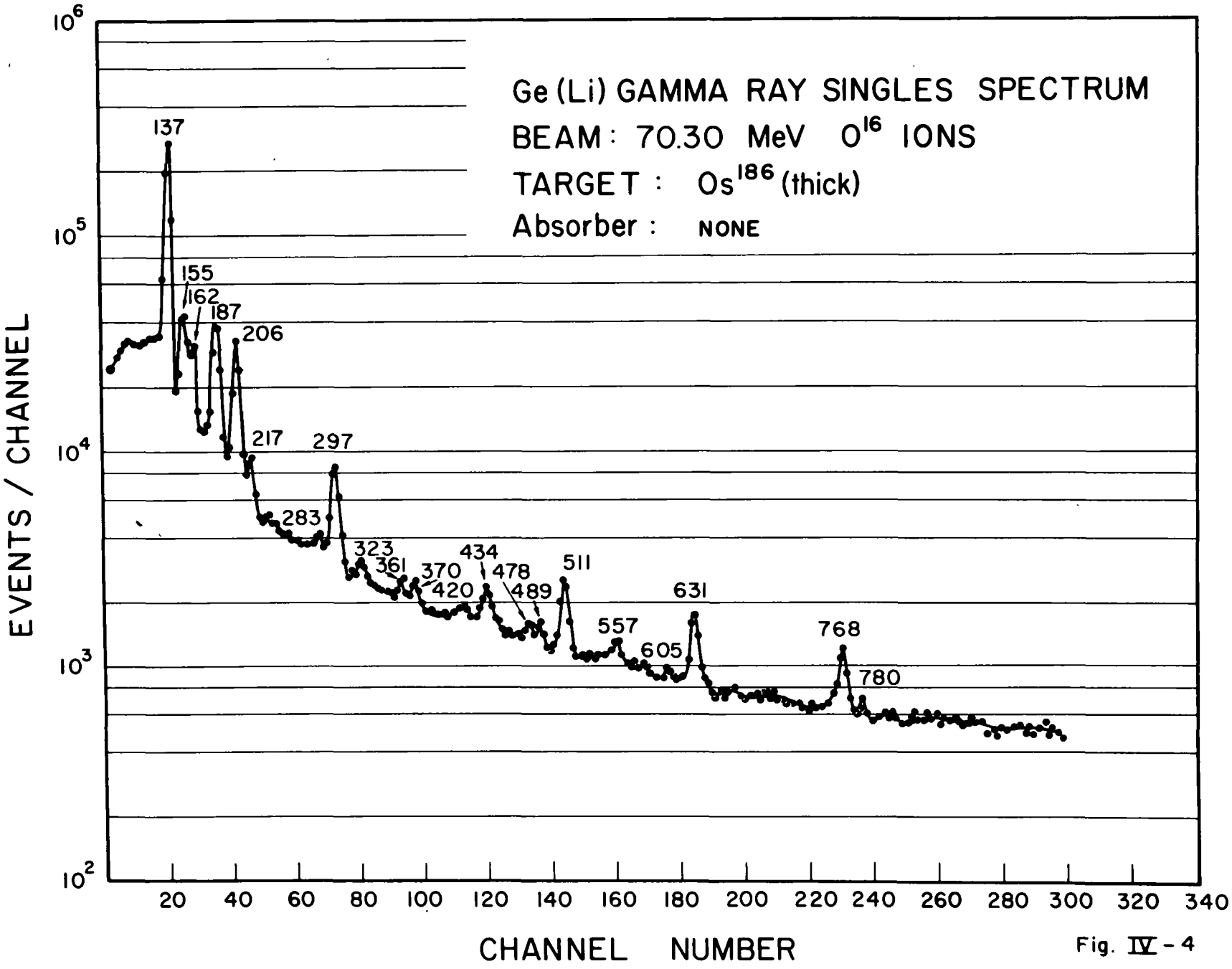
Ge(Li) GAMMA RAY SINGLES SPECTRUM
BEAM: 70.30 MeV O^{16} IONS
TARGET: Os^{186} (thick)
Absorber: NONE
EVENTS / CHANNEL
CHANNEL NUMBER
10^6
10^5
10^4
10^3
10^2
20 40 60 80 100 120 140 160 180 200 220 240 260 280 300 320 340
137
155
162
187
206
217
297
283
323
361
370
420
434
478
489
511
557
605
631
768
780

Fig. IV - 4

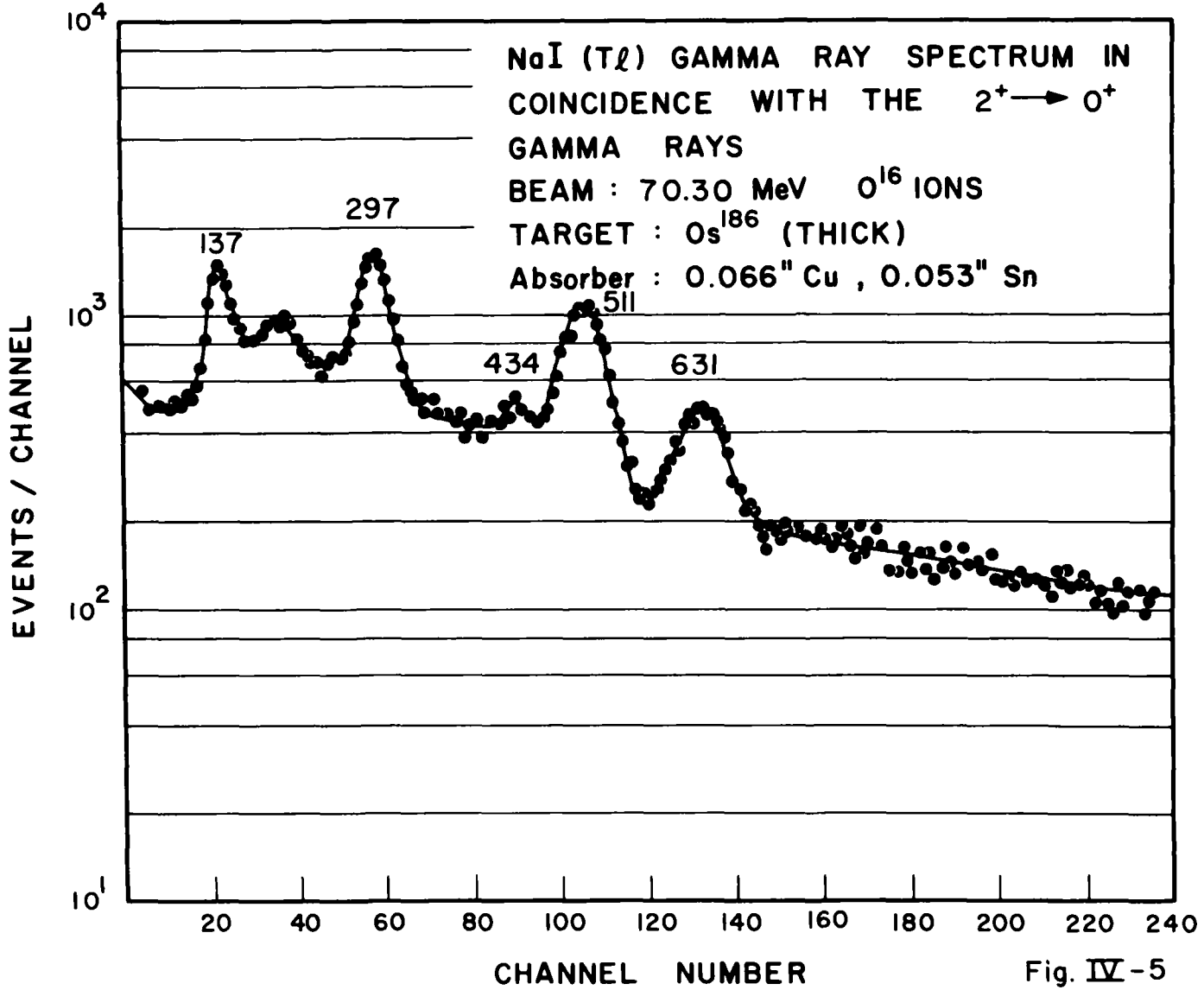
NaI (Tℓ) GAMMA RAY SPECTRUM IN COINCIDENCE WITH THE 2+ → 0+ GAMMA RAYS
BEAM : 70.30 MeV O16 IONS
TARGET : Os186 (THICK)
Absorber : 0.066" Cu , 0.053" Sn
137
297
434
511
631
EVENTS / CHANNEL
CHANNEL NUMBER
10^4
10^3
10^2
10^1
20
40
60
80
100
120
140
160
180
200
220
240

Fig. IV-5

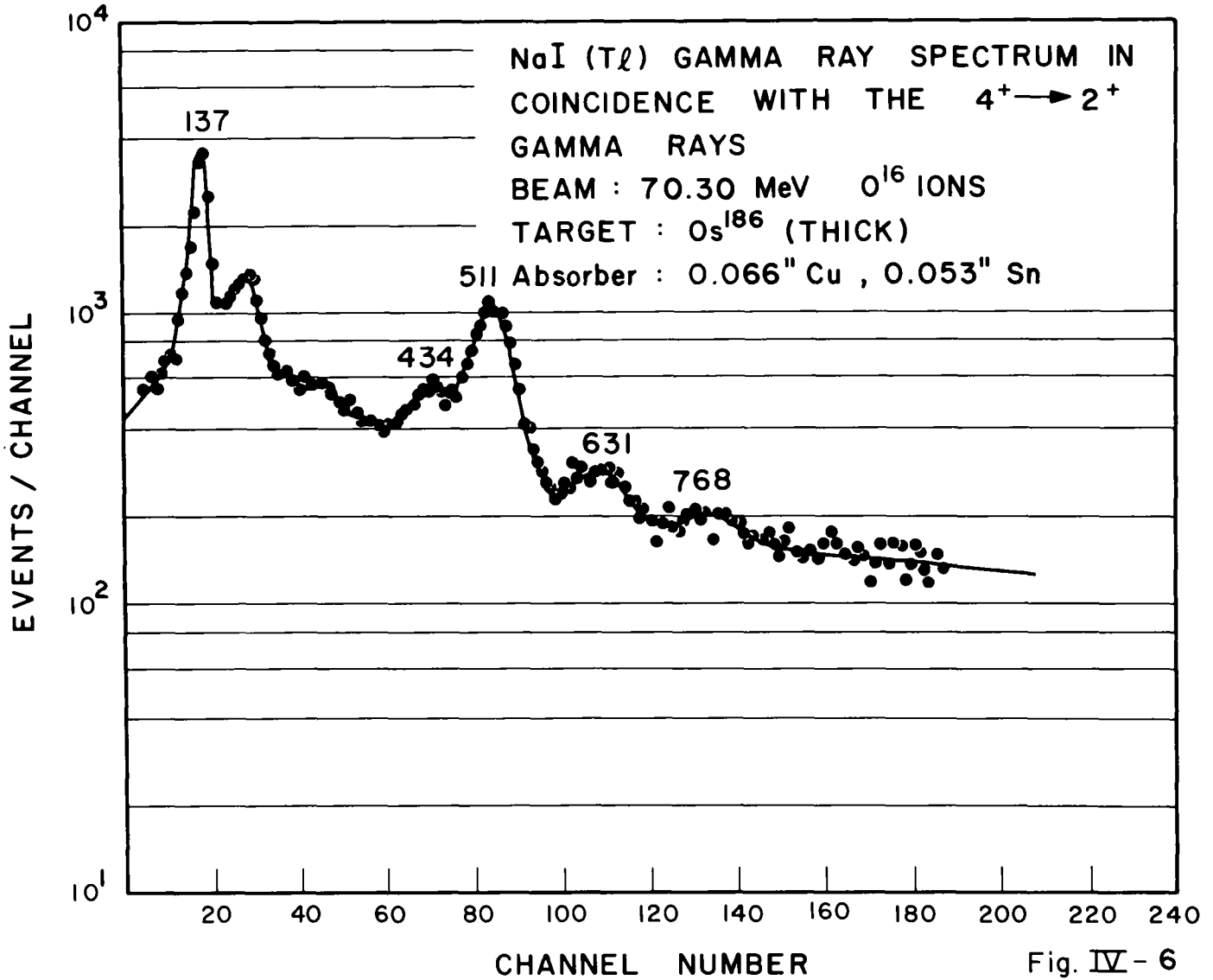
NaI (Tℓ) GAMMA RAY SPECTRUM IN COINCIDENCE WITH THE 4+ → 2+ GAMMA RAYS
BEAM : 70.30 MeV O16 IONS
TARGET : Os186 (THICK)
511 Absorber : 0.066" Cu , 0.053" Sn
137
434
511
631
768
EVENTS / CHANNEL
CHANNEL NUMBER
10^4
10^3
10^2
10^1
20
40
60
80
100
120
140
160
180
200
220
240

Fig. IV - 6

confirming its assignment as due to the $6^+ \rightarrow 4^+$ transition.

γ-particle coincidence spectra were taken at 48.26 MeV, 62.10 MeV and 70.30 MeV and are shown in Figs. IV-7, IV-8 and IV-9. In addition to the peaks at 137, 297, 631 and 768 kev which are due to the transitions $2^+ \rightarrow 0^+$, $4^+ \rightarrow 2^+$, $2^{+'} \rightarrow 2^+$, $2^{+'} \rightarrow 0^+$, photopeaks are seen at 434 and 933 kev. These, as noted previously, are due to the $6^+ \rightarrow 4^+$ and $4^{+'} \rightarrow 2^+$ transitions, respectively. The 6^+ and $4^{+'}$ levels have not been previously Coulomb excited and B(E2) values associated with them are obtained here for the first time (See Chapter VI). The energy dependences in the γ-particle spectra of the various transition intensities are consistent with the level assignments in the decay scheme of Fig. IV-2. (Again, see Chapter VI).

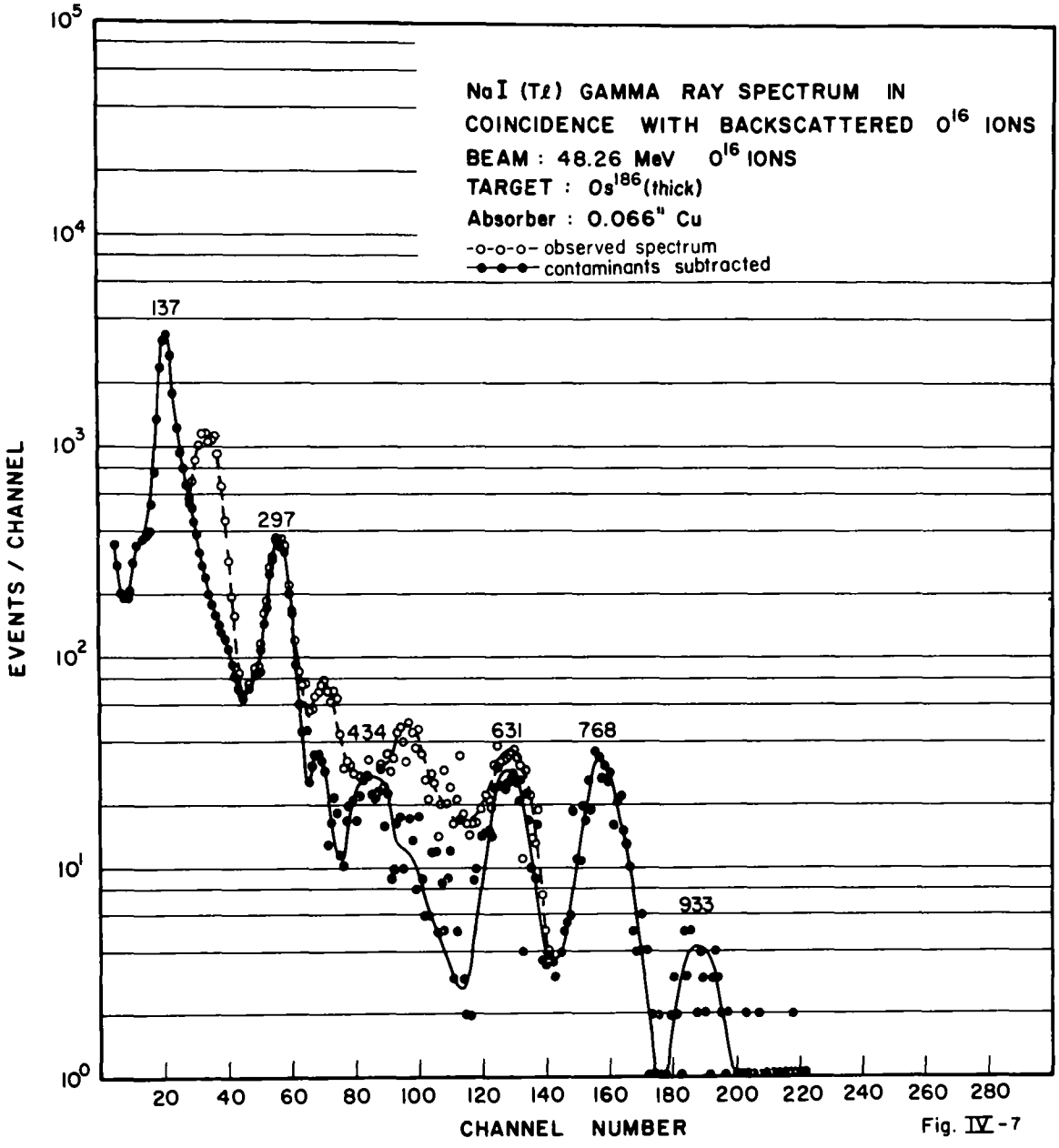
NaI (Tℓ) GAMMA RAY SPECTRUM IN
COINCIDENCE WITH BACKSCATTERED O16 IONS
BEAM : 48.26 MeV O16 IONS
TARGET : Os186(thick)
Absorber : 0.066" Cu
-o-o-o- observed spectrum
—●—●—● contaminants subtracted
EVENTS / CHANNEL
CHANNEL NUMBER
137
297
434
631
768
933

Fig. IV-7

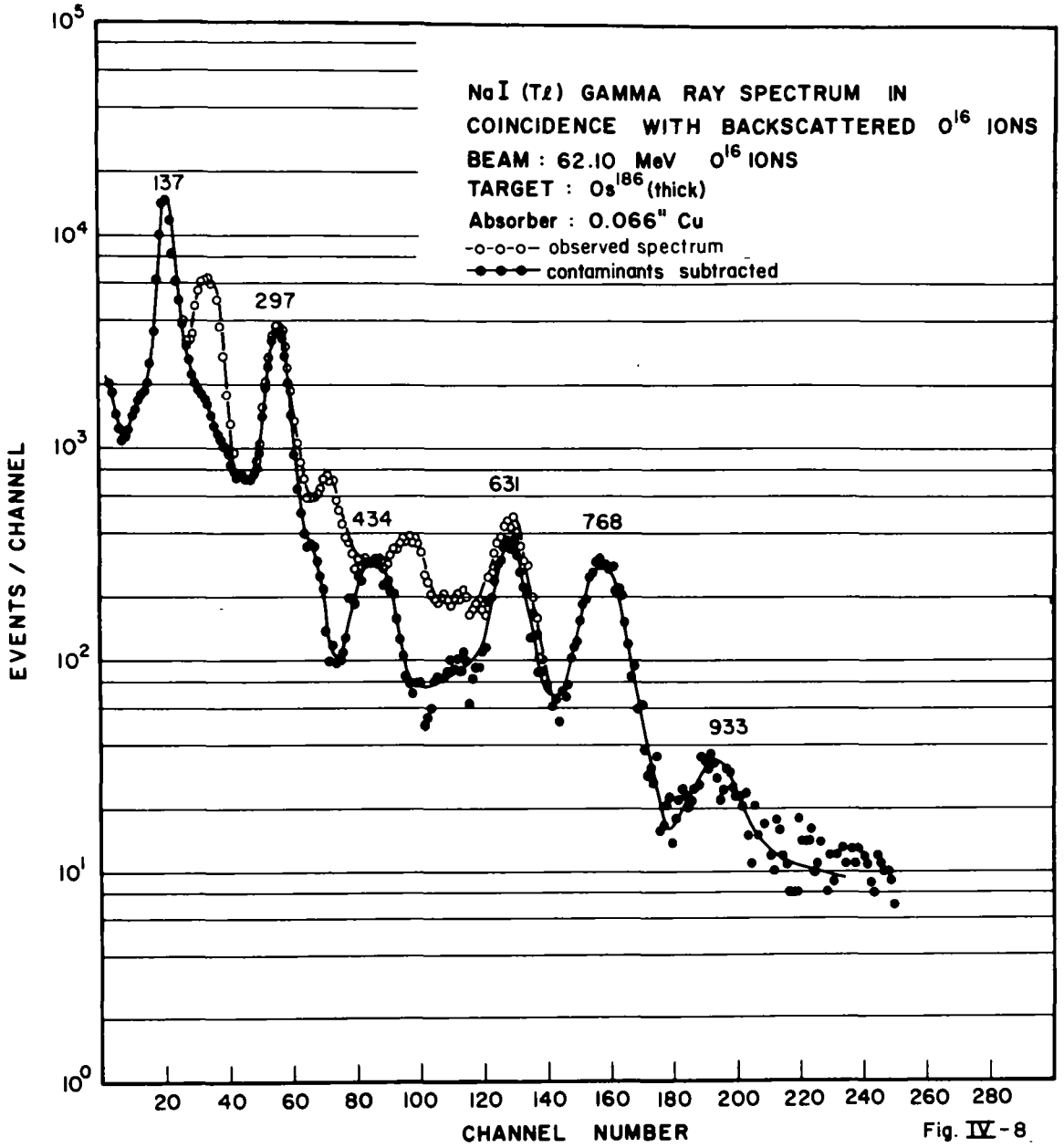
NaI (Tℓ) GAMMA RAY SPECTRUM IN
COINCIDENCE WITH BACKSCATTERED O16 IONS
BEAM : 62.10 MeV O16 IONS
TARGET : Os186 (thick)
Absorber : 0.066" Cu
-o-o-o- observed spectrum
-●-●-● contaminants subtracted
137
297
434
631
768
933
EVENTS / CHANNEL
CHANNEL NUMBER
10^5
10^4
10^3
10^2
10^1
10^0
20 40 60 80 100 120 140 160 180 200 220 240 260 280

Fig. IV-8

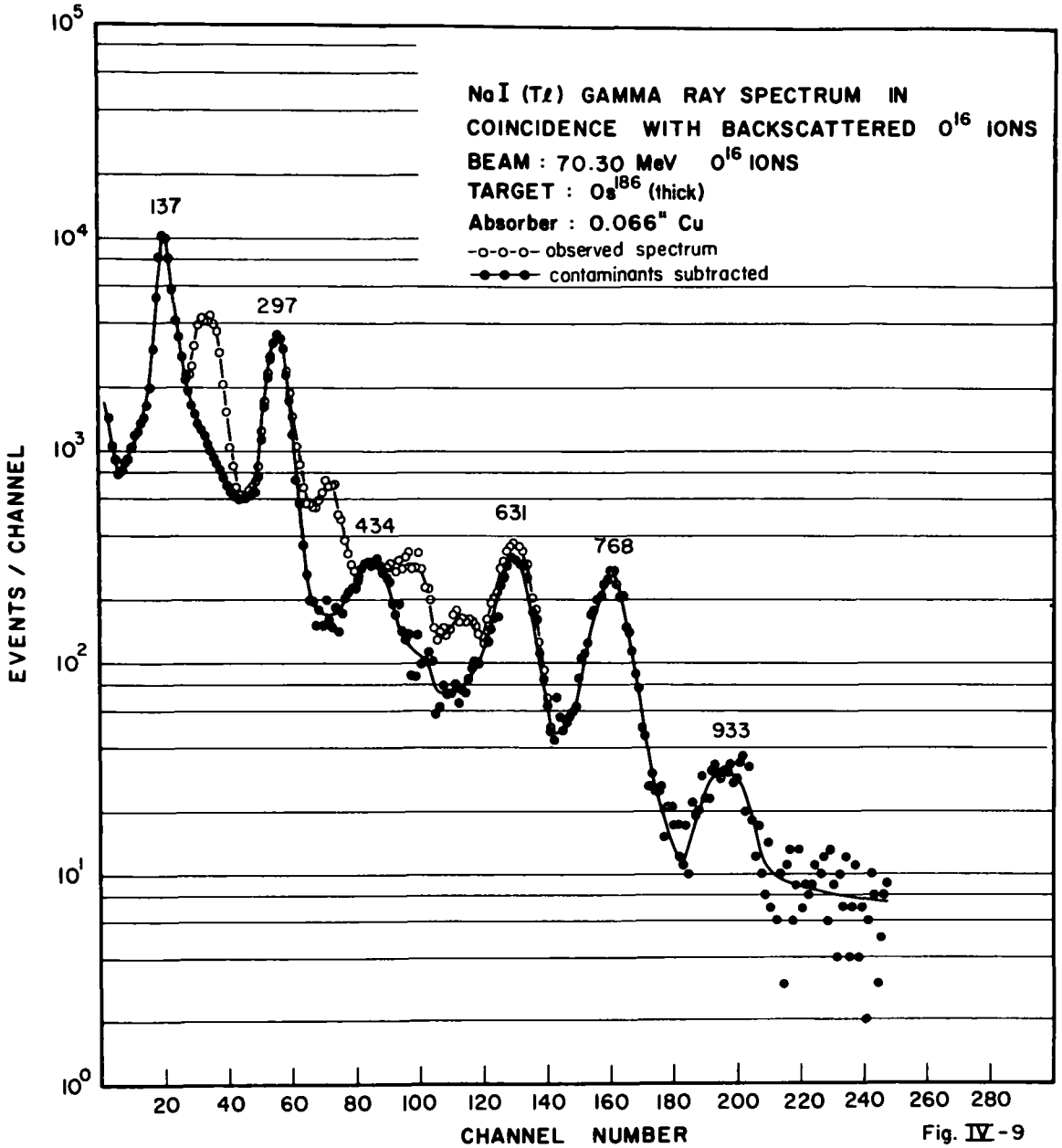
NaI (Tℓ) GAMMA RAY SPECTRUM IN
COINCIDENCE WITH BACKSCATTERED O16 IONS
BEAM : 70.30 MeV O16 IONS
TARGET : Os186 (thick)
Absorber : 0.066" Cu
-o-o-o- observed spectrum
-●-●-● contaminants subtracted
137
297
434
631
768
933
EVENTS / CHANNEL
CHANNEL NUMBER
10^5
10^4
10^3
10^2
10^1
10^0
20 40 60 80 100 120 140 160 180 200 220 240 260 280

Fig. IV-9

C. Os^{188}

Like many of the even-even osmium isotopes Os^{188} has been extensively studied by the (α, xn) reaction[79, 80] and by techniques related to the use of the radioactive decay[72, 75, 87-90]. These studies have established a detailed level structure and decay scheme up to an energy greater than 2.0 MeV. Using experimental branching ratios, energy level systematics and model predictions, the low-lying levels of Os^{188}, like those of Os^{186} and Os^{190}, have usually been grouped into two rotational bands built respectively on the ground state and on the second excited 2^+ level. The low-lying levels and transitions seen here are indicated in the partial decay scheme of Fig. IV-10.

Unlike Os^{186}, Os^{188} has been studied several times via Coulomb excitation[58, 70, 71, 91-93]. The first three excited states have been seen in these studies and B(E2) values for their excitation have been obtained. Unfortunately, due to target problems and to lower energy projectiles than were available in these studies, counting statistics in earlier work were very poor and the B(E2) values were quoted with errors of $\pm$ 30-40%. Furthermore, disagreements among different observers on B(E2) values (other than on the $B(E2{:}0^+ \rightarrow 2^+)$ value which is known from lifetime measurements[85, 86] also) often amount to factors of two to four. In the present studies cleaner targets and a variety of O^{16} energies from 42-80 MeV have enabled us to obtain new measurements on these low-lying states and to extract B(E2) values accurate to about $\pm$ 10-15 %. Furthermore, several higher-lying states, not previously excited, have been observed and B(E2) values for their excitation obtained. In addition, the data cited below are consistent with the observation of two new transitions emanating from a previously unknown level at about 780 kev. More will be said below about this tentative assignment.

Figs. IV-11 and IV-12 show sample direct spectra taken with NaI(Tl) and with Ge(Li) detectors. Other singles spectra were taken at incident O^{16} energies of 42.00, 48.26, 62.10 and 80.00 MeV. These spectra have been useful for verifying branching ratios obtained from the γ-particle data. In $Os^{186, 188}$ there is a peak or shoulder in the direct and γ-particle coincidence spectra at about 200 kev. This is shown by the Ge(Li) data to be due mainly to the deexcitation of the first excited

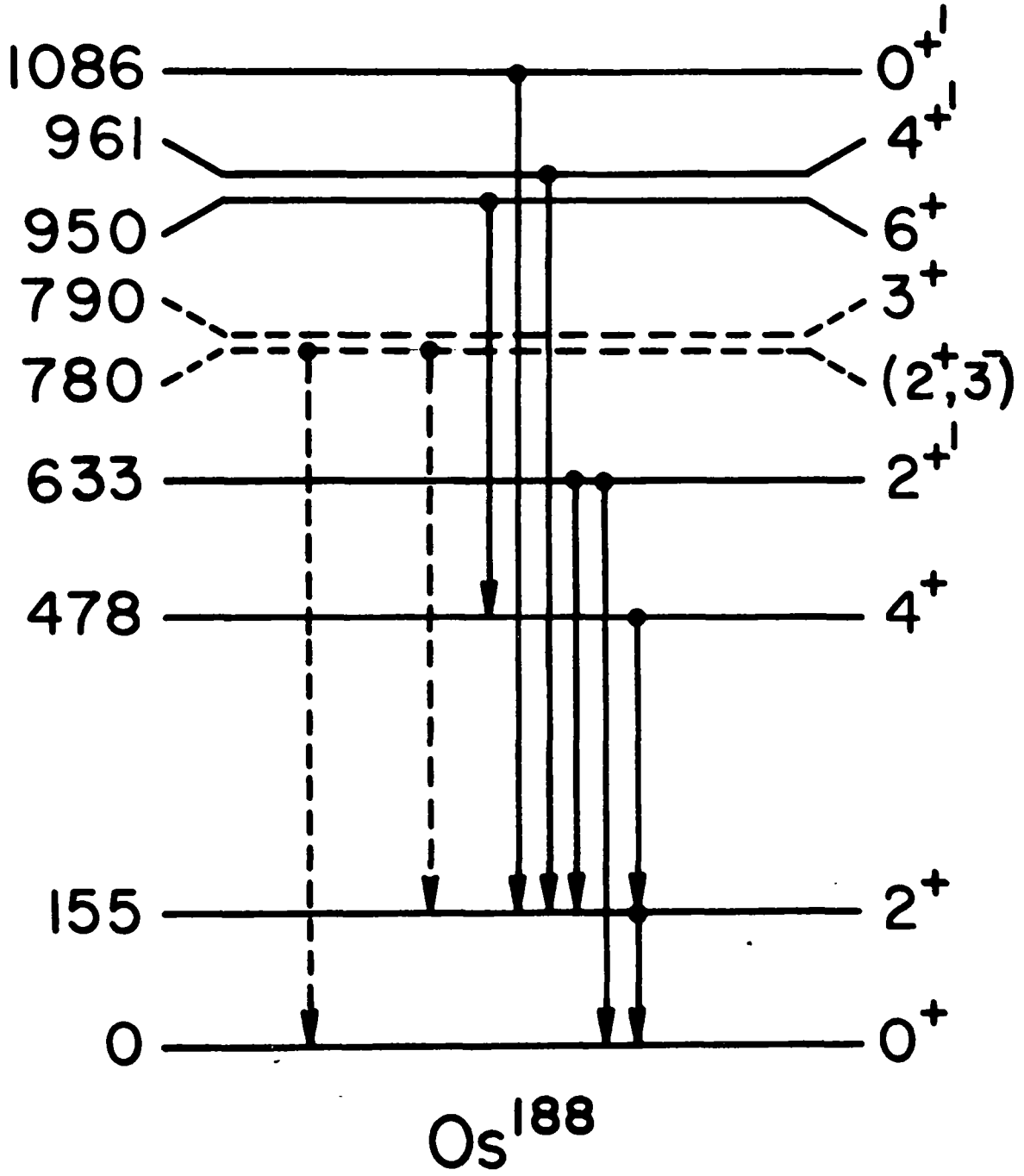

Fig. IV-10

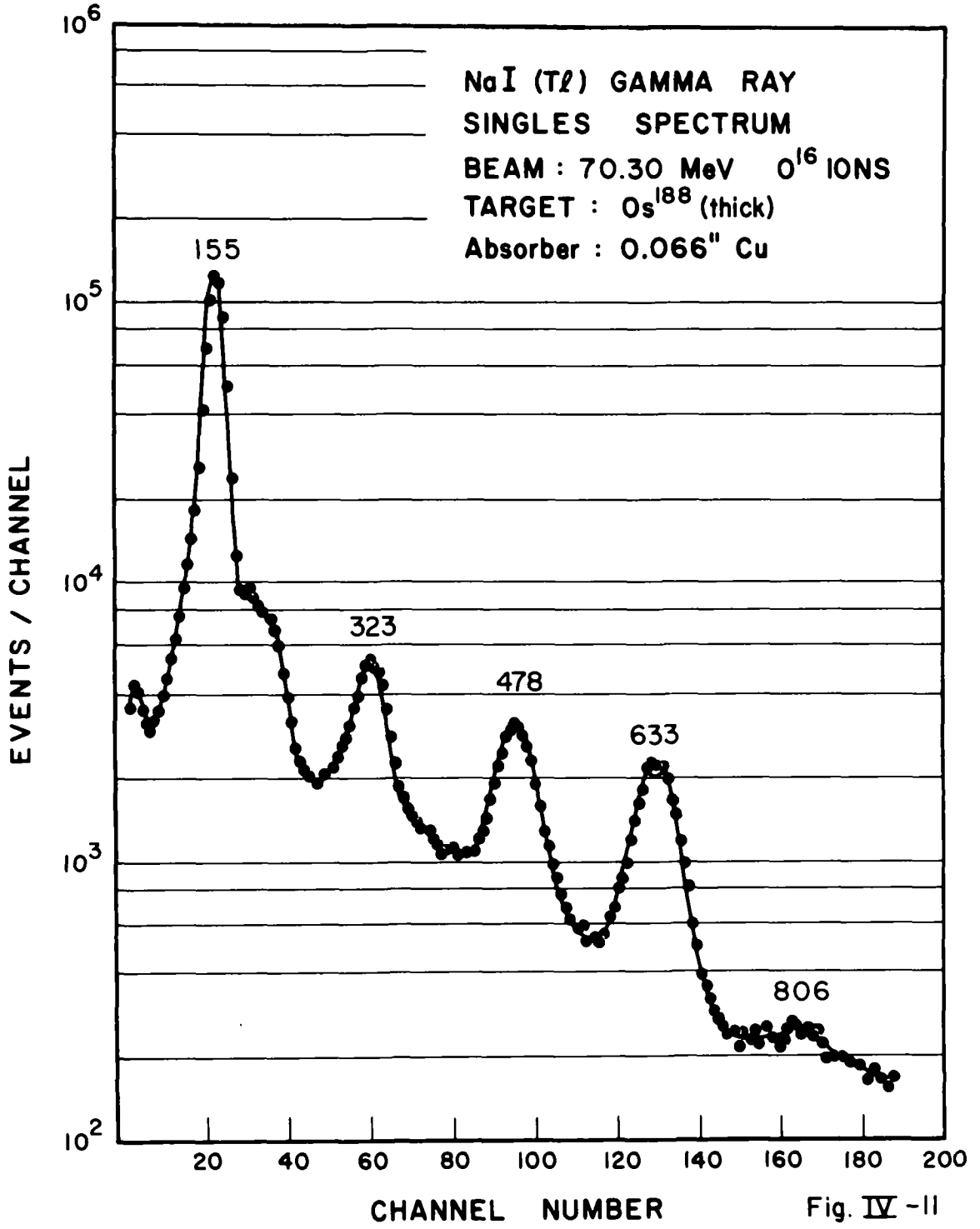
NaI (Tℓ) GAMMA RAY
SINGLES SPECTRUM
BEAM : 70.30 MeV O^{16} IONS
TARGET : Os^{188} (thick)
Absorber : 0.066" Cu
155
323
478
633
806
10^6
10^5
10^4
10^3
10^2
EVENTS / CHANNEL
20
40
60
80
100
120
140
160
180
200
CHANNEL NUMBER

Fig. IV -11

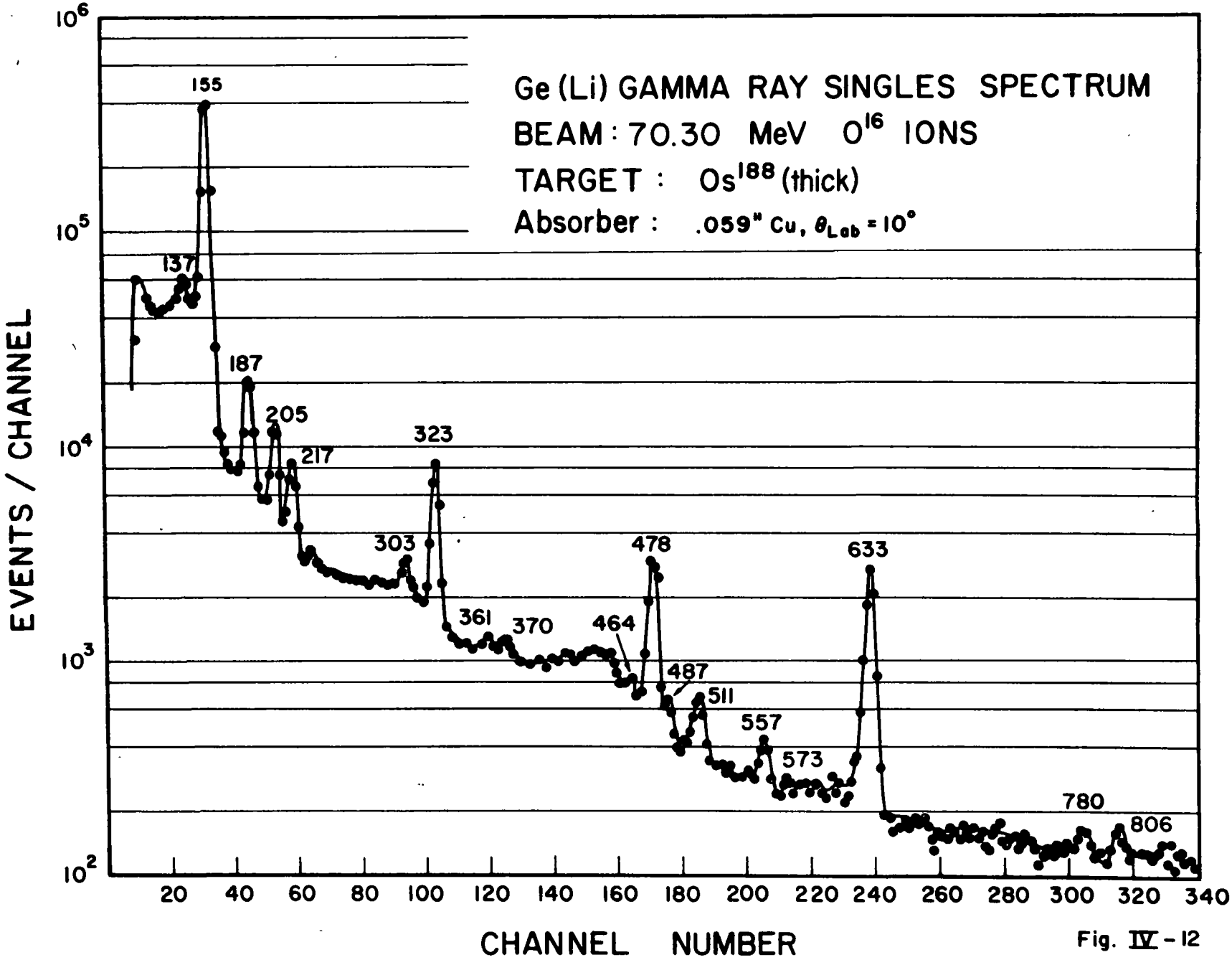
Ge (Li) GAMMA RAY SINGLES SPECTRUM
BEAM : 70.30 MeV O^{16} IONS
TARGET : Os^{188} (thick)
Absorber : .059" Cu, $\theta_{Lab} = 10°$
EVENTS / CHANNEL
CHANNEL NUMBER
10^6
10^5
10^4
10^3
10^2
155
137
187
205
217
323
303
361
370
464
478
487
511
557
573
633
780
806
20 40 60 80 100 120 140 160 180 200 220 240 260 280 300 320 340

Fig. IV - 12

states of several target contaminants. Many of the other peaks shown in the Ge(Li) data are from transitions in Os^{188} itself as can be seen by comparison with the decay scheme of Fig. IV-10. The other peaks can usually be identified with transitions in target contaminants. One peak in particular which should be noted in the Ge(Li) spectrum shown is the transition at 780 kev. Admittedly, the peak is seen only weakly above the background but it appears in two of the higher energy Ge(Li) spectra and the statistics are sufficient for it to merit acceptance. The γ - singles data do not determine its origin, however. Further discussion of this transition is given shortly and also in Section IV-E.

Again, γ-γ coincidence spectra with the $2^+ \rightarrow 0^+$ and $4^+ \rightarrow 2^+$ transitions were taken (at 70.30 MeV) and are shown in Figs. IV-13 and IV-14. γ-particle spectra were recorded at 42.00, 48.26, 62.10, 70.30 and 80.00 MeV on thick Os^{188} targets and at 62.10 and 70.30 MeV on thin Os^{188} targets. These are shown in Figs. IV-15 to IV-21. The structures at 155, 323, 478 and 633 kev are predominantly due to the $2^+ \rightarrow 0^+$, $4^+ \rightarrow 2^+$, $2^{+\prime} \rightarrow 2^+$ and $2^{+\prime} \rightarrow 0^+$ transitions, respectively. The energy dependence of these peaks, the angular distribution measurements and the analysis of the γ-γ data are consistent with the above assignments. As will be shown, however, both the 478 and 633 kev peaks have small contributions from other transitions in them. Corrections for this have, of course, been made. The γ-particle data taken at 62.10 and 70.30 MeV on both thick and thin targets clearly show additional peaks at 806 and 931 kev. The energies of these peaks are consistent with their being due to the $4^{+\prime} \rightarrow 2^+$ and $0^{+\prime} \rightarrow 2^+$ deexcitation of states at 961 and 1086 kev, respectively. These assignments are confirmed by the γ-γ data. Both transitions are present in the spectrum of coincidences with the $2^+ \rightarrow 0^+$ transitions but are absent from the spectrum of coincidences with the $4^+ \rightarrow 2^+$ transitions. Furthermore, the energy dependence of the intensities of these transitions is satisfactorily accounted for by assuming the above assignments (see Chapter VI)

A very weak transition at about 780 kev is observed in the γ-particle spectra taken on thick targets at 62.10 and 70.30 MeV. Presumably it would appear more clearly in the thin target results if statistics in those spectra were better. This transition cannot be fit into the known decay scheme of the low-lying levels of Os^{188} [94]. Search for a 780 kev transition in the γ-γ coincidence data reveals none.

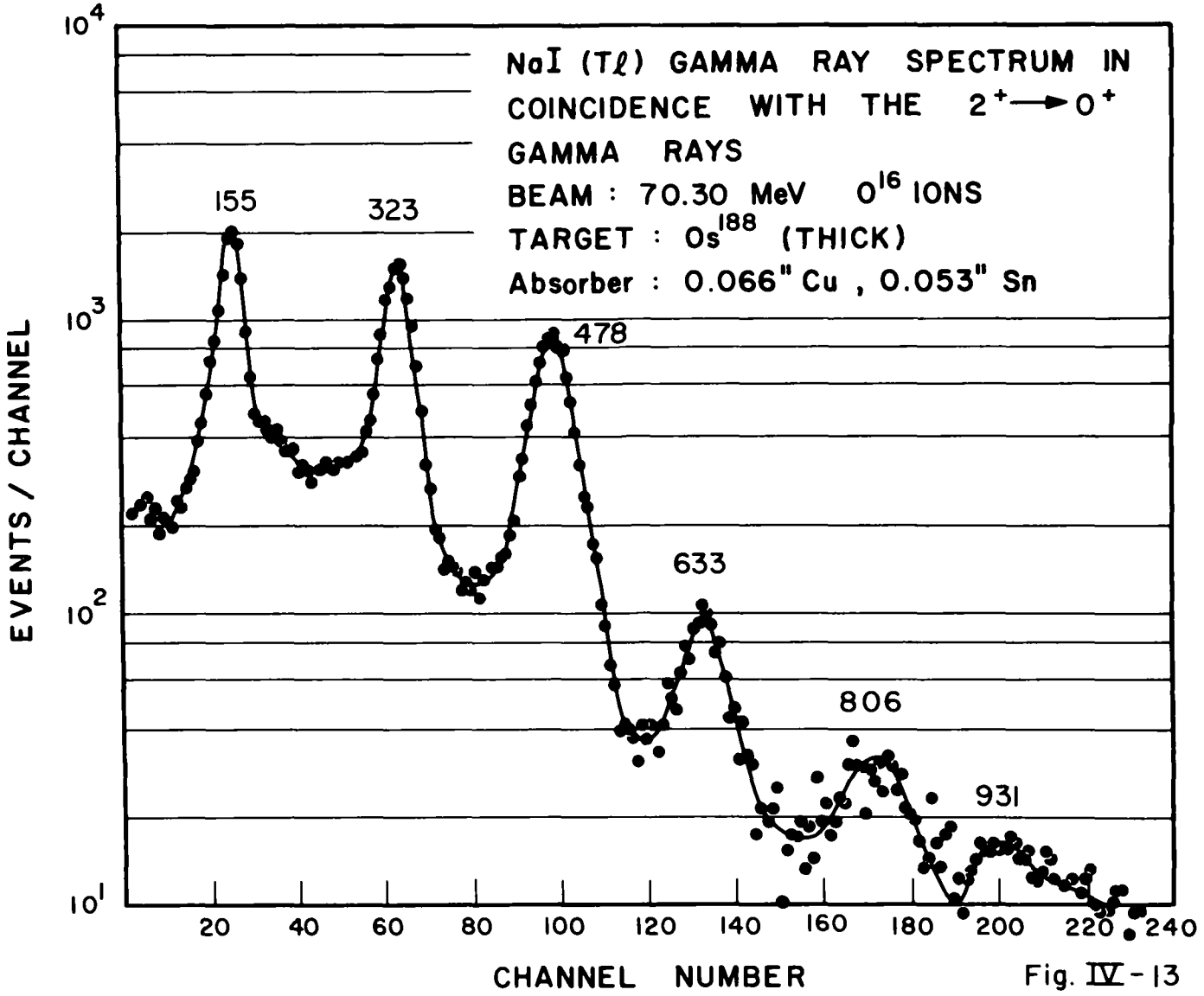
NaI (Tℓ) GAMMA RAY SPECTRUM IN
COINCIDENCE WITH THE 2+ → 0+
GAMMA RAYS
BEAM : 70.30 MeV O16 IONS
TARGET : Os188 (THICK)
Absorber : 0.066" Cu , 0.053" Sn
155
323
478
633
806
931
EVENTS / CHANNEL
CHANNEL NUMBER
10^4
10^3
10^2
10^1
20
40
60
80
100
120
140
160
180
200
220
240

Fig. IV-13

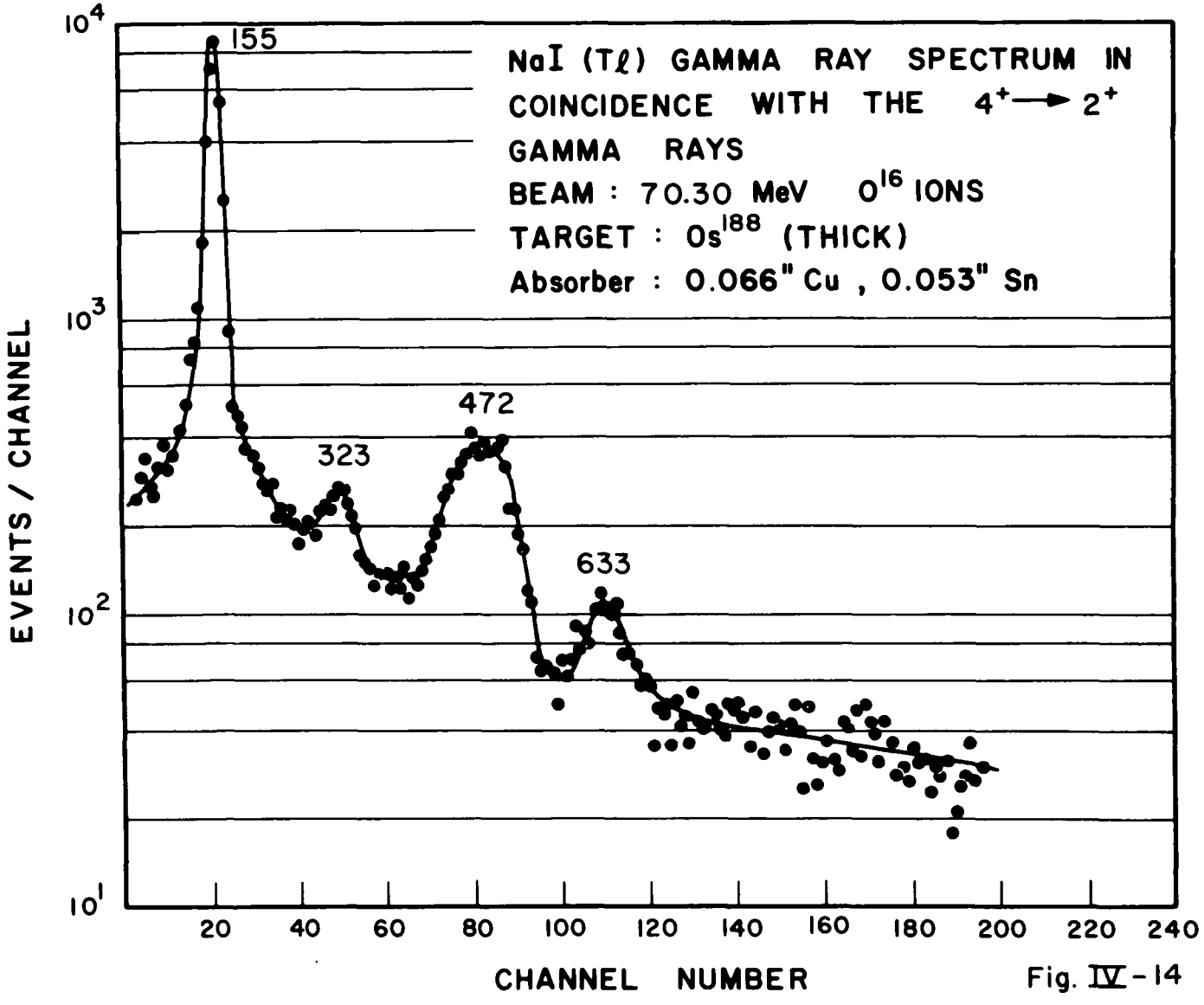
NaI (Tℓ) GAMMA RAY SPECTRUM IN COINCIDENCE WITH THE 4+ → 2+ GAMMA RAYS
BEAM : 70.30 MeV O16 IONS
TARGET : Os188 (THICK)
Absorber : 0.066" Cu , 0.053" Sn
155
323
472
633
EVENTS / CHANNEL
CHANNEL NUMBER
10^4
10^3
10^2
10^1
20
40
60
80
100
120
140
160
180
200
220
240

Fig. IV-14

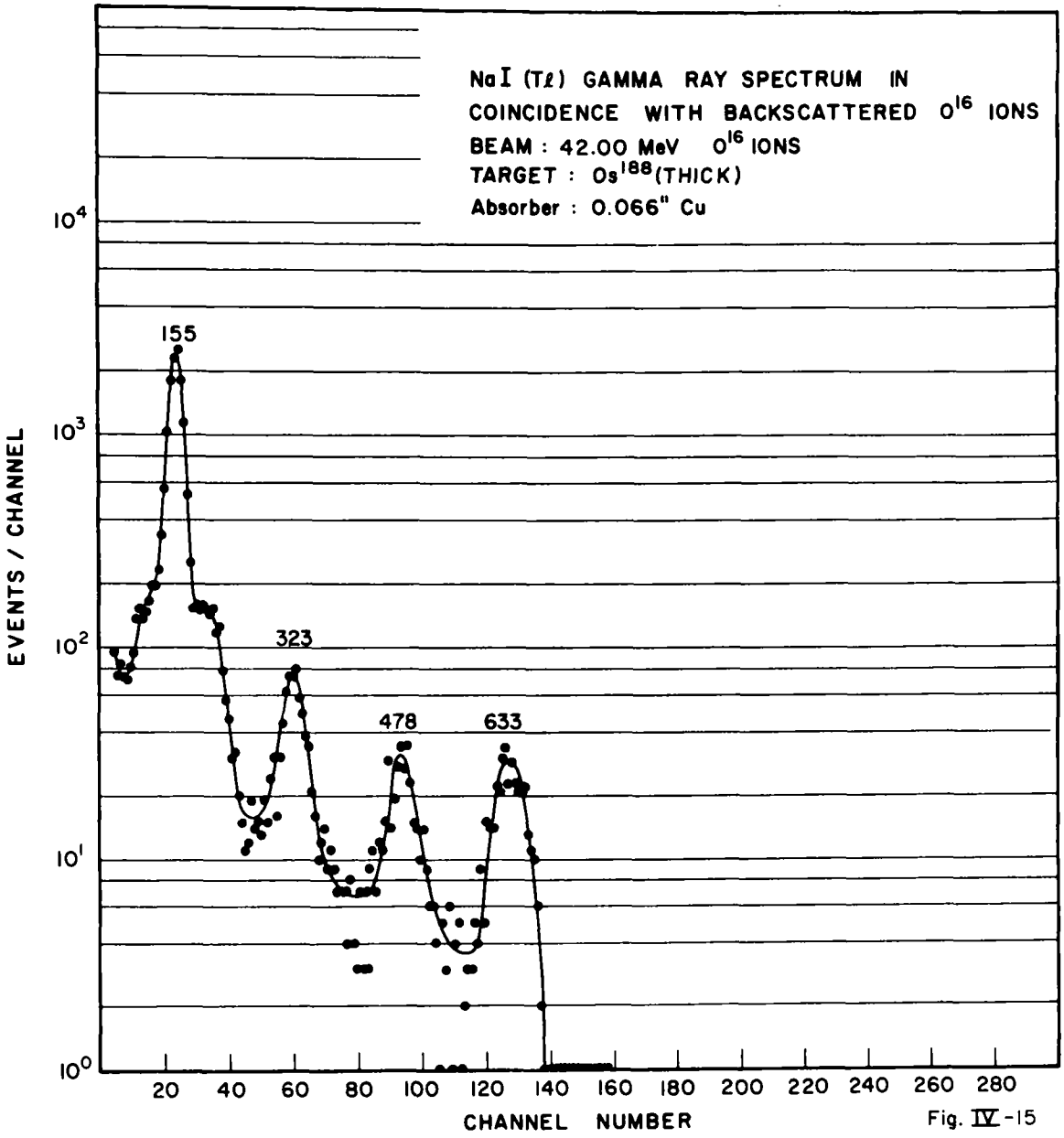
NaI (Tℓ) GAMMA RAY SPECTRUM IN
COINCIDENCE WITH BACKSCATTERED O16 IONS
BEAM : 42.00 MeV O16 IONS
TARGET : Os188(THICK)
Absorber : 0.066" Cu
EVENTS / CHANNEL
10^4
10^3
10^2
10^1
10^0
155
323
478
633
20 40 60 80 100 120 140 160 180 200 220 240 260 280
CHANNEL NUMBER

Fig. IV-15

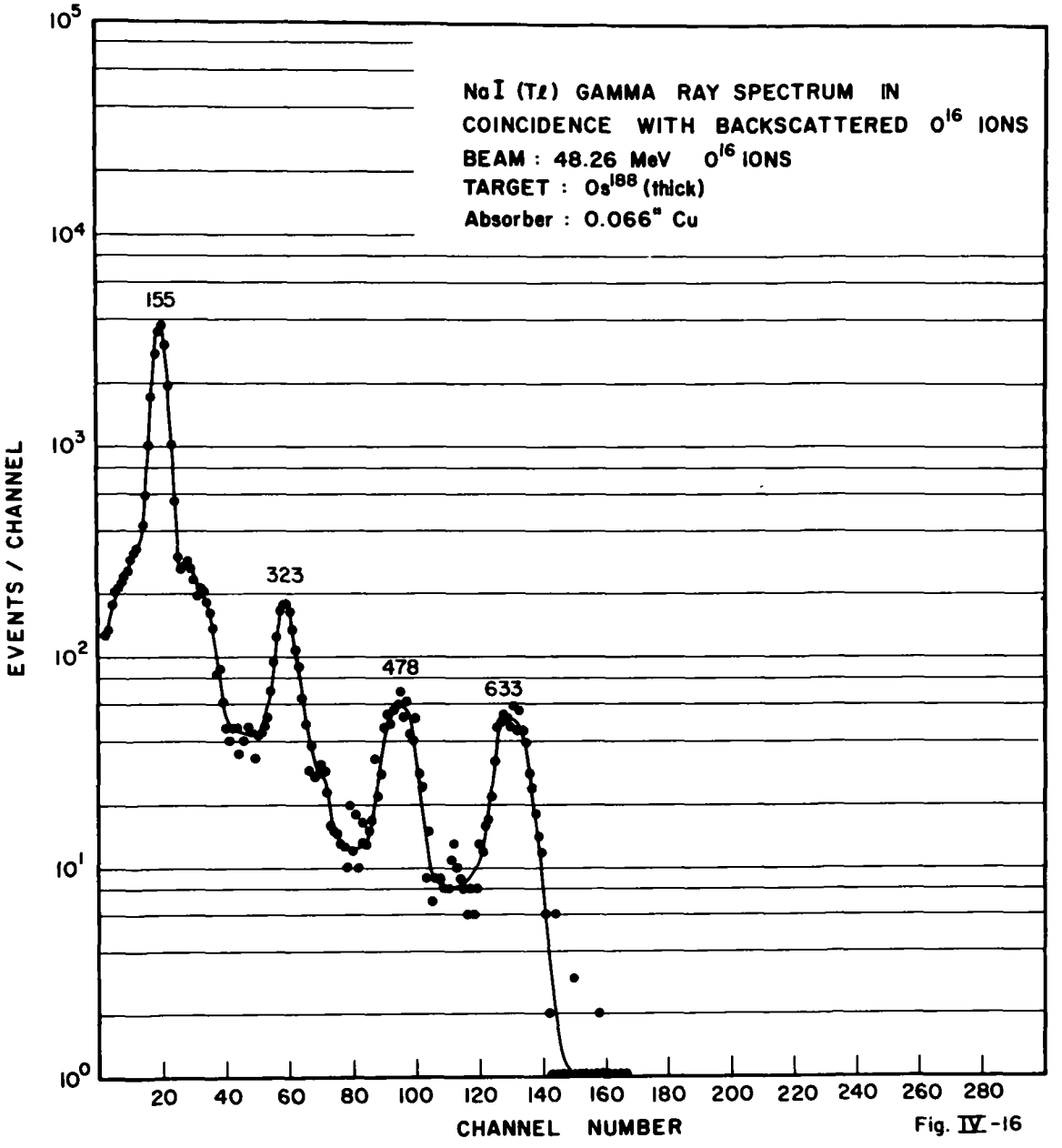
NaI (Tℓ) GAMMA RAY SPECTRUM IN
COINCIDENCE WITH BACKSCATTERED O16 IONS
BEAM : 48.26 MeV O16 IONS
TARGET : Os188 (thick)
Absorber : 0.066" Cu
155
323
478
633
EVENTS / CHANNEL
CHANNEL NUMBER
10^5
10^4
10^3
10^2
10^1
10^0
20 40 60 80 100 120 140 160 180 200 220 240 260 280

Fig. IV-16

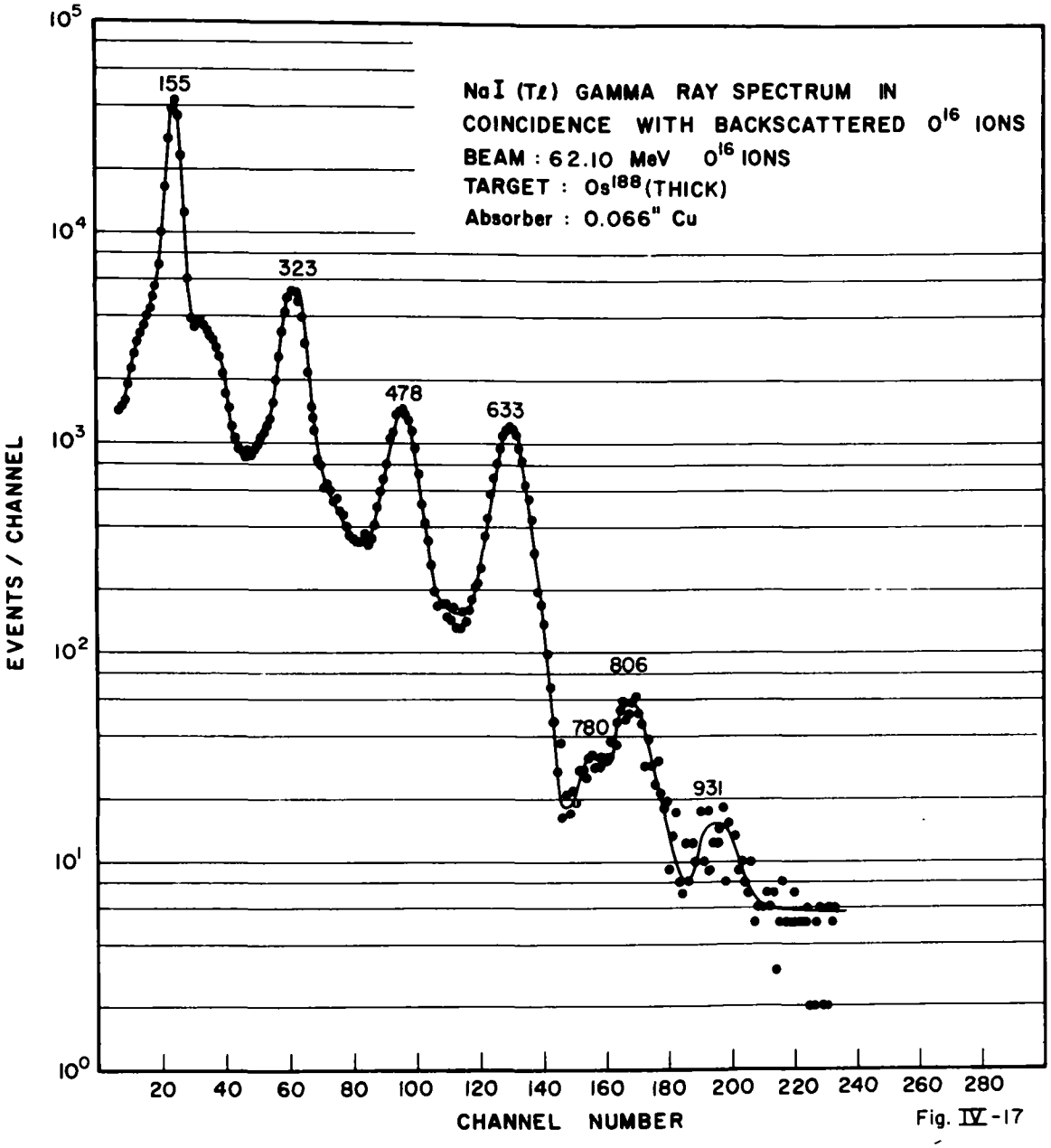
NaI (Tℓ) GAMMA RAY SPECTRUM IN
COINCIDENCE WITH BACKSCATTERED O16 IONS
BEAM : 62.10 MeV O16 IONS
TARGET : Os188 (THICK)
Absorber : 0.066" Cu
155
323
478
633
806
780
931
EVENTS / CHANNEL
CHANNEL NUMBER
10^5
10^4
10^3
10^2
10^1
10^0
20 40 60 80 100 120 140 160 180 200 220 240 260 280

Fig. IV-17

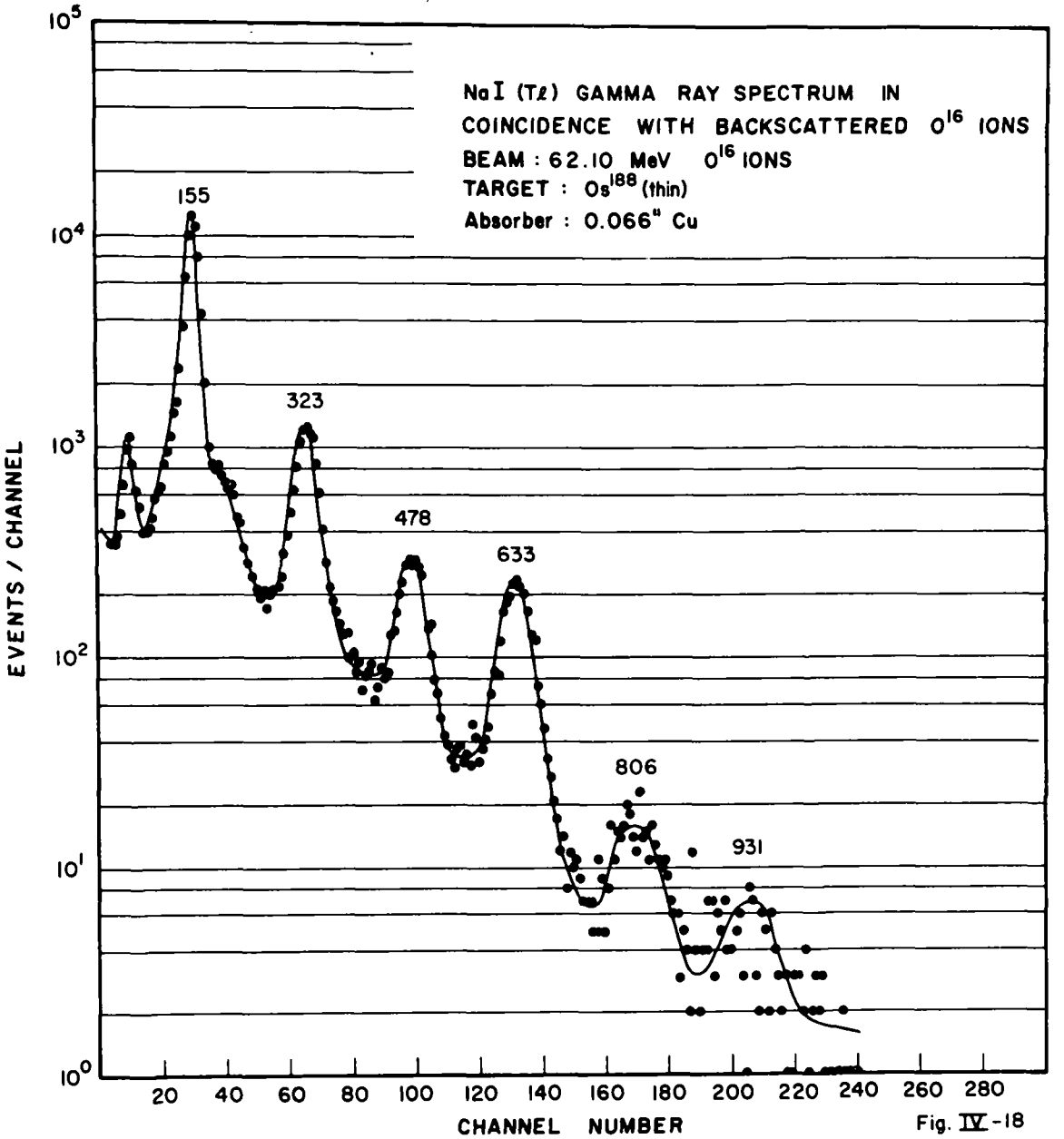
NaI (Tℓ) GAMMA RAY SPECTRUM IN
COINCIDENCE WITH BACKSCATTERED O16 IONS
BEAM : 62.10 MeV O16 IONS
TARGET : Os188 (thin)
Absorber : 0.066" Cu
155
323
478
633
806
931
EVENTS / CHANNEL
CHANNEL NUMBER
10^5
10^4
10^3
10^2
10^1
10^0
20 40 60 80 100 120 140 160 180 200 220 240 260 280

Fig. IV-18

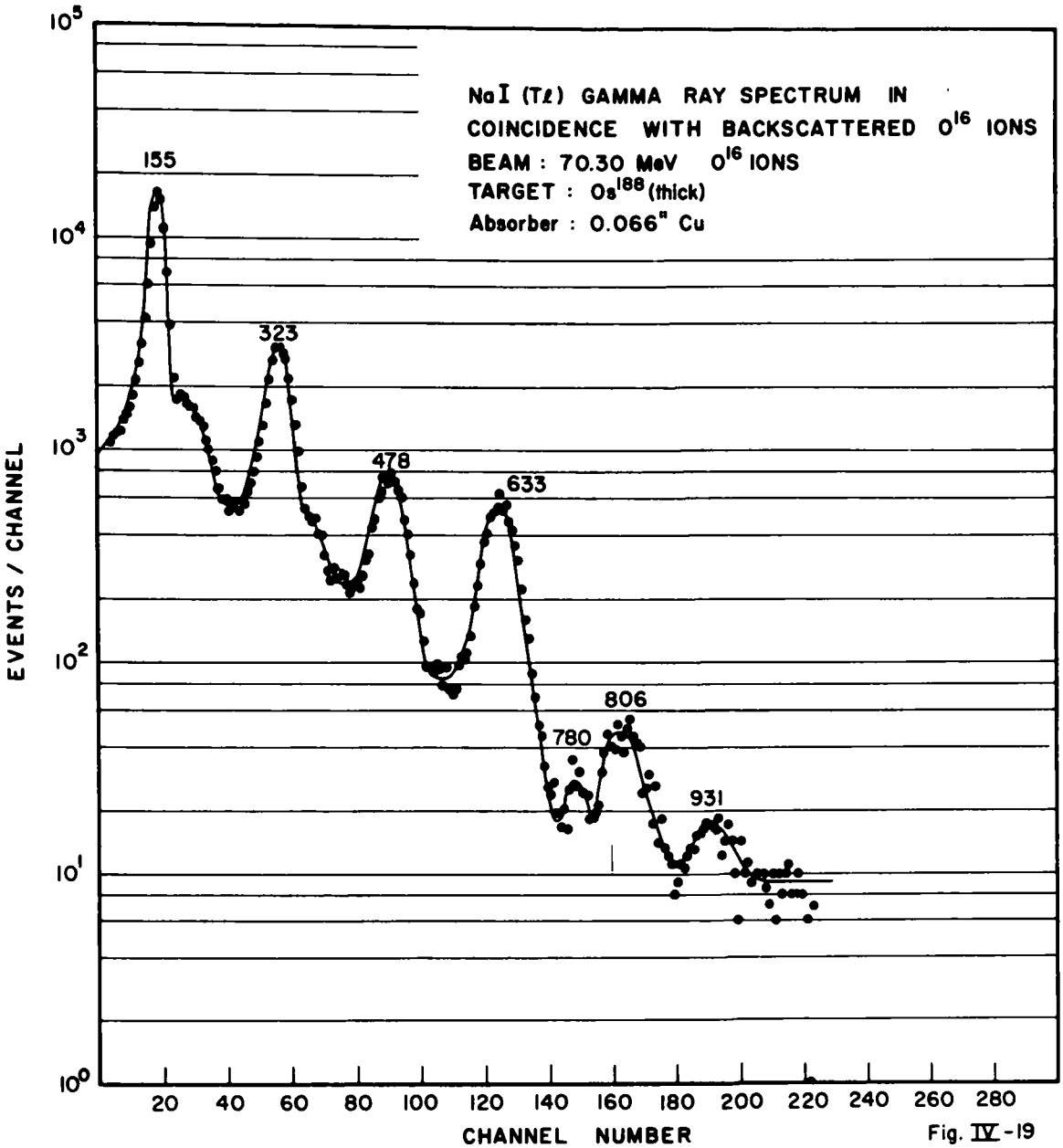
NaI (Tℓ) GAMMA RAY SPECTRUM IN
COINCIDENCE WITH BACKSCATTERED O16 IONS
BEAM : 70.30 MeV O16 IONS
TARGET : Os188 (thick)
Absorber : 0.066" Cu
155
323
478
633
780
806
931
EVENTS / CHANNEL
CHANNEL NUMBER
10^5
10^4
10^3
10^2
10^1
10^0
20 40 60 80 100 120 140 160 180 200 220 240 260 280

Fig. IV-19

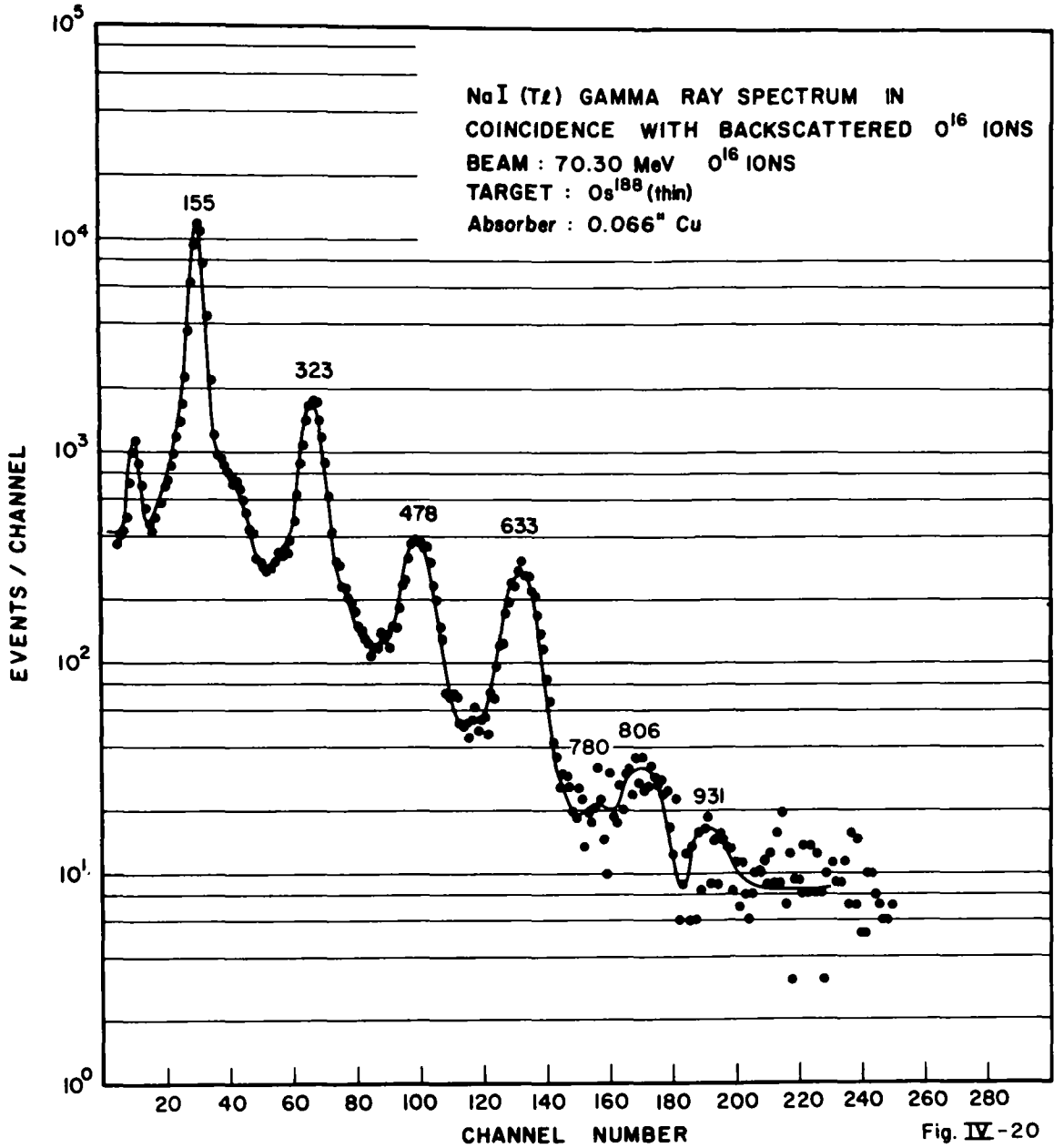
NaI (Tℓ) GAMMA RAY SPECTRUM IN
COINCIDENCE WITH BACKSCATTERED O16 IONS
BEAM : 70.30 MeV O16 IONS
TARGET : Os188 (thin)
Absorber : 0.066" Cu
155
323
478
633
780
806
931
EVENTS / CHANNEL
CHANNEL NUMBER
10^5
10^4
10^3
10^2
10^1
10^0
20 40 60 80 100 120 140 160 180 200 220 240 260 280

Fig. IV-20

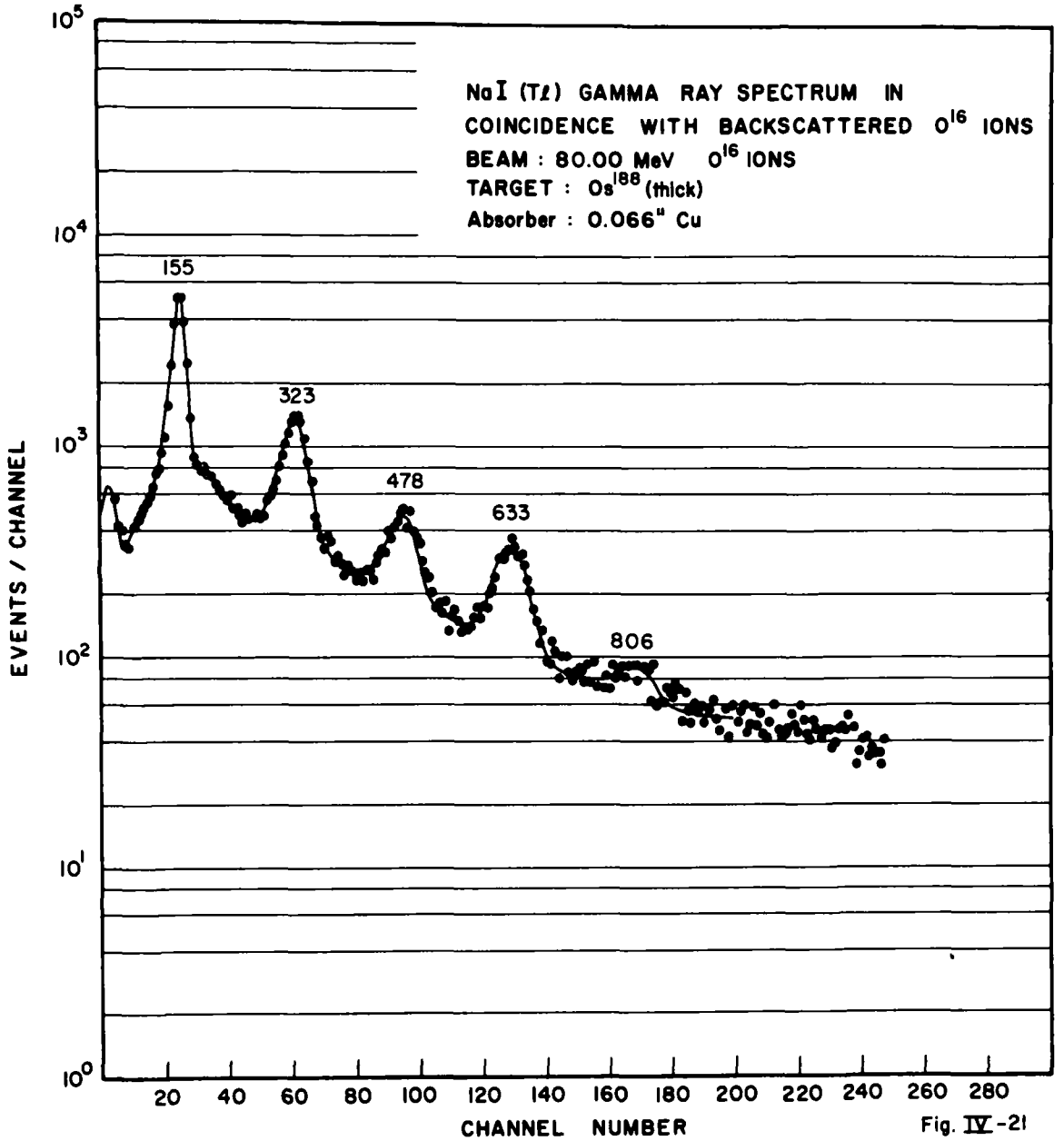
NaI (Tℓ) GAMMA RAY SPECTRUM IN
COINCIDENCE WITH BACKSCATTERED O16 IONS
BEAM : 80.00 MeV O16 IONS
TARGET : Os188 (thick)
Absorber : 0.066" Cu
155
323
478
633
806
EVENTS / CHANNEL
CHANNEL NUMBER
10^5
10^4
10^3
10^2
10^1
10^0
20 40 60 80 100 120 140 160 180 200 220 240 260 280

Fig. IV-21

However, the 633 kev peak in the spectrum of coincidences with the $2^+ \rightarrow 0^+$ transitions does not vanish when accidentals are subtracted as it should were it due to the $2^{+'} \rightarrow 0^+$ deexcitations. Note, however, that 155 + 633 = 788 and so a consistent interpretation is afforded by postulating a new level at $\cong$ 780 kev which decays both to the ground state and to the first excited state. The $\cong$ 630 kev γ-ray would not be seen in the direct or γ-particle spectra because of the strong 633 kev transition. It would also not be resolved even with the Ge(Li) detector. The absence, after subtraction of accidentals, of a $\cong$ 630 kev transition in the γ-γ spectrum in coincidence with the $4^+ \rightarrow 2^+$ transitions is consistent with the above interpretation. The spin of this level is not known and not established by the data. In principle it could be determined by the transition's energy dependence but the photopeak is so weak that experimental errors are large. Furthermore, for weakly excited states the excitation is dominated by factors (df(ξ)) which do not have sharply different dependencies on energy (see Chapter II). The decay routes of the state do, however, imply that it is not a 0^+ state but that it could have spin and parity of 2^+ or 3^-.

If one determines the relative intensities of the $2^{+'} \rightarrow 0^+$ and $2^{+'} \rightarrow 2^+$ transitions one finds a variation with energy of up to 25% in their ratio. This implies the existence of another transition building up the intensity of the 478 kev photopeak. The variation is such as to imply a very rapid increase in intensity of this transition with O^{16} energy. This in turn is a signal of a state principally populated by higher order processes (see Chapter II). The γ-rays from the deexcitation of this level are not resolved from the 478 kev ($2^{+'} \rightarrow 2^+$) γ-rays even with the Ge(Li) detector. All these points are consistent with the interpretation that the transition is due to the $6^+ \rightarrow 4^+$ deexcitation. If this is true, a transition at 472 kev should remain in the γ-spectrum in coincidence with the $4^+ \rightarrow 2^+$ γ-rays after accidentals are removed. (If the 478 kev transitions were all due to the $2^{+'} \rightarrow 2^+$ deexcitations this would not be so). In fact, such a transition does remain, adding confirmation to the above hypothesis. The observation of the excitation of the 6^+ state is also consistent with its clear observation in the two surrounding nuclei, $Os^{186, 190}$. One would also like to be able to obtain a measure of the $6^+ \rightarrow 4^+$ transition intensity in the γ-particle data. Being masked by the $2^{+'} \rightarrow 2^+$ transitions makes this difficult. The only recourse is to extract it by realizing that the 6^+ state is negligibly excited at 42 MeV, and by defining the true branching ratio of the $2^{+'}$ level by its value at

that energy. Then, the variation of this ratio with O^{16} energy can be ascribed to the $6^+ \rightarrow 4^+$ transition. Thus a measure of its intensity as a function of energy is crudely obtained. The branching ratio varies from energy to energy typically by 2-5% and the process of subtracting large numbers to obtain results of less than 5% their size is quite suspect. This procedure has nevertheless been carried out and the results are fairly gratifying. The excitation probabilities thus obtained for the 6^+ state fall below those for Os^{186} and very near those for Os^{190}. This is not inconsistent with expectations based on systematics. Thus a $B(E2:6^+ \rightarrow 4^+)$ value can be obtained from the data although errors will be slightly larger than for other B(E2) values (see Chapter VI).

It should be noted that the photopeak from the $4^{+'} \rightarrow 4^+$ transition is also found under the strong 478 kev peak. However, from our observations of the $4^{+'} \rightarrow 2^+$ transition intensities, and from the known branching ratio of the $4^{+'}$ state[72], the contribution to the 478 kev peak from the $4^{+'} \rightarrow 4^+$ transitions can be approximately eliminated. Although another source of error is thereby added to the determination of the $6^+ \rightarrow 4^+$ intensities the above does not prohibit the extraction of the latter from the spectra.

D. Os^{190}

Like $Os^{186, 188}$, Os^{190} has been extensively studied by radioactive decay methods and a complex decay scheme evolved[72, 88, 95, 96]. The spins and parities of many levels are known. The partial decay scheme shown in Fig. IV-22 illustrates the levels excited in these experiments. (At 840 kev a (dotted) new transition is seen.)

Previous Coulomb excitation studies of Os^{190} have obtained B(E2) values for the transition $2^+ \rightarrow 0^+$[71, 91, 58]. These are confirmed by lifetime measurements.[97] In addition, the $2^{+'}$ and 4^+ levels have been Coulomb excited weakly and with poor statistics[58, 71]. However, since the $2^{+'} \rightarrow 2^+$ and $4^+ \rightarrow 2^+$ transitions are nearly degenerate and unresolved by NaI(Tl) scintillation detectors, extraction of quantitative information concerning the excitation probabilities of these states is beset by another major source of error. Thus the previously measured B(E2) values for transitions involving the 4^+ and $2^{+'}$ states are subject to very large uncertainties (on the order of 40% or greater). In the experiments here these problems were avoided with the use of the Ge(Li) detector and more accurate B(E2) values have been obtained.

The γ-singles spectra taken at energies of 70.30 MeV with a NaI(Tl) counter and at 48.26 and 70.30 MeV with the Ge(Li) detector are shown in Figs. IV-23, 24 and 25. The most prominent feature of the NaI(Tl) spectra is the presence of three rather than four major peaks. This is due to the just mentioned near-degeneracy of the transitions $4^+ \rightarrow 2^+$ and $2^{+'} \rightarrow 2^+$. However, as Figs. IV-24, 25 show, these transitions of 361 and 370 kev are resolved by the Ge(Li) detector. By using the relative intensities of the $2^{+'} \rightarrow 0^+$ and $2^{+'} \rightarrow 2^+$ transitions at 557 and 370 kev as obtained from the Ge(Li) data, and by demanding the same ratio in the γ-particle NaI(Tl) data, the relative amount of the 370 kev component of the composite 361-370 kev peak was determined. The remainder of the peak is due to the $4^+ \rightarrow 2^+$ transition whose intensity is thereby also determined.

An interesting point graphically evidenced in the Ge(Li) spectra is the considerable variation with energy in the relative intensities of the $4^+ \rightarrow 2^+$ and $2^{+'} \rightarrow 2^+$ transitions. As expected, the excitation of the 4^+ state has a generally stronger

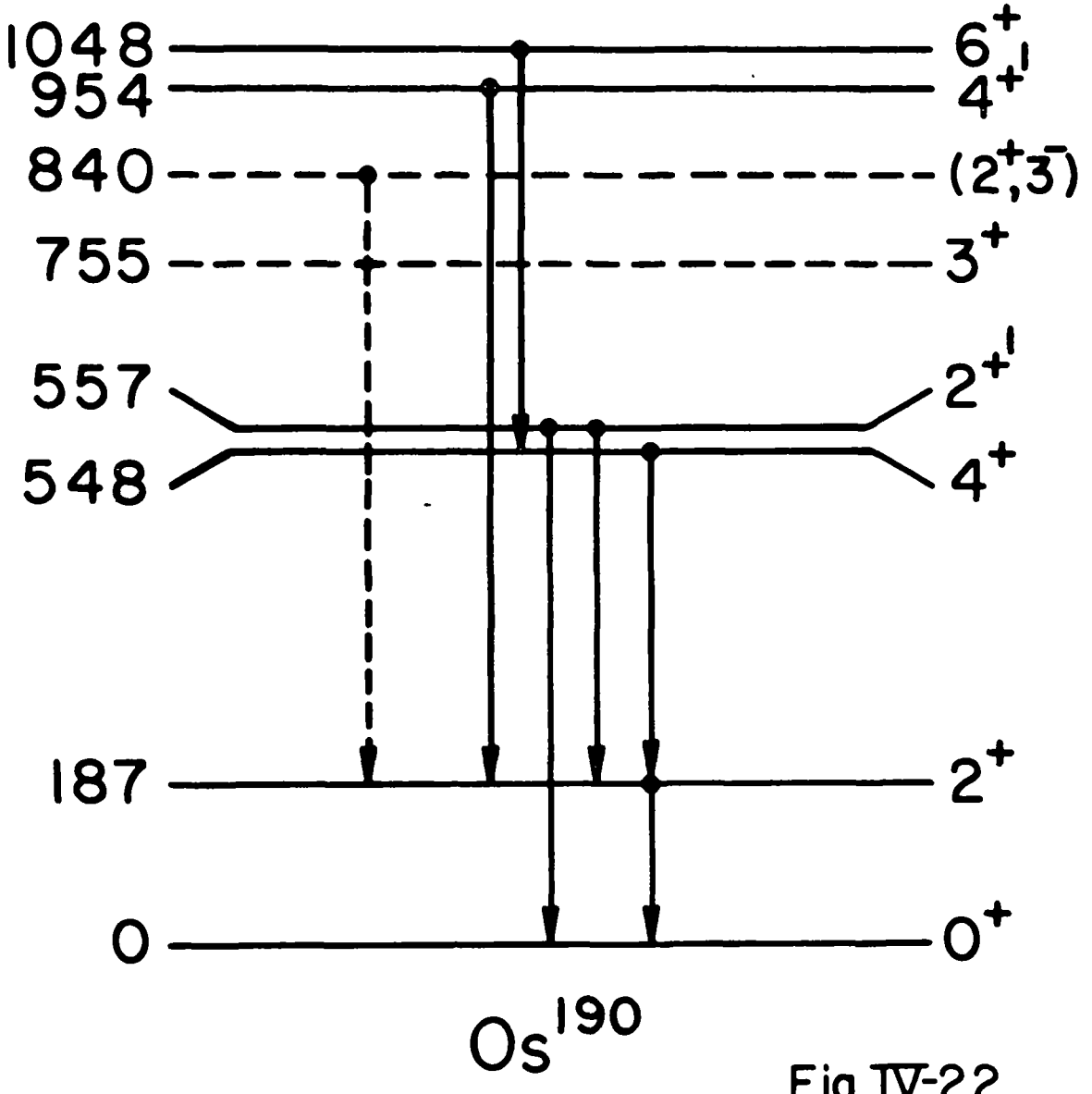

Fig. IV-22

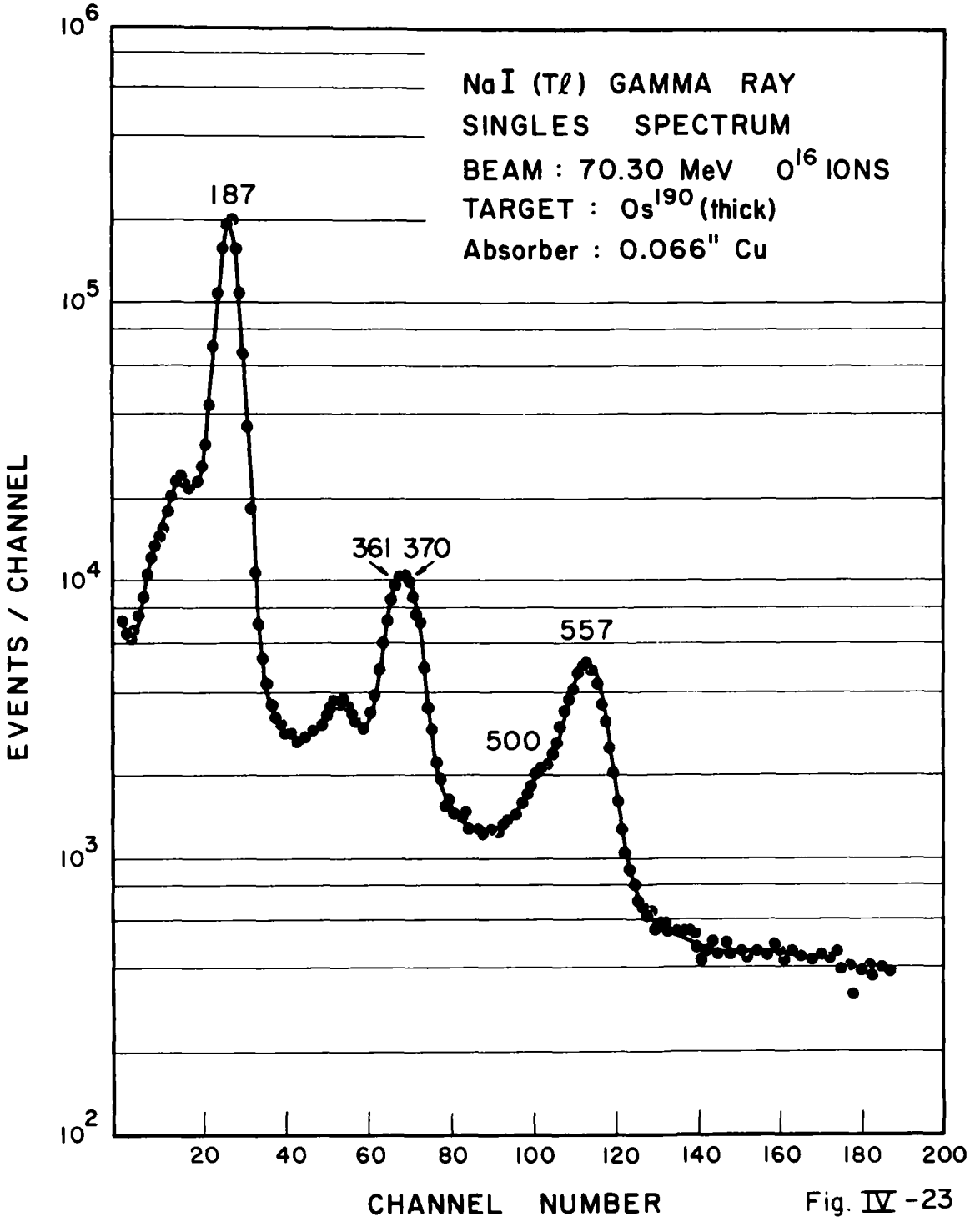
NaI (Tℓ) GAMMA RAY
SINGLES SPECTRUM
BEAM : 70.30 MeV O^{16} IONS
TARGET : Os^{190} (thick)
Absorber : 0.066" Cu
187
361 370
557
500
10^6
10^5
10^4
10^3
10^2
EVENTS / CHANNEL
20
40
60
80
100
120
140
160
180
200
CHANNEL NUMBER

Fig. IV-23

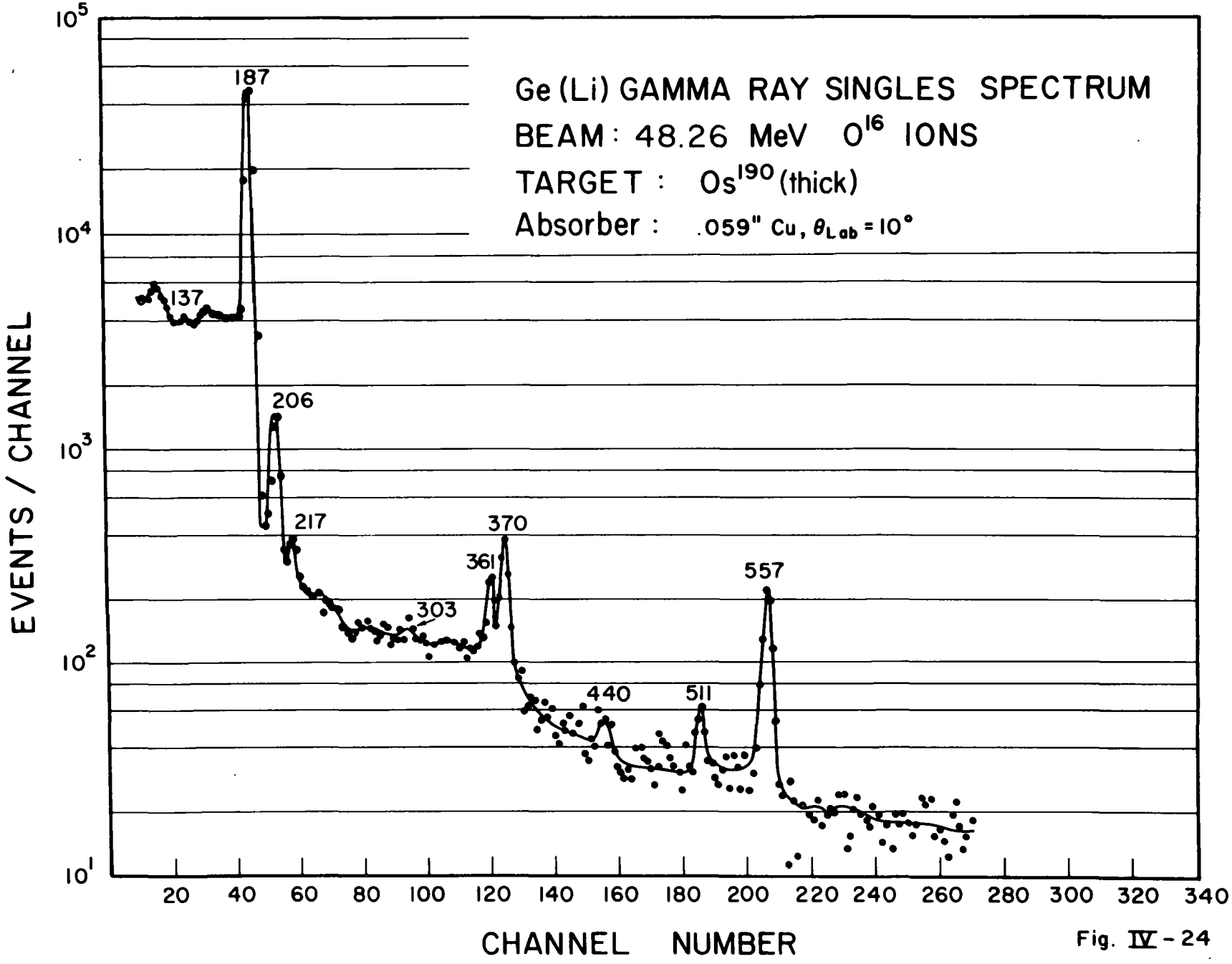
Ge (Li) GAMMA RAY SINGLES SPECTRUM
BEAM: 48.26 MeV O^{16} IONS
TARGET: Os^{190} (thick)
Absorber: .059" Cu, $\theta_{Lab} = 10°$
EVENTS / CHANNEL
CHANNEL NUMBER
10^5
10^4
10^3
10^2
10^1
20 40 60 80 100 120 140 160 180 200 220 240 260 280 300 320 340
187
137
206
217
370
361
303
557
440
511

Fig. IV - 24

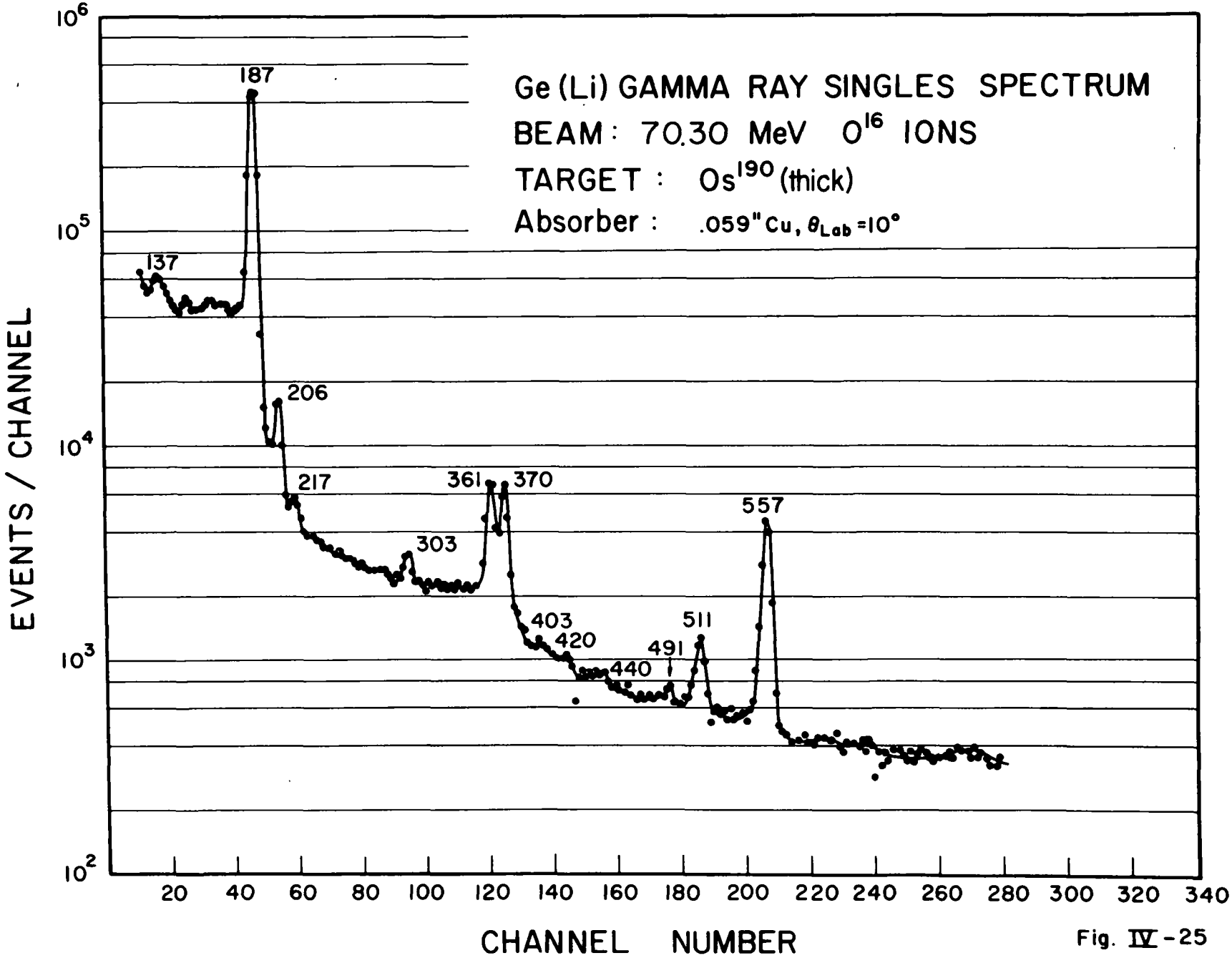
Ge (Li) GAMMA RAY SINGLES SPECTRUM
BEAM: 70.30 MeV O^{16} IONS
TARGET: Os^{190} (thick)
Absorber: .059" Cu, θ_{Lab} = 10°
EVENTS / CHANNEL
CHANNEL NUMBER
10^6
10^5
10^4
10^3
10^2
20 40 60 80 100 120 140 160 180 200 220 240 260 280 300 320 340
137
187
206
217
303
361
370
403
420
440
491
511
557

Fig. IV-25

energy dependence than does that of the $2^{+'}$ state. We, indeed, note that the 361 kev ($4^{+} \rightarrow 2^{+}$) peak is smaller than the 370 kev ($2^{+'} \rightarrow 2^{+}$) peak at lower bombarding energies but larger at 70.30 MeV.

The γ-γ and γ-particle coincidence spectra are shown in Figs. IV-26-31. The main peaks of 187, 361, 370 and 557 kev are due to the transitions: $2^{+} \rightarrow 0^{+}$, $4^{+} \rightarrow 2^{+}$, $2^{+'} \rightarrow 2^{+}$, $2^{+'} \rightarrow 0^{+}$, respectively. These assignments are confirmed by the transition energies, the γ-γ data and the energy dependence of the transition intensities (see Chapter VI), as well as by our angular distribution measurements.

The 500 kev ($6^{+} \rightarrow 4^{+}$) transition is partially obscured in the γ-particle data by the much stronger 557 kev transition, but emerges clearly, as it should, in both γ-γ spectra. There is little doubt as to its origin.

In the γ-particle spectra at 62.10 and 70.30 MeV a wide peak at or around 800 kev is seen. From the level scheme and the systematics in this region one expects a 765 kev transition from the known $4^{+'}$ level to the 2^{+} level. Such a transition is in coincidence with the $2^{+} \rightarrow 0^{+}$ γ-rays and should be seen in the appropriate γ-γ spectrum.In fact, it is, as can be seen from Fig. IV-26. In order to complete the analysis of the corresponding peak in the γ-particle data we must determine if it is composite. Its width there, as well as its asymmetric shape, indicates that it is. The asymmetry in shape is especially clear if one pair averages the γ-particle spectra in this region. Evidence for a composite peak, the second (higher-lying) member of which is not in coincidence with the $2^{+} \rightarrow 0^{+}$ transitions is also obtained by comparing the shape of this peak in the γ-particle and γ-γ spectra which have the same γ-ray energy calibration (Figs. IV-26, 31).

Thus we conclude that there is a transition at about 840 kev in addition to the $4^{+'} \rightarrow 2^{+}$ transition at 765 kev. The nature of the former transition is not known. It can probably be presumed from its absence in the γ-γ data that it represents a transition to the ground state. Furthermore, no transition of energy around 840 - 187 = 653 kev is seen in any of the γ-ray spectra, precluding at least a strong decay branch of the level involved to the first excited state. Reasonable spins for this level would be 2^{+} or 3^{-}. If there actually is a weak and unobserved branch to the 2^{+} state, then this level could be analogous to the 780 kev level proposed in Os^{188}, and perhaps to the 855 kev level to be proposed in Os^{192}. See the following section for a more complete discussion of this triad of levels.

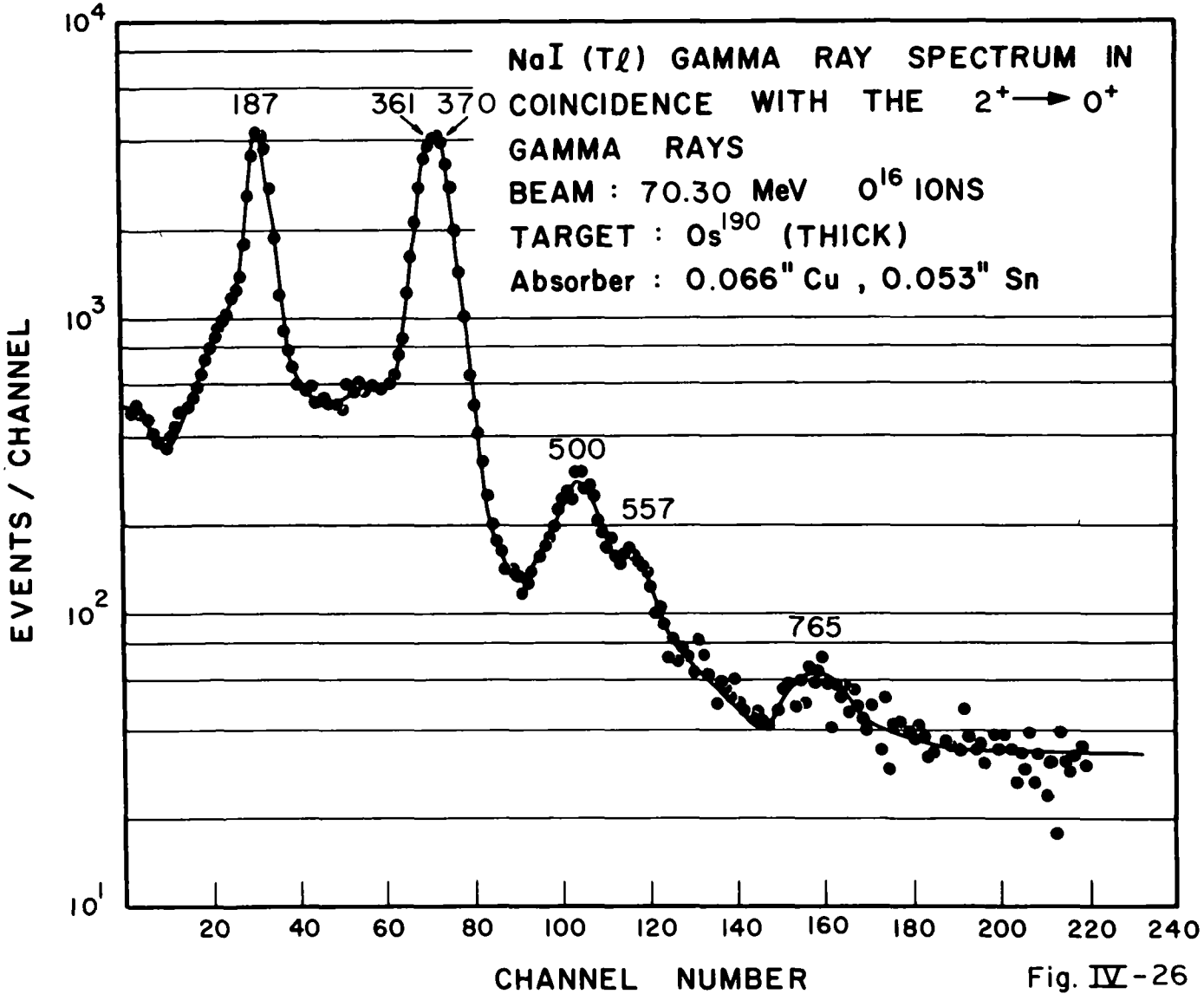
NaI (Tℓ) GAMMA RAY SPECTRUM IN COINCIDENCE WITH THE 2⁺ → 0⁺ GAMMA RAYS
BEAM : 70.30 MeV O¹⁶ IONS
TARGET : Os¹⁹⁰ (THICK)
Absorber : 0.066" Cu , 0.053" Sn
187
361 370
500
557
765
EVENTS / CHANNEL
CHANNEL NUMBER
10⁴
10³
10²
10¹
20
40
60
80
100
120
140
160
180
200
220
240

Fig. IV-26

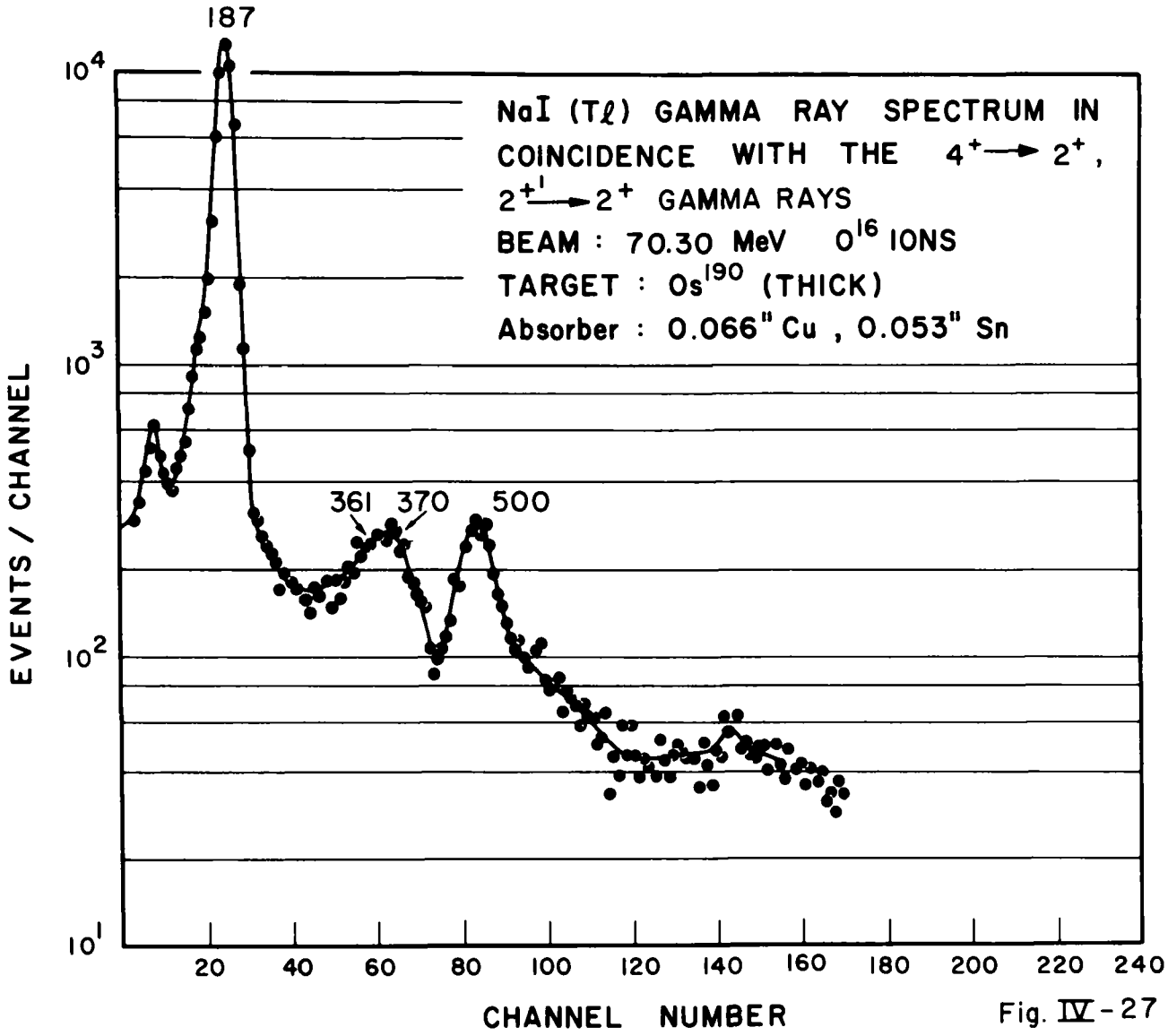
187
10^4
10^3
10^2
10^1
NaI (Tℓ) GAMMA RAY SPECTRUM IN COINCIDENCE WITH THE $4^+ \longrightarrow 2^+$, $2^{+'} \longrightarrow 2^+$ GAMMA RAYS
BEAM : 70.30 MeV O^{16} IONS
TARGET : Os^{190} (THICK)
Absorber : 0.066" Cu , 0.053" Sn
361
370
500
EVENTS / CHANNEL
20
40
60
80
100
120
140
160
180
200
220
240
CHANNEL NUMBER

Fig. IV-27

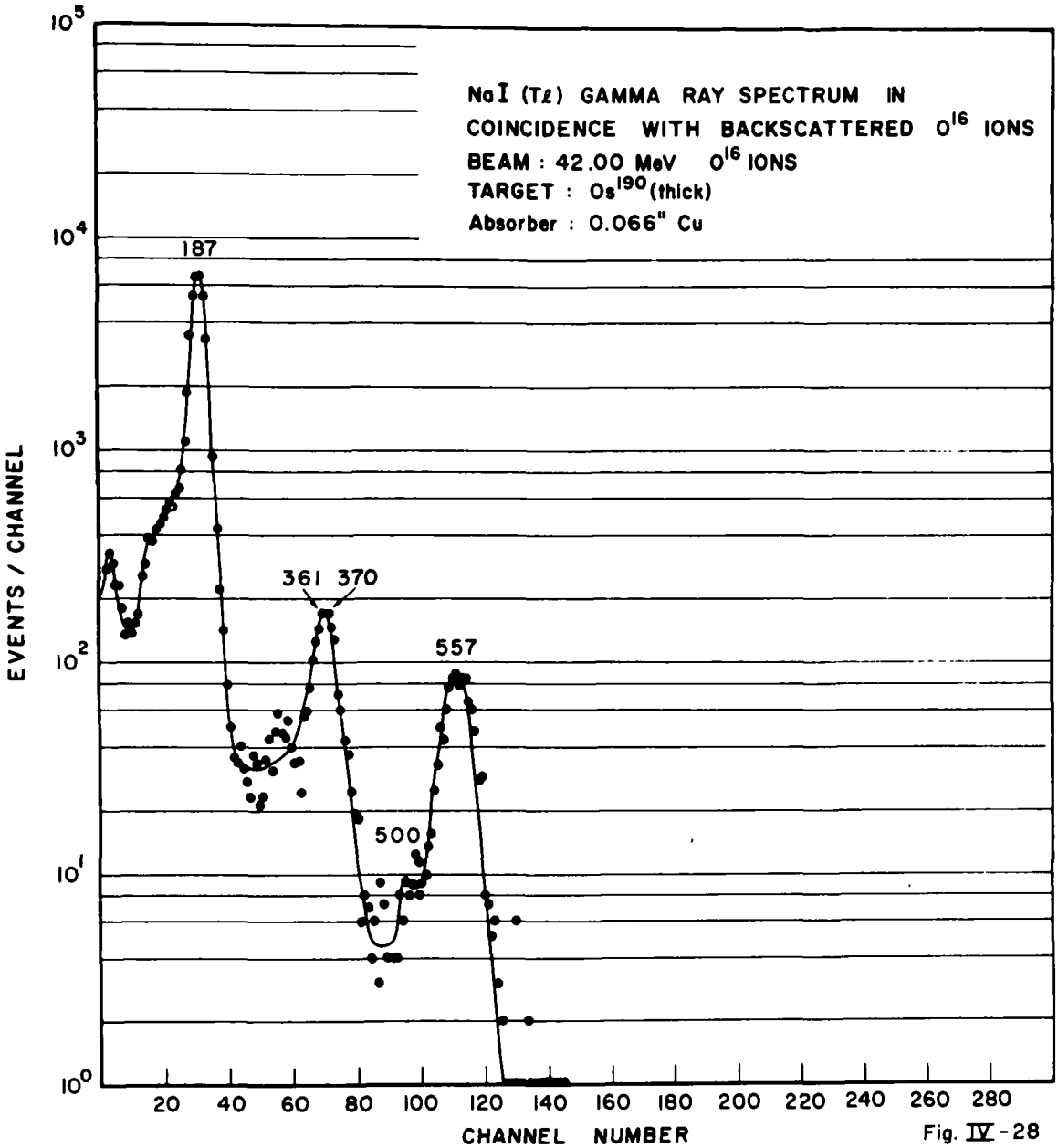
NaI (Tℓ) GAMMA RAY SPECTRUM IN
COINCIDENCE WITH BACKSCATTERED O16 IONS
BEAM : 42.00 MeV O16 IONS
TARGET : Os190 (thick)
Absorber : 0.066" Cu
187
361 370
557
500
EVENTS / CHANNEL
CHANNEL NUMBER
10^5
10^4
10^3
10^2
10^1
10^0
20 40 60 80 100 120 140 160 180 200 220 240 260 280

Fig. IV-28

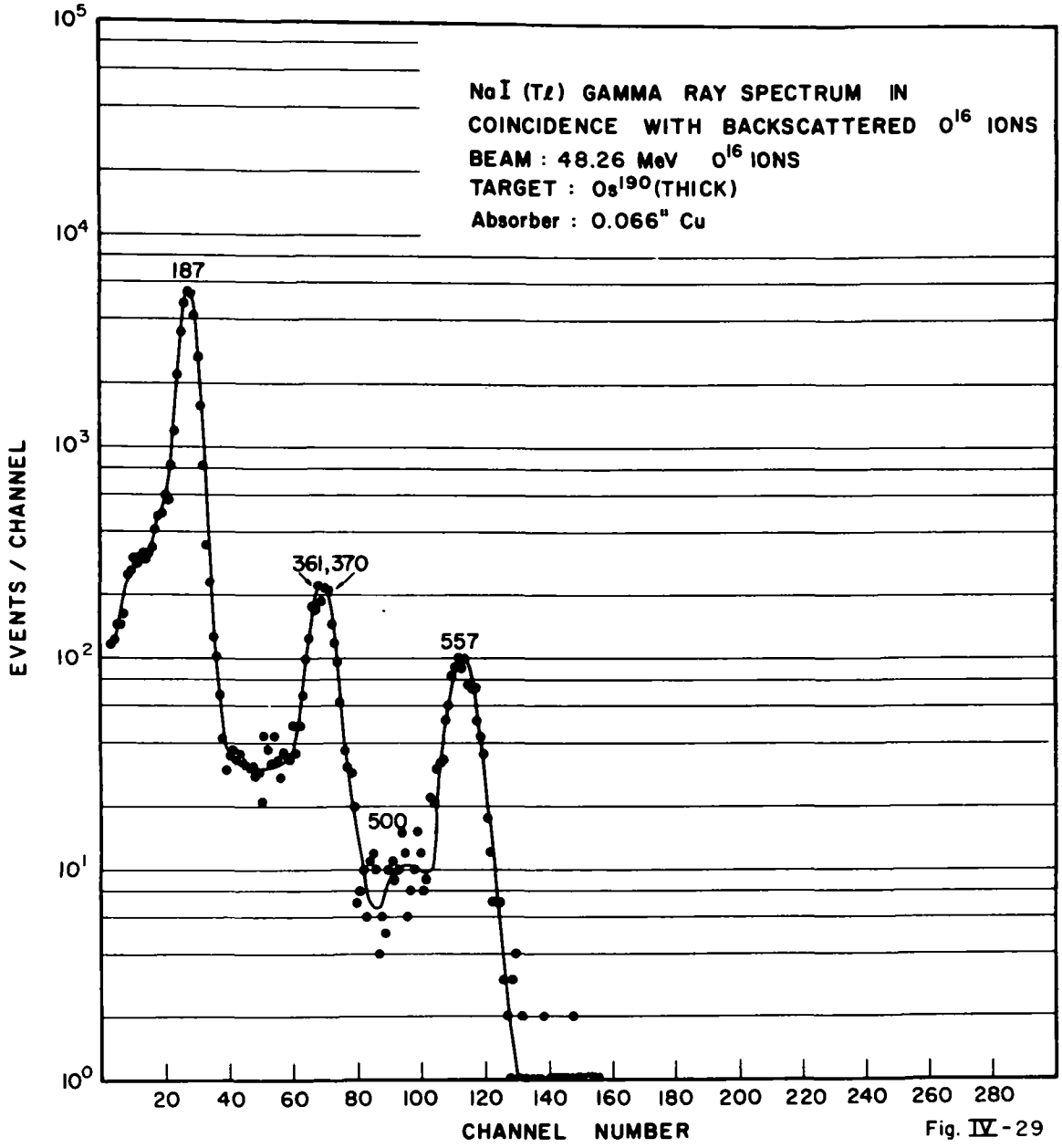
NaI (Tℓ) GAMMA RAY SPECTRUM IN
COINCIDENCE WITH BACKSCATTERED O16 IONS
BEAM : 48.26 MeV O16 IONS
TARGET : Os190(THICK)
Absorber : 0.066" Cu
187
361,370
557
500
EVENTS / CHANNEL
CHANNEL NUMBER
10^5
10^4
10^3
10^2
10^1
10^0
20 40 60 80 100 120 140 160 180 200 220 240 260 280

Fig. IV-29

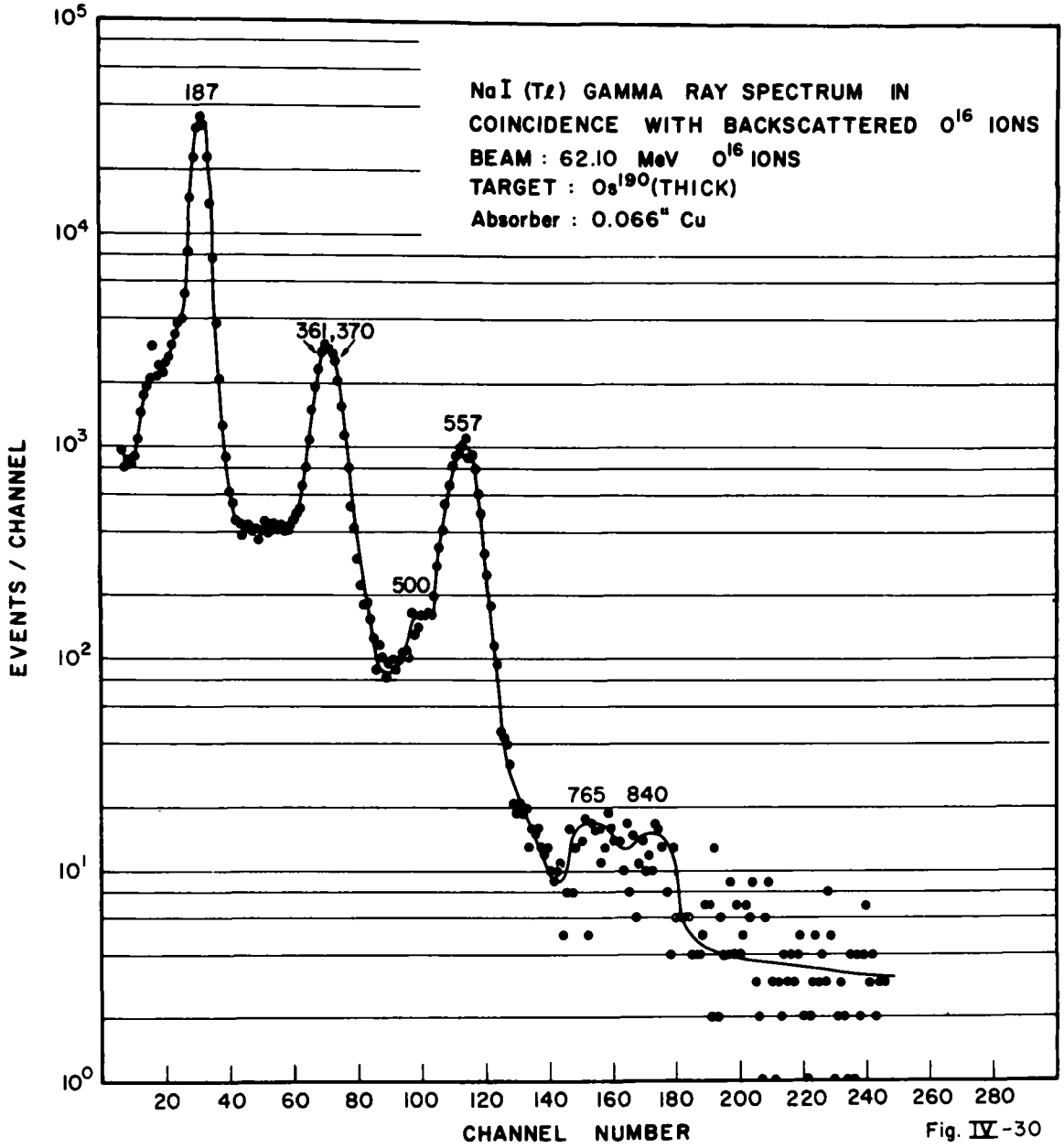
NaI (Tℓ) GAMMA RAY SPECTRUM IN
COINCIDENCE WITH BACKSCATTERED O16 IONS
BEAM : 62.10 MeV O16 IONS
TARGET : Os190(THICK)
Absorber : 0.066" Cu
187
361,370
557
500
765 840
EVENTS / CHANNEL
CHANNEL NUMBER
10^5
10^4
10^3
10^2
10^1
10^0
20 40 60 80 100 120 140 160 180 200 220 240 260 280

Fig. IV-30

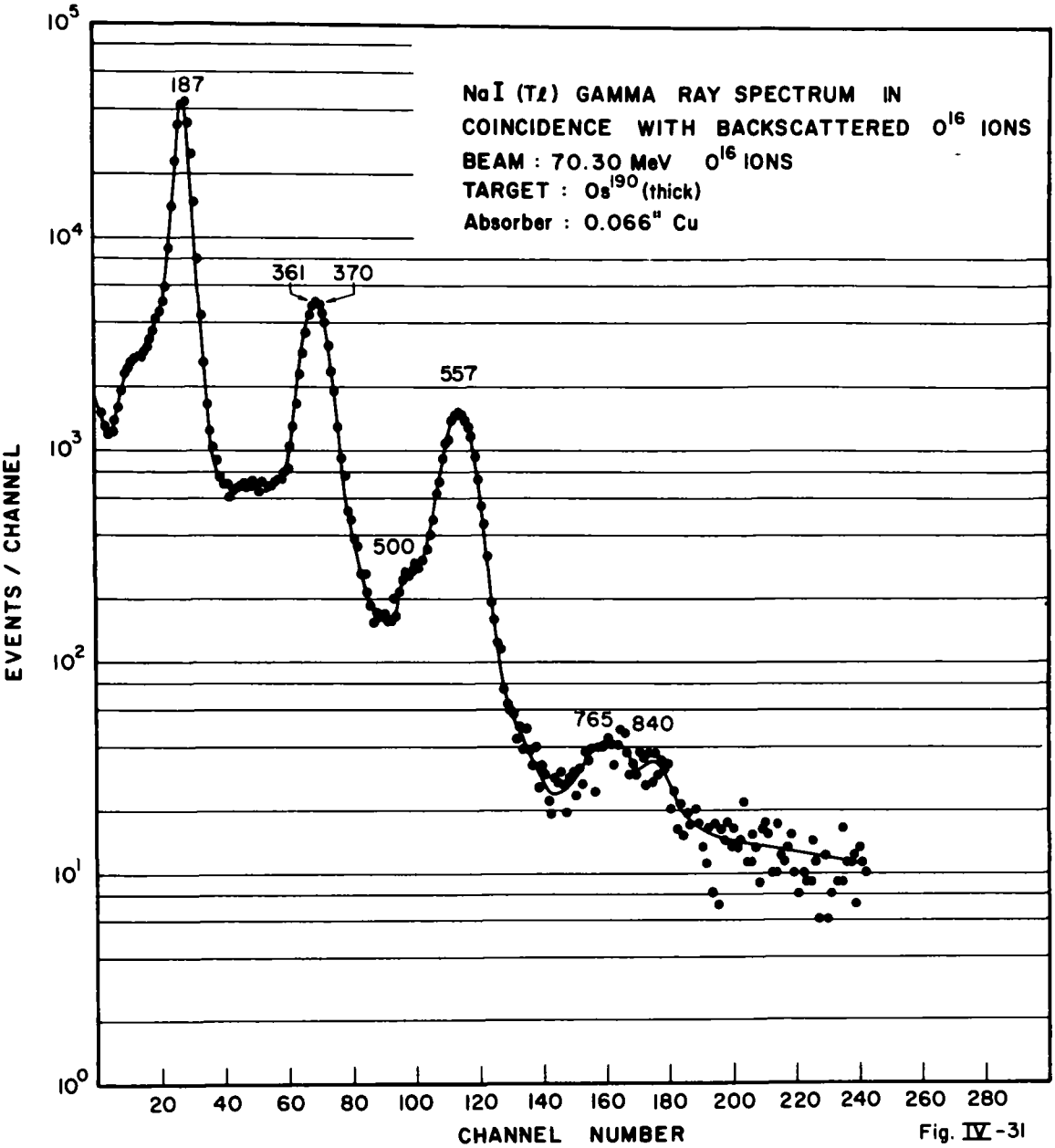
NaI (Tℓ) GAMMA RAY SPECTRUM IN
COINCIDENCE WITH BACKSCATTERED O16 IONS
BEAM : 70.30 MeV O16 IONS
TARGET : Os190 (thick)
Absorber : 0.066" Cu
187
361
370
557
500
765
840
EVENTS / CHANNEL
CHANNEL NUMBER
10^5
10^4
10^3
10^2
10^1
10^0
20
40
60
80
100
120
140
160
180
200
220
240
260
280

Fig. IV-31

E. Os^{192}

The structure of Os^{192} is much less well-known than that of the other isotopes discussed[78]. Radioactive decay studies have only revealed four excited states[72, 76, 98, 99]. The 2^+, 4^+ and $2^{+'}$ states have also been Coulomb excited[70, 71, 82] although, once again, uncertainties in obtaining B(E2) values have been large. As before, quoted errors are in the region of $\pm$ 30-40%. The decay scheme for Os^{192} shown in Fig. IV-32 contains the levels seen in the experiments performed here. (The proposed and heretofore unseen transition at 855 kev is discussed below.) Sample γ-singles spectra taken with NaI(Tl) and Ge(Li) detectors are shown in Figs. IV-33, 34, 35. Figs. IV-36-43 consist of the γ-γ and γ-particle coincidence spectra. Data has been taken on both thick and thin targets as indicated in the figures. The thick and thin target NaI(Tl) singles spectra at 62.10 MeV illustrate one advantage of thick targets in experiments not involving coincidences with backscattered particles: namely, they have much smaller surface-to-volume ratios than thin targets and thus, percentagewise, less surface contamination and oxidation and therefore larger peak-to-valley ratios emerge in the γ-ray spectra.

The level scheme, γ-γ data, angular distributions, variation of γ-ray intensities with energy and the general systematics in this region are all consistent with correspondences of the 206, 283, 374 and 489 kev peaks to the $2^+ \rightarrow 0^+$, $2^{+'} \rightarrow 2^+$, $4^+ \rightarrow 2^+$, and $2^{+'} \rightarrow 0^+$ transitions, respectively. The "hump" on the high energy side of the 489 kev peak in the γ-particle data is a sum peak resulting from coincidences of the $4^+ \rightarrow 2^+$ and $2^+ \rightarrow 0^+$ transitions.

No evidence for the excitation of $4^{+'}$ or 6^+ levels is seen in the spectra taken on Os^{192}. This is consistent with the view that, with Os^{192}, we are finally nearly out of the region of large stable deformations and of well-developed rotational structures. One would now expect that rotational band structures would be highly impure and would not persist through nearly as many levels as in the other Os isotopes. (α, xn) reactions would be a useful tool for investigating more thoroughly whether or not 6^+ and 8^+ levels exist as part of a ground state rotational band in Os^{192}.

A new transition is seen, in the data taken at higher O^{16} energies, at about

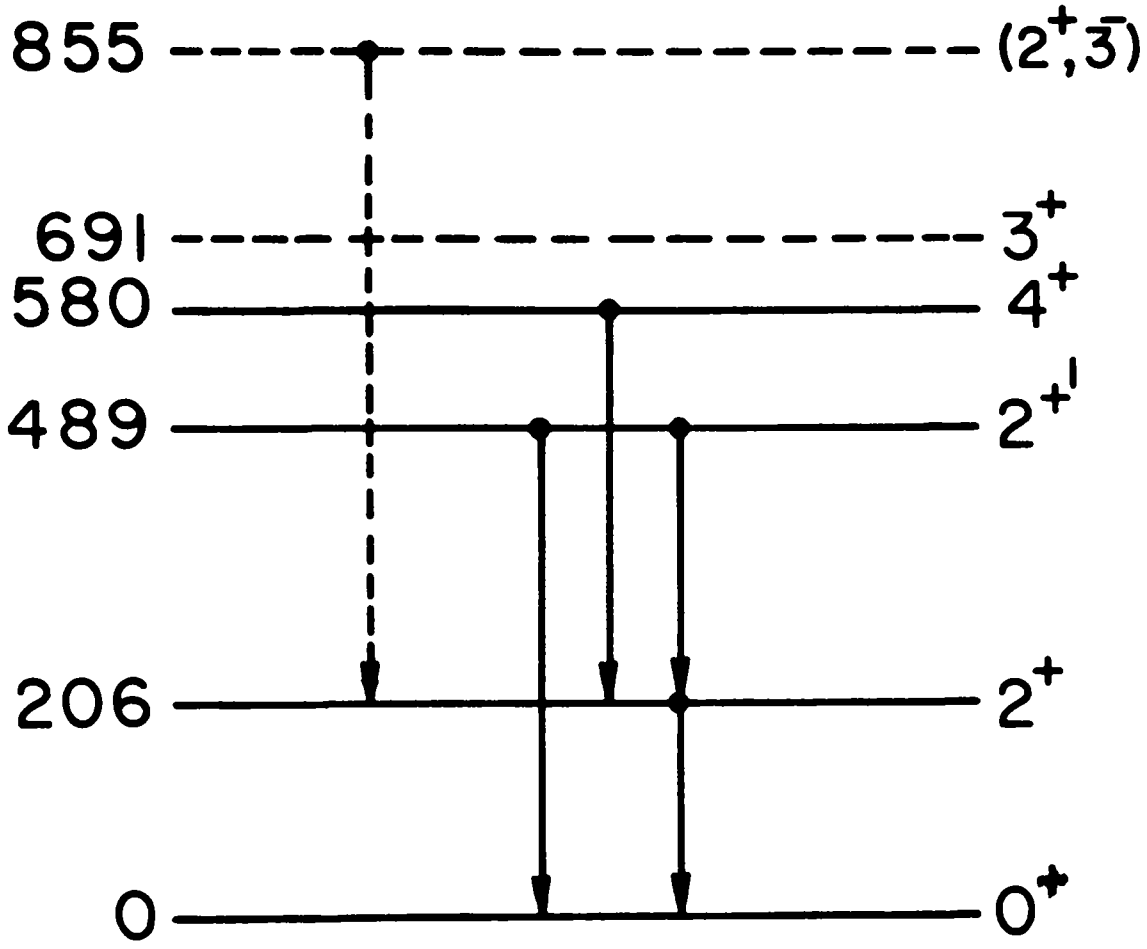

Os^{192}

Fig. IV-32

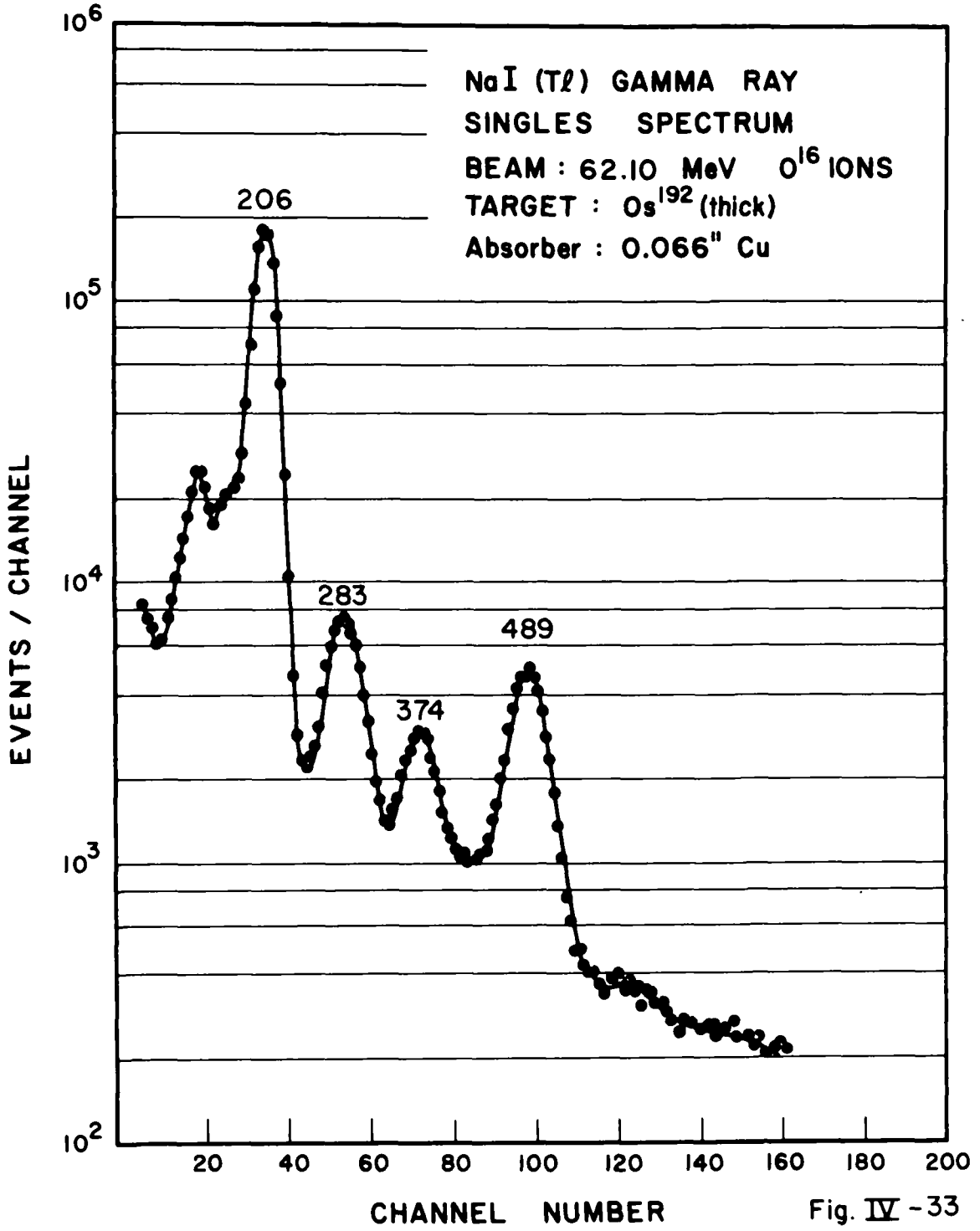
NaI (Tℓ) GAMMA RAY
SINGLES SPECTRUM
BEAM : 62.10 MeV O^{16} IONS
TARGET : Os^{192} (thick)
Absorber : 0.066" Cu
206
283
374
489
10^6
10^5
10^4
10^3
10^2
EVENTS / CHANNEL
20
40
60
80
100
120
140
160
180
200
CHANNEL NUMBER

Fig. IV-33

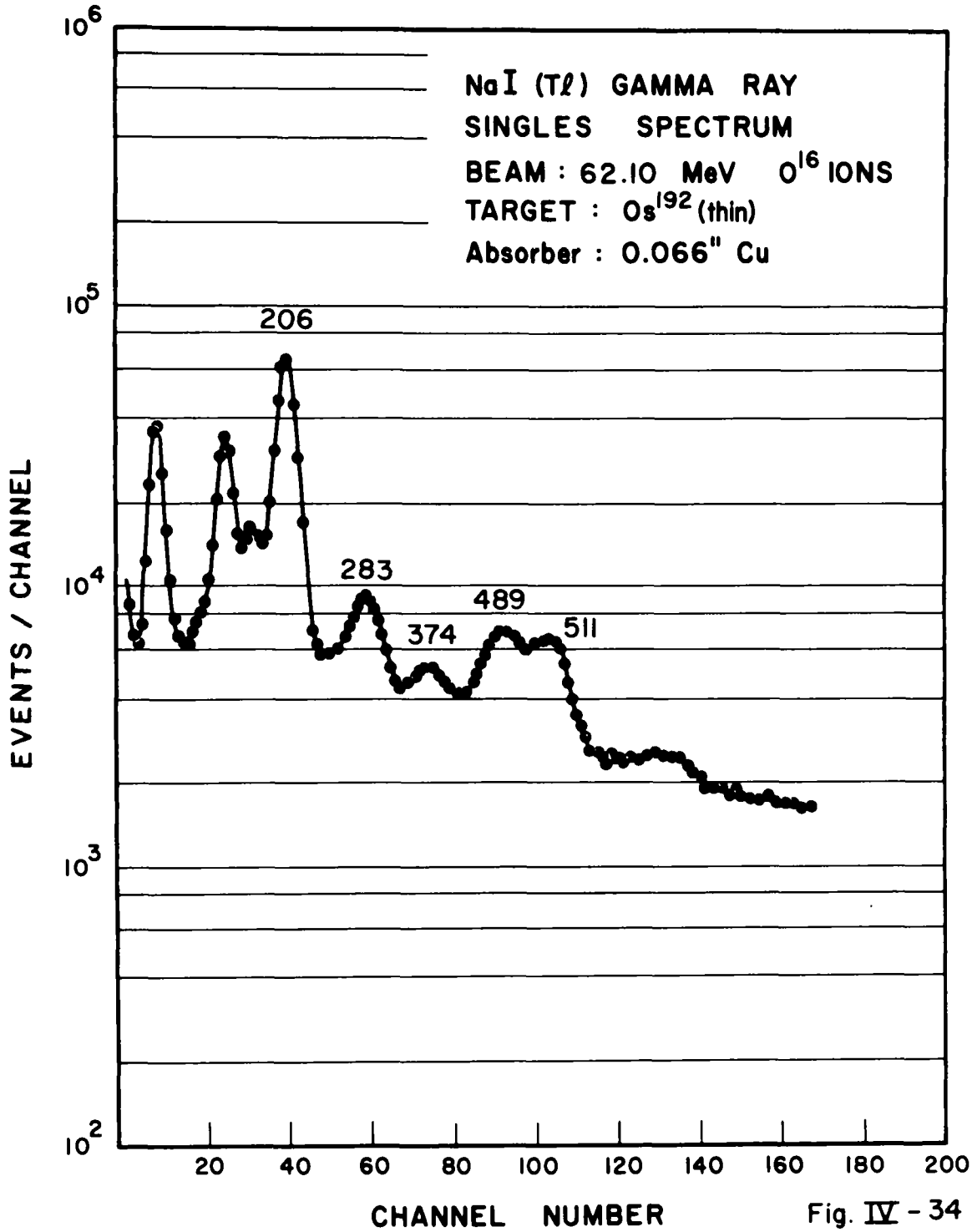
NaI (Tℓ) GAMMA RAY
SINGLES SPECTRUM
BEAM : 62.10 MeV O16 IONS
TARGET : Os192 (thin)
Absorber : 0.066" Cu
206
283
374
489
511
EVENTS / CHANNEL
CHANNEL NUMBER
10^6
10^5
10^4
10^3
10^2
20
40
60
80
100
120
140
160
180
200

Fig. IV - 34

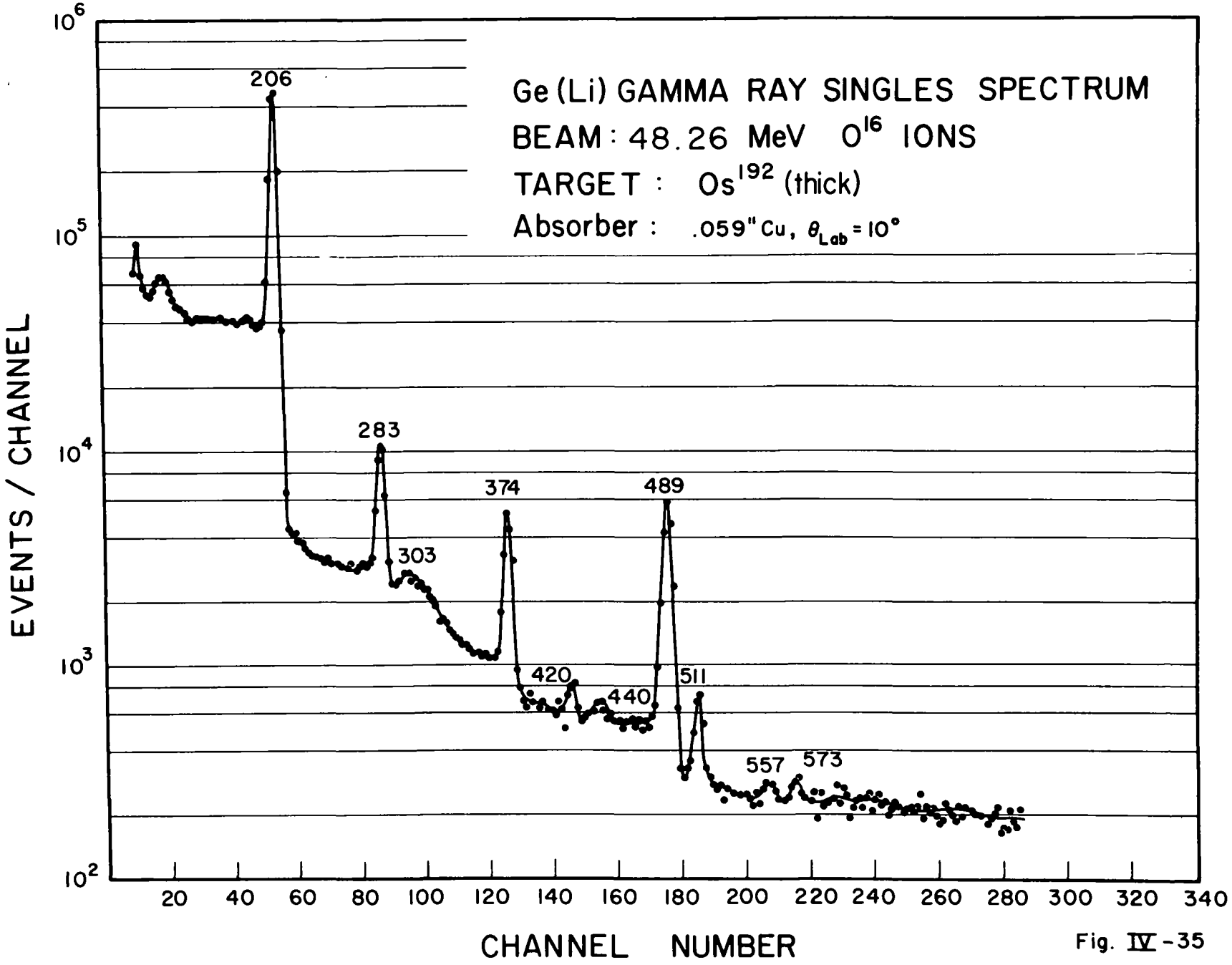
Ge(Li) GAMMA RAY SINGLES SPECTRUM
BEAM: 48.26 MeV O^{16} IONS
TARGET: Os^{192} (thick)
Absorber: .059" Cu, $\theta_{Lab} = 10°$
206
283
303
374
420
440
489
511
557
573
10^6
10^5
10^4
10^3
10^2
EVENTS / CHANNEL
20 40 60 80 100 120 140 160 180 200 220 240 260 280 300 320 340
CHANNEL NUMBER

Fig. IV-35

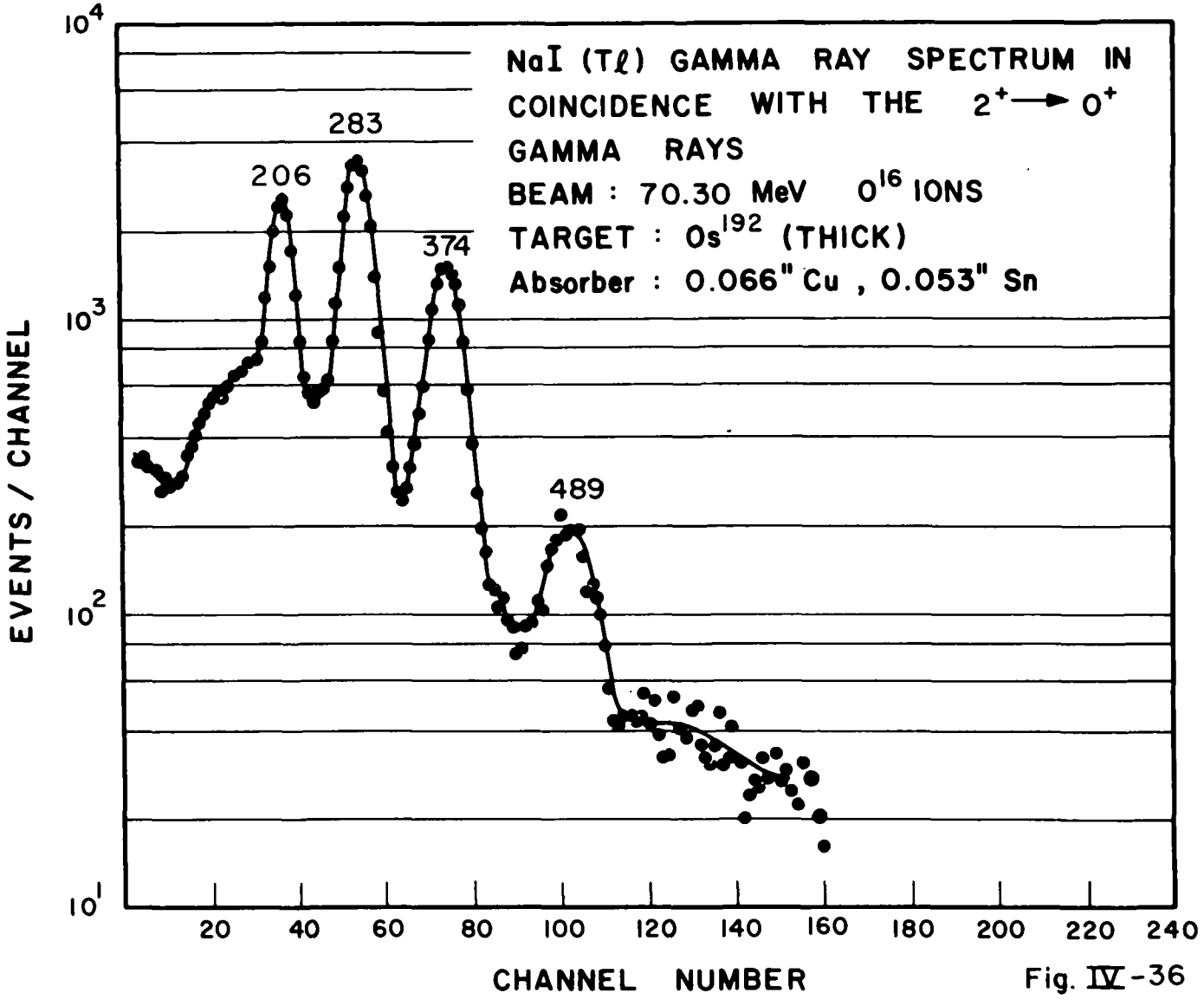
NaI (Tℓ) GAMMA RAY SPECTRUM IN COINCIDENCE WITH THE 2+ → 0+ GAMMA RAYS
BEAM : 70.30 MeV O16 IONS
TARGET : Os192 (THICK)
Absorber : 0.066" Cu , 0.053" Sn
283
206
374
489
EVENTS / CHANNEL
CHANNEL NUMBER
10^4
10^3
10^2
10^1
20
40
60
80
100
120
140
160
180
200
220
240

Fig. IV-36

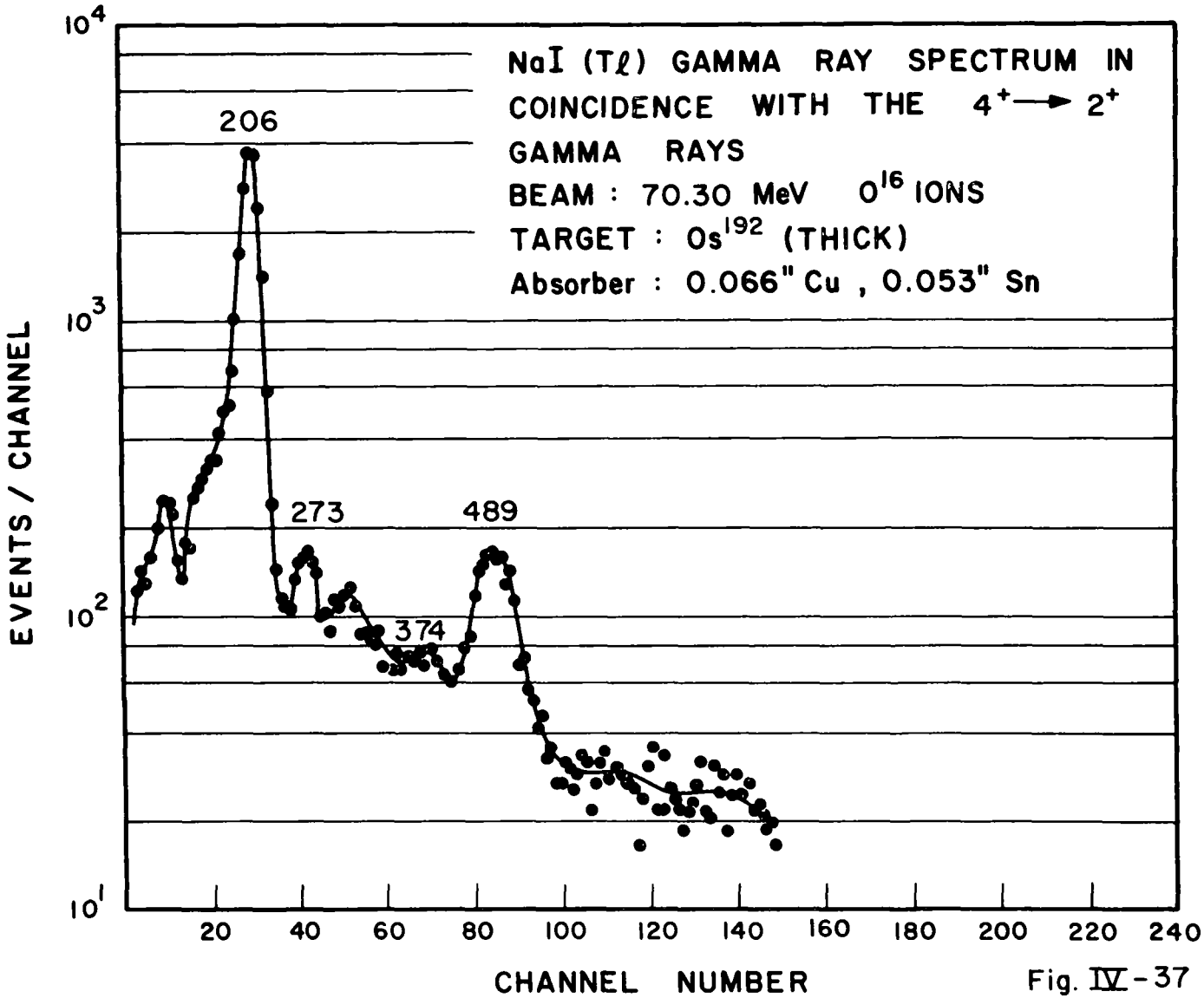
NaI (Tℓ) GAMMA RAY SPECTRUM IN
COINCIDENCE WITH THE 4+ → 2+
GAMMA RAYS
BEAM : 70.30 MeV O16 IONS
TARGET : Os192 (THICK)
Absorber : 0.066" Cu , 0.053" Sn
206
273
374
489
EVENTS / CHANNEL
CHANNEL NUMBER
10^4
10^3
10^2
10^1
20
40
60
80
100
120
140
160
180
200
220
240

Fig. IV-37

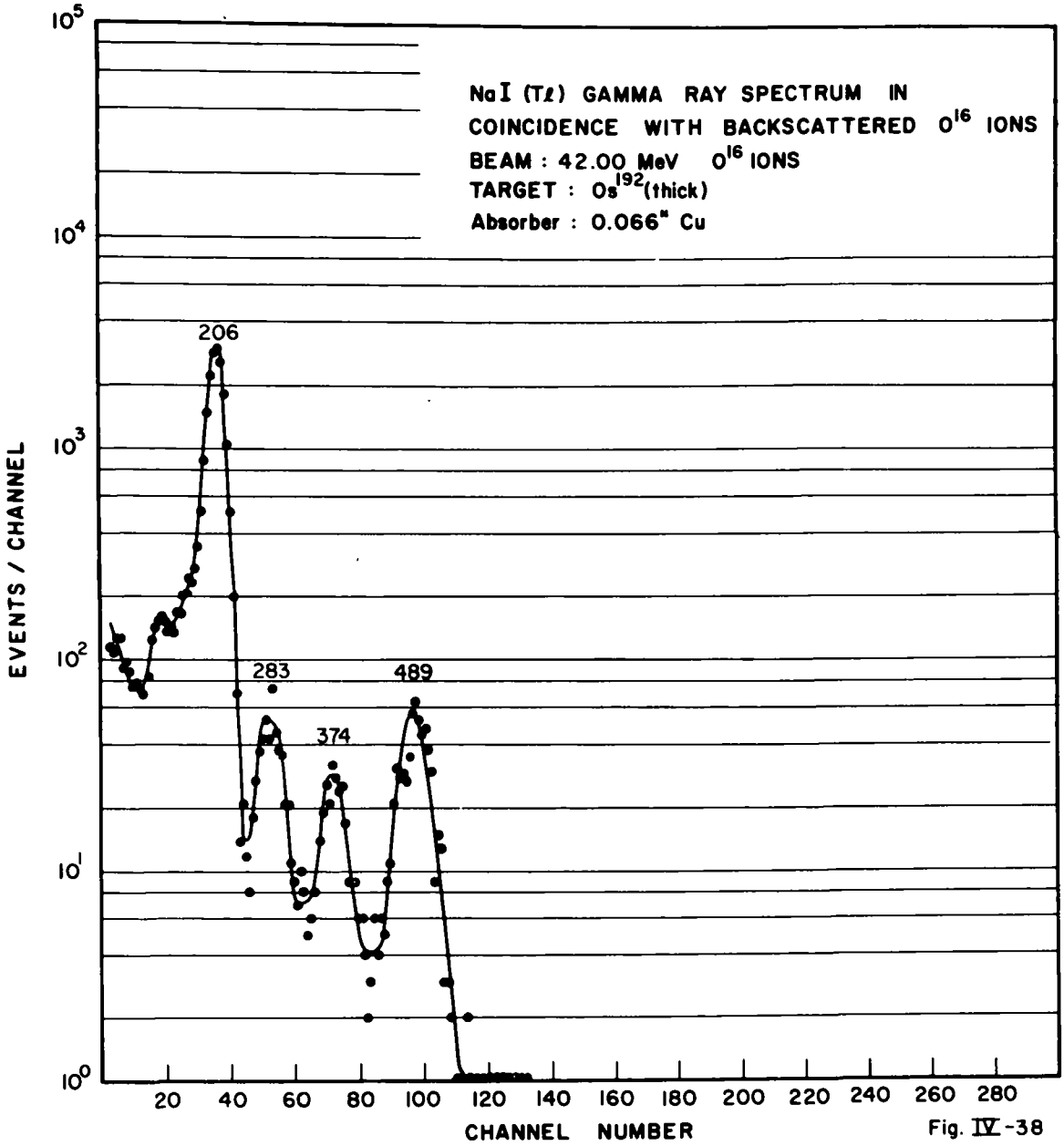
NaI (Tℓ) GAMMA RAY SPECTRUM IN
COINCIDENCE WITH BACKSCATTERED O16 IONS
BEAM : 42.00 MeV O16 IONS
TARGET : Os192(thick)
Absorber : 0.066" Cu
206
283
374
489
EVENTS / CHANNEL
CHANNEL NUMBER
10^5
10^4
10^3
10^2
10^1
10^0
20 40 60 80 100 120 140 160 180 200 220 240 260 280

Fig. IV-38

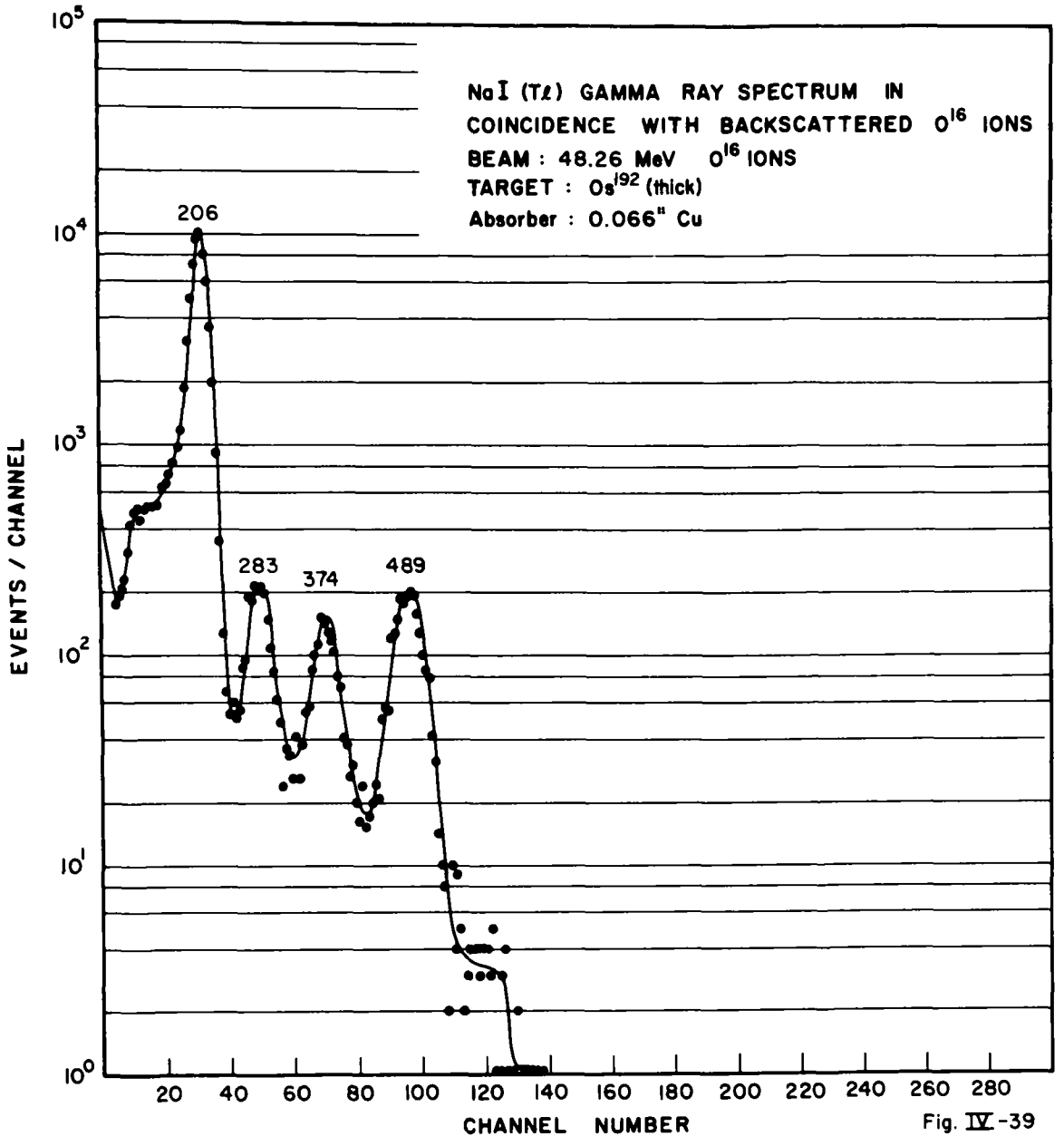
NaI (Tℓ) GAMMA RAY SPECTRUM IN
COINCIDENCE WITH BACKSCATTERED O16 IONS
BEAM : 48.26 MeV O16 IONS
TARGET : Os192 (thick)
Absorber : 0.066" Cu
206
283
374
489
EVENTS / CHANNEL
CHANNEL NUMBER
10^5
10^4
10^3
10^2
10^1
10^0
20 40 60 80 100 120 140 160 180 200 220 240 260 280

Fig. IV-39

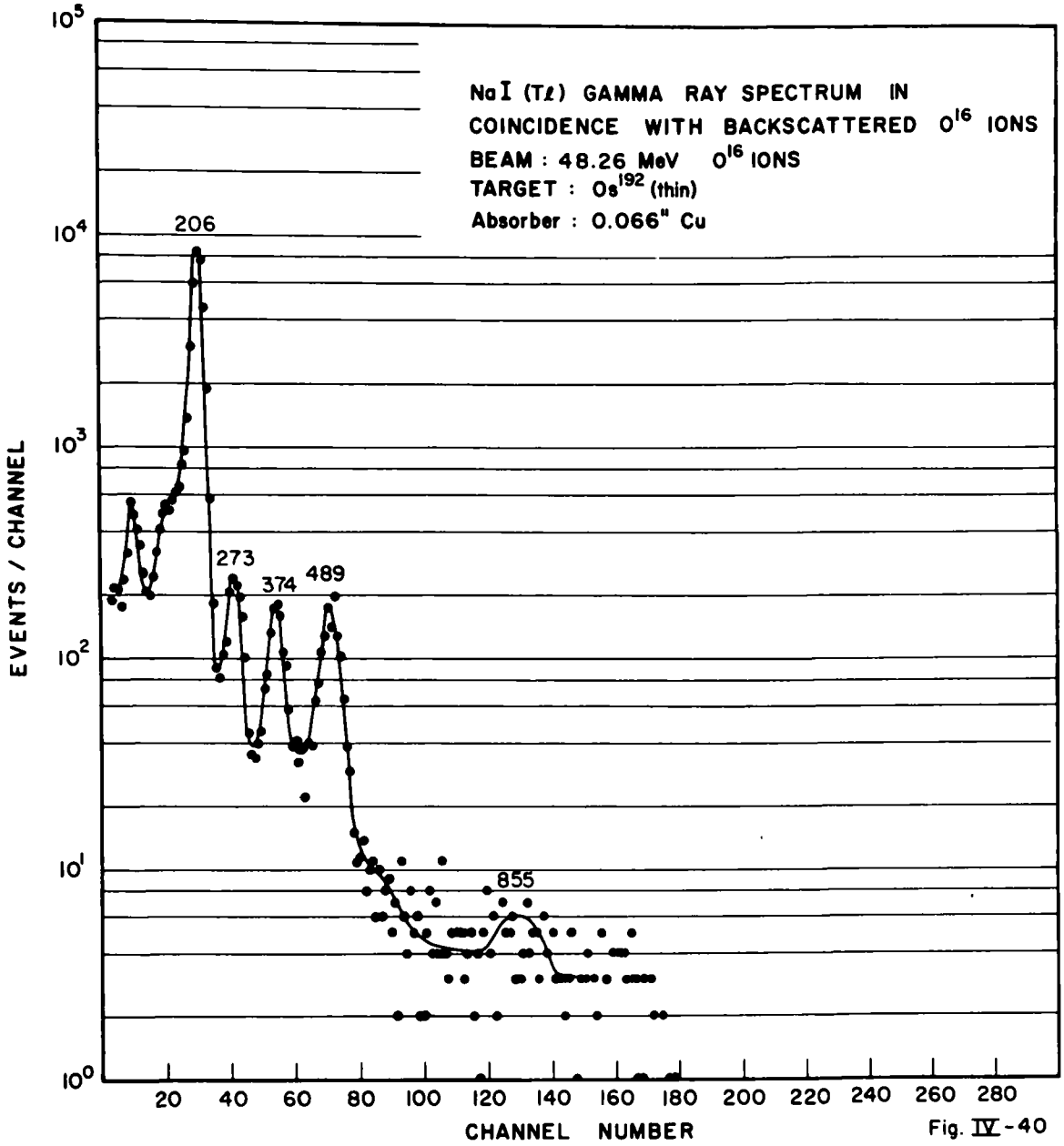
NaI (Tℓ) GAMMA RAY SPECTRUM IN
COINCIDENCE WITH BACKSCATTERED O16 IONS
BEAM : 48.26 MeV O16 IONS
TARGET : Os192 (thin)
Absorber : 0.066" Cu
206
273
374
489
855
EVENTS / CHANNEL
CHANNEL NUMBER
10^5
10^4
10^3
10^2
10^1
10^0
20 40 60 80 100 120 140 160 180 200 220 240 260 280

Fig. IV-40

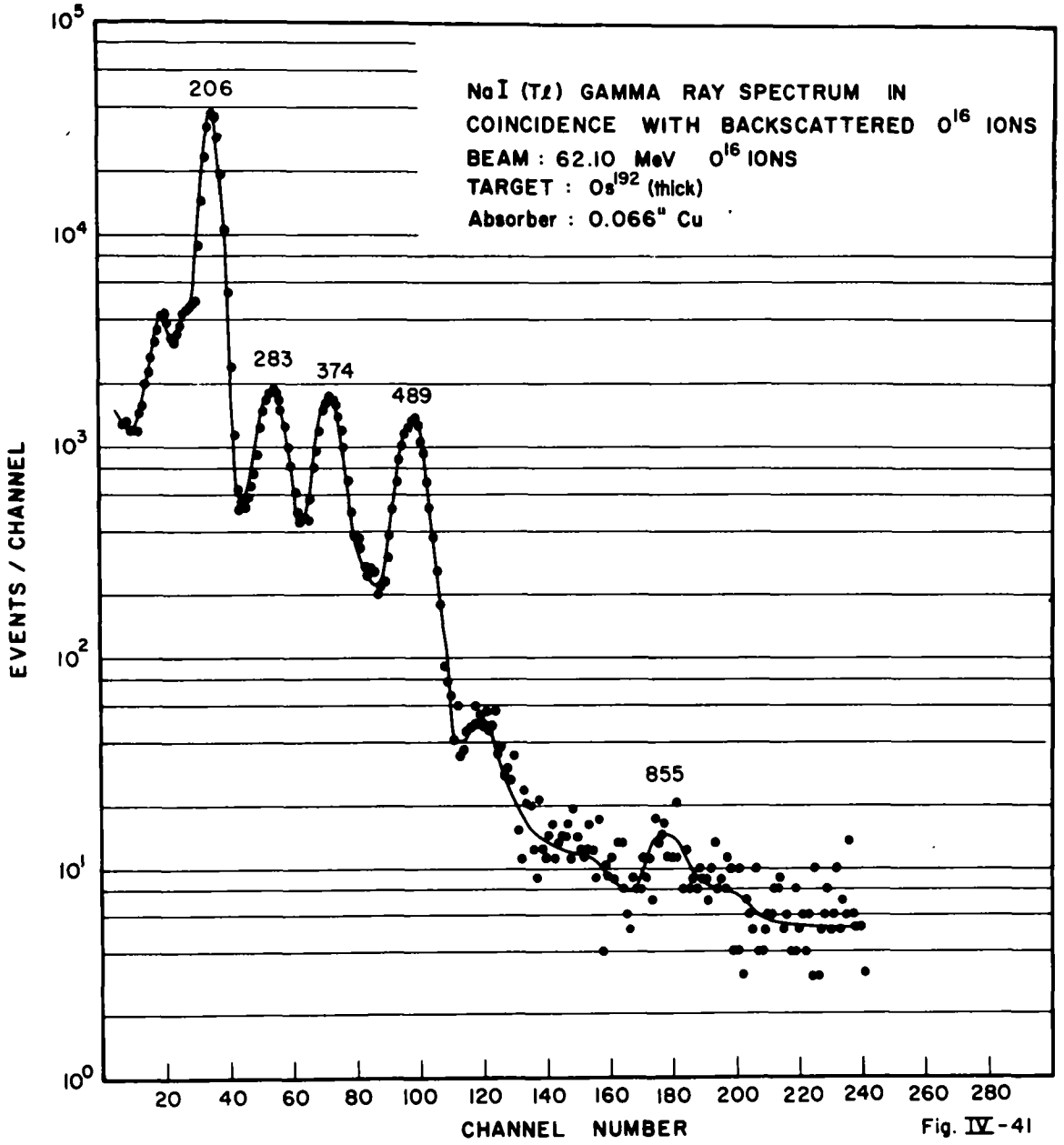
NaI (Tℓ) GAMMA RAY SPECTRUM IN
COINCIDENCE WITH BACKSCATTERED O16 IONS
BEAM : 62.10 MeV O16 IONS
TARGET : Os192 (thick)
Absorber : 0.066" Cu
206
283
374
489
855
EVENTS / CHANNEL
CHANNEL NUMBER
10^5
10^4
10^3
10^2
10^1
10^0
20 40 60 80 100 120 140 160 180 200 220 240 260 280

Fig. IV-41

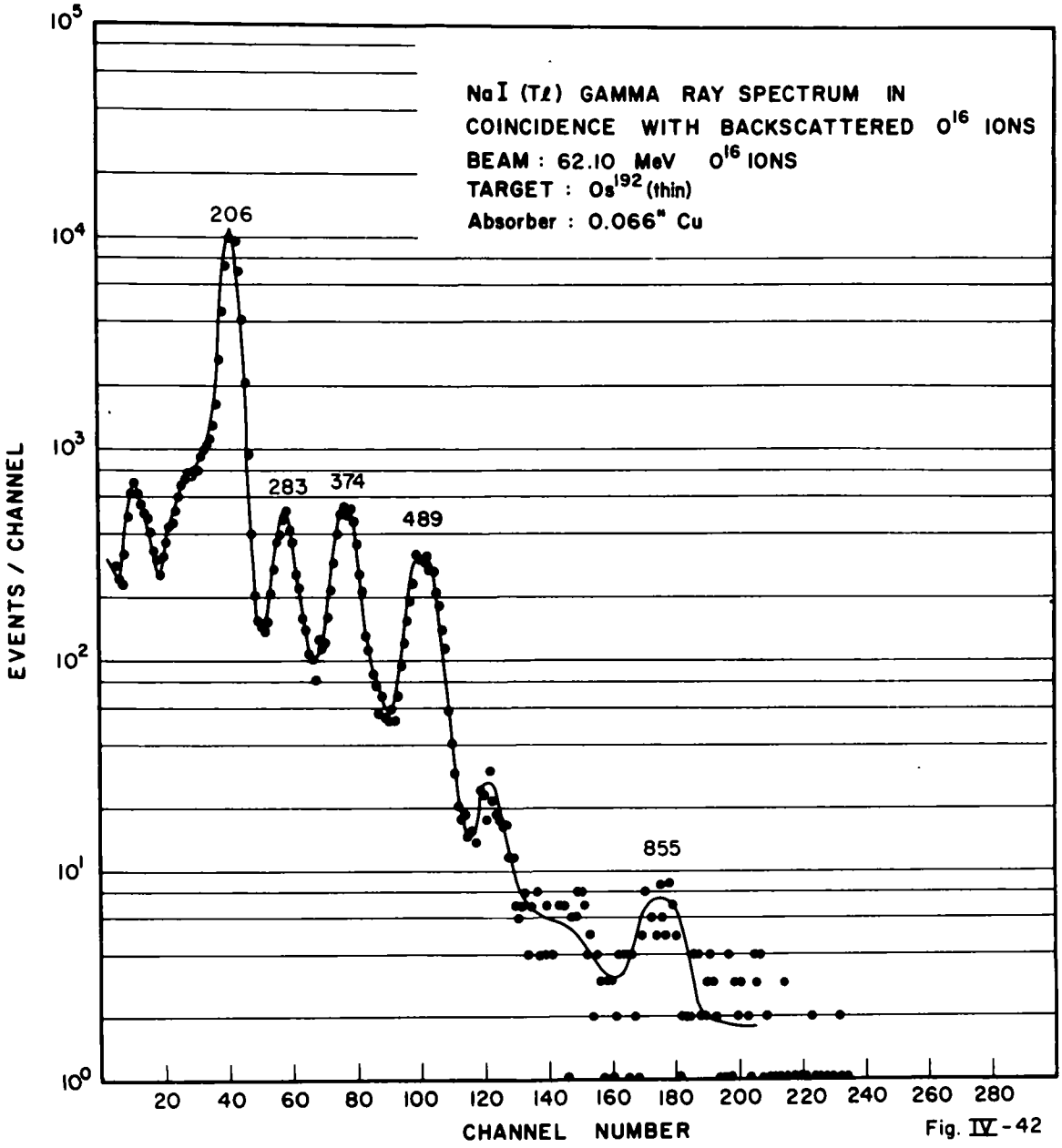
NaI (Tℓ) GAMMA RAY SPECTRUM IN
COINCIDENCE WITH BACKSCATTERED O16 IONS
BEAM : 62.10 MeV O16 IONS
TARGET : Os192 (thin)
Absorber : 0.066" Cu
206
283
374
489
855
EVENTS / CHANNEL
CHANNEL NUMBER
10^5
10^4
10^3
10^2
10^1
10^0
20 40 60 80 100 120 140 160 180 200 220 240 260 280

Fig. IV-42

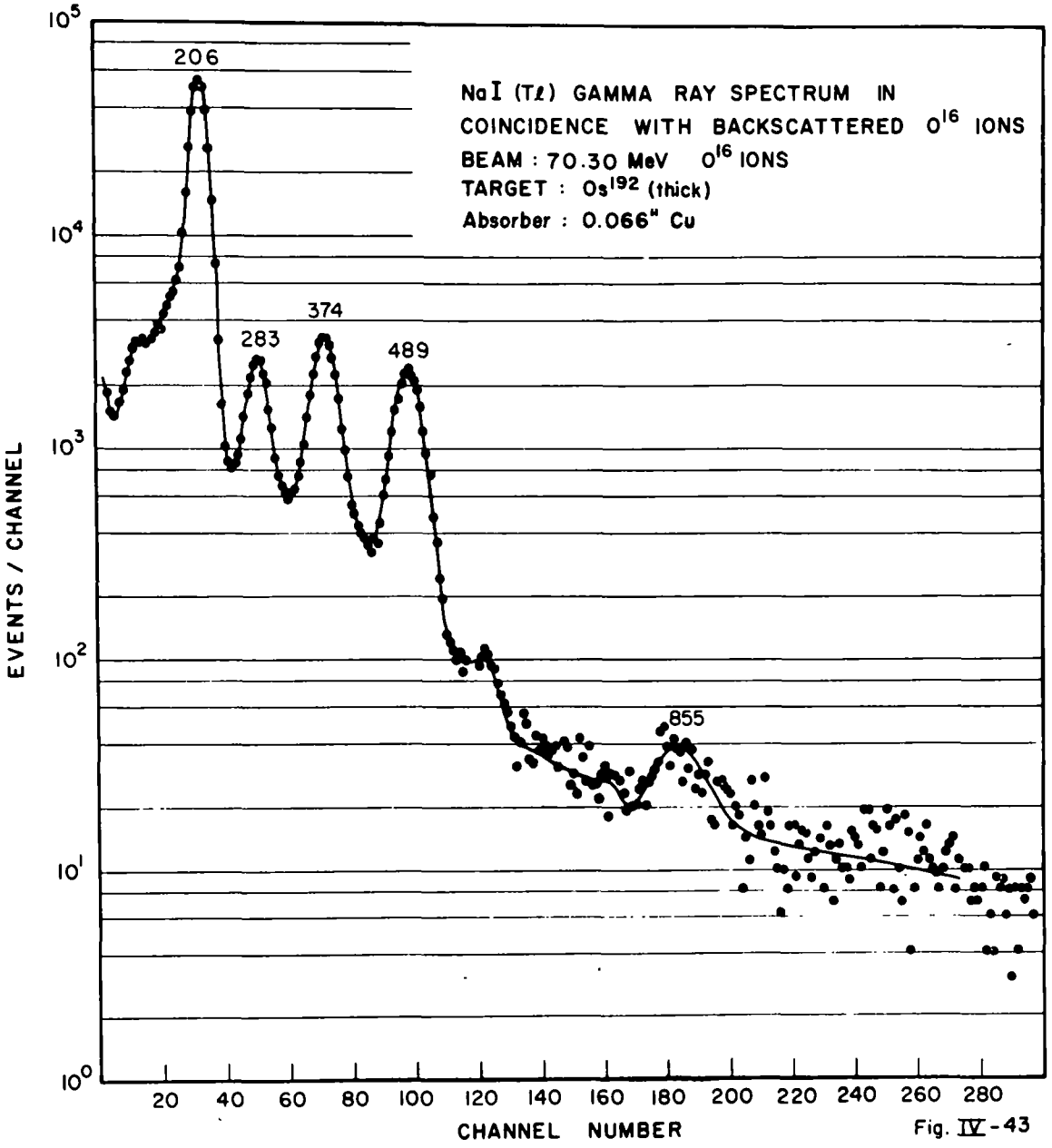
NaI (Tℓ) GAMMA RAY SPECTRUM IN
COINCIDENCE WITH BACKSCATTERED O16 IONS
BEAM : 70.30 MeV O16 IONS
TARGET : Os192 (thick)
Absorber : 0.066" Cu
206
283
374
489
855
EVENTS / CHANNEL
CHANNEL NUMBER
10^5
10^4
10^3
10^2
10^1
10^0
20 40 60 80 100 120 140 160 180 200 220 240 260 280

Fig. IV-43

855 kev. This transition is not seen in either of the γ-γ spectra and so possibly represents the decay of a new level at that energy to the ground state. Reasonable and consistent J^{π} assignments for this level are 2^+ or 3^-. Thus, referring to the discussions of Os^{188} and Os^{190}, we see that it is likely that previously unobserved levels exist in $Os^{188, 190, 192}$, at energies of about 780, 840 and 855 kev, respectively, which decay predominantly or solely to the ground state, and which can perhaps be suspected of having J^{π} assignments of 2^+ or 3^-. It is hard to see how an isolated 2^+ state could be present at these energies unless it is the second member of a K = 0 rotational band built on an unobserved (β vibrational ?) 0^+ state. Most nuclear models, indeed, do predict 0^+ levels at around 500 to 1200 kev in these nuclei but none have yet been found except for the well-known 1086 kev level in Os^{188}. However, if these 0^+ states are present, they should have been seen in the γ-particle spectra, for their excitation is enhanced relative to the 2^+ states of the same band when coincidences with backscattered particles are recorded. Also, if these three states are indeed of similar character and are assumed to be 2^+ levels with associated 0^+ states at lower energy, this would imply the existence of three 0^+ states in Os^{188}, in addition to the ground state, below 1800 kev. This would be difficult to explain with most theories of nuclear structure in this region.

On the other hand, collective 3^- states have recently been found[25, 100] in the low A end of the rare earth region and it would not be surprising if they were also present here. No definite conclusion can be drawn from these considerations and final spin assignments should await further experiments. For example, (p,t) reactions leading to residual even-even Os isotopes would tend to preferentially excite any collective 0^+ or 3^- levels in these nuclei[101]. Determination of transferred ℓ-values might be able to help pin down the spin of these levels and to determine if, indeed, they are all of similar structure.

V. DATA ANALYSIS

A. Data Reduction

In this chapter the techniques for data analysis will be described. Most of the emphasis will be placed on the analysis of the γ-particle data. Logically, the chapter is divided into two parts in which are described, respectively, the reduction of the experimental data to a form convenient for extraction of nuclear information, and the actual extraction of that information.

The raw γ-particle data consist simply of spectra of γ-rays known to be in coincidence with incident O^{16} ions backscattered, with energies greater than a certain minimum value, E_{min}, into an annular surface barrier detector. The γ-rays result from the decay of nuclear states whose excitation has been induced by O^{16} ions of energies ranging from the incident energy to a lower energy, E_{cut}. E_{cut} is the energy, just prior to backscattering, of an O^{16} ion such that it enters the detector, at the most backward sensitive angle, with the minimum energy, E_{min}, accepted by the single channel analyzer of the linear particle signals (see Section III-E). As an example, in several runs, the energy, E_{min}, in the particle detector spectrum was set at 23.30 MeV. For 70.30 MeV incident O^{16} ions only those that were backscattered prior to being reduced in energy below about 57.1 MeV due to energy loss in the target, could be scattered through 165^{o}, pass out through the target and yet be detected with energies greater than E_{min}. More will be said about the matter of cutoff energy later.

The first step in data reduction consists of obtaining the number of counts in each γ-ray photopeak. Technically speaking, prior to this, correction for accidental coincidences should be made by subtracting from the coincidence spectrum the direct spectrum normalized by the ratio of accidental to true coincidences. This correction can be quite large in many cases. Fortunately, however, in these experiments, target cleanliness was sufficient that corrections for accidentals were always less than 2%.

Having corrected for random coincidences, one can then analyze the experimental spectra for peak areas by subtracting out, in turn, the entire spectrum

resulting from each γ-ray transition, starting with that one highest in energy. The subtraction may be performed by employing standard γ-ray spectra, recorded with point sources placed at the target spot and in geometries identical to those pertaining to actual running conditions, to fit each photopeak intensity. The use of the standard spectra then enables accurate estimation of photopeak widths and areas and provides a means for quantitatively eliminating Compton edges and backscatter peaks. However, if the coincidence spectrum is relatively free of contaminants and the number of peaks is moderate, such a detailed procedure is not always necessary. Such was indeed the case in these spectra. Peak areas obtained with seriously different and extreme background estimates differed only by a few percent and areas obtained with different but "reasonable" backgrounds differed by even less. From a knowledge of the general shape of the standard spectra or from a knowledge of photopeak-to-Compton ratios[102], the effects of Compton scattered photons could be easily eliminated with considerable accuracy.

Peak areas themselves were obtained in three ways, the results of which never differed from one another by more than 5%. The first consisted simply of summing up the counts/channel under the photopeak after a sloping background had been subtracted. This background included the effects of multiple processes that should not be included in the photopeak as the latter is defined by Heath[102] and as it is construed in Heath's tabulations of photopeak-to-total ratios.

The second, and third, more accurate, methods, used whenever statistics were sufficient for photopeak shapes to be well-defined, may be called the parabola and the modified Gaussian methods.[102] (The γ-ray peak is approximately a Gaussian or modified Gaussian in shape.) These two methods use this fact to fit a Gaussian (parabola on semi-log paper) or modified Gaussian to the peak involved.

Such a procedure is especially useful if for some reason only part of a peak is suitable for obtaining areas. Thus, if another γ-ray peak is superposed on the high-or low-energy side of the peak of interest, the top and opposing side may be used to reconstruct the actual peak (See the 557 kev transition in Os^{190} for an example of a case in which the utility of this approach is clear). The backgrounds used in these methods should properly include only the effects of detector efficiency variation

and of the gradually rising Compton and nuclear reaction background since asymmetric effects, such as those due to forward scattered Comptons, are automatically eliminated by the symmetrization inherent in these methods.

The final peak areas obtained must be corrected for detector efficiency and solid angle, photopeak-to-total ratios, γ-ray absorption prior to entrance into the detector proper, and internal conversion effects. For a given transition, these corrections are combined in the formula:

$$T'_{i\rightarrow f} = \frac{(1+\alpha)}{\eta A} T''_{i\rightarrow f} \qquad \text{V-1}$$

where: $T'_{i\rightarrow f}$ = total number of nuclear deexcitations from level i into level f assuming isotropic distribution of the deexcitation γ-rays,

$T''_{i\rightarrow f}$ = the number of counts in the photopeak corresponding to this transition,

α = the internal conversion coefficient,

η = photopeak efficiency times photopeak-to-total ratio,

and A = the fraction of γ-rays not deleted by absorbers.

The internal conversion coefficients were obtained from calculations by Sliv and Band[103] which include corrections for finite nuclear size. The coefficient α is taken as given by:

$$\alpha = \alpha_K + 1.33 \sum_{i=1}^{3} \alpha_{L_i} \quad . \qquad \text{V-2}$$

The experimental internal conversion coefficients for the decay of the first excited states in $Os^{186, 188}$ differ considerably from the theoretical ones[104]. This is an unavoidable source of error in the results for these two transitions. For consistency, theoretical coefficients have been used throughout.

The absorption correction factors, A, were obtained from calculations based on attenuation coefficients given in Wapstra[105]. The absorption was also checked experimentally. To within the accuracy of the experimental results the accord between calculated and measured absorption factors was quite good. With

the thick Os targets, the strongest absorber was the target itself. Although monoenergetic calibrated "point" sources[106] were used in these measurements, it was difficult to determine if the sources were located precisely behind the small Os targets. However, the consistency of the data taken on thick and thin targets provides an internal confirmation of the thick target contributions to the absorption.

The efficiency factors, η, were obtained by interpolation from tabulations of efficiencies and photopeak-to-total ratios by Heath[102] for a 3 x 3 inch NaI(Tl) detector for various γ-ray energies and source-detector distances.

The result of eq. 1, $T'_{i\rightarrow f}$, would be the total number of transitions from level i to level f were the γ-rays representing this mode of decay isotropically distributed. As it is, $T'_{i\rightarrow f}$ must be multiplied by $1/W(\theta)$ where $W(\theta)$ is equal to the value of the angular distribution at the mean angle of the γ-ray detector and is normalized so that

$$\oint W(\theta)\, d\Omega = 4\pi \qquad \text{V-3}$$

Thus, if $T_{i\rightarrow f}$ = the total numer of deexcitations (via γ-rays or conversion electrons) of level i to level f, then

$$T_{i\rightarrow f} = \frac{T'_{i\rightarrow f}}{W(\theta)} . \qquad \text{V-4}$$

The anisotropies, which may in principle be large, are greatly reduced by placement of the γ-ray counter at 55^{o} to the beam direction. Then the second order term in a multipole expansion of $W(\theta)$ (see below) vanishes and only the relatively small fourth order term can lead to deviations from isotropy. The angular distribution correction, $W(\theta)$ was calculated theoretically and measured experimentally as well. Agreement between experimental and theoretical values is within 20%. Since $W(\theta)$ itself generally entails only a 5-10% correction (or typically 25% for the $2^{+}\rightarrow 0^{+}$ transitions), a 20% error in $W(\theta)$ results in small overall error.

A general expression for the angular distribution of γ-rays corresponding to the transition $I \rightarrow I_f$ following Coulomb excitation from initial level I_i is given by[107]:

$$W(\theta_\gamma, \varphi_\gamma) = \sum_{\substack{\text{even } k \\ \lambda\lambda'}} F_k (\lambda\, \lambda'\, I_f\, I)\, \delta_\lambda\, \delta_{\lambda'} \sum_{K'} g_{k K'}\, D^{k\,*}_{K'\,0} (\theta_\gamma, \varphi_\gamma, 0) \qquad \text{V-5}$$

where

$$g_{k K'} = 2 \left(\frac{2k+1}{2I+1} \right)^{1/2} \frac{(-1)^I}{(2I_i+1)} \sum_{\substack{K, M, \\ M'}} \begin{pmatrix} I & I & k \\ -M & M & K \end{pmatrix} D^{k\,*}_{K\,K'} \left(\frac{\pi}{2}, \frac{\pi+\theta}{2}, 0 \right) (-1)^M \times \sum_{M_i} a^{I_i\, M_i\,*}_{I\quad M}\; a^{I_i\, M_i}_{I\quad M}$$

and where the $F_k (\lambda\, \lambda'\, I_f\, I)$ are well-known geometrical coefficients[108], δ_λ is the relative amplitude for the 2^λ- pole transition, θ_γ and φ_γ describe the direction of emission of γ radiation with respect to the incoming beam, θ is the asymptotic scattering angle of the incident projectile and $a^{I_i\, M_i}_{I\quad M}$ is the amplitude for excitation of the magnetic substate M of a nuclear level of spin I, from an initial state with quantum numbers $I_i\ M_i$.

In general, the angular distribution must be integrated over φ_γ, particle scattering angle and energy and is quite complicated. However if an annular particle detector symmetrically located with respect to the incident beam is employed, only the $K' = 0$ terms survive and the resulting $D^{k\,*}_{00}(\theta_\gamma, \varphi_\gamma, 0)$ functions reduce to Legendre polynomials, $P_k (\cos \theta_\gamma)$. Furthermore if γ-rays are detected only in coincidence with particles scattered backward through large angles an additional simplification occurs. In this case, for zero spins in the entrance channel, the so-called $\mu = 0$ approximation (see Section II-C) applies in which only $M = 0$ magnetic substates are considered to be populated. Then the summation, over M and M', degenerates to a single term. The same factor, $a^{I_i\, 0}_{I\quad 0} \cdot a^{I\, 0}_{I\, 0}$ then occurs in all terms of $W(\theta)$ and hence may be factored out. Thus the angular distribution becomes independent of excitation mechanism and so also of incident ion energy. Thus, no integration over particle energy is required, and furthermore the calculation becomes model-independent. (See Section II-C for a more detailed discussion of the $\mu = 0$ approximation). It also turns out that an error of less

than 2% is introduced into the experimental cross sections if, in addition, one uses a single mean particle scattering angle, θ_{mean}, and omits the integration over particle scattering angle. In the calculations for this thesis a mean scattering angle varying from 165^{o} to 170^{o} has been used.

With the simplifications just discussed the γ-ray angular distribution for the case of particles backscattered into an annular detector becomes (for E2 radiation)

$$W(\theta) = \sum_{k \text{ even}} F_k (2\ 2\ I_f\ I) g_{k0} D^{k*}_{00} (\theta_\gamma, \varphi_\gamma\ 0) \qquad V\text{-}6$$

or, explicitly written out:

$$W(\theta) = F_0 (2\ 2\ I_f\ I) g_{00} + F_2 (2\ 2\ I_f\ I) g_{20} P_2 (\cos\theta_\gamma) + F_4 (2\ 2\ I_f\ I) g_{40} P_4 (\cos\theta_\gamma) \qquad V\text{-}7$$

Dividing by $F_0 (2\ 2\ I_f\ I) g_{00} = g_{00}$ gives:

$$W(\theta) = 1 + F_2 (2\ 2\ I_f\ I) \frac{g_{20}}{g_{00}} P_2 (\cos\theta_\gamma) + F_4 (2\ 2\ I_f\ I) \frac{g_{40}}{g_{00}} P_4 (\cos\theta_\gamma) \qquad V\text{-}8$$

g_{k0} is now given by (setting $I_i = 0$):

$$g_{k0} = 2 \left(\frac{2k+1}{2I+1} \right)^{1/2} \begin{pmatrix} I & I & k \\ 0 & 0 & 0 \end{pmatrix} D^{k*}_{00} \left(\frac{\pi}{2}, \frac{\pi + \theta_{mean}}{2}, 0 \right) \qquad V\text{-}9$$

Once again, the advantages and simplifications of the γ-particle coincidence technique are manifest, for, clearly, if γ-rays in coincidence with all particles are recorded, neither the annular detector, $\mu = 0$ approximation nor the single mean angle simplifications are possible.

In the experiments performed here the γ counters were placed at $\theta = 55^{o}$ to the beam direction and so the $P_2 (\cos\theta_\gamma)$ term in $W(\theta)$ vanishes. Since the coefficient of the $P_4(\cos\theta_\gamma)$ term is generally small, $W(\theta = 55^{o})$ is close to 1.0 and the angular distribution correction factor ultimately alters the experimental

numbers very little. Eq. 8 for $W(\theta)$ is not yet quite complete, though, for it neglects the smearing out of the angular distribution due to the finite size of the γ counter. A complete expression, valid for these experiments (annular particle detector, with $\theta_{min} \geq 155^{o}$, $\theta_{\gamma} = 55^{o}$), and which includes the appropriate solid angle corrections, is:

$$W(\theta = 55^{o}) = 1 + Q_2 \frac{A_2}{A_0} P_2 (\cos 55^{o}) + Q_4 \frac{A_4}{A_0} P_4 (\cos 55^{o})$$

$$= 1 + Q_4 \frac{A_4}{A_0} P_4 (\cos 55^{o})$$

or

$$= 1 - 0.3852 \, Q_4 \frac{A_4}{A_0} \qquad \text{V-10}$$

where $A_k = F_k (22I_f I) g_{ko}$ and where Q_4 is a finite solid angle correction factor for the γ-ray counter. Values of Q_4, corresponding to the geometry of these experiments, were obtained by interpolation from a tabulation by Yates[104]. Eq. 10 was used in the analysis of all the γ-particle data taken. Typical values of $W(\theta_{\gamma} = 55^{0})$ for most transitions are about 1.07. For $2^{+} \rightarrow 0^{+}$ transitions $W(\theta_{\gamma} = 55^{o})$ is typically about 1.30. In the γ singles and γ-γ data the angular distribution correction, though energy dependent, is always less than 1.10 for $\theta_{\gamma} = 55^{o}$.

Tests of the independence of $W(\theta)$ of incident energy and of excitation mechanism were made using the Winther and de Boer computer program[61] with the five magnetic substates through M = 2 considered. The independence was verified to within 1%.

Finally the angular distributions of γ-rays from the stronger transitions were experimentally measured in both direct and γ-particle modes for 48.26 MeV O^{16} ions incident on thick $Os^{186, 188, 192}$ targets and for 70.30 MeV O^{16} ions incident on thick $Os^{188, 192}$ targets. The experimental measurements were carried out at 0^{o}, 55^{o} and 90^{o} to the incident beam and, for the γ-particle cases, are compared, for several transitions, with the theoretical results obtained from eq. 10, in Fig. V-1. $W(\theta)$ is normalized to 1.0 at 55^{o} in these figures. Agreement of experiment with theory is quite good except perhaps for the lowest $2^{+} \rightarrow 0^{+}$ transitions

COMPARISON OF THEORETICAL AND EXPERIMENTAL ANGULAR DISTRIBUTIONS FOR CERTAIN PROMINENT GAMMA RAY TRANSITIONS

(Normalized to 1.0 at 55°,
only sample error bars are shown)

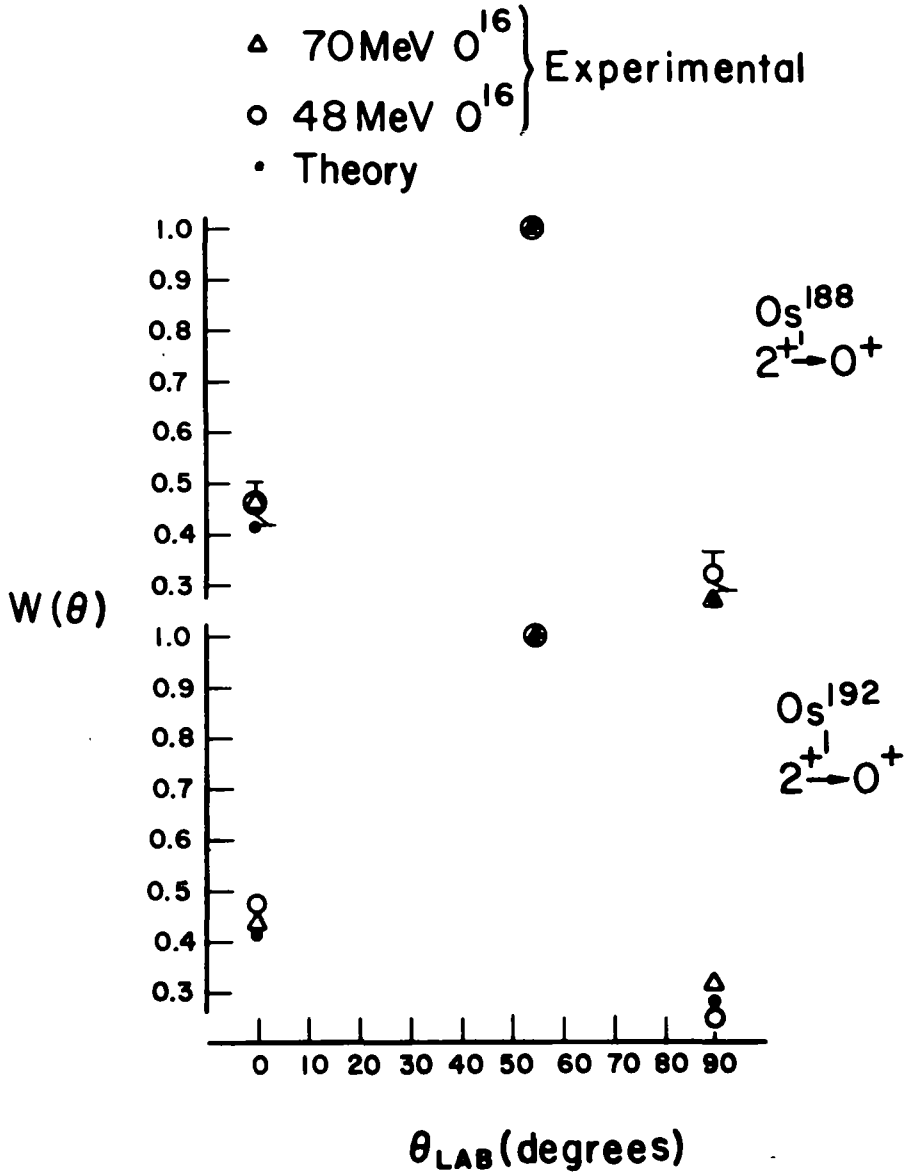

Fig. V-1

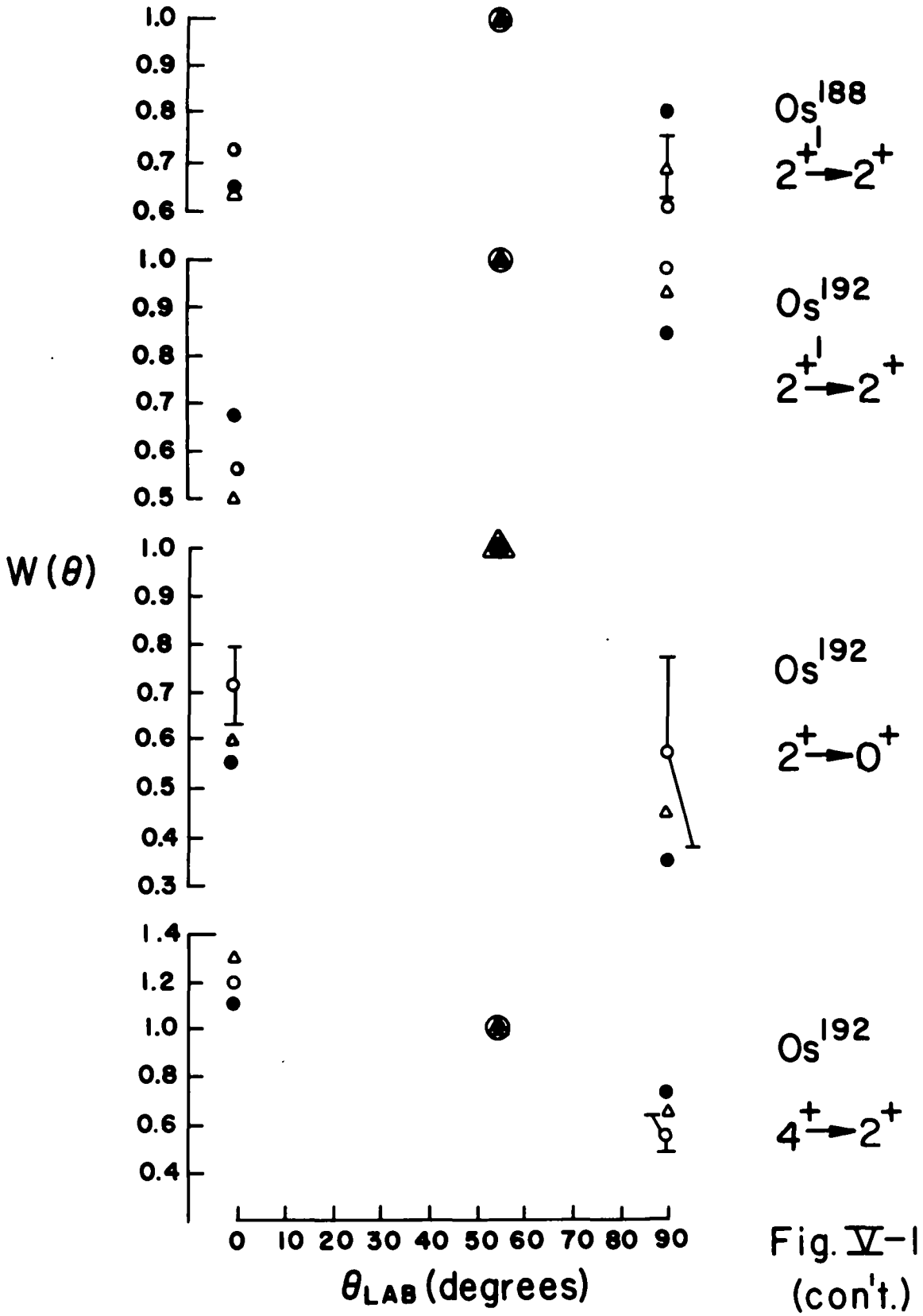
W(θ)
1.0
0.9
0.8
0.7
0.6
0.5
0.4
0.3
1.4
1.2
0 10 20 30 40 50 60 70 80 90
θLAB (degrees)
Os188
2+1 → 2+
Os192
2+1 → 2+
Os192
2+ → 0+
Os192
4+ → 2+

Fig. V-1
(con't.)

at 90^{o}. Here, however, the γ-rays had to pass through large amounts of target material before entering the γ-ray detector and absorption calculations and measurements at 90^{o} for these lowest energy γ-rays are subject to very large errors. Theoretical angular distribution correction factors have been used throughout the data analysis and errors from this source are expected to be always less than 5% .

Returning to a consideration now of eq. 4, we see that in order to extract the total number of real excitations of a given level i, one must sum the fully-corrected quantities $T_{i\rightarrow f}$ over all levels, f, into which level i can decay, and must subtract from this result the sum of all $T_{n\rightarrow i}$, that is, of all contributions to observed transitions $T_{i\rightarrow f}$ due to population of level i via cascades from higher levels. The resulting number for the i^{th} level is called Y_i and is given by

$$Y_i = \sum_{f<i} T_{i\rightarrow f} - \sum_{n>i} T_{n\rightarrow i} \qquad \text{V-11}$$

Strictly speaking, there is a slight error in subtracting the $T_{n\rightarrow i}$'s directly since the angular distribution of γ-rays from level i to some level f is not the same if level i was populated via Coulomb excitation as it is if population resulted from deexcitation of a higher state. In practice, this effect consists of, at most, a 10% correction to a 5% cascade correction, or less than a 1% overall error.

The experimental results at this point have been reduced to a set of numbers, Y_i, representing the total yield of excitations of each nuclear state arising from Coulomb excitation by those O^{16} ions in the energy range $E_{cut} \leq E \leq E_{inc}$ which were backscattered into an annular detector. It is convenient to convert these into probabilities of excitation instead. By doing this one tends to minimize certain sources of error in the calculation of the theoretical numbers corresponding to these experimental results[25]. Thus we now divide the yield for each state by the total integrated numbers of particles, denoted by N, backscattered into the detector with energies above the minimum, E_{min}. The result, $P_{i_{ave}}$, is thus given by

$$P_{i_{ave}} = \frac{Y_i}{N} \qquad \text{V-12}$$

$P_{i_{ave}}$ is an average probability for excitation of state i under the conditions cited above. The theoretical result for the same quantity may now be calculated and the only unknowns remaining, the nuclear matrix elements, may be obtained by fitting the theoretical $P_{i_{ave}}$'s to the experimental. There are several techniques for calculating the theoretical results and to each one corresponds a slightly different manner of comparison with experiment. These considerations are dealt with in the following sections.

B. Extraction of Nuclear Information

We wish to evaluate theoretically the same quantities as obtained experimentally, namely the numbers, $P_{i_{ave}}$. A suitable theoretical expression which achieves this is:

$$P_{i_{ave}} = \frac{\int_{\theta_{min}}^{\theta_{max}} d\Omega \int_{E_{cut_i}}^{E_{inc}} \frac{d\sigma_i}{d\Omega}(\theta, E) \frac{dS}{dE} dE}{\int_{\theta_{min}}^{\theta_{max}} d\Omega \left[\sum_i \int_{E_{cut_i}}^{E_{inc}} \frac{d\sigma_i}{d\Omega}(\theta, E) \frac{dS}{dE} dE \right]} \qquad \text{V-13}$$

The numerator is essentially the thick target integral of the differential cross section for excitation of level i. The denominator is also a thick target integral, but essentially of the number of particles Rutherford scattered into the detector. This becomes clear when it is recalled that $d\sigma_i/d\Omega\ (\theta, E) = \{ d\sigma/d\Omega\ (\theta, E) \}_{Ruth} P_i(\theta, E)$ (see eq. II-61). Thus the denominator may be written as:

$$\text{Den} = \int_{\theta_{min}}^{\theta_{max}} d\Omega \left[\sum_i \int_{E_{cut_i}}^{E_{inc}} \left[\frac{d\sigma}{d\Omega}(\theta, E) \right]_{Ruth} P_i(\theta, E) \frac{dE}{dE/dS} \right] \qquad \text{V-14}$$

The Rutherford cross section must be weighted by the probabilities only because the proper cutoff energies, E_{cut_i}, are functions of the excitation energy of the level i. Thus the inner integral cuts off at different lower limits for each state i.

In practice, the range of integration differs by only about 5% for the ground state and states at about 1 MeV. The integrand also in general decreases rapidly with energy and so the additional range of integration corresponds to the smallest contributions of the integrand to the integral. Furthermore, the weighting factors $P_i(\theta, E)$ for states other than the ground or low-lying first excited states are always less than .10. Consequently, omission of $P_i(\theta, E)$ altogether, and evaluation of the integral from E_{inc} to an E_{cut} corresponding to an excitation energy in the target nucleus midway between the ground and first excited states, leads to errors less than 1%. Thus we can write the theoretical expression to be evaluated as:

$$P_{i_{ave}} = \frac{\int_{\theta_{min}}^{\theta_{max}} d\Omega \int_{E_{cut_i}}^{E_{inc}} \frac{d\sigma_i}{d\Omega}(\theta, E) \frac{dE}{dE/dS}}{\int_{\theta_{min}}^{\theta_{max}} d\Omega \int_{E_{cut}(\Delta E = E_{2^+}/2)}^{E_{inc}} \left[\frac{d\sigma}{d\Omega}(\theta, E)\right]_{Ruth} \frac{dE}{dE/dS}} \qquad V\text{-}15$$

Finally, it has been found that the variation as a function of angle in the value of the integrand over the angular range of interest is essentially negligible for the lowest states excited and about 5% for those excited by the highest order processes. Consequently, as mentioned previously, deletion of the angular integration and replacement of it by evaluation at a mean angle, θ_{mean}, is a highly accurate approximation. Resulting errors thus introduced are less than 2% at most. An additional advantage of this approach is that now $d\Omega$, the solid angle subtended by the particle detector, drops out and errors associated with definition of the sensitive area of the detector are avoided.

The final expression for $P_{i_{ave}}$ is therefore

$$P_{i_{ave}} = \frac{\int_{E_{cut_i}}^{E_{inc}} \frac{d\sigma_i}{d\Omega}(\theta_{mean}, E) \frac{dE}{dE/dS}}{\int_{E_{cut}(\Delta E = E_{2^+}/2)}^{E_{inc}} \left[\frac{d\sigma}{d\Omega}(\theta_{mean}, E)\right]_{Ruth} \frac{dE}{dE/dS}} \qquad V\text{-}16$$

or

$$P_{i_{ave}} = \frac{\int_{E_{cut_i}}^{E_{inc}} \frac{d\sigma}{d\Omega}(\theta_{mean}, E)_{Ruth} P_i(\theta_{mean}, E) \frac{dE}{dE/dS}}{\int_{E_{cut}(\Delta E = E_{2^+}/2)}^{E_{inc}} \left[\frac{d\sigma}{d\Omega}(\theta_{mean}, E)\right]_{Ruth} \frac{dE}{dE/dS}} \qquad V\text{-}17$$

Some of the advantages of considering probabilities rather than yields are now apparent from eq. 17 which shows that errors in E_{inc}, E_{cut}, θ_{mean}, dE/dS and $\left[\frac{d\sigma}{d\Omega}\right]_{Ruth}$ tend to cancel[25]. Eq. 17 is general and is applicable to any Coulomb excitation process provided the P_i appropriate to that process is inserted. In the discussion, therefore, of perturbation theory, model-dependent analyses and the Winther and de Boer program calculations, it is usually necessary

only to consider the evaluation of P_i.

In eq. 17 $\left[\frac{d\sigma}{d\Omega}(\theta, E)\right]_{Ruth}$ is evaluated according to the expression just below eq. II-61. E_{cut_i} is obtained by a straight forward energy loss and kinematics calculation from a knowledge of the minimum acceptible energy in the particle detector spectrum, the excitation energy of level i and the differential energy loss in the target, dE/dS. The latter is obtained by interpolation in Z in range-energy curves of Northcliffe[110]. An expression, quadratic in energy, for the range, S, was fitted[111] to the resulting curve for O^{16} incident on Os. The result, which reproduced the curve to within 0.8% from 24 to 80 MeV is

$$S_{Os}\left(\frac{mg}{cm^2}\right) = 3.1722 + 0.29317E + 0.00178E^2 \qquad V\text{-}18$$

where E is in MeV. Differentiation yields

$$\left(\frac{dE}{dS}\right)_{Os} = \frac{1}{0.29317 + 0.00356E} \qquad V\text{-}19$$

as the final result.

The cutoff energy, E_{min}, in the particle detector spectrum is obtained after energy calibration of the detector is made using several accurately known incident beam energies as essentially monoenergetic sources of O^{16} ions. Some extrapolation to low energies usually had to be made to obtain E_{min}. The values of E_{cut_i} ranged from about 36 MeV to about 66 MeV in the different runs. Errors associated with E_{cut_i} are certainly less than $\pm$ 1 MeV and probably, more realistically, about $\pm$ 0.5 MeV. The thick target integrations generally involve an energy range of 6-13 MeV.

Once dE/dS and E_{cut} are known, the denominator of eq. 17 can be evaluated once and for all for a given run on a given nucleus. This was done in all cases using a computer program[25, 27] which evaluated the integrand at a series of energies and performed a numerical integration via Simpson's rule. The numerator of eq. 17 was likewise usually evaluated by a similar thick target integration routine into which the probabilities P_i were inserted as data or were calculated in a subprogram.

In this and the preceding section several approximations have been discussed. These have been related to estimation of peak areas, evaluation of W (θ), calculations of the theoretical $P_{i_{ave}}$, and the like. In practice, the data analysis has indeed been performed with these approximations but additional treatments have been performed without them both to obtain more accurate final numbers and to check on the magnitudes of the errors involved as a result of the set of approximations. The overall errors stemming from these sources is, in all cases, less than 4% and are much less, therefore, than other sources of error.

C. Perturbation Theory Analysis

If the probabilities for excitation in a given scattering event are small, then first or second order perturbation theory may be applied. This method has the advantage that the calculated probabilities of excitation are directly proportional to B(E2) values which are therefore easy to extract from the data by equating theoretical and experimental expressions for the quantities $P_{i_{ave}}$. Such calculations have been applied to the excitation of the 2^+, 4^+ and $2^{+\prime}$ states in $Os^{186, 188, 190, 192}$ for both 48.26 and 70.30 MeV incident O^{16} ions.

The expressions for the cross sections from perturbation theory were discussed briefly in Chapter II. Here, we give results in a form convenient for numerical calculations. In all the results cited below we have substituted $Z_{O16} = 8$, $A_{O16} = 16$, $Z_{Os} = 76$ and $A_{Os} = 189$ and have set all factors $(1 + \frac{\Delta E}{E})^n$ equal to 1.0. $\Delta E/E$ is typically about .01. The use of $A_{Os} = 189$ is an approximation for convenience here which is nevertheless quite accurate since A_{Os} enters the expressions only through the factor $(1 + A_{O_{16}}/A_{Os})$. In actual calculations for each nucleus the correct value for A_{Os} was used. All the results below correspond to excitations induced by an incident O^{16} ion of energy E scattered through a center of mass angle θ.

The probability for excitation of a 2^+ state by direct E2 excitation is obtained from eq. II-71 in first order perturbation theory, and is given by

$$P_{2^+}^{(1)} = \frac{d\sigma_{2^+}^{(1)}}{d\sigma_{Ruth}} = \frac{0.203\, E^3\, df^{(1)}(\theta, \xi)}{\sin^{-4}(\theta/2)} B(E2{:}0^+ \rightarrow 2^+) \qquad V\text{-}20$$

where ξ, the adiabaticity parameter, $B(E2{:}0^+ \rightarrow 2^+)$, and $df^{(1)}$ are quantities defined in Chapter II. The superscript (1) denotes a first order process.

Second order perturbation theory is applicable to the excitation of 4^+ states and to the route 0^+ (E2) 2^+ (E2) $2^{+\prime}$ which accounts for some of the excitation of the $2^{+\prime}$ states. From ABHMW we obtain for $P_J^{(2)}$ the result:

$$P_J^{(2)} = \frac{1.02 \times 10^{-10}\, E^6\, dF(\xi_1, \xi_2, \theta, J)}{\sin^{-4}(\theta/2)} B(E2{:}0^+ \rightarrow 2^+) \times B(E2{:}2^+ \rightarrow J^+) \qquad V\text{-}21$$

where, again, the quantities are all defined in Chapter II or reference 60. J is the spin of the final state and E is in MeV in eq. 21 (and below, eq. 23, as well).

In the excitation of the $2^{+'}$ state the cross section is actually given to second order by eq. II-73, namely,

$$d\sigma_{2^{+'}} = d\sigma^{(1)}_{2^{+'}} + d\sigma^{(2)}_{2^{+'}} + d\sigma^{(1,2)}_{2^{+'}} \qquad \text{V-22}$$

as discussed in Chapter II. There is an uncertainty in a calculation using eq. 22 since the relative sign of the reduced matrix elements $<0^{+} \| E2 \| 2^{+'}>$ and $<2^{+} \| E2 \| 2^{+'}>$ in general is not known. It may in principle be determined if measurements are made at several bombarding energies. Then that sign is chosen which yields constant B(E2) values as a function of incident energy. Such a procedure has been used here and indicates that a relative plus sign is to be favored as more consistent with the data. The negative sign is not entirely ruled out. Since the excitation amplitudes are complex the interference term may actually be larger than the double excitation term and should not be ignored. It ranges from approximately 7% to 25% of $d\sigma_{2^{+'}}$ as one goes from Os^{192} to Os^{186}. (For $E_{2^{+'}} = 2E_{2^{+}}$ it is zero and generally increases as $E_{2^{+'}}$ departs further and further from this value. This explains the variation in percentage cited just above.) The result for the probability of excitation via the interference term is given by

$$P^{(1,2)}_{2^{+'}} = 2.52 \times 10^{-8} E^{9/2} df^{(1,2)}(\xi_1, \xi_2, \theta) \left[B(E2{:}0^{+} \rightarrow 2^{+'}) \, B(E2{:}0^{+} \rightarrow 2^{+}) \times B(E2{:}2^{+} \rightarrow 2^{+'}) \right]^{1/2} \qquad \text{V-23}$$

See ABHMW for a definition and tabulation of $df^{(1,2)}$. $\mathrm{Sin}^{-4}(\theta/2)$ appears in eqs. 20 and 21 for $P^{(1)}$ and $P^{(2)}$, respectively, but not in eq. 23 for $P^{(1,2)}$ merely because the df functions are defined slightly differently in the two cases.

In the calculation of the excitation probabilities for the $2^{+'}$ states the full expression to second order is analogous to eq. 22:

$$P_{2^{+'}} = P^{(1)}_{2^{+'}} + P^{(2)}_{2^{+'}} \pm P^{(1,2)}_{2^{+'}} \qquad \text{V-24}$$

(This neglects effects of finite quadrupole moments (see Chapter VI).) If we denote by A, B and C all the factors in eqs. 20, 21 and 23 respectively except for the B(E2) values, then the expression for the excitation probability of a $2^{+'}$ state may

be written:

$$P_{2^{+'}} = \left[A + B \left[B(E2{:}0^{+} \rightarrow 2^{+}) R \right] \pm C \left[B(E2{:}0^{+} \rightarrow 2^{+}) R \right]^{1/2} \right] \times B(E2{:}0^{+} \rightarrow 2^{+'}) \quad V\text{-}25$$

where R is the branching ratio: $B(E2{:}2^{+} \rightarrow 2^{+'})/B(E2{:}0^{+} \rightarrow 2^{+'})$ and is known experimentally. From the excitation of the first excited state $B(E2{:}0^{+} \rightarrow 2^{+})$ can also be determined and so the only unknown in eq. 25 is $B(E2{:}0^{+} \rightarrow 2^{+'})$ which can then be determined by comparison with experimental excitation probabilities.

For thick targets, the method of analysis, via perturbation theory, consists then of simply inserting the appropriate P_i into eq. 17 and integrating. For thin targets the analysis is simpler for no integration is needed. A further discussion of the validity of the perturbation expansion and of the contributions to it from neglected terms of the same orders as those included is contained in Chapter VI.

D. Model Dependent Calculations

As discussed previously (Section II-C), when the excitation probabilities are too high for perturbation theory to be valid one must either fit the experimental data using a full set of nuclear matrix elements by solving the coupled Schrodinger equations (eqs. II-68) or one must assume some model relationship among these matrix elements. Calculations of the latter kind have been carried out for the ground band states of the even-even Os nuclei studied using Alder's theory of multiple Coulomb excitation (See Section II-C). The probabilities to be inserted in eq. 17 are obtained by interpolation from tables given by Alder[64]. The interpolation is done by a computer program[27] which evaluates the probabilities P_J, as functions of the parameters q and ξ, defined in Chapter II, by equating them to seventh degree polynomials in $\chi = \frac{q}{1.6771}$. With these values of P_J the code can then evaluate the integrand of the numerator of eq. 17 at any desired energy and proceed to perform the numerical integrations. The input data to the program consists of A_1, Z_1, A_2, Z_2, E_{min}, dE/dS, E_{inc}, the excitation energy, ΔE_{2+}, of the first excited state, and the $B(E2:0^+ \rightarrow 2^+)$ value. Other ground band energies and B(E2) values are calculated from the last two quantities using eqs. II-12, 14, respectively. Tests of the degree to which the rotational model is applicable to each nucleus are obtained by comparing theoretical and experimental excitation probabilities as a function of beam energy.

In actual nuclei, the energies of the ground state rotational band members do not rigorously obey eq. II-12, as assumed by the Alder theory, but rather an equation of the form of eq. II-17. Thus a source of error is implicitly introduced into the calculations. This can, however, be partially avoided[25, 70] by using for ΔE_{2+}, not its actual value, but a separate, mocked-up number for each state J. These latter are obtained by using, in eq. II-12, an effective moment of inertia for the state J calculated so that eq. II-12 gives the correct energy difference $(E_J - E_{J-2})$. Since the excitation probability P_J depends more strongly on $\Delta E_{(J \rightarrow J-2)}$ than on any other transition energy, a significant improvement in its calculation can thereby be obtained. One thus removes errors in excitation energies from the calculations and resulting discrepancies with experimental numbers can

then be attributed to deviations of the actual B(E2) values from those assumed by the rotational model.

Model-dependent calculations based on the multiple Coulomb excitation theory of Lutkin and Winther[65] have also been performed. This theory has been discussed in Section II-C and, like the Alder theory, involves the assumption of the rotational model. It enables one to extract $B(E2:0^+ \rightarrow 2^{+\prime})$ values by assuming the direct first order perturbation theory result for the transition between the ground state and γ-vibrational bands and by including the effects of virtual multiple Coulomb excitation in factors B(q) which essentially "redistribute" the final state excitation probabilities within the γ-band.

E. Complete Calculation via the Coupled Schrodinger Equations

If possible one would like to avoid both the perturbation expansion and the model-dependent calculations. To do this one must solve the coupled Schrodinger equations (eqs. II-68) for the time dependent excitation amplitudes. Winther and de Boer[61] have written a computer code which does precisely this. For given bombarding conditions, the program solves eq. II-68 by numerical integration over time, that is, over the orbit of the incident projectile.

The nuclear matrix elements M_{ij} or $M_{J_i \rightarrow J_j}$ in the equations are considered as theoretical input data to the program and their values are determined by fitting the calculated excitation probabilities for the several states to the corresponding experimental results. (Further discussion of the program is contained in Section II-C.)

As mentioned several times previously, it was found in the Coulomb excitation calculations with this program that, frequently, only the M = 0 magnetic substate was required. Occasionally (for lower bombarding energies and more indirectly excited states), the $M = \pm 1$ substates were also used. The code has an accuracy control which is specified by the quantity, a_c, defined in reference 61. Accuracies in excitation cross sections and probabilities of $\pm$ 1% are obtained for O^{16} ions incident on Os and backscattered at angles $\theta \geq 155^{\circ}$ if $a_c \leq 0.001$.

The Winther and de Boer program is especially suitable for thin target experiments since it calculates the excitation probabilities at a given incident energy. For thick targets the probabilities P_i must be inserted in eq. 17 and the integrations over energy performed. This involves the repeated use of the code at many different energies. Since this can be quite an expensive computational chore, the program was modified in certain respects and major portions of it were incorporated as a subprogram into a main program which performs the integrations over energy for each of the excited states. Cost considerations necessitated a modified integration routine which lessened the number of energies at which the P_i were required. Details of this thick target version of the code are given in Appendix II. The output of the new code is a set of fully evaluated

numerators of eq. 17, each one corresponding to the excitation of a different excited state.

With the use of both the thick and thin target programs considerably greater insight was obtained concerning the Coulomb excitation mechanism and the role of the various matrix elements involved in the excitation processes. In particular it was found that the set of matrix elements required to fit the experimental results at a given incident energy was not unique but that if data at several energies was available a unique set could often be obtained. This is particularly so if the states involved are predominantly excited via only one route, as is the case for levels in the ground state rotational band. When two common excitation routes are present, other information (such as branching ratios) is generally needed in order to pin down the matrix elements. Further discussions of the results of this form of data analysis are contained in the next chapter.

F. Errors

The largest sources of error involved are often those concerned with determination of photopeak areas. These errors vary greatly from transition to transition depending on the intensity of the transition, the ease of estimation of backgrounds and the proximity in energy of other transitions. The errors assigned to the determination of peak ares vary from about 5% or less for the most intense peaks to about 20-30% for very weak peaks containing less than 100-200 counts.

In obtaining the experimental yields, errors in absorber corrections, detector efficiency factors, photopeak-to-total ratios, angular distributions, electron conversion coefficients, cascade corrections, analyzer dead time and accidental coincidence corrections must all be included. Several of these have already been discussed in previous sections. Most are quite small. Except for the uncertainty in conversion coefficients for the decay of the first excited states of $Os^{186, 188}$, the largest errors are often due to absorber corrections. This is especially the case for the lower energy transitions. The resultant of these sources of error is about 18% for the $2^+ \rightarrow 0^+$ transition in Os^{188}, about 15% for the same transition in Os^{186} and about 5-10% for the other transitions observed.

In view of the above, the experimental quantities $P_{i_{ave}}$ are assigned overall errors ranging from 10 to 40%, with most values having assigned errors of 10-15%. Estimations of certain sources of error (such as those due to disagreement of theoretical and experimental internal conversion coefficients) involve value judgements that make it difficult to quote uncertainties as standard deviations. This has, however, been attempted as far as possible.

Additional uncertainties arise in the calculation of the averaged theoretical excitation probabilities. Among these are uncertainties in the previously defined quantities dE/dS, E_{cut} and θ_{mean}, as well as in interpolation in tables of functions needed in the evaluation of the quantities P_i in eq. 17. The magnitudes of these errors have been analyzed both here and elsewhere[25, 27]. As has been noted in the discussion of eq. 17, many of these tend to cancel. The degree of consistency of both thick and thin target results is itself a check and limitation

on the errors involved in the calculation of eq. 17 and on absorber corrections as well.

All the experimental B(E2) values tabulated in later sections have been assigned resultant uncertainties that take into account all known sources of error.

VI. PRESENTATION AND INTERPRETATION OF EXPERIMENTAL RESULTS

This chapter contains a consideration of the most important results and conclusions of these studies. Conceptually, it can be divided into three topics centering on the experimental excitation probabilities themselves, on the Coulomb excitation reaction mechanism and its relation to the various calculational techniques, and on the comparison of the experimental results (chiefly B(E2) values and branching ratios) with the predictions of the various macroscopic and microscopic nuclear models. The first topic is dealt with immediately below and, while the next two are in part discussed in order, they are closely related (e.g., the rotational model and Alder's multiple Coulomb excitation theory) and consequently the discussion of each is largely intermingled with that for the other.

From the discussion of Section V-A we recall that the primary experimental results obtained in this research consists of the numbers, $P_{i_{ave}}$. These are equal to the average excitation probabilities, per backscattered ion (with $E \geq E_{min}$), of the various levels (indexed by i). They have been obtained as a function of incident O^{16} energy and the results are tabulated below. The experimental conditions under which the $P_{i_{ave}}$ were obtained were all quite similar in their essential aspects. The data used for this purpose were the γ-particle coincidence measurements. Details as to the position of the γ-ray and particle detectors, and the absorbers used to eliminate low energy γ-rays, are found in Section III-A.

Table VI-1 presents a complete tabulation of all experimental excitation probabilities obtained. The top row of the table lists the incident O^{16} energy and the nature of the target bombarded (i.e., thick or thin). The first column on the left indicates the level whose excitation is being considered. All entries relate to a specific run except those for 62.10 MeV O^{16} ions incident on a thin Os^{192} target which are an average of two runs. The two relevant runs in this case actually gave results consistent with each other to better than 5% for all excitation probabilities.

Table VI-2 lists similar results for the three transitions, of uncertain origin, at energies of 780, 840, and 855 kev in $Os^{188, 190, 192}$. The entries in this table are not excitation probabilities since we only observed weak deexcitation γ-rays

TABLE VI-1. EXPERIMENTAL EXCITATION PROBABILITIES

Excitation probabilities of the indicated levels obtained with O^{16} ions incident on thick or thin targets at various energies.

E(MeV) / Level	42.00 Thick	48.26 Thick	48.26 Thin	62.10 Thick	62.10 Thin	70.30 Thick	70.30 Thin	80.00 Thick
Os^{186}								
2^+		.250		.396		.465		
4^+		.0121		.0511		.0868		
$2^{+'}$		.00439		.0167		.0276		
6^+		.00042		.00292		.00635		
$4^{+'}$		.00057		.00256		.00592		
Os^{188}								
2^+	.132	.188		.354	.403	.433	.436	.367
4^+	.00271	.0054		.0328	.0480	.0615	.0790	.0880
$2^{+'}$	.00326	.00566		.0238	.0291	.0366	.0449	.0553
6^+	------	------		.00036	.00063	.00142	.00241	.0040
$4^{+'}$	------	------		.00195	.00473	.00592	.0090	.0117
$0^{+'}$	------	------		.00022	.00046	.00055	.0015	----
Os^{190}								
2^+	.1169	.167		.332		.399		
4^+	.00168	.00348		.0227		.0452		
$2^{+'}$	.00438	.00814		.0308		.0493		
6^+	------	------		.00057		.00144		
$4^{+'}$	------	------		.00138		.00248		
Os^{192}								
2^+	.107	.1445	.180	.311	.337	.382		
4^+	.00108	.00249	.00527	.0179	.0298	.0327		
$2^{+'}$	.00478	.00795	.0135	.0283	.0395	.0479		

TABLE VI-2. EXPERIMENTAL PROBABILITIES OF OBSERVATION OF HERETOFORE UNOBSERVED TRANSITIONS

Target Nucleus	Transition Energy (kev)	O^{16} Bombarding Energy (in MeV) Target Descriptions		
		62.10 Thick	62.10 Thin	70.30 Thick
Os^{188}	780	0.00019	-----	0.00030
Os^{190}	840	0.00020	-----	0.00043
Os^{192}	855	0.00015	0.00046	0.00062

of the above energies and cannot be certain that no other decay branches exist. (In Os^{188} a second deexcitation path via the first excited state is, in fact, indicated by the γ-γ data.) Thus the entries in Table VI-2 are only probabilities (again, per backscattered ion) of observation of the relevant deexcitation transitions.

From the experimental γ-ray intensities one can obtain branching ratios for those states that decay by more than one route. Since such a ratio is independent of excitation mechanism, it is independent of mode of detection. We present, in Table VI-3, for the four isotopes studied, the ratios

$$\frac{I_{2^{+'}\rightarrow\ 2^{+}}}{I_{2^{+'}\rightarrow\ 0^{+}}} \qquad \text{and} \qquad \frac{B(E2{:}2^{+'}\rightarrow\ 2^{+})}{B(E2{:}2^{+'}\rightarrow\ 0^{+})}$$

obtained from both the γ-particle and γ-singles measurements. The branching ratios extracted from runs at different bombarding energies are internally consistent to within $\pm$ 4% in all cases.

Tables VI-1, 2, 3 summarize most of the quantitative information garnered. In Chapter III we presented other information, obtained from a composite consideration of all three modes of measurement, pertaining to the nature (J^{π}) of the levels excited and to the decay schemes of the four osmium isotopes.

The excitation probabilities from Table VI-1 are of interest in themselves for they reveal neatly the systematics in this transition region. In order to illustrate this more clearly we present graphs, in Fig. VI-1, of the excitation probabilities for the various states as a function of O^{16} energy. For the measurements on thick targets the O^{16} energies used are not the bombarding energies but rather weighted mean energies in the target, determined separately for each state. That is, for each state we determine, from the Winther and de Boer program calculations, the energy at which the excitation probability for that level is the same as the experimentally weighted average excitation probability for the thick target. It is the energy obtained by this procedure that we call the mean energy and use in Fig. VI-1. Due to somewhat different cutoff energies, E_{min}, the mean energies for each type of state in Os^{186} are not necessarily identical to the mean energies for a similar state in the other three isotopes.

From Table VI-1 and Fig. VI-1 then, we see that, in going from Os^{186} to Os^{192}, the ground state band excitation probabilities gradually decrease in a smooth

TABLE VI-3. EXPERIMENTAL RATIOS OF γ-RAY INTENSITIES AND B(E2) VALUES

Isotope	Mode of Measurement	$\frac{I_{2^{+'} \rightarrow 2^{+}}}{I_{2^{+'} \rightarrow 0^{+}}}$	$\frac{B(E2:2^{+'} \rightarrow 2^{+})}{B(E2:2^{+'} \rightarrow 0^{+})}$
Os^{186}	γ-particle	1.00	2.66
	γ-singles	1.04	2.77
Os^{188}	γ-particle	0.862	3.54
	γ-singles	0.850	3.45
Os^{190}	γ-particle	-----	----
	γ-singles	0.892	6.90
Os^{192}	γ-particle	0.763	11.76
	γ-singles	0.753	11.60

(Errors on the entries in the table are $\pm$ 5%.)

EXPERIMENTAL EXCITATION PROBABILITIES

(For clarity only sample error bars are shown)

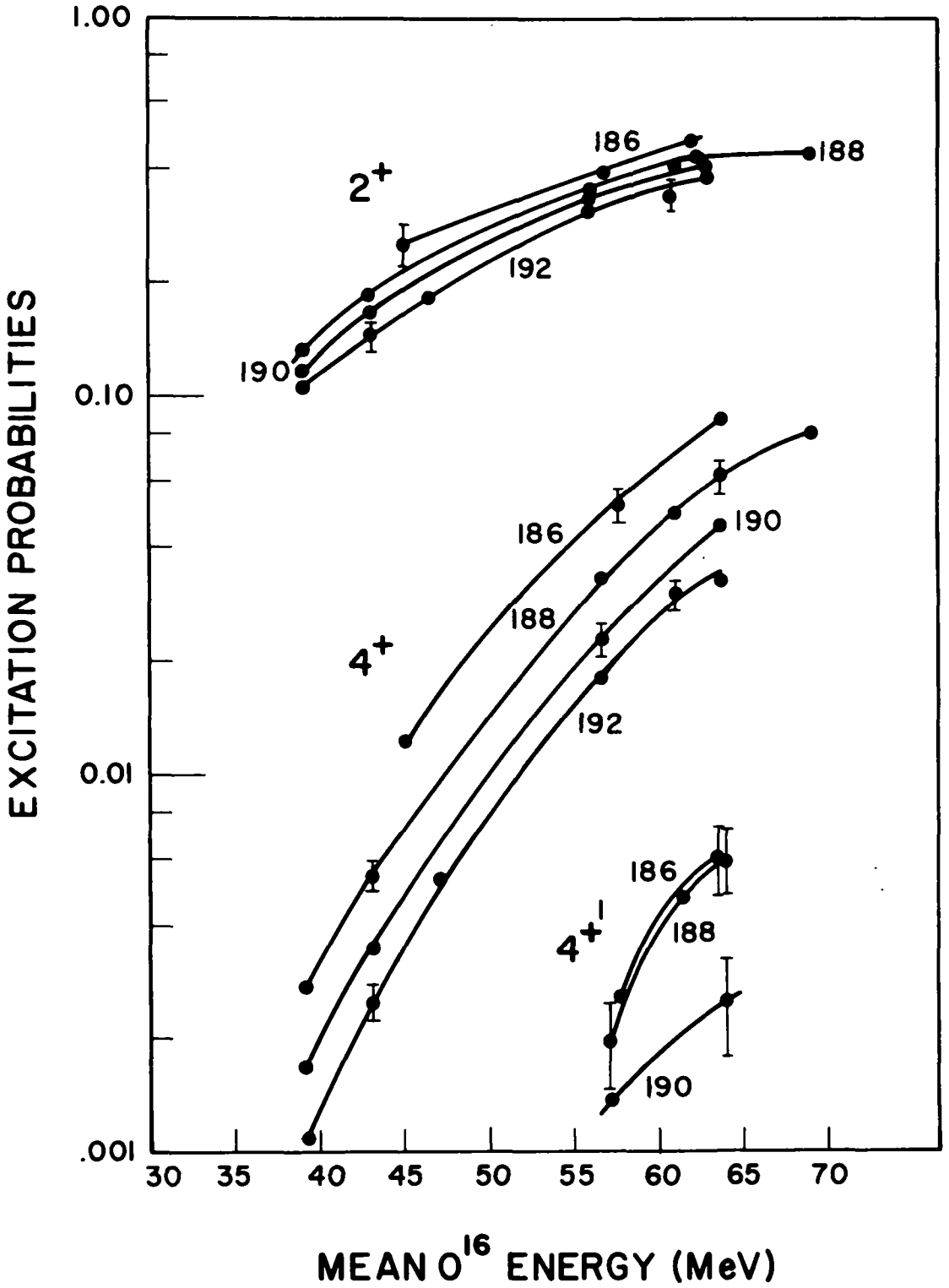

Fig. VI-1

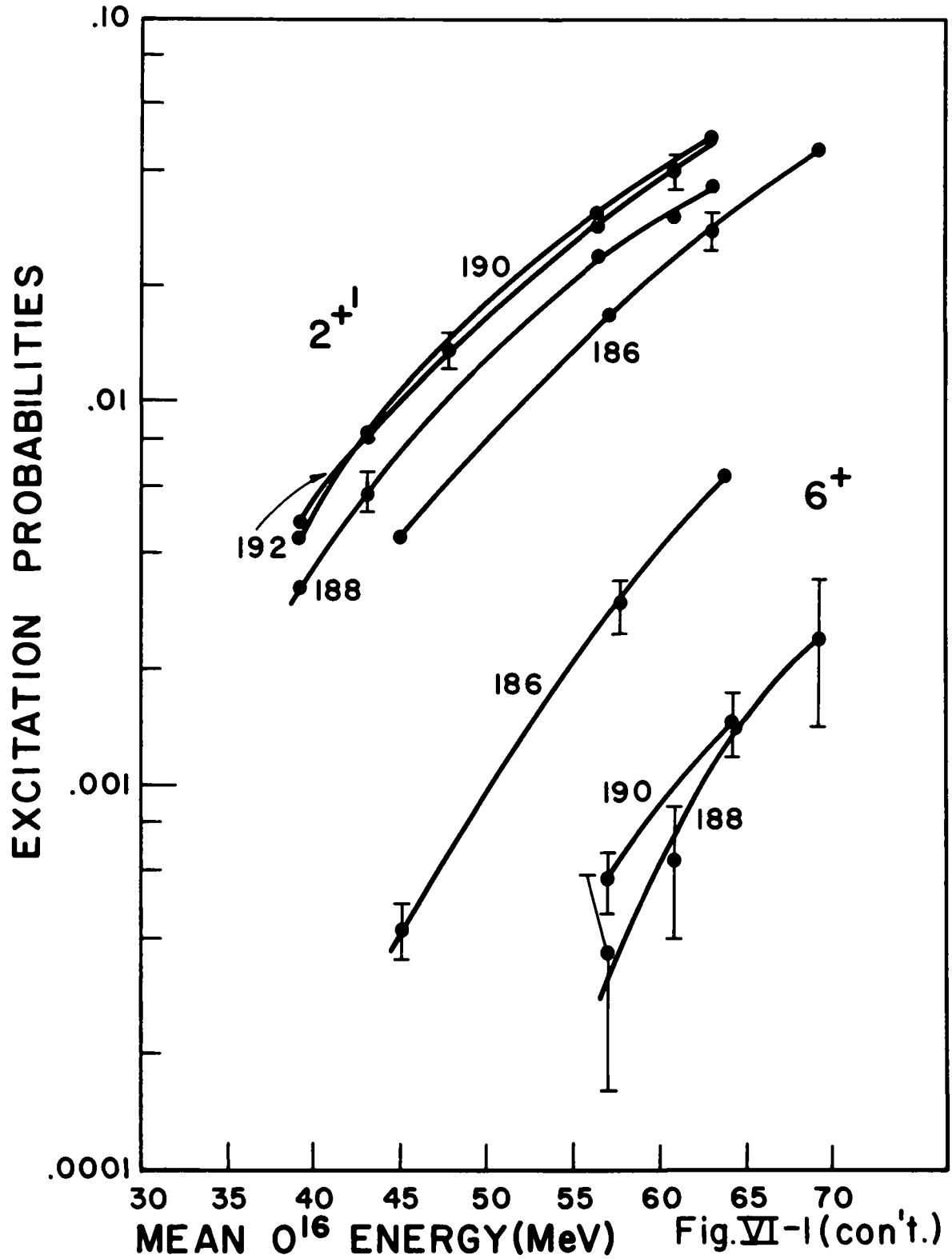
.10
.01
.001
.0001
EXCITATION PROBABILITIES
2+1
190
186
192
188
6+
186
190
188
30
35
40
45
50
55
60
65
70
MEAN O16 ENERGY(MeV)

Fig. VI-1 (con't.)

manner. This is in line with what the general systematics in this region would indicate since, as one approaches Os^{192}, nuclear deformation is decreasing, ground band excitation energies are increasing, and mixing with other (e.g., $2^{+'}$ or quasi-particle) states is reducing the mutual overlap integrals and E2 transition moments of the ground band states. All these factors point to smaller B(E2) values and excitation probabilities.

The only exceptions to the empirical observations above are the excitation probabilities for the 6^+ state in Os^{188}. They are less than or equal to the analogous numbers in Os^{190} whereas one would expect them to lie between those for Os^{190} and Os^{186}. The systematics is otherwise so consistent that this inconsistency in fact makes one tend to suspect the experimental numbers for this state in Os^{188}. It will be recalled (Section III-C) that the $6^+ \rightarrow 4^+$ deexcitation γ-rays in Os^{188} are masked by the $2^{+'} \rightarrow 2^+$ and $4^{+'} \rightarrow 4^+$ transitions and that extraction of the $6^+ \rightarrow 4^+$ intensity was indeed beset by large errors. Thus one should not lay too great reliance on results obtained later in this chapter pertaining to the 6^+ state in Os^{188} although the large uncertainties ($\pm$ 40%) associated with such results almost certainly include any experimental errors. As can be seen, an error of only 20% on the low side for the 6^+ state's excitation probabilities would be sufficient to remove the apparent inconsistency noted above with this region's systematics.

Continuing our comments on systematics, we observe that the $2^{+'}$ state excitation probability increases from Os^{186} to $Os^{190, 192}$. This is consistent with that state's gradual decrease in energy and with its transformation from a "γ-vibrational" state weakly coupled to the 0^+ and 2^+ states to a "two phonon" state strongly coupled to the 2^+ state. The $4^{+'}$ state, on the other hand, should be successively less readily populated in $Os^{186, 188, 190, 192}$ since it changes in structure from an ordinary γ-band member to a complicated state probably approximated somewhat by a "three phonon" excitation not directly coupled at all to the 0^+ or 2^+ states. This trend is indeed evidenced by the data and in fact no $4^{+'}$ excitation is observed at all in Os^{192}.

This feature in the latter nucleus is nicely complemented by the corresponding lack of observation of any 6^+ state excitation. If a 6^+ level does exist in Os^{192} it can hardly be expected to be a good ground state rotational band member any more than the $4^{+'}$ level has remained a pure γ-vibrational state. Rather, again like

the $4^{+'}$ state, it is approaching in nature a structure somewhat like "a three phonon" excitation. The analogous decrease in excitation probabilities of the 6^+ and $4^{+'}$ states in $Os^{186, 188, 190}$ and the sudden lack of any observed excitation of either in Os^{192} is thus consistent with the view that both states are undergoing similar transformations in this region.

The branching ratios of Table VI-3 can also be considered in the light of general trends in the osmium nuclei. The ratio is 2.66 for Os^{186} and 11.76 for Os^{192} with a smooth increase in between. As the vibrational limit is being approached in Os^{192} the $2^{+'}$ state is becoming weakly coupled to the ground state and more strongly coupled (through a quadrupole phonon excitation) to the 2^+ state. Thus a large branching ratio is consistent (recall eq. II-6) in Os^{192}. On the other hand, in a rotational nucleus, the intrinsic matrix elements connecting the $2^{+'}$ state to the 2^+ and 0^+ states are identical and the branching ratio is determined only by "geometric" details, i.e., mathematically, by a ratio (= 1.43) of Clebsch-Gordan coefficients (see eq. II-15).

A more quantitative consideration of the applicability of the phenomenological models (the rotational model, in particular) to the osmium nuclei can also be approached via the model-dependent multiple Coulomb excitation theories outlined in Section II-C. The Alder[64] theory has been applied to the calculation of the excitation probabilities for the members of the ground state band.

Since the best way to measure the required input numbers, $B(E2:0^+ \rightarrow 2^+)$, in the Alder theory is not with high energy O^{16} ions but with lower energy protons or alpha particles or by lifetime measurements, the $B(E2:0^+ \rightarrow 2^+)$ values used in these calculations have been taken from the literature[58, 70, 71, 116]. An effective moment of inertia (see Section V-D) for each state has been used to mock up the energy difference $\Delta E_{2^+ \rightarrow 0^+}$ so that the latter correctly reproduces the larger and more important energy difference $\Delta E_{J \rightarrow (J-2)}$. The results of these calculations are contained in Table VI-4 which gives the calculated excitation probabilities for the four isotopes at the various bombarding energies on both thick and thin targets. Fig. VI-2 is a plot of the ratio of experimental to calculated probabilities as a function of "mean" O^{16} energy (the manner in which to construe "mean" is described above). In interpreting this figure one obtains a somewhat clearer picture of the applicability of the rotational model to the ground band states

TABLE VI-4. THEORETICAL GROUND STATE BAND EXCITATION PROBABILITIES CALCULATED ACCORDING TO ALDER'S MULTIPLE COULOMB EXCITATION THEORY

This table is to be compared with Table VI-1. Therefore, entries are inserted only for those cases in which corresponding results were measured and inserted in Table VI-1.

E(MeV) / Level	42.00 Thick	48.26 Thick	48.26 Thin	62.10 Thick	62.10 Thin	70.30 Thick
Os^{186}						
2^+		0.236		0.414		0.482
4^+		0.00111		0.0510		0.0885
6^+				0.00229		0.00593
Os^{188}						
2^+	0.144	0.188		0.375	0.440	0.458
4^+	0.00274	0.00632		0.0371	0.0586	0.0716
6^+		-------		0.00138	0.00266	0.00416
Os^{190}						
2^+	0.110	0.153		0.322		0.409
4^+	0.00122	0.00377		0.0255		0.0506
6^+		--------		0.00080		0.00244
Os^{192}						
2^+	0.0921	0.128	0.179	0.285	0.350	0.371
4^+	0.00066	0.00250	0.00597	0.0190	0.0312	0.0386

COMPARISON OF EXPERIMENTAL GROUND STATE BAND EXCITATION PROBABILITIES WITH THOSE CALCULATED USING ALDER'S THEORY OF MULTIPLE COULOMB EXCITATION

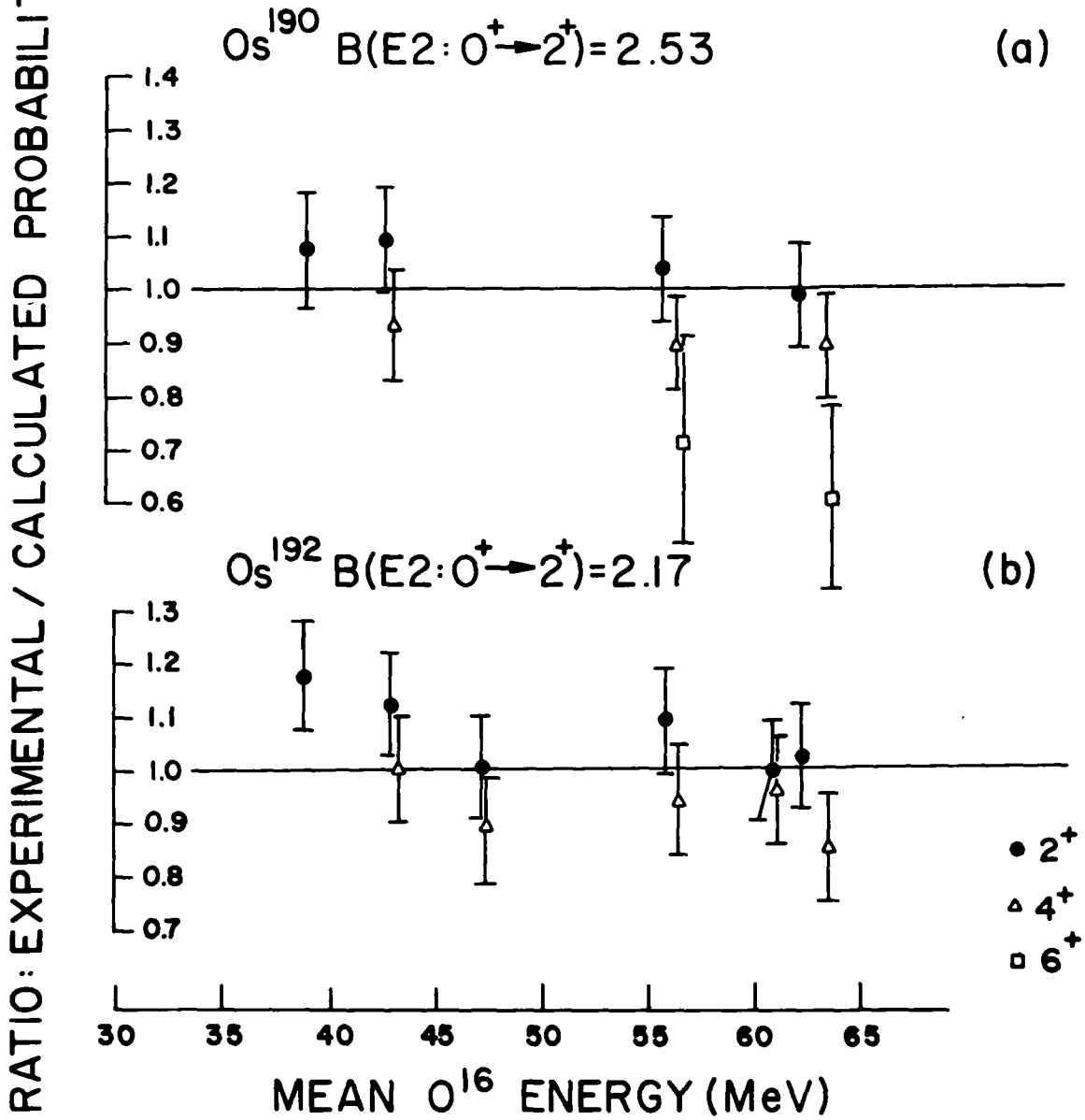

Fig. VI-2

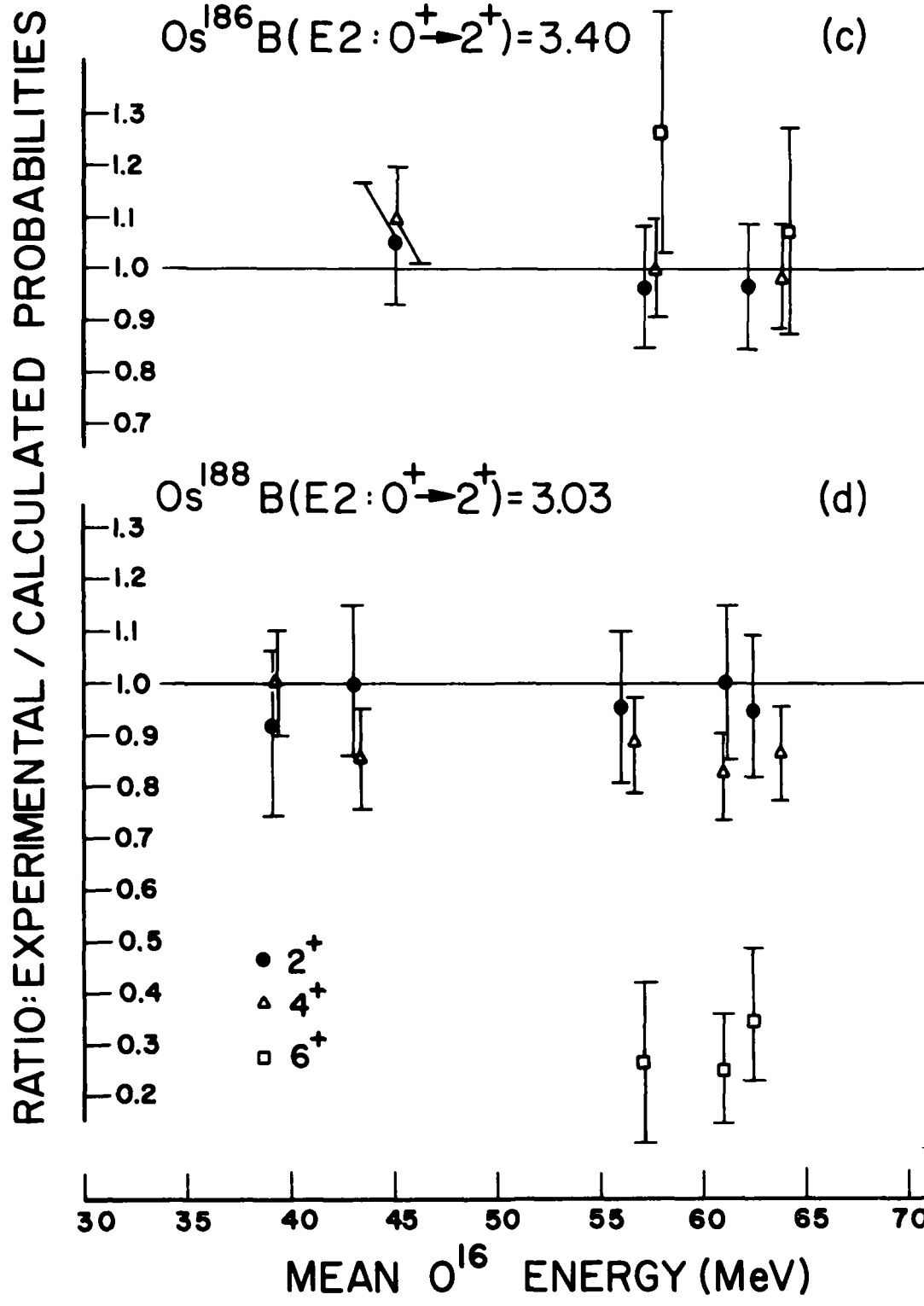
Os^{186} B(E2 : $0^+ \rightarrow 2^+$) = 3.40
(c)
Os^{188} B(E2 : $0^+ \rightarrow 2^+$) = 3.03
(d)
RATIO: EXPERIMENTAL / CALCULATED PROBABILITIES
1.3
1.2
1.1
1.0
0.9
0.8
0.7
0.6
0.5
0.4
0.3
0.2
2^+
4^+
6^+
30
35
40
45
50
55
60
65
70
MEAN O^{16} ENERGY (MeV)

Fig. VI-2 (con't.)

if the deviations of the ratios for the 4^+ and 6^+ states are taken as those that would result were the $B(E2:0^+ \rightarrow 2^+)$ values adjusted to normalize the 2^+ state ratios to 1.0. In any case, it is clear that the results are actually quite close to unity, the ideal case for a pure rotor, with mildly increasing deviations from this value as the transition region is traversed.

One would, of course, expect fairly good agreement for the first excited state since the experimental value for the quantity $B(E2:0^+ \rightarrow 2^+)$ is actually used in the calculations. Thus, if the predicted 4^+, 6^+ state excitation probabilities are given even remotely correctly, the virtual depopulation (only $\cong$ 15% at most anyway) of the 2^+ state will be decently approximated and the final 2^+ excitation probabilities accurately predicted. This is indeed seen to be the case. However, if the rotational model in these nuclei is not accurate then one would expect populations of the higher levels to be incorrectly given. Deviations toward the vibrational (or spherical) limit would weaken the coupling among the ground state band members. Thus the excitation probabilities for 4^+ and 6^+ states, calculated as they are in the rotational limit, should exceed the experimental or, at least the ratios for these states should be lower than for the 2^+ state. In almost all cases this is so, as Fig. VI-2 shows.

Since one cannot obtain B(E2) values from this approach we cannot go further into a comparison with the rotational model now but must await the extraction of the full set of B(E2) values obtained by using the Winther and de Boer program. We can, however, apply the Lutken and Winther theory[65] to obtain the quantities $B(E2:0^+ \rightarrow 2^{+'})$. By comparing the results so obtained, as a function of energy, with the model-independent results we may gain some insight into the accuracy with which the theory accounts for the redistribution of γ-band population, and thereby into the degree to which the γ-band is structured as a pure rotational band. Performance of this admittedly only semi-quantitative comparison for the four osmium isotopes will also provide a measure of the accuracy of the Lutken and Winther technique for extraction of $B(E2:0^+ \rightarrow 2^{+'})$ values in a variety of nuclear situations.

Table VI-5 presents the calculated $B(E2:0^+ \rightarrow 2^{+'})$ values for the four nuclei for bombarding energies of 48.26, 62.10 and 70.30 MeV. A clear trend is evidenced in that the B(E2) values increase considerably with higher beam energies. From a

TABLE VI-5. $B(E2{:}0^{+} \rightarrow 2^{+'})$ VALUES EXTRACTED FROM THE DATA USING THE MODEL DEPENDENT LUTKEN AND WINTHER ANALYSIS

$B(E2)$ values listed were obtained from thick target measurements. Units are $e^2 \times 10^{-48} cm^4$.

Isotope	Bombarding O^{16} Energy (MeV)		
	48.26	62.10	70.30
Os^{186}	0.125	0.138	0.140
Os^{188}	0.134	0.150	0.151
Os^{190}	0.150	0.169	0.177
Os^{192}	0.121	0.136	0.152

comparison with the results obtained later in this chapter (Table VI-10) it is apparent that the highest energy Lutken and Winther results are the best. This is to be expected since, at higher projectile energies, the $\xi = 0$ approximation for all levels within each rotational band is most nearly satisfied (recall: $\xi \propto \Delta E/E^{3/2}$) It will also be noted that the variation in B(E2) values obtained as a function of energy gradually decreases from Os^{192} to Os^{186}, that is, as the rotational band states become more closely spaced and as the $\xi = 0$ approximation becomes more accurate even at lower beam energies. In all the nuclei, though, the results even at 70.30 MeV deviate considerably from the model-independent calculations, indicating, as will be confirmed later in this chapter, that the population of lthe $2^{+'}$ state via Coulomb excitation is not well described by a reaction mechanism that treats this state as the leading member of a pure rotational band.

We now consider the B(E2) values for excitation of the 2^+, 4^+ and $2^{+'}$ states obtained from first and second order perturbation theory. These are given in Table VI-6. The values given are those calculated at lower beam energies since for higher projectile energies the perturbation expansion to second order is a poor approximation. This is even true for states weakly excited ($2^{+'}$, 4^+ levels) by second order processes since the excitation of the intermediate first 2^+ state is incorporated into the higher order expressions and is incorrectly calculated. First and second order perturbation theory further overestimates excitation probabilities because it neglects virtual depopulation of 2^+, 4^+ and $2^{+'}$ states. The effects of this neglect are, again, smallest at lower beam energies and in fact, in the 48.26 and 42.00 MeV cases, are negligible. This error can, however, be approximately offset to some degree at any energy by adding to the experimental excitation probability for the state of interest (e.g., a 4^+ state) the excitation probabilities of higher states (e.g., 6^+ levels) predominantely populated via the lower level. This procedure has been incorporated into all the perturbation calculations performed. (These calculations neglect the effects of finite excited state quadrupole moments (see below) which, though generally small, may involve contributions of lower than second order.)

In the calculations of the excitation probabilities for the $2^{+'}$ state by perturbation theory the unknown sign of the interference term (eqs. V-24, 25) introduces

TABLE VI-6. B(E2) VALUES EXTRACTED USING FIRST AND SECOND ORDER PERTURBATION THEORY

Entries are in units of $e^2 \times 10^{-48} cm^4$. The $B(E2:0^+ \rightarrow 2^{+'})$ values were calculated using an overall + sign for the interference term. See text and Table VI-7 for more details on this matter.

Isotope	$B(E2:0^+ \rightarrow 2^+)$	$B(E2:2^+ \rightarrow 4^+)$	$B(E2:0^+ \rightarrow 2^{+'})$
Os^{186}	3.10	1.77	0.193
Os^{188}	2.58	1.36	0.201
Os^{190}	2.38	1.09	0.225
Os^{192}	2.11	0.938	0.178

an uncertainty ranging from 7% in Os^{192} to 25% in Os^{186}. However, the sign of this term can in principle be determined by demanding that the B(E2) values extracted be constant as a function of beam energy.

In practice, this is difficult for three reasons. First the interference terms are not large ($\leq$ 15%, except for Os^{186}). Secondly, their relative size (compared to "direct" plus "double" terms) remain almost precisely constant as a function of beam energy. Thirdly, perturbation theory is invalid at the higher energies anyway, thereby reducing the number of validly calculable quantities with which to test for constancy of the extracted matrix elements. Despite the first and second points the appropriate calculations were carried out. The third problem was partially obviated by slightly modifying the perturbation calculation at the higher energies. This was done by using in eq. V-25, not the correct $B(E2:0^+ \rightarrow 2^+)$, but an incorrect one obtained from a first order perturbation calculation of the 2^+ level's excitation at this energy. Since perturbation theory overestimates the excitation probability at higher energies, the B(E2) value needed to give the experimental 2^+ excitation probability will be lower than the correct one. Use of this lower value in V-25 then prevents a similar overestimate of that portion of the excitation route in the second order calculation of the $2^{+'}$ state's excitation probability. (This technique gives results very similar to those obtained with the use of $P_{2^+}/(1 + P_{2^+})$ for the perturbation probability instead of P_{2^+}.) Calculations using these procedures result in two sets of $B(E2:0^+ \rightarrow 2^{+'})$ values, one for each sign of the interference term. Neither set is exactly constant but that corresponding to an overall plus sign for the interference term is favored by the computations. The $B(E2:0^+ \rightarrow 2^{+'})$ values obtained at 48.26 and 70.30 MeV for each sign of the interference term are listed in Table VI-7. The plus sign is also consistent with the rotational model which predicts equal signs for the reduced matrix elements $< 0^+ \| M(E2) \| 2^{+'} >$ and $< 2^+ \| M(E2) \| 2^{+'} >$ (and a relative plus sign between these two quantities leads in turn to a plus sign for the interference term[70]).

A final comment on the perturbation theory B(E2) values is that in Os^{192} they should be in better agreement with the results of the "correct" Winther and de Boer calculations than is the case in the other nuclei. (This is due to the combined

TABLE VI-7. $B(E2;0^{+} \rightarrow 2^{+'})$ VALUES OBTAINED FROM PERTURBATION THEORY FOR EACH SIGN OF THE INTERFERENCE TERM

Units are $e^2 \times 10^{-48} cm^4$. Results are given for 48.26 and 70.30 MeV O^{16} ions on thick osmium targets.

Isotope	48.26 MeV		70.30 MeV	
	+	-	+	-
Os^{186}	0.193	0.280	0.177	0.244
Os^{188}	0.201	0.265	0.192	0.244
Os^{190}	0.225	0.278	0.215	0.254
Os^{192}	0.178	0.199	0.168	0.183

reasons of higher excitation energy of the 2^+ state and generally weaker coupling among all states, resulting in lower excitation probabilities and less virtual depopulation of low-lying levels via higher order processes.) A detailed comparison of Tables VI-6 and VI-10 does in fact bear out this expectation. Actually, though, in all four nuclei and at lower beam energies, it must be stressed that the results of perturbation theory are in general remarkably close to the "correct" results (obtained using eqs. II-68) for those states that can be reached by first or second order excitations. As expected, however, they are generally lower than the more accurate results.

In order to delve further into the structure of the osmium region we now need to consider the complete calculation of all the B(E2) values through the solution of the coupled Schrodinger eqs. II-68. These considerations will allow us finally to extract B(E2) values for excitation of the 2^+, 4^+ and $2^{+'}$ levels that are no longer imbued with large uncertainties stemming from model assumptions or from poor conversion of perturbation expansions. They will also now allow us to obtain B(E2) values relating to any state observed.

Determination of the best set of matrix elements using the code[61] for the solution of eqs. II-68 is not a priori a trivial task. In all nuclei but Os^{192} there are at least six states to be included in the calculations. Thus, in principle, the code must be supplied with 36 or more matrix elements none of which are initially known in either magnitude or sign. Extensive simplifications are, however, possible.

First, many matrix elements can be arbitrarily set equal to zero. Thus, for example, the quantity $B(E2{:}0^+ \rightarrow 4^+)$ is a contradiction since the two levels cannot be directly coupled via E2 radiation. Thus immediately we have $M_{0^+ \rightarrow 4^+} = 0$. There are many such cases. Secondly, the matrix M is symmetric and thus its size is effectively cut by nearly a factor of two. Thirdly, and most importantly, the magnitudes and relative magnitudes of many matrix elements are approximately known from other sources such as perturbation theory calculations and experimental branching ratios.

Still unknown, however, are the signs of all the matrix elements and the magnitudes of the diagonal one (quadrupole moments) and of those pertaining

to states not susceptible at all to practical analysis via perturbation theory.

If the signs of the matrix elements are considered as arbitrary one has a totally preposterous number of parameters to vary. The number of different sign combinations can be extremely large and one would have to attempt to fit the data with each choice of relative signs. Then comparison of all these myriad fits would needs be made to determine the best overall set of matrix elements. Fortunately, this problem can be nearly totally avoided with what is felt to be, in the osmium nuclei at least, an excellent assumption. The assumption is that the relative signs of the matrix elements be those given by the rotational model. This does not determine all relative signs but it reduces the number of choices from over one hundred down to less than four.

The assumption merits several comments. It is not considered to constitute a transformation at all of the calculation into the model-dependent variety. The main reason is that, while the absolute magnitudes of the matrix elements may deviate sharply from the rotational model, the relative signs will still be correctly given by that model. Were this not true it is hard to see how even weak vestiges of rotational structure could remain for the implication would be that the wave functions would be drastically altered from the rotational form. Yet, in the osmium nuclei, and especially in $Os^{186, 188, 190}$, rotational patterns are clearly evident. For example, the ground state rotational band structure persists at least up through the 8^+ level and, in the γ-band, states past the $4^{+'}$ level are also known. The argument in Os^{192} is twofold. First, it is certainly true that considerable rotational structure is still evident, at least in the ground band. Secondly, if one considers the trends in the matrix elements determined, on the rotational assumption, in $Os^{186, 188, 190}$ it becomes quite unlikely that an abrupt change in sign would occur for Os^{192} although such a possibility is not thereby utterly excluded.

Even if the rotational assumption concerning signs were not made, it turns out that observable effects due to sign changes occur only in isolated cases. Virtually the only situation in which the effect is serious is in the excitation of the $2^{+'}$ states, and as noted earlier, the rotational model's predictions here are in fact probably also favored by the model-independent perturbation theory analysis of the interference term. Furthermore, the size of the effects of relative sign

changes in the excitation of the $2^{+'}$ states is directly related to the magnitude of that interference term. Thus, in the one nucleus (Os^{192}) in which certain doubts might be raised about the validity of the rotational model signs, the effect is the smallest, being only 5-7% in size.

Adopting then this assumption, the only uncertainties in signs are the absolute values of any one sign for a matrix element between bands and of the sign of one matrix element within each band. It turns out that the resulting excitation probabilities are not at all a function of the former sign: either choice gives identical results. For the signs within the two bands one can test the four combinations possible. Again no effects are observed, mainly due to the fact that within a band there are no interference terms to consider. Since no theory or model of this region predicts oblate shape we have assumed the four nuclei to be prolate in both ground and γ-bands. This is sufficient to fix the signs of all intraband matrix elements.

At this point the only matrix elements whose magnitudes are completely unknown are those for the 6^{+}, 4^{+} and $0^{+'}$ (if any) states and those related to the quadrupole moments of the various levels. As a starting point for the former, one can assume rotational model results and probe from there. For the $4^{+'}$ state experimental branching ratios are known so that the existence of several excitation routes does not essentially complicate the analysis.

The matrix elements pertaining to the nuclear quadrupole moments cannot, however, be obtained by fitting the data, as will be seen from the discussion that follows. In a perturbation expansion analysis, the main effect of a finite quadrupole moment, Q_f, in the excitation of the state f from an initial state i arises in an interference term between first and second order contributions. The relative size of the interference term, $P^{(1,\,2)}_{i\to f\to f}$, compared to the first order term, $P^{(1)}_{i\to f}$, is given by[56]

$$\rho = \frac{P^{(1,\,2)}_{i\to f\to f}}{P^{(1)}_{i\to f}} = \frac{A_1}{Z_2}\,\frac{1}{\left(1+\frac{A_1}{A_2}\right)}\,\Delta E'_{if}\,M_{ff}\,K(\xi_{if},\,\theta) \qquad \text{VI-1}$$

where $\Delta E'_{if}$ is in MeV and where K is defined in reference 56. $\Delta E'_{if} = (1+\frac{A_1}{A_2})\,\Delta E_{if}$.

$M_{ff} = < f \| M(E2) \| f >$ is proportional to the quadrupole moment of state f. Numerically, in osmium, it turns out that

$$\rho \cong -.8 \frac{A_1}{Z_2} \Delta E_f M_{ff} \cong .01 A_1 \Delta E_f M_{ff} \qquad \text{VI-2}$$

Thus ρ is proportional to the magnitude and sign of the quadrupole moment, to the excitation energy of the state f and to the mass of the projectile. If only one projectile is used, however, it is extremely difficult to extract accurate values of Q_f since other matrix elements involved in the excitation would then need to be known very accurately. If however, several different projectiles are employed, extraction of Q_f is greatly facilitated. Only O^{16} beams were used here, though. If "reasonable" values of M_{ff} are used, ρ is found to vary, in Os, from .03-.20 for the various states. Thus percentage errors of these magnitudes could arise if one has no knowledge at all of the Q_f's. However, this situation is not encountered here for, despite the fact that the Q_f's were not actually measured, other results indicate very plausible approximate values for them. Using these values, estimated possible errors from this source are reduced to acceptable levels ($\leq 3\%$) for all states in $Os^{186, 188}$ and for most states in $Os^{190, 192}$. In Os^{192} it is possible that an error from this source of $\pm 5\%$ may remain for the $2^{+'}$ state's B(E2) values.

The technique for delimitation of the possible values for the quadrupole moments rests on the fact that B(E2) values for the low-lying states are, in any case, known to within $\pm 15\%$ without any knowledge at all of the Q_f's. Thus a comparison can be made of the experimental B(E2) values with the predictions of the calculations of Kumar and Baranger[13] and the rotational model. The predictions of the models are related in one of two ways: either they are nearly identical in which case they also predict similar values for the Q_f's or they differ widely in which case the 15% errors in the experimental B(E2) values (due to lack of knowledge of the Q_f's) makes no difference in the general comparison. In the second case it turns out that the experimental results tend to lie in between the two models and so Q_f for each state can be chosen in accordance with this general comparison. In light of the comparisons to be made below, it would be very surprising and unlikely if any of the Q_f were to lie outside the range determined in this way by the two models. Thus, in summary, in the extraction of B(E2) values from the data with the Winther

and de Boer code[61] values for the diagonal matrix elements were used that implied quadrupole moments situated in magnitude relative to the rotational model and the Kumar and Baranger predictions in the same way as were the other matrix elements and branching ratios for the low-lying states. Errors remaining due to this source are included in the ± uncertainties associated below with the tabulated experimentally determined B(E2) values. In addition, in Table VI-8, we present a listing of the percent changes in various excitation probabilities were the quadrupole moments used in these calculations here to be altered (increased or decreased) by 30%. In $Os^{186, 188, 190}$ a change of this size almost certainly leads to an overestimate of the errors in the quadrupole moments actually employed. In Os^{192} a ± 30% uncertainty on the quadrupole moments is probably realistic.

With these considerations in mind, then, the initial input matrix elements consist of "reasonably" chosen diagonal moments, dynamic moments connecting the ground state, 2^+, 4^+ and $2^{+'}$ levels as obtained from á perturbation analysis and from experimental branching ratios and rough (e.g., rotational model) estimates of other dynamic moments for higher-lying states. With these one obtains excitation probabilities for all states for all bombarding conditions. Comparison of these with their experimental counterparts leads to a new, hopefully improved, set. This process of successive approximations is repeated until an "acceptable" fit to the experimental results is obtained.

Five comments are relevant here. First, one must attempt to fit all observed levels of a given nucleus at once. Otherwise later inclusion of higher levels would upset prior agreement for the initial states. Secondly, it is not generally sufficient to consider only one bombarding energy at a time. It is entirely possible, in some cases, to fit observed excitation probabilities at one energy but not at another, or to fit experimental results at one energy with one set of matrix elements and at another energy with another set.

Thirdly, it is not necessary to use the thick target computer program for each new set of matrix elements. Since that program prints out all excitation probabilities at each energy, all one needs to do is estimate the percentage change required in certain matrix elements, perform the new calculations at some intermediate energy (largely arbitrary) and determine if the excitation probabilities

TABLE VI-8. DEPENDENCE OF EXCITATION PROBABILITIES ON QUADRUPOLE MOMENTS

Percent changes in the excitation probabilities listed in Table VI-11, and used in obtaining Table VI-10, that result for + and - 30% changes in all quadrupole moments. The results are given for two incident O^{16} energies and pertain to Os^{190} although similar percent variations were obtained in analogous calculations on the other osmium isotopes. The Winther and de-Boer code was used in obtaining the results. Entries are given to the nearest 0.5%.

Level	63.30 MeV		43.30 MeV	
	+30%	-30%	+30%	-30%
2^+	2.0	2.0	2.0	1.0
4^+	2.0	2.0	3.0	2.0
6^+	7.0	5.0	5.5	3.5
$2^{+'}$	3.0	1.5	---	---
$4^{+'}$	1.5	0.5	---	---

do change by the desired percentages at this energy. If they do, they one generally has an excellent approximation to the changes that will occur in the thick target results. Thus one can probe with the inexpensive thin target program, returning occasionally to the thick target version for confirmation.

Fourthly, due to the intricate coupling of the amplitudes in eqs. II-68, it is not easily practicable to "search" automatically with many sets of matrix elements. For example, it might turn out that a $2^{+'}$ state's excitation probabilities are better fit to the data if the matrix element connecting the 2^{+} and 4^{+} levels is altered. The changes one makes in matrix elements in attempting to fit the data are frequently dictated by composite considerations of the relative slopes (with energy) of theoretical and experimental excitation probabilities, the "confidence" one has in certain experimental numbers relative to others and the degree to which one can tolerate disagreement with the data for isolated probabilities for the sake of better overall agreement in other cases.

Finally, a comment on uniqueness: provided one fits "satisfactorily" the $P_{i_{ave}}$'s for all levels at all energies and provided branching ratios are known for all levels excitable by more than one route, the final set of matrix elements obtained can be considered unique. This uniqueness is, strictly speaking, obtained only for the specific choice of relative signs used unless one has tested other such combinations or has reasonably sound arguments in favor of a given set. The uniqueness is also subject to the small errors involved if quadrupole moments were not measured. Of course, one must also assess the accuracy of the experimental results in placing $\pm$ errors on the final matrix elements.

One additional comment for the experimentalist is appropriate here. For guidance in the initial choice of matrix elements, and for accuracy in determining branching ratios, it is often extremely beneficial to have run at least at one very low beam energy. This is especially true if transitions from higher states are nearly degenerate with any deexcitations of lower-lying levels.

In the computations leading to the results now to be cited the number of magnetic substates considered and the accuracy control in the code were set so that errors from these sources in the excitation probabilities for the 2^{+}, 4^{+} and $2^{+'}$ states were less than 1% and for the 6^{+}, $4^{+'}$ and $0^{+'}$ states were less than 3%.

This criterion ensures that calculational errors are in all cases much less than other sources of uncertainty.

The same criterion was observed in determining the number of angles at which calculations were necessary. As it turned out, computations at one mean angle, and generally in the M = 0 substate only, were sufficient. Table VI-9 tabulates the percentage changes in the excitation probabilities of the states of the intermediate nucleus Os^{188} that result if either the $M = \pm 1, \pm 2$ substates are included or the mean angle is altered by 5^{o} toward the forward direction. The latter change can be taken as a considerable overestimate of the errors involved in assuming one mean angle. (See discussion in Section II-C.)

Having considered in some detail now the implementation and accuracy of our solutions to eqs. II-68 we can finally present the results obtained. In Table VI-10 are given all the B(E2) values derived from the present experiments. The quantities $B(E2{:}2^{+'} \rightarrow 4^{+'})$ and $B(E2{:}4^{+} \rightarrow 4^{+'})$ actually could not be determined "internally" since the relevant γ-ray transitions were not observed. Rather, known branching ratios[72] were used together with the observed $4^{+'} \rightarrow 2^{+}$ γ-ray intensities to determine the actual excitation probabilities of the $4^{+'}$ state and the corresponding B(E2) values just mentioned.

In order to assess the accuracy with which the listed B(E2) values allow one to fit the data, Table VI-11 gives the theoretical excitation probabilities obtained with this set of B(E2) values. The entries in this table should be compared with those of Table VI-1. In almost all cases the agreeement, especially as a function of energy, is impressive. This is revealed in Fig. VI-3 in which the ratios of the experimental to theoretical excitation probabilities are plotted. In most cases the ratio is equal to unity to well within 5% and the error bars on the ratio (not shown: see caption) almost invariably include 1.0 within their ranges. Since the experimental errors for the excitation probabilities of the 6^{+} and $4^{+'}$ states at the lowest energies at which they are observed are extremely large one should not consider the deviations from unity of 20-30% for these few cases as indicating poor agreement. For these states, excitation probabilities at the higher bombarding energies should be given considerably heavier "weightings" in determining the quality of the fits. Table VI-10 thus summarizes the quantitative

TABLE VI-9. DEPENDENCE OF EXCITATION PROBABILITIES ON BACKSCATTERING ANGLE AND MAGNETIC SUBSTATE POPULATION

Excitation probabilities were calculated with the Winther-deBoer code that included the $M = \pm 1, \pm 2$ magnetic substates. Analogous calculations were also performed for $\theta = 160^{o}$. The results were compared with the excitation probabilities calculated assuming $M = 0$ only and assuming $\theta = 165^{o}$, respectively. The percentage changes that were found for the excitation probabilities of various levels are given below. The calculations were performed for Os^{188} but analogous results are obtained in the other osmium nuclei. Entries are given to the nearest 0.5%.

Level	Percent Changes in Excitation Probabilities	
	$M = \pm 1, \pm 2$ relative to $M = 0$	$\theta = 160^{o}$ relative to $\theta = 165^{o}$
2^{+}	0.0	0.0
4^{+}	0.0	1.0
6^{+}	1.5	3.0
$2^{+'}$	0.0	1.0
$4^{+'}$	1.0	1.5

TABLE VI-10. FINAL EXPERIMENTAL B(E2) VALUES

The B(E2) values listed here were obtained by the full, model-independent solution of the Schrodinger eqs. II-68 using both thick and thin target versions of the Winther - de Boer computer code to fit theoretical to experimental excitation probabilities as a function of O^{16} energy. Units are $e^2 \times 10^{-48} cm^4$. (For discussion of errors, see Section IV-F).

Reduced Transition Probability	Os^{186}	Os^{188}	Os^{190}	Os^{192}
$B(E2:0^+ \rightarrow 2^+)$	3.42±.55	2.80±.56	2.54±.35	2.37±.33
$B(E2:2^+ \rightarrow 4^+)$	1.79±.21	1.42±.17	1.16±.14	.950±.110
$B(E2:4^+ \rightarrow 6^+)$	1.68±.34	.557±.222	.840±.17	--------
$B(E2:0^+ \rightarrow 2^{+'})$	.231±.028	.245±.029	.243±.029	.180±.021
$B(E2:2^+ \rightarrow 2^{+'})$	.123±.015	.173±.021	.335±.040	.420±.050
$B(E2:2^+ \rightarrow 4^{+'})$	.0289±.0058	.0205±.0041	.00699±.0021	---------
$B(E2:4^+ \rightarrow 4^{+'})$	.147±.029	.163±.032	.149±.045	---------
$B(E2:2^{+'} \rightarrow 4^{+'})$	1.15±.23	.899±.180	.338±.100	---------
$B(E2:2^+ \rightarrow 0^{+'})$	--------	.00612±.0015	---------	---------

TABLE VI-II. THEORETICAL EXCITATION PROBABILITIES

Excitation probabilities calculated with the Winther-de Boer code for those matrix elements that yield the B(E2) values given in Table VI-10. The notation is the same as that of Table VI-1 to which these entries should be compared (see also Fig. VI-3). The experimental results for O^{16} ions of 70.30 MeV on a thin Os^{188} target and of 80.00 MeV on a thick Os^{188} target are not reliable since the Coulomb barrier is almost exceeded and profuse nuclear reactions occur in addition to Coulomb excitation. The corresponding theoretical entries are, therefore, omitted in the table below.

E(MeV) / Level	42.00 Thick	48.26 Thick	48.26 Thin	62.10 Thick	62.10 Thin	70.30 Thick
Os^{186}						
2^+		.244		.417		.475
4^+		.0114		.0515		.0879
$2^{+'}$		.00445		.0170		.0263
6^+				.00240		.00643
$4^{+'}$				.00261		.00608
Os^{188}						
2^+	.135	.180		.354	.422	.432
4^+	.00261	.00544		.0322	.0524	.0630
$2^{+'}$	.00319	.00585		.0232	.0336	.0373
6^+				.000441	.00090	.00142
$4^{+'}$				.00228	.00430	.00581
$0^{+'}$				.000224	.00042	.000546
Os^{190}						
2^+	.116	.157		.331		.411
4^+	.00161	.00348		.0226		.0448
$2^{+'}$	.00443	.00785		.0311		.0512
6^+				.000450		.00147
$4^{+'}$				.00100		.00263
Os^{192}						
2^+	.104	.143	.202	.311	.377	.394
4^+	.00111	.00248	.0052	.0172	.0287	.0355
$2^{+'}$	.00446	.00771	.0134	.0300	.0438	.0505

RATIO OF EXPERIMENTAL EXCITATION PROBABILITIES TO THOSE CALCULATED FROM THE COUPLED SCHRODINGER EQUATIONS II - 68

(The calculated excitation probabilities listed in Table VI-11 and used to obtain the ratios here were calculated assuming the B(E2) values of Table VI-10. The accuracy of those B(E2) values is thus measured in part by the degree to which the ratios here approximate unity. For clarity error bars are omitted: the errors are 1-3% greater than those indicated in Fig. VI-1.)

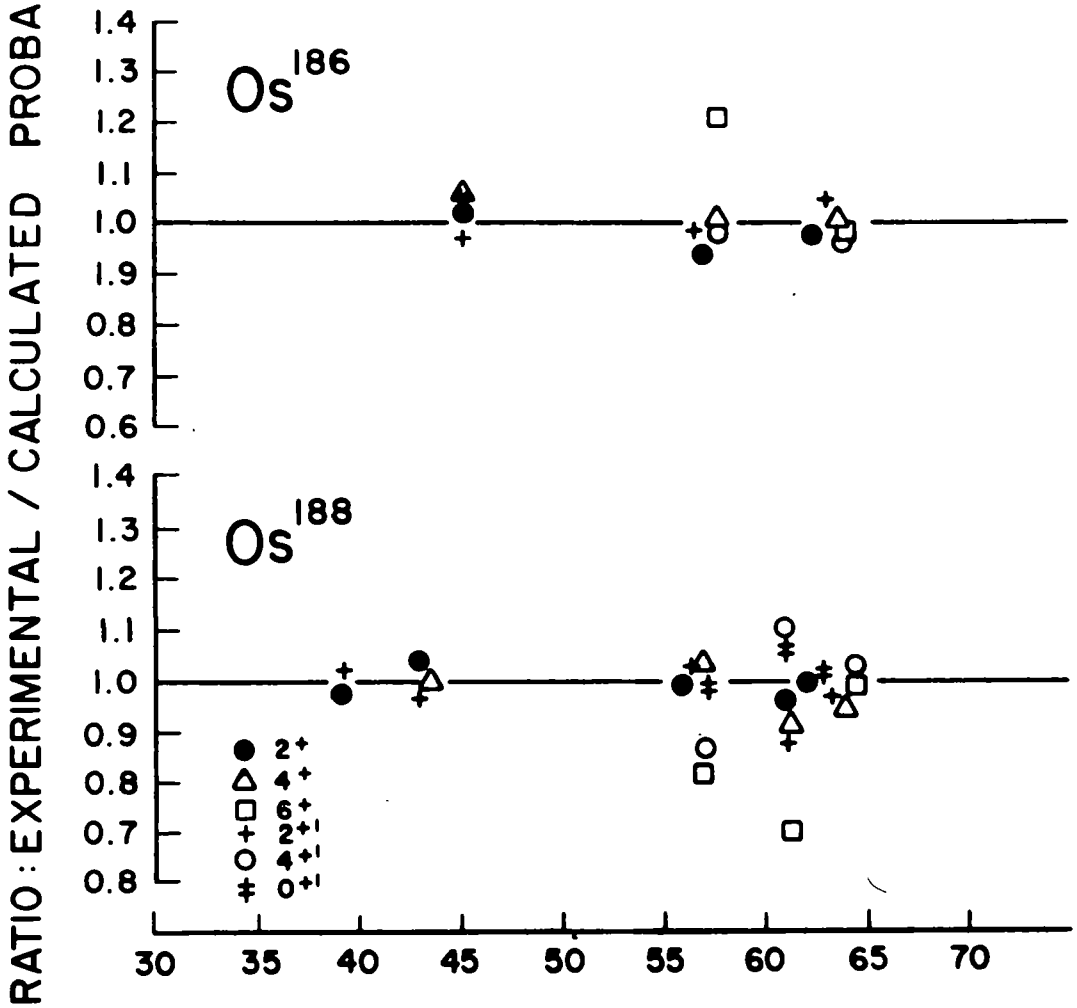

Fig. VI - 3

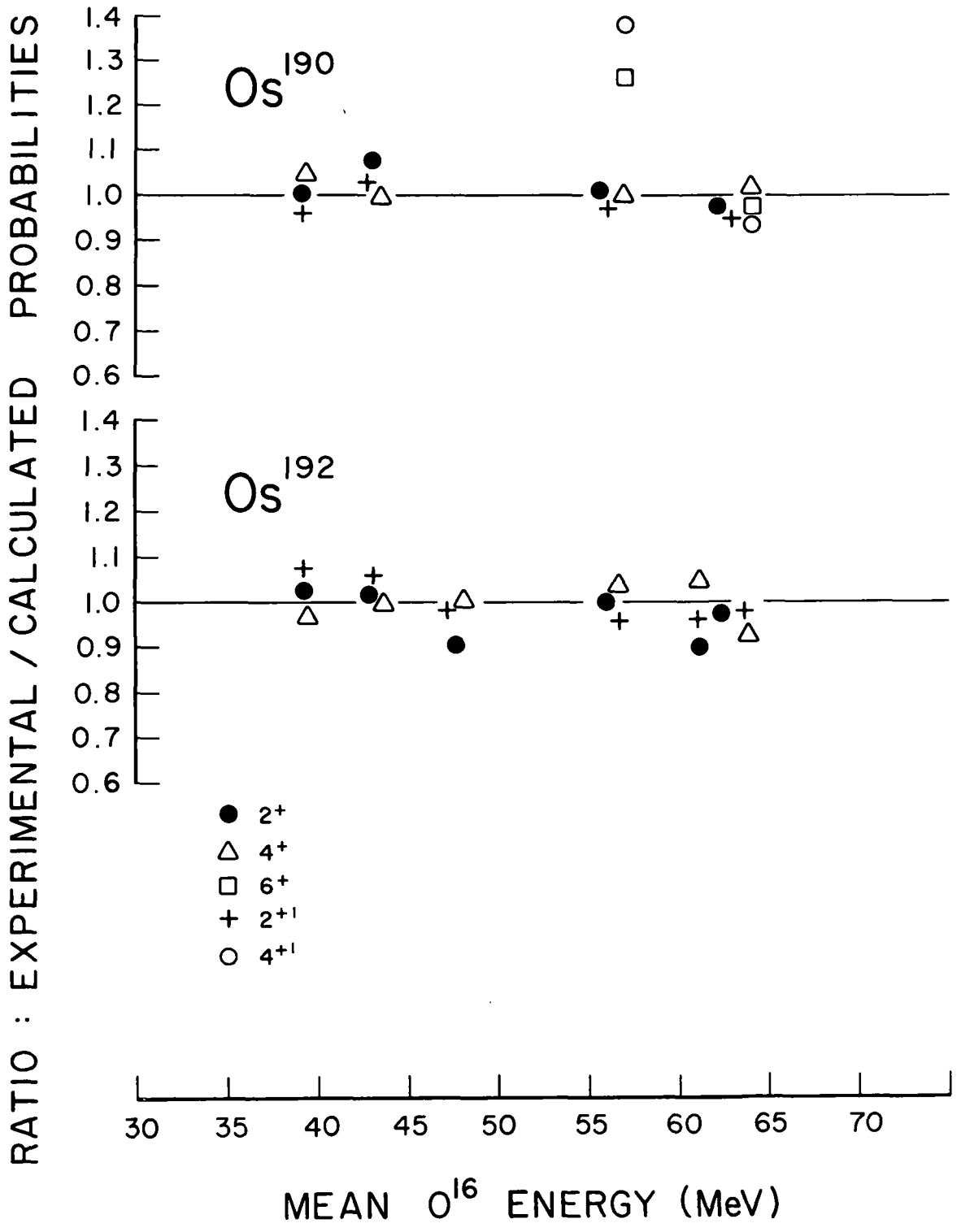
RATIO : EXPERIMENTAL / CALCULATED PROBABILITIES
Os190
Os192
1.4
1.3
1.2
1.1
1.0
0.9
0.8
0.7
0.6
2+
4+
6+
2+1
4+1
30
35
40
45
50
55
60
65
70
MEAN O16 ENERGY (MeV)

Fig. VI - 3 Con't

information on transition rates obtained in these experiments. We now turn to a comparison of these quantities (essentially absolute squares of nuclear matrix elements) with various nuclear models.

Physically, the most revealing approach is afforded by simultaneous comparison with the predictions of the rotational model and of the calculations of Kumar and Baranger. The latter have calculated, to date, B(E2) values involving the 2^+, 4^+, $2^{+'}$ and $0^{+'}$ excited states but not involving the $4^{+'}$ and 6^+ states. Absolute B(E2) values in the former model are obtained from the quantity $B(E2{:}0^+ \rightarrow 2^+)$ which in turn specifies the intrinsic quadrupole moment by eq. II-13 and thus allows calculation of the other ground band B(E2) values. Assumption of the same quadrupole moment for the γ-band permits evaluation of B(E2) values for this band as well. (The Kumar and Baranger calculations also predict approximately equal quadrupole moments for the two bands). The $B(E2{:}2^+ \rightarrow 2^{+'})$ values are obtained in the rotational model by using eq. II-15 and the experimentally determined $B(E2{:}0^+ \rightarrow 2^{+'})$ values. Thus three parameters are needed for each nucleus to specify the model's predictions. Table VI-12[119] presents the overall comparison of the three sets of B(E2) values. The experimental (exp.) numbers included are simply repeated for convenience from Table VI-10.

Fig. VI-4 illustrates in graphical form some of the comparisons of Table VI-12. Several conclusions are clear. The rotational model is quite accurate for the low-lying ground state band members. Thus, given the quantity $B(E2{:}0^+ \rightarrow 2^+)$ the $B(E2{:}2^+ \rightarrow 4^+)$ value is impressively predicted. In addition, for $Os^{186, 188, 190}$, the $B(E2{:}4^+ \rightarrow 6^+)$ values are not badly accounted for although the experimental fall-off of these numbers near Os^{192} is not fully reproduced. In Os^{192}, in fact, no 6^+ excitation is observed but yet the rotational model still predicts a fairly large matrix element for its excitation. This generally good agreement for the ground state band, however, explains in part why the Alder calculations (see Fig. VI-2) were able to account so nicely for the ground state band excitation probabilities. The deviations from the rotational model are in such a direction as to imply, physically, that the rotational character of the ground band wave functions disappears more rapidly for 4^+ and (especially) 6^+ states than it does for the 2^+ level. This is, of course, reasonable since effects such as mixing with single particle (or quasi-

TABLE VI-12. COMPARISON OF EXPERIMENTAL B(E2) VALUES WITH THE ROTATIONAL MODEL AND WITH THE CALCULATIONS OF KUMAR AND BARANGER

$B(E2:J_i \rightarrow J_f)$ values (Exp.) obtained from the present work are compared with the predictions, where relevant or calculable, of the rotational model (R. M.) and with the theory of Kumar and Baranger (K + B). Units are $e^2 10^{-48} cm^4$.

Isotope		$J_i \rightarrow J_f$						
		$0^+ \rightarrow 2^+$	$2^+ \rightarrow 4^+$	$4^+ \rightarrow 6^+$	$0^+ \rightarrow 2^{+'}$	$2^+ \rightarrow 2^{+'}$	$2^+ \rightarrow 4^{+'}$	$2^+ \rightarrow 0^{+'}$
Os^{186}	Exp.	3..42	1. 79	1. 68	0. 231	0. 123	0 . 0289	-----
	K+B	2. 95	1. 632	----	0..190	0. 256	-----	0. 0316
	R. M.	----	1. 76	1. 55	----	0. 0661	0. 0495	-----
Os^{188}	Exp.	2. 80	1. 42	0. 557	0. 245	0. 173	0. 0205	0. 0061
	K+B	2. 731	1. 509	----	0. 184	0. 403	------	0. 022
	R. M.	----	1. 44	1. 27	----	0. 0700	0. 0525	-----
Os^{190}	Exp.	2. 54	1. 16	0. 840	0. 243	0. 335	0. 00699	-----
	K+B	2. 595	1. 429	----	0. 143	0. 539	------	0. 016
	R. M.	----	1. 31	1. 16	----	0. 695	0. 0520	-----
Os^{192}	Exp.	2. 37	0. 950	----	0. 180	0. 420	------	-----
	K+B	2. 576	1. 405	----	0. 035	0. 743	------	0. 008
	R. M.	----	1. 22	1. 08	----	0. 515	0. 0386	-----

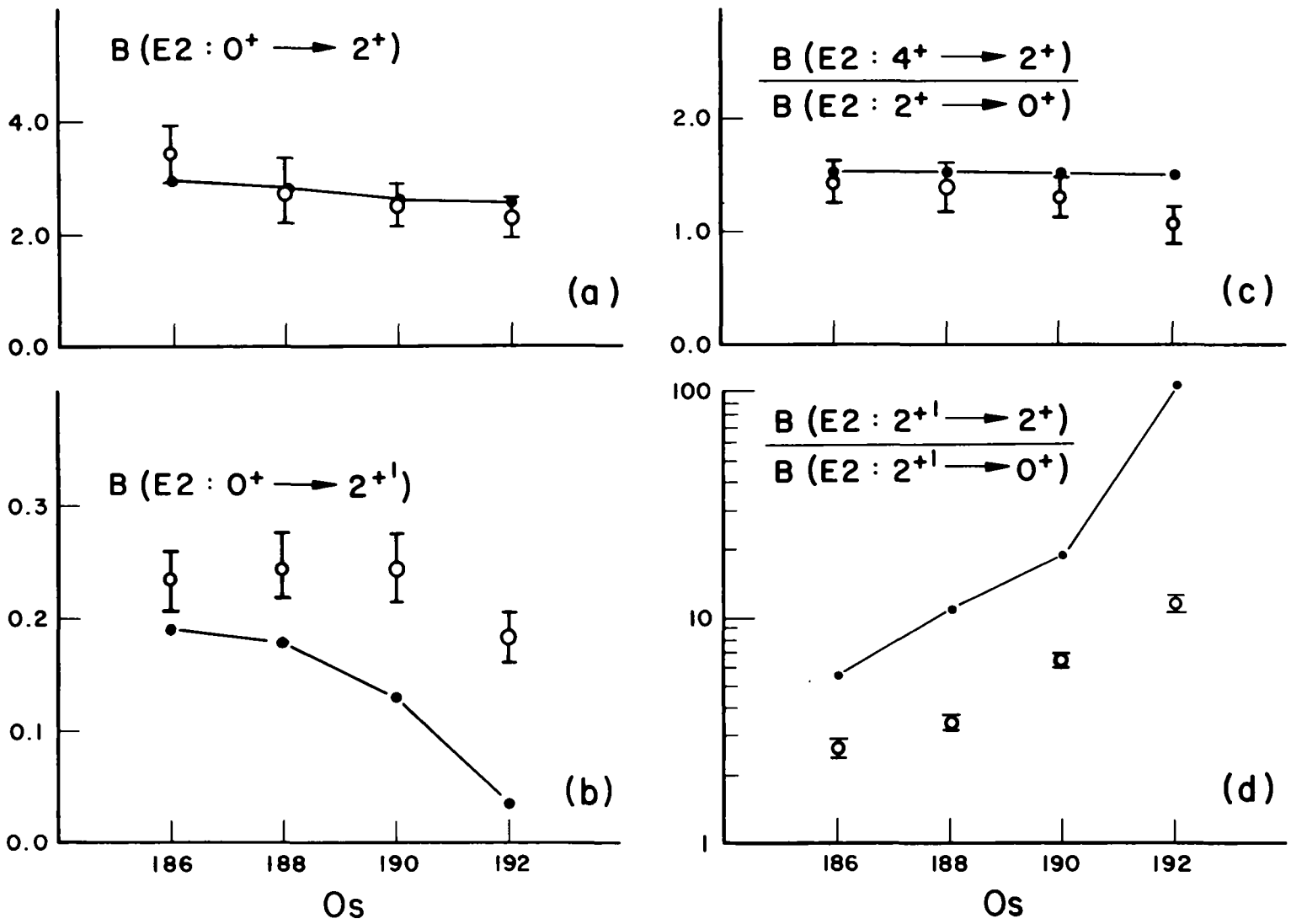
B (E2 : 0+ → 2+)
4.0
2.0
0.0
(a)
B (E2 : 4+ → 2+) / B (E2 : 2+ → 0+)
2.0
1.0
0.0
(c)
B (E2 : 0+ → 2+1)
0.3
0.2
0.1
0.0
(b)
B (E2 : 2+1 → 2+) / B (E2 : 2+1 → 0+)
100
10
1
(d)
186
188
190
192
Os
186
188
190
192
Os

Fig.VI-4

particle) states, centrifugal stretching, CAP forces and the like are more important for the higher-lying states with larger angular momenta.

For the 4^+ levels the Kumar and Baranger results are likewise in satisfactory accord with experiment although they are not noticeably better than those of the rotational model. Of course, the former calculations also predict absolute numbers for the $B(E2:0^+ \rightarrow 2^+)$ values that are extremely close to the measured results and, furthermore, require no parameter fitting for each nucleus.

The real difference between the two models arises when one considers their respective predictions for interband matrix elements. Here, the rotational model, as expected, is totally unable to account for the sharp increase in the $B(E2:2^+ \rightarrow 2^{+'})$ values as the vibrational limit is approached (compare eqs. II-6 , 15). Moreover, even in $Os^{186, 188}$, absolute values for this quantity differ from the experimental results by factors of two or more. This failure to account for the properties of the γ-band states, even in $Os^{186, 188}$, now makes it reasonable that the Lutken and Winther analysis, discussed above, should have given B(E2) values for the transition $0^+ \rightarrow 2^{+'}$ that differed seriously from model-independent results. The rotational model likewise fails to account for the experimental $B(E2:2^+ \rightarrow 4^{+'})$ values.

The Kumar and Baranger theory, on the other hand, accurately predicts not only the region in which the transition to spherical nuclei occurs but also the magnitude of the transition in terms of its effects on reduced transition probabilities. Fig. VI-4 and Table VI-12 show, though, that this theory predicts too sharp a transformation to vibrational character in Os^{192}. However, the trend of interband B(E2) values, in the four isotopes, is correctly tracked by the theory and some slight variation in the input parameters might well be able to reduce the specific numerical differences with experiment (see the next chapter for further discussion of this.).

To summarize thus far, the microscopic calculations of Kumar and Baranger are in generally impressive agreement with experiment in all four nuclei. With no parameter fitting specific to each nucleus they are equally as good as the rotational model for the ground state band and significantly better for other states. The trends in the systematics are qualitatively reproduced. Large numerical disagreements with experiment occur only in Os^{192} and may perhaps be rectified. Furthermore,

though it has not been stressed here, a complete comparison of their theory with experiment shows that it also correctly predicts the energies of the 4^+ and $2^{+'}$ levels in all four Os nuclei to within 50 kev. In addition, experimental ground state band moments of inertia are quite accurately reproduced.

Before considering two other predictions of the Kumar and Baranger theory, it is well to consider what its success in this region implies as to the physical structure of the osmium isotopes. The theory calculates both potential wells and wave functions and these are illustrated (the latter in contour plots) in detail in reference 13. We conclude, then, that $Os^{186, 188}$ are prolate in their ground states with a potential minimum of a few hundred kev. A second, shallower potential minimum exists on the oblate side. In $Os^{190, 192}$ the minima are both very shallow (< 150 kev) and there is only slight preference for prolate over oblate shapes. In these two nuclei the zero point motion in the ground state actually carries the nucleus through many configurations. The mean or time-averaged condition is thus not far from the spherical and so properties analogous to vibrational nuclei reasonably arise. However, the slight preference for a non-spherical equilibrium configuration permits finite quadrupole moments to remain[122]. Finally, as regards deformation, the equilibrium value of β is predicted to gradually decrease from Os^{186} to Os^{192}.

Considering now the contour plots of the wave functions of reference 13 we see that the latter in general are quite spread out in the β-γ plane. Again, maxima are meager. A marginal preference for slightly asymmetric shapes in the ground state is found in Os^{190} and Os^{192}. All four nuclei are extremely soft to γ vibrations although this tendency is the greatest in $Os^{190, 192}$. Thus we expect (and get) low-lying γ-vibrational excitations with the $2^{+'}$ state decreasing in energy as Os^{192} is approached.

The wave functions for the first excited 2^+ states have both K = 0 and K = 2 components although in $Os^{186, 188}$ the former dominates. For $Os^{190, 192}$, however, the two components have nearly equal magnitudes and the wave functions are not at all localized. This results in a structure similar to that for a one phonon harmonic oscillation of a spherical nucleus. It is also reasonable that the matrix elements connecting the 2^+ and $2^{+'}$ states should thus be rapidly increasing as the transition

to nearly spherical shape is being consummated.

One of the most important points to note is that the calculated wave functions are "spread all over the place"[13] and thus the common calculational approximations of small oscillations in β and γ are not really valid in this region. This result of the Kumar and Baranger theory is thus in part a retrospective justification of the exact treatment given by them to β and γ vibrations.

It must be remarked that the above description of the wave functions assumes full agreement of observable quantities with the predictions of the Kumar and Baranger theory. This is not true, as has been indicated. However, the degree of agreement obtained is sufficient to allow one to consider the model wave functions as good approximations to the physical ones. These wave functions are considerably different from those of previous models in several respects, and, in so far as this is the case, some insights into the detailed nature of collective behaviour have emerged.

It is now necessary to consider two other features of the Kumar and Baranger model. First, it does predict finite quadrupole moments for the excited states. Since the other predictions of the model are fairly accurate it can be presumed that the wave functions obtained are not seriously in error either. Since, furthermore, experimental disagreements with the theory are in the rotational model (larger quadrupole moment) direction, it is thus highly likely that finite quadrupole moments of 2^+ states do exist in all the osmium isotopes studied. The microscopic theory, with its shallow potential wells, thus provides a physical picture of the origin of these moments in otherwise apparently spherical nuclei. Even partial success in this area is of interest for it may well lead to other detailed calculations that, similarly, do not restrict β and γ to small oscillations.

The other prediction of interest is that of excited 0^+ levels around 1 MeV or slightly lower. Almost all models, in fact, predict such levels in this region. The only observed candidates in osmium, however, are the 1086 and 1765 kev 0^+ states in Os^{188}. Non-existence of 0^+ levels in the other nuclei could constitute a significant failure in the theories of collective motion in this region. The question of 0^+ states is closely linked to the degree of coupling with quasi-particle excitations and so an accurate interpretation of such states requires a microscopic approach.

Bès[6] has calculated the properties of 0^+, β-vibrational, states using the pairing-plus-quadrupole formalism without the adiabatic approximation (see Section II-B). He predicts 0^+ states at about 1.5 MeV in $Os^{186, 188, 190}$ with $B(E2:0^{+'} \rightarrow 2^+)$ values in the range: $0.002 - 0.009 \times 10^{-48} e^2 cm^4$. His predicted excitation energies, however, bring these levels to within a 100 kev of the energy gap, that is, of the minimum excitation energy for intrinsic two quasi-particle excitations. Thus strong mixing occurs and the so-called β-vibrational states are not very collective in nature. If the 1765 kev 0^+ level in Os^{188} is considered as the β-vibration in that nucleus, then its energy is, in fact, not badly accounted for in Bès' model. However, if the 1086 kev 0^+ level is chosen then Kumar and Baranger more accurately calculate its energy. Moreover, their predicted $B(E2:0^{+'} \rightarrow 2^+)$ value in Os^{188} (See Table VI-12) is nearly adequate, especially when one recalls that their model neglects mixing with quasi-particle states and hence the calculated B(E2) values should be taken as upper limits only. Also, in Os^{188}, the two 0^+ states undoubtedly mix strongly with one another as well and so neither should be considered to contain the entire predicted collective character.

On the assumption of Bès' results, the 0^+ levels in the osmium isotopes would be nearly impossible to observe via Coulomb excitation due both to their high energy and to their small collective enhancements. In fact, even Kumar and Baranger's predictions for the 0^+ levels are barely sufficient to render them observable in these experiments. Therefore, we can say nothing definite about this important test of the various models except that, thus far, the experimental attacks on the 0^+ states have not yielded results inconsistent with the theories and have, barring degeneracies of the kind mentioned below, indicated upper limits on the $B(E2:2^+ \rightarrow 0^{+'})$ values in these isotopes of about $0.015 \times 10^{-48} e^2 cm^4$.

One initially disturbing aspect of the comparison of experimental results with both microscopic theories, though, is that, since the $B(E2:0^{+'} \rightarrow 2^+)$ values are predicted to increase for the lighter osmium isotopes, observation of a 0^+ state in Os^{188} would seem to imply even more facile detection of one in Os^{186}. No such state is seen, however. Assuming it exists, it is not hard, though, to explain its lack of observation for it might well be in the 700-1000 kev range and its de-excitation to the 2^+ state could yield a γ-ray nearly degenerate with the strong, relatively high energy, $2^{+'} \rightarrow 0^+$ or $2^{+'} \rightarrow 2^+$ transitions in this nucleus.

For several reasons the stress thus far has been on mainly a single microscopic model. For one, it predicts finite quadrupole moments in nearly spherical nuclei and, for another, its more general and exact treatment of β and γ vibrations is conceptually more satisfying than the approximations usually made. The comparisons with experiments have not belied the expectations initially held for it. It is, nevertheless, appropriate to consider certain other microscopic calculations in the osmium region.

We shall limit ourselves to two representative examples of calculations of the properties of the γ-band states.

The calculations by Marshalek and Rasmussen[8] actually were not performed for the osmium nuclei but rough values for energies and B(E2) values in osmium can be obtained by extrapolation from the trends evidenced in Hf and W. The calculations are based on the so-called vibrating potential model which is a generalization of the cranking model and which avoids the adiabatic approximation.

The $2^{+'}$ γ-vibrational state energies are found to decrease as the region of strong deformation is left behind. This is likewise found experimentally and also predicted by Kumar and Baranger. Extrapolation indicates that $2^{+'}$ energies are fairly well accounted for. $B(E2{:}0^{+} \rightarrow 2^{+'})$ values appear to be increasing as the osmium region is approached and numerical values are roughly 12 single particle units. Experimentally, the B(E2) values are typically 6-8 single particle units, but are constant or decrease as Os^{192} is approached.

For more detailed comparison with alternate calculations of γ-vibrational states we turn now to the work of Bès and coworkers[6, 54]. Calculations in the adiabatic approximation and in the more general framework of the linearized equations of motion were performed (for both approaches, see Section II-B). We shall mainly consider the latter model. In it, an extension is made in that the interaction Hamiltonian (see eqs. II-36, 56) is not simply $H_{Q\text{-}Q}$ but rather

$$H_{int} = H_{Q\text{-}Q} + H_{Cor} \qquad \text{VI-3}$$

where $H_{Cor} = -\frac{\hbar^2}{I} \bar{J} \cdot \bar{R}$ ($\bar{J}$ is the total and $\bar{R}$ the intrinsic angular momentum). H_{Cor} thus represents the Coriolis interaction between intrinsic and rotational degrees of freedom. As usual, the collective energy levels are obtained by solving a dis-

persion equation (see eq. II-37).

In the osmium region the $2^{+'}$ state energies are calculated to be rapidly decreasing. Although $E_{2^{+'}}$ for Os^{186} is closely approximated by the model, the $2^{+'}$ energies in the heavier osmium isotopes have already become imaginary and the nuclei are γ-unstable. Bès et al.[54] point out that results here are extremely sensitive to deformation because of the behaviour of certain Nilsson orbits. Thus, in the light of the Kumar and Baranger finding that the wave functions are not at all well localized at a single value of β, it is not surprising that the calculations run into trouble. Hence it is only for Os^{186} that Bès et al.[54] can calculate a $B(E2:0^{+} \rightarrow 2^{+'})$ value. They obtain $0.51 \times 10^{-48} cm^4 e^2$ or about twice the experimental value. This added enhancement is consistent with the slightly low value they obtained for $E_{2^{+'}}$. In the earlier, adiabatic calculations of Bès[6], which also neglect the Coriolis interaction, $B(E2:0^{+} \rightarrow 2^{+'})$ values can be calculated in $Os^{186, 188, 190}$ since large values for γ, but not γ instability, are derived for these nuclei. The calculations give 0.22, 0.23, and 0.37 ($\times 10^{-48} cm^4 e^2$), respectively. These are in better numerical accord with our results than the later, more general, theory, but the theoretical trend, especially as seen in Os^{190}, opposes the experimental.

Thus, in conclusion, it appears that the best and more complete microscopic calculations in the osmium region are those of Kumar and Baranger. Their model is far from being perfectly satisfactory since it is based on the unrealistic[13, 44] pairing-plus-quadrupole approximation to the nuclear force. Nonetheless, the calculations, though crude in this sense, have permitted a fairly detailed interpretation of the osmium isotopes and should motivate subsequent, more exact, treatments. It may now be of interest, therefore, to determine if the same overall picture is mirrored by two rather more refined macroscopic models: the rotational model with rotation-vibration interactions[29, 30] and the asymmetric rotor model of Davydov and co-workers[32, 35] in its later forms.

We recall from the discussion of Section II-A that the first order correction to the ground state band wave functions arising from mixing with the γ-band leads, in turn, to a term that is proportional to $J^2 (J+1)^2$ in the expression (eq. II-17) for the ground state band energy levels. The physical origin of this interband

mixing can be pictured as due to small dynamic departures from axial symmetry in the ground state band wave functions. One must be careful in applying this analysis to the osmium nuclei for it is not at all clear that a first order treatment of the mixing is sufficient. Kumar and Baranger indeed found that the wave functions in $Os^{190, 192}$ were actually smeared over large regions of the β-γ plane. Even in $Os^{186, 188}$, the preference for axial symmetry was not overwhelming. In the mixing analysis the amplitude of the γ-vibrational wave functions in the ground state is proportional to the quantity ϵ_γ which is, itself, a function of the branching ratio $B(E2:2^{+'} \rightarrow 2^+)/ B(E2:2^{+'} \rightarrow 0^+)$. In $Os^{190, 192}$ this ratio deviates so much from the rotational limit (1.43) that it is unlikely that a mixing analysis would be meaningful. Even in $Os^{186, 188}$ the validity of this approach is not certain but we have performed the mixing calculations on these nuclei anyway.

A priori, we might actually expect an accurate mixing analysis to contribute a larger fraction of B in eq. II-17 in the osmium nuclei than it has provided elsewhere[25, 27, 30, 120] since lower γ- band energies and higher $B(E2:0^+ \rightarrow 2^{+'})$ values indicate that the $2^{+'}$ and 0^+ state wave functions may be considerably mixed. In a microscopic calculation of B by Marshalek and Rasmussen[9], in fact, other factors, besides mixing, such as the CAP effect and the reduction in Δ due to the Mottelson-Valatin effect were found to contribute relatively less to B in the high A end of the rare earth region than in the low A end. Therefore we might expect a large fraction of the experimental value of B to be accounted for by mixing with the γ-band.

Using the ratios

$$\frac{B(E2:\, 2^{+'} \rightarrow 2^+)}{B(E2:\, 2^{+'} \rightarrow 0^+)} \qquad \text{and} \qquad \frac{B(E2:\, 0^+ \rightarrow 2^+)}{B(E2:\, 0^+ \rightarrow 2^{+'})}$$

to determine z_γ and α_γ, values for ϵ_γ (eq. II-18) were found and the quantities B calculated using eqs. II-16, 17. The results, and a comparison with the experimental values, B_{exp}, are given in Table VI-13. The B_{exp} were obtained by fitting the observed energy levels with an expression for E_J analogous to eq. II-17 but containing a term cubic in $J(J+1)$ as well.

From the table it is apparent that the γ-band-ground band mixing correction accounts for 25-50% of B. This is to be contrasted sharply with typical values of

TABLE VI-13. COMPARISON WITH EXPERIMENT OF ROTATIONAL MODEL WITH ROTATION-VIBRATION INTERACTION

The rotational model with rotation-vibration interaction was used to calculate, in $Os^{186, 188}$, the coefficient $B_{R.V.}$ in the energy expansion of eq. II-17. Experimental branching ratios were used to determine the parmeters of the theory The results for $B_{R.V.}$ are compared with the analogous experimental quantities, $B_{exp.}$

	Os^{186}	Os^{188}
z_γ	-0.10	-0.163
α_γ	3.46	2.80
ϵ_γ	-0.0059	-0.0119
$B_{R.V.}$ (ev)	-26	-89
$B_{exp.}$ (ev)	-100	-175

5-10% in Nd, Sm and Gd[25, 117, 120]. Previous evaluations[30] of the contribution to B from the mixing in Os[186, 188] used less well-known ratios of B(E2) values and obtained results somewhat lower than those of Table VI-13. However, the general conclusion remains that the mixing apparently accounts, as might be expected, for a decent portion of the perturbations on the J(J + 1) law but that other microscopic effects are needed to account for at least half the observed deviations from the simple law. The fraction of B contributed by the mixing is also seen to increase as E_{2^+} decreases and as , according to Kumar and Baranger, the first 2^+ state begins to contain K = 2 components in increasing amounts.

Another way to consider the rotation-vibration analysis, that is, to include K = 2 components in the ground state band wave functions,is afforded by the asymmetric rotor model of Davydov and co-workers[32-35]. In fact, to first order, the Davydov model obtains expressions for the ground band energies and for certain branching ratios that are similar in form to those obtained in the Bohr-Mottelson model with rotation-vibration interaction[88]. It has been pointed out that the two models are actually equivalent for all predictions concerned with K = 0 and K = 2 bands[38]. Recently Yamazaki et al.[39] have cast some doubt, however, on the reliability of the physical basis of the model in the osmium region by pointing out that analysis of beta decay studies shows that the structure of the 2^+ state is significantly different from that of the ground state. In the asymmetric rotor model this state is rather depicted as just another rotational excitation built on an axially asymmetric structure. Nevertheless, particularly because the Kumar and Baranger calculations indicate the likelihood of γ instability or of actually asymmetric equilibrium values of γ, it is worthwhile to consider briefly how well this model accounts for the properties of the osmium isotopes.

Such comparisons in the osmium region with the Davydov – Filippov version of the asymmetric rotor model have previously been published[70, 71, 95, 40]. This version, however, assumes rotations about fixed values of both β and γ. In light of our previous discussions this is a dubious approximation. Davydov and Chaban[34] have relaxed this restriction somewhat by allowing at least small amplitude β-vibrations. Numerical results for the case of variable γ are not yet available.

We present, in Table VI-14, a comparison of our results with the Davydov-

TABLE VI-14. COMPARISON OF ASYMMETRIC ROTOR MODEL WITH EXPERIMENTAL RESULTS

In this table we compare experimental energy level and B(E2) ratios with those predicted by the asymmetric rotor model. For the theoretical ratio $B(E2:2^{+'} \rightarrow 0^{+})/B(E2:2^{+'} \rightarrow 2^{+})$ and for the energy level predictions we use the Davydov-Chaban model which allows for softness in β. This model's predictions are specified by the parameters γ and μ which are also listed. γ and μ were determined from the ratios E_{4+}/E_{2+} and $E_{2+'}/E_{2+}$. For the other B(E2) ratios listed calculated values in the Davydov-Chaban model are not available. We therefore have used the similar Davydov-Filippov model which, however, assumes fixed β.

		Os^{186}	Os^{188}	Os^{190}	Os^{192}
γ		16^{o}	19^{o}	21^{o}	25.2^{o}
μ		.26	.25	.25	.25
$\frac{B(E2:2^{+'} \rightarrow 0^{+})}{B(E2:2^{+'} \rightarrow 2^{+})}$	Th.	0.32	0.21	0.15	0.05
	Exp.	0.38	0.28	0.145	0.085
$\frac{B(E2:4^{+} \rightarrow 2^{+})}{B(E2:2^{+} \rightarrow 0^{+})}$	Th.	1.37	1.37	1.37	1.36
	Exp.	1.46	1.41	1.25	1.11
$\frac{B(E2:6^{+} \rightarrow 4^{+})}{B(E2:2^{+} \rightarrow 0^{+})}$	Th.	1.57	1.60	1.64	1.70
	Exp.	1.70	0.70	1.15	----
$\frac{B(E2:4^{+'} \rightarrow 2^{+})}{B(E2:2^{+'} \rightarrow 0^{+})}$	Th.	0.006	0.001	0.002	0.021
	Exp.	0.0236	0.020	0.0077	----
E_{6+}/E_{4+}	Th.	6.2	5.8	5.45	5.20
	Exp.	6.34	6.13	5.73	----

Chaban model. For the reader's convenience we do not adopt the notation of the latter authors but rather continue to designate the various levels as we have previously done in this thesis. The model predictions are fully determined by the parameters γ and μ which are also listed in the table. The observed trends are fairly well predicted and, in many cases, quantitative accord is attained. It is especially in its predictions of ratios of reduced transition probabilities involving the $2^{+'}$ state that the Davydov-Chaban model is seen to be a significant improvement over the simple symmetric rotor model.

The large values of both γ and μ imply that the osmium nuclei are both "soft" to β vibrations and have, in this model, large equilibrium values of γ. Furthermore, the asymmetry increases from Os^{186} to Os^{192}. These conclusions, especially those concerning the equilibrium values of γ are not necessarily quantitatively correct. What is most probably correct, however, is that the qualitative picture of either axial asymmetry or near γ-instability is a reasonably accurate one in this transition region. This statement, moreover, is more or less independent of the specific phenomenological model to which one turns in order to correlate the experimental observations and corroborates the analysis of the several microscopic theories we have considered.

We are not, after all, seeking to obtain a detailed knowledge of the nucleus with these macroscopic models. Rather, we wish to use them to point out gross nuclear characteristics and to indicate, frequently by their own failures, the need for inclusion of other, often microscopic, effects. In this way, they may serve as guide-lines indictating certain desired features of the macroscopic nuclei that the more fundamentally-oriented theories must ultimately produce out of their superpositions of myriad microscopic elements. This correlation of approach has, in fact, been fruitful in the osmium nuclei for it has turned out that those microscopic calculations which derive the same resultant macroscopic structures as inferred from the successes and failures of the phenomenological models are also those that best account for the detailed properties of these isotopes. The result is that we now at least partially understand both the general structure and even the microscopic makeup of the even-even osmium nuclei and of the transition region in which they lie.

VII. SUMMARY AND SUGGESTIONS

The four even-even isotopes of osmium, $Os^{186, 188, 190, 192}$, have been studied using Coulomb excitation induced by O^{16} ions with bombarding energies between 42 and 80 MeV. The isotopes listed span the transition region from highly deformed to nearly spherical nuclei at the high A end of the rare earth region of deformation. The emphasis has been on a detailed quantitative study of the low-lying collective levels in these nuclei. In particular, the major effort has gone into extracting a large number of absolute reduced transition probabilities and branching ratios from the data. Confirmations and tentative extensions of already published decay schemes have also resulted.

The reasons for studying these nuclei have been several. They span an important region which has long been a traditional testing ground for collective theories. As much data as can possibly be garnered here is thus of use. Secondly, previous studies resulting in B(E2) values in these isotopes have been beset by large errors and limited in scope to consideration of only the lowest three states. Thirdly, the recent microscopic theory of Kumar and Baranger[13], as well as other microscopic calculations[6, 8, 54] have never been seriously tested in a detailed manner in this region. Due particularly to the enthusiasm generated of late for the Kumar and Baranger model, it appeared desirable to provide that model with accurate experimental values for comparison with its predictions. Fourthly, by complementing earlier studies in this laboratory[117, 118, 120] on the sharper transition region at the low A end of the rare earths, it was hoped that we could obtain a more comprehensive understanding of the detailed interactions in nuclei intermediate between the limiting cases of the simple collective models. In particular, by offering a gradual transition region, the osmium isotopes are specifically well-suited to a study of some of the more subtle effects that arise in transitional nuclei.

In $Os^{186, 188, 190}$ all levels up through the 6^+ state of the ground state rotational band and the $2^{+'}$ and $4^{+'}$ states of the γ-band have been excited. In Os^{188} an additional $0^{+'}$ level at 1086 kev was observed. In Os^{192} all known levels except the 3^+ were excited. For all these states, reduced transition probabilities for

their excitation have been extracted from the results. In addition, transitions of 780, 840 and 855 kev in $Os^{188, 190, 192}$ respectively, have been observed. They cannot be fit consistently into present decay schemes. Hence, using in particular the γ-γ coincidence data, we have tentatively predicted new levels at these energies. The spins and parities are not known although 2^+ or 3^- assignments are not inconsistent with our observations. Aside from results concerning the decay schemes of the four nuclei, the principal experimental results of this research are tabulated in Tables VI-1, 2, 3 and 10.

In extracting B(E2) values from the data several approaches have been used. First and second order perturbation theory were employed to calculate the excitation probabilities of the 2^+, 4^+ and $2^{+\prime}$ states. The model-dependent multiple Coulomb excitation theories of Alder and of Lutken and Winther have been applied in the analysis, respectively, of the ground state band and γ band excitation probabilities. The emphasis here was less on extracting B(E2) values than on investigating the rotational and vibrational excitations in these nuclei through comparison of these B(E2) values with ones obtained in a model-independent manner. Finally, full sets of such model-independent B(E2) values have been obtained via use of the Winther and de Boer computer code for the solutions of eqs. II-68. A fairly detailed discussion of the application of this code, and of a thick target version of it, was also presented in which was considered the accuracy of several approximations ($M = 0$, one mean angle θ, etc.) as well as techniques for the choice of signs and magnitudes for the various matrix elements required in attempts to fit the data.

The B(E2) values obtained with this code were compared, along with other properties of the osmium isotopes, with the predictions of several macroscopic and microscopic nuclear models. These included the rotational model of Bohr and Mottelson, the same model with rotation-vibration interaction, the Davydov and Chaban model, the microscopic calculations of Bès and of Marshalek and Rasmussen and, in particular, the microscopic theory of Kumar and Baranger.

We shall not attempt to summarize all of these comparisons here. Suffice it to say that the Kumar and Baranger model proved highly encouraging and accurate in most of its predictions. Variations with neutron number of all predicted B(E2) values follow the experimental trends quite well. Absolute magnitudes are also in

quite creditable agreement although the quantities $B(E2:2^{+}\rightarrow 2^{+'})$ are consistently somewhat larger than observed. Energy levels, g factors and moments of inertia are impressively reproduced. The model's principal shortcoming is that the transition to spherical nuclei is predicted to be too sharp. Specifically, the observed B(E2) values for excitation of the $2^{+'}$ states in $Os^{190, 192}$ actually lie between the rotational limit and the Kumar and Baranger predictions. In particular, the calculated $B(E2:0^{+}\rightarrow 2^{+'})$ values tend toward zero in these nuclei more rapidly than is observed to be the case. This shortcoming is perhaps rectifiable if the input parameters (e.g., the single particle energy levels or the quadrupole force strength, χ) are varied somewhat so as to produce a slightly deeper potential minimum in these nuclei. Then the wave functions would not be quite so spread out in β and γ and the deviations from sphericity would be correspondingly greater. Calculated wave functions would exhibit less overlap with those of a simple harmonic oscillator and the E2 matrix elements between the ground and $2^{+'}$ states would not decrease as precipitously.

One other possible failing of the model is its prediction of $0^{+'}$ states which are not (except in Os^{188}) observed. However, the predicted B(E2) values for excitation of these levels are sufficiently low that experimental observation of the latter is expected to be very difficult anyway. The experimental results reported here thus can make no definite conclusions about this matter.

In general, however, all the models investigated, and in particular that of the above authors, have indicated that a correct picture of the osmium nuclei depicts them as possessing shallow potential wells with weak minima for slightly prolate shapes (with somewhat axially asymmetric equilibrium configurations in $Os^{190, 192}$). The wave functions can be considered to be extensively smeared out in the β-γ plane. The conclusion is that a serious treatment of these isotopes cannot limit itself to fixed or slightly varying values of these parameters, but must, like the Kumar and Baranger model, admit of an exact treatment with no limitations on β and γ oscillations and with no a priori assumptions of weak coupling between rotations and β and γ vibrational excitations. Furthermore, the overall comparison of the osmium nuclei with the rotational model and with that of Kumar and Baranger makes it quite likely that finite, even large, excited state quadrupole moments exist in all four nuclei.

It is thus of interest at this juncture to mention some other attempts to calculate finite quadrupole moments in nearly spherical nuclei. Such alternate calculations have not concerned themselves with osmium but rather more commonly with the isotopes of cadmium. Therefore they are not strictly relevant here except as they illustrate certain features apparently required of such (nearly spherical, finite Q_{2^+}) nuclei. Calculations of the kind referred to have been carried out by Tamura and Udagawa[122], by Do Dang et al.[122] and by B. Sørensen[122]. All three calculations obtain the "correct" 2^+ state quadrupole moment in Cd^{114} by the inclusion of anharmonicities. Those of Tamura and Udagawa, however, are also in error by a factor of five for the $2^{+'}$ state's branching ratio while the other two models do not calculate this quantity. Do Dang et al. and Tamura and Udagawa mix phonon excitations in the construction of the first 2^+ state. As is well known[24], the anharmonicities thus introduced are closely related to the substitution of the HRPA for the RPA in a microscopic calculation. In fact, Tamura and Udagawa point this out and indicate that an improved use of the HRPA in their calculations might correct the $2^{+'}$ state branching ratio. The work of Do Dang et al. involves the somewhat different mathematical technique of a self-consistent perturbation theory approach. However, they similarly comment that the linearization inherent in the RPA is inadequate here.

Recollection that, in the RPA, pairs of Fermion operators are assumed to obey Boson commutation relations leads to another means for the introduction of anharmonicities. This so-called quasi-boson approximation may be acceptable if the number of available states is much greater than the number of particles outside the last closed shell. In any case, inadequacies in the approximation may be partially obviated[24] by the addition of correction terms in the Hamiltonian that result from an expansion of pairs of Fermion operators in a series of Boson operators. Investigations of this type have been considered by Belyaev and Zelevinsky[24]. The work by Sørensen, mentioned above, is, in fact, structured along these lines.

The question of axial asymmetry merits inclusion at this point. We note that such a condition is obtained for the ground state wave function by Kumar and Baranger for $Os^{190, 192}$. Furthermore, Tamura and Udagawa point out that, for large values of the axial asymmetry parameter γ, the asymmetric rotor model of Davydov and co-workers[32-35] can also predict finite quadrupole moments of the same magnitude and sign as found experimentally in cadmium. The latter model also yields

$Q_{2^+} \cong -1.0$ barns in Os^{190} and $Q_{2^+} \cong -0.5$ barns in Os^{192}. These are quite close to the Kumar and Baranger results of -0.89 and -0.36 barns for the same quantities. Finally, axial asymmetry, anharmonicity, and finite excited state quadrupole moments are again interrelated by the fact that Belyaev and Zelevinsky, by the technique described above, obtain a formula for the $2^{+'}$ state's branching ratio of the same form as that calculated with the Davydov model.

Thus certain conclusions may be drawn from this general confluence of ideas. It is apparent that there is a strong kinship between the existence of finite quadrupole moments in otherwise nearly spherical nuclei and the presence of axial asymmetry and of anharmonicity. Since the models which successfully treat the osmium region characteristically predict both anharmonicity and asymmetry (or at least near γ-instability) this rather general three-fold relationship indicates the likelihood of a corresponding presence of non-zero excited state quadrupole moments in these nuclei. Also, from a microscopic viewpoint, the collective excitations in such nuclei must be quite complicated structures, including, in part, coherent superpositions of two particle-hole (or four quasi-particle) excitations. An adequate treatment of these nuclei must thus involve a fairly sophisticated approach such as is provided, for example, by the model of Kumar and Baranger or by calculations with the HRPA.

It is thus of extreme interest to determine if indeed the osmiumnuclei do possess finite quadrupole moments. If they do, the triple relationship mentioned above will again be manifested, and added credence may be conferred on the calculations of Kumar and Baranger and impetus given to further treatments along similar lines. Furthermore, such an eventuality would imply that a detailed understanding of the osmium nuclei, of their transition region, and of similar nuclei may now be near at hand, although a fully acceptable theory should employ more realistic forces than the pairing-plus-quadrupole interactions used so often now.

The investigation of the osmium nuclei is not completed by this study. There are several puzzles remaining and experimental attacks directed toward their elucidation are urgently needed. Several specific suggestions for future research in this region will now be considered. Many have been mentioned in passing earlier.

1) It is very important to determine once and for all whether or not excited 0^+ states exist in these isotopes. For this purpose, (p,t) reactions leading to even-even osmium nuclei should be an appropriate tool. Such reactions tend to

preferentially populate collective 0^+, 2^+ and 3^- levels and so any existing 0^+ states would be likely to be observed. This reaction is also not limited to low excitation energies as is Coulomb excitation. Any 0^+ levels populated could be identified by the transferred ℓ values. Furthermore, other states such as the tentative ones found here at 780, 840 and 855 kev in $Os^{188, 190, 192}$ might be investigated in a similar manner.

2) It is likewise important, as mentioned above, to measure the quadrupole moments of the excited states in osmium. This would be a significant test of the Kumar and Baranger theory. For this purpose one could make use of the so-called "reorientation effect"[56] (see pages 97—98), employing Coulomb excitation with several different projectiles (e.g., C^{12}, O^{16}, S^{32}) to extract the signs and magnitudes of these quantities.

3) To complement the comparison of the properties of the Os nuclei with the calculations of Kumar and Baranger, it is desirable to study the neighboring isotopes of Pt and W to which these authors have also applied their model. In this way the model could be confronted with data on the entire transition region and its merits tested in even greater detail. Specifically, its ability to deal with variations in proton, as well as neutron, number could then be subjected to scrutiny.

4) In order to more fully investigate the structure of Os^{192}, (α, xn) reaction studies leading to this nucleus in the final state would be useful. This reaction is known to preferentially populate the ground band states up to very high angular momenta and thus would reveal any 6^+ and 8^+ states that might exist in this nucleus.

5) Finally, further tests of the rotational structure of the osmium isotopes would also be provided with Coulomb excitation studies using heavier projectiles such as S^{32}. If these latter ions could be accelerated to 100-150 MeV then one would be in the region of oscillation of the relative population curves for the various rotational band members (see Section II-C). The degree to which the the excitation probabilities track the predicted ones would provide a test both of the rotational character of the levels excited and of the accuracy of the model-dependent multiple Coulomb excitation theories. In addition, a similar approach might be applicable to the states of unknown spin and parity suggested earlier at

about 800 kev in $Os^{188, 190, 192}$. It might be feasible to obtain at least a model-dependent set of spin assignments if these levels could be excited with sufficient frequency so that accurate experimental excitation probabilities could be extracted for comparison with the relative population curves. In such an analysis, however, the serious inability of the rotational model to describe accurately the excitation of levels in osmium that are not members of the ground state rotational band would render such assignments helpful but still only very tentative.

The experiments suggested above, and especially the first two and the fourth, would serve to complement our present, quite detailed knowledge of E2 transition probabilities in the osmium nuclei (the latter provided in large part by the experiments described in this thesis). Coupled with the third suggestion, they would thus tend to round out the experimental attack on this important transitional region. A relatively complete body of experimental knowledge would then exist, for these nuclei, with which future generations of theoretical calculations could compare their predictions in the ongoing hope of finally approaching a comprehensive knowledge of collective behaviour in atomic nuclei.

Appendix I

Targets

A. Thin target fabrication

In this appendix two methods of fabrication of self-supporting Os targets will be described. As indicated in Section III-D thin self-supporting evaporated targets of Os have not previously been made and evaporated Os targets on backings have been limited to thicknesses $< 1\ \mu g/cm^2$. For experiments of the type described herein targets of several hundred $\mu g/cm^2$ would be desirable. Other experiments, perhaps involving separation of elastically from inelastically scattered particles would require even thinner foils. These, too, should be producible by the evaporation and floatation method described below.

Os cannot conveniently be evaporated from the usual "boat" arrangement for making many targets due to its high melting point of 2700° C.[113] An electron gun would indeed be suitable for evaporation of osmium powder but most such guns are much less efficient than a directional boat. This can be a serious disadvantage with an expensive material such as osmium. Another problem associated with use of a gun is the possibility of evaporating some of the gun's own base material. Finally, a third problem is that once osmium powder melts it tends to coagulate and, for a fixed beam spot size, to subtend a smaller fraction of the electron beam target area. Compensation by increased power output of the gun leads to recurrence of the second problem mentioned above, even if the gun's base is water-cooled.

This third problem implies that one must avoid magnetically focussing electron guns and use electrostatically operated ones. In the latter, the spot struck by the beam is determined by the electric potentials involved and, by situating the evaporant as physically the closest material to the filament and focussing shield, one will insure that the electron beam will track the evaporant even if the latter should coagulate.

The first two problems mentioned above are soluble by employing as inherently efficient and adaptable a gun as possible and by designing the boat or substrate on which the evaporant rests so as to maximize efficiency and to prevent substrate evaporation.

A suitable gun for these purposes is the MRC V4-200 Electron Vapor Deposition Gun illustrated in Fig. A-1, and described in reference 112. For our needs here it is sufficient to note that, in use, the entire shield and filament assembly is raised to a high positive voltage relative to the grounded, water-cooled copper base assembly into which the boat is screwed. The low voltage, high current power supply used to heat the filament is thus at high negative potential and suitable insulating precautions are necessary. The electrons emitted from the filament are focussed downward onto the boat. The power input into the boat is approximately equal to the product of electron current and shield voltage and can be varied easily from a few watts to almost 2 kw. An advantage of this gun is that the figure of merit is power and any combination of voltage and current giving the desired power is sufficient. Thus, if for some reason high voltages are undesirable or unattainable (due to sparking, for example), one can employ higher currents instead.

The design of the boat is critical and the most successful version is shown in Fig. A-1 (insert). It consists of a cylindrical tungsten rod .250" in diameter and about $\frac{1}{4}$" long press-fitted into a .240" diameter hole in a copper holder which in turn screws into the electron gun's water-cooled base. The press fitting assures good thermal contact (and hence cooling efficiency) between the tungsten and copper. This, plus its greater thermal conductivity, is one reason tungsten is used instead of carbon. Even better thermal contact is achieved by melting the top of the copper so that it flows into intimate contact with the tungsten. The top of the tungsten should previously have been scooped out into a cup-shaped cavity into which small amounts of osmium powder can be placed. This scooping is done with either an abrasive blasting with fine (50 μ) silica pellets using an S. S. White Airbrasive machine or by an "Agietron" Electrical Discharge Machine (EDM).

The cup size should be sufficient so that about 30 mg of Os can be inserted at once. It has been found necessary to load the boat and evaporate several successive charges of Os in order to obtain film thicknesses sufficient to be self-supporting. Employing a larger cup size initially is not an acceptable substitute. Regardless of the amount of Os inserted into the boat only about 15 to 20 mg can be evaporated at once. This is partially due to the coagulation problem mentioned above. The coagulated globules of Os, though "attracting" most of the electron

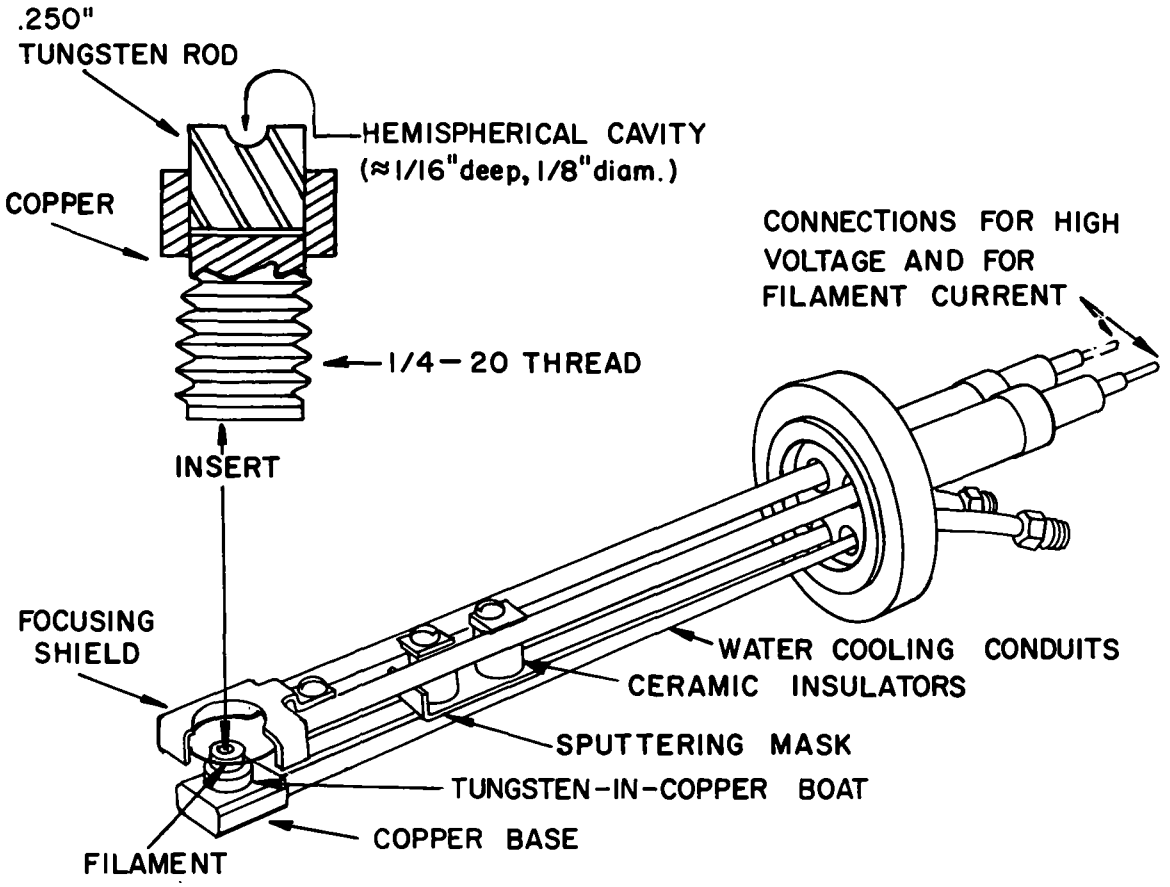

MRC ELECTRON GUN USED IN FABRICATION OF Os TARGETS FIG. A-1

beam, are not nearly as susceptible to evaporation due to their drastically reduced surface area.

The evaporation procedure is described below. It should be noted, however, that the precise timing and characteristics of each step vary considerably with each evaporation due to variations in granular size of the Os powder and to different amounts of globulation.

1) The first step in the thin target fabrication procedure consists a thorough cleaning of the entire gun with water, acetone, and ethanol. If necessary, the shields and copper base may have to be cleaned with acid or sandpaper.

2) Further cleaning is accomplished in this step also. The boat is inserted into the vacuum system with no charge of osmium in it. The high voltage and filament current are gradually raised until about . 8-1. 2 kw of power are striking the tungsten surface. With no Os in the boat the copper is being almost directly heated (despite water-cooling) and care must be taken to insure that the copper does not melt and destroy the boat. After about 10 minutes the power can be gradually reduced to zero and after the system has cooled sufficiently the gun may be removed and a charge of Os powder inserted. Pressures during all stages are not critical but should be at least in the low 10^{-4} mm. Hg. range or high 10^{-5} mm. Hg range at the start of evaporation. Pressures of 2×10^{-6} mm. Hg are typical at the conclusion of an evaporation stage.

3) In order to later float the Os films from the substrate onto which they have been evaporated, the substrate must be coated with some material that easily dissolves in a convenient solvent. The most suitable combination has been found to be an ordinary laboratory glass slide coated by evaporation with reagent grade NaCl. The NaCl film should be quite thin and not powdery or streaked in appearance. These slides may be prepared prior to use and stored in air for up to several days before excessive quantities of adsorbed moisture render them useless.

The use of NaCl has several advantages: 1) It is extremely soluble in water and hence contamination problems are minimized; 2) The contaminants that do remain are known; 3) Floatation success probabilities with NaCl approach 100% even with poorly prepared NaCl films.

4) With 20-30 mg. of Os powder piled high in the boat and with the NaCl-coated glass substrate inserted about 2 inches vertically above the osmium, the chamber may be re-evacuated and the high voltage and filament current may be increased gradually over a period of about 20 minutes so that total power input reaches about .6 kw. Typical settings are: high voltage 4000 V, filament current $\cong$ 150 ma. Somewhere in this power range the osmium will begin to evaporate very slowly and it is of the utmost importance that the electron beam power be set just at the lowest threshold of evaporation. Otherwise coagulation will occur and evaporation will cease. Evaporation should continue at these settings (which may be slightly and gradually raised as evaporation proceeds and fewer electrons are actually striking the remaining Os powder) until no further darkening of the glass slide occurs. Voltage and current should then be reduced slowly to zero and the system let stand to cool for about 30 minutes. Osmium tetra-oxide is poisonous and so care should be taken not to expose the Os to the air while it is at elevated temperatures. Osmium will suffer negligible oxidation at room temperature. Once cooled and removed from vacuum the boat should be recharged and step 4 repeated.

5) Repetition of step 4 should continue until the glass slide is nearly opaque. An alternate test is that the gun's filament with about 16 amperes flowing through it should be merely a dull red when viewed through the glass. When this occurs the glass slide should be removed and (after the Os film is scored into conveniently sized target shapes) placed in the floatation apparatus. This latter merely consists of a holder for the slide which suspends the glass at about 30° to the horizontal in a beaker into which distilled, deionized water can be gradually introduced. The water should be allowed to rise gradually, so that it seeps under the osmium film and dissolves the NaCl. The Os film then floats off and may be picked up on thin metallic holders. These holders must be no more than $\cong$ .020" thick or else water adhering to the perimeter of the central hole will be heavy enough to pull the Os film through and destroy it. Finally, the Os film must be lifted nearly vertically out of the water to reduce surface tension effects. (No contamination problems occurred in these experiments if ethanol was added to the water to reduce surface tension and facilitate picking up of the films.) The resulting Os films must

now be allowed to dry thoroughly before being moved or vibrated. It is during this drying stage that most unsuccessful attempts actually fail. After having dried, the films are quite sturdy.

Approximately 80 mg. of Os is needed for the production of these targets. As many as five or six targets may, however, be obtained in one application of these procedures.

B. Thick target fabrication

The thick targets were considerably easier to fabricate, required only 20-30 mg. of the enriched Os and were somewhat cleaner due in part to reduced surface-to-volume ratios. They were truly thick, being .0029 $\pm$ .0002" thick in all cases. The beam was thus fully stopped in the first few percent of the targets. The difficulty with mechanical methods of production of Os targets such as are to be described is that Os is, mechanically, completely unworkable and non-ductile[113]. Consequently, it cannot be rolled but only pressed or compacted. The reason for these properties is that Os is both the heaviest element known (density = 22.48g/cm^3) and one of the hardest. (Its hardness on the Moh scale is 7.0[114].)

The fabrication procedure consists of forming about 20 mg. of the Os powder into a disk shape on a flat, carefully cleaned slab of carborundum. A second identical carbordundum slab is gently placed on top of the Os powder, care being taken not to disturb the shape of the Os disk. The resulting sandwich is then mechanically pressed. The use of carborundum stems from the fact that it is one of the few substances harder than Os (Moh scale hardness of carborundum = 9.0[114]). Pressure must be applied and released gradually and monotonically. Especially during its initial application, fluctuations in pressure tend to "work" the Os, resulting in entanglement of the embryonic crystallites and preventing further compacting[115]. Pressure may be released after about 30 seconds of constant application.

The amount of pressure necessary is largely irrelevant. Identical results were obtained when 300 lbs. of force were applied at the end of a 3 foot long lever arm of a standard Dake Arbor machine shop mechanical press and when approximately

seven million pounds pressure were applied using the 100 ton hydraulic press of the Yale University High Pressure Laboratory of the EAS Department.*

At this stage the Os is solidified into a flat disk which, though, self-supporting , has a powdery, non-uniform surface and which often exhibits large quantities of contaminants. It is necessary to clean the targets and to fuse their crystallites by annealing. For this purpose one uses the same electron gun as described in part A of this Appendix. The Os disk is placed on a boat identical to the tungsten-in-copper one described in part A except that the top of the tungsten is flat rather than scooped out. Once in the vacuum system, the high voltage and filament current are applied to the electron gun very slowly over a period of about 20 minutes until the Os disk is nearly white hot corresponding to a temperature of about 1300^{0} C. After maintaining this condition for about 20 minutes the power should be reduced slowly over a period of another 20 minutes and the Os allowed to cool gradually to room temperature. During the application of the electron beam care must be taken not to let the heat rise enough that the disk begins to curl at the edges. It is better, if necessary, to anneal for a longer duration at lower temperatures.

Removal of the Os disks from the vacuum system yields resulting targets which are very strong and clean, and are ready to be mounted in their holders. Microscopic examination of these targets reveals a much shinnier, more uniform and fused surface.

* I would like to thank Dr. Carl Nelson and Dr. Lance Davis of that laboratory for several informative discussions concerning the metallurgy of the osmium isotopes and for their help in the use of the hydraulic press.

Appendix II

Computer Programs

The computer programs used in the data analysis were mentioned in Chapter V. Existing programs[25, 27] were used for calculating the weighted integrals of Rutherford cross sections according to the denominator of equation V-17 and for certain portions of the first and second order perturbation theory analyses. An existing program[27] for calculating thick target integrals of weighted Alder Coulomb excitation probabilities based on the rotational model[64] was modified and improved somewhat and used for the calculation of ground state band excitation probabilities.

Most of the data analysis, however, was carried out using two versions of the Winther and de Boer Coulomb excitation program[61] discussed in Sections II-C and V-E. The first was nearly identical to the published version of the program and was used for calculation of Coulomb excitation probabilities and cross sections for the case of given incident projectile energy and backscattering angle. The second was a highly modified version included as a subprogram providing the cross sections for a main program which calculated thick target integrals of the weighted Coulomb excitation cross sections.

As this last program turned out to be a very convenient tool of analysis, a listing of the Fortran IV deck is given below. The program has been run successfully on the Yale Computer Center 7094-7040 system. A typical calculation of the numerator of eq. V-17 for 7 nuclear states over an energy range of approximately 12 MeV, using the M = 0 magnetic substate only, requires about 25 seconds of computer time. The integration is performed numerically via Simpson's rule with an additional remainder term which corrects for non-integral numbers of steps in the range of integration. The number of magnetic substates to be included in the calculations and the accuracy of the computation of the cross sections are selectable in the same way as in the original Winther-de Boer program[61]. Immediately following the program listing is a typical set of data cards relevant to the computation of the Coulomb excitation of 7 states of Os^{188} by 70.30 MeV incident O^{16} ions.

Many of the data cards are identical to those used in the standard Winther-de-Boer thin target program[61] and will not be discussed here. It will be noted, however, that the card controlling the calculation of the angular distribution coefficients has been deleted since the thick target program only computes excitation probabilities and cross sections. Besides charge and mass information, the bombarding energy and the backscattering angles at which the integrals are to be computed, new input data consists of the number of levels, k, for which integrals are desired (last entry, card # 1), the set of cutoff energies, E_{cut_i}, which specify the lower limit on the thick target integrals for each state i (card # 3), and the coefficients of the energy loss formula, dx/dE (last entries, card # 2). The format specifications for the new data entries may, of course, be determined from the appropriate statements in the listing below.

```
C       THICK TARGET INTEGRALS OF WINTHER DEBOER COULOMB EXCITATION PROBS
        COMMON/B/DSIG(40,10)
        DIMEMSION DED(3), TE(500), ESUM(500), EMIN(10)
        NI= 5
        NO=6
  111   READ(NI,2) EMAX, ESTEP, TMAX, TMIN, TSTEP, K
    2   FORMAT(5F10.5,I2)
        READ(NI,3) Z1, A1, Z2, A2
    3   FORMAT(4F10.2)
        READ(5,6) DED(1), DED(2), DED(3)
    6   FORMAT(3F10.5)
        READ(NI,10)(EMIN(N), N = 1,K)
   10   FORMAT(10F7.3)
        WRITE(NO,4) EMAX, ESTEP, TMAX, TMIN, TSTEP
    4   FORMAT(1H1,5F10.3)
        WRITE(6,5) A1, Z1, A2, Z2, DED(1), DED(2), DED(3)
    5   FORMAT(1H0,4F6.1,12H    DX/DE = F8.5,5H  +  F8.5,7H*E  +  F8.5,4H*E*E)
       /E*E)
        WRITE(NO,12)(EMIN(N),N=1,K)
   12   FORMAT(1H0,10F7.3)
  610   TCMAX = TMAX
        TCMIN = TMIN
  620   KMAX = (TCMAX - TCMIN)/TSTEP + 1.0
        WRITE(NO,8) TCMAX,TCMIN,KMAX
    8   FORMAT (1H0,5X,17HTHETAMAX(C.M.) = F8.3,20H   THETAMIN(C.M.) = F8.
       3,10H   KMAX = I5)
        T = TCMAX
C       DO LOOP OVER ANGLES
        DO 2000 KA = 1,KMAX
        ECUT = EMIN(1) - 1.0
        LMAX = (EMAX - ECUT)/ESTEP  +  2.0
        E = EMAX
C       DO LOOP OF DEBOER-WINTHER PROBS OVER ENERGY
        CALL PROT(E,T,LMAX, ESTEP, DSIG)
C       DO LOOP OVER STATES
        DO 3000 N = 1,K
        E = EMAX
  102   PLMAX = (EMAX - EMIN(N))/ESTEP + 1.0
        LMAX = PLMAX
        ELMAX=LMAX
        IF(AMOD(FLMAX,2.0)) 106,150,106
  150   LMAX=LMAX+1
        FLMAXN = LMAX
        RLMAXO = (FLMAXN - PLMAX)*ESTEP
        WRITE(6,189) RLMAXO
  189   FORMAT(1H0,9HRLMAXO = ,F10.5)
        WRITE(6,444)
  444   FORMAT(1X,4HOVER//)
        GO TO 114
C       DO LOOP FOR INTEGRATION OVER ENERGY.
  106   RLMAXU = (PLMAX - FLMAX)*ESTEP
        WRITE(6,191) RLMAXU
  191   FORMAT(1H0,9HRLMAXU = ,F10.5)
  114   LMAXN = LMAX + 1
        DO 4000 L = 1,LMAXN
        TE(L) = DSIG(L,N)*(DED(1) + E*DED(2) + E*E*DED(3))
 4000   E = E - ESTEP
C       SIMPSONS RULE FOR INTEGRATION OVER ENERGY.
  105   ESUM(KA)=TE(1)+4.0*TE(LMAX-1)+TE(LMAX)
        LMAXL = LMAX - 2
        DO 300 L = 3,LMAXL,2
  300   ESUM(KA) = ESUM(KA) + 4.0*TE(L-1) + 2.0*TE(L)
        ESUM(KA) = ESUM(KA)*ESTEP/3.0
        IF (AMOD(FLMAX,2.0)) 107,151,107
  151   ESUM(KA) = ESUM(KA) - RLMAXO*(TE(LMAX) + TE(LMAX - 1))/2.0
        GO TO 29
  107   ESUM(KA) = ESUM(KA) + RLMAXU*(TE(LMAX) + TE(LMAX + 1))/2.0
   29   WRITE(NO,30) N,ESUM(KA), KA, T
```

```
   30 FORMAT(1H0,5X53HTHICK TARGET INTEGRAL OF CROSS SECTION FOR STATE N
     /(= I3,4H) = E12.5,8H    KA =I2,18H    THETA(C.M.) = F8.3)
 3000 CONTINUE
 2000 T = T - TSTEP
      GO TO 111
      END
$IBFTC PROTE   DECK
      SUBROUTINE PROT(E,THETA,LMAX, ESTEP, DSIG)
C
C     DEBOER-WINTHER MULTIPLE COULOMB EXCITATION PROGRAM
C
      COMMON COT1,COT2
      COMMON/B/DSIG(40,10)
      COMMON/Y/ACC10
      COMMON /XX/NMAX,EN(10),SPIN(10),MATRIX(10,10),FMT4(6),XNUM(10)
      REAL MATRIX
      INTEGER OUXI,OUPSI,OUAMP,OUPROW
      DIMENSION XI(10,10),PSI(10,10),QU(10,10,6),P(10)
      DIMENSION Q1(180,4),PROB(90),AMPP(180,4),F(180,4,4)
      DIMENSION CAT(90,3),ZETA(90,90),AMPDOT(180,4),AMP(180,4)
      DIMENSION DSIGLB(10),TCMDG(10),ZLBDG(10)
      DIMENSION R3(10),R4(10),EPP(10)
      DIMENSION FMT(7),FMT1(9),FMT2(7),FMT3(6)
      DIMENSION FT(17),FT1(5),FT2(6),FT3(8),FT4(13),FT5(5)
      DATA FMT(1)/41H(1H0,6X1HW2X       (6X2HP(I2,1H))6X4HPTOT)/
      DATA FMT1(1)/54H(34H0ENERGY SPECTRUM     LEVEL INDEX N,          (I
     1 9))/
      DATA FMT2(1)/37H(1H0,20X13HENERGY IN MEV       (F9.4))/
      DATA FMT3(1)/32H(1H0,20X4HSPIN,9X        (F9.4)/)/
      DATA FT(1)/98H(28H0EXECUTION TERMINATED AT W= F10.6,6HPTOT= F14.
     1        ,33H ERROR IN PTOT EXCEEDS 20 * ACCUR)/
      DATA FT1(1)/25H(1XF10.3,11F11.          )/
      DATA FT2(1)/32H(1XF5.1,F12.1,1X2(1XF20.       ))/
      DATA FT3(1)/43H(5XI3,11XF15.            ,8XE15.           )/
      DATA FT4(1)/73H(2XI3,13XF7.2,5XF15.           ,8XE15.           , 8XF8
     1XF8.3,12XF7.2,12XF9.5)/
      DATA FT5(1)/25H(1H ,3I7,2F20.           )/
C
C     READ IN STARTS
C
  500 READ(5,106) INTERV,NTIME,NCM,ACCUR
  106 FORMAT(3I5,F10.7)
C     INTERV - PRINT OUT OF P(N) WILL OCCUR EVERY INTERV-TH STEP
C     NTIME IS THE TIME IN MIN ALLOWED FOR THE JOB
C     NCM PICKS LEVEL FOR WHOSE CM SCATTERING ANGLE ORBIT IS CALCULATED
C     ACCUR IS ACCURACY WITH WHICH INTEGRATION IS PERFORMED
C
      IF(INTERV) 46,46,47
   46 CALL EXIT
C     INTERV .LE. ZERO ON LAST DATA CARD INDICATES NO MORE DATA
   47 READ(5,102)XIMAX,EMMAX,NMAX
  102 FORMAT(2F10.0,I5 )
C     XIMAX IS LARGEST XI CONSIDERED
C     EMMAX IS LARGEST MAGNETIC QUANTUM NUMBER CONSIDERED
C     NMAX IS NUMBER OF NUCLEAR LEVELS CONSIDERED
      READ(5,104) OUXI,OUPSI,OUAMP,OUPROW
  104 FORMAT(4I5)
C     IF THE OUTS ARE ENTERED AS ZERO NO OUTPUT WILL OCCUR
C
      READ(5,100) Z1,A1,Z2,A2
  100 FORMAT(4F10.2)
```

```
  101 READ(5,105)(EN(N),SPIN(N),N=1,NMAX)
  105 FORMAT(2F10.0)
C     PRINT OUT OF INPUT DATA .
      WRITE(6,430)
  430 FORMAT(54H1DE BOER - WINTHER MULTIPLE COULOMB EXCITATION PROGRAM/)
      EP = E
      WRITE(6,431) Z1,A1,EP
  431 FORMAT(32H0PROJECTILE CHARGE NUMBER  Z1 = F6.2,14H,  MASS  A1 =
     1F8.3,23HAMU,  LAB ENERGY  EP = F8.3,3HMEV)
  435 WRITE(6,437) Z2,A2
  437 FORMAT(28H0TARGET CHARGE NUMBER  Z2 = F6.2,14H,  MASS  A2 = F8.3,
     113HAMU/)
      FMT1(8) = XNUM(NMAX)
      WRITE(6,FMT1)(N,N=1,NMAX)
      FMT2(5) = XNUM(NMAX)
      WRITE(6,FMT2)(EN(N),N=1,NMAX)
      FMT3(4) = XNUM(NMAX)
      WRITE(6,FMT3)(SPIN(N),N=1,NMAX )
C     THE QUADRUPOLE MATRIX ELEMENTS ARE PRODUCED IN THE MAT SUBROUTINE
      CALL MAT
C
C     DECIMAL PLACES FOR PRINTOUT
      IJ=0
      AC=ACCUR
   30 AC=AC*10.0
      IJ=IJ+1
      IF(1.0-AC) 31,30,30
   31 CONTINUE
C     IJ HOLDS NO. OF DECIMAL PLACES WANTED IN PRINT OUT OF RESULTS
C     ACCORDING TO ACCURACY OF INTEGRATION
  451 CONTINUE
      SWITCH = 0.0
      DO 1000 MEN = 1, LMAX
      WRITE(6,994)EP
  994 FORMAT(1H0,5HEP = F10.5)
C     COMPUTATION OF XI MATRIX
C
      CXI = Z1*Z2*SQRT(A1)/6.325
      DO 3 M=1,NMAX
      DO 3 N=1,NMAX
      XI(N,M) = 100.0
      IF(MATRIX(N,M))4,3,4
    4 RX1 = 1.0/SQRT(EP-(1.+(A1/A2))*EN(N))
      RX2 = 1.0/SQRT(EP-(1.+(A1/A2))*EN(M))
      XI(N,M) = CXI*(RX1-RX2)
    3 CONTINUE
      IF(OUXI)5,452,5
    5 WRITE(6,203)
  203 FORMAT(10H0XI MATRIX)
      DO 7 N = 1,NMAX
    7 WRITE(6,207) N,(XI(N,M),M=1,NMAX)
  207 FORMAT(4H0N =I2,10F12.4)
C
C     DETERMINATION OF THE LARGEST XI VALUE IN XI MATRIX
  452 XIM = 0.0
      DO 25 M = 1,NMAX
      DO 25 N = 1,NMAX
      IF(XI(N,M).GT.XIMAX)GO TO 25
      IF(XI(N,M).LE.XIM)GO TO 25
      XIM = XI(N,M)
   25 CONTINUE
      WRITE(6,300)XIM
  300 FORMAT(7H0XIM = F10.4)
C
```

```
C      COMPUTATION OF PSI MATRIX
C
       CPSI = 14.36*SQRT(A1)/((1.+(A1/A2))**2 * Z1*Z2*Z2)
       DO 8 M=1,NMAX
       DO 8 N = 1,NMAX
       PP1 = (EP- (1.+(A1/A2))*EN(N))**.75
       PP2 = (EP- (1.+(A1/A2))*EN(M))**.75
    8  PSI(N,M)=CPSI*PP1*PP2*MATRIX(N,M)
       IF(OUPSI)10,11,10
   10  WRITE(6,204)
  204  FORMAT(11H0PSI MATRIX)
       DO 12 N = 1,NMAX
   12  WRITE(6,207) N,(PSI(N,M),M=1,NMAX)
   11  CONTINUE
       IF(SWITCH)446,441,446
  441  WRITE(6,442)
  442  FORMAT(84H0PERFORMANCE CONTROLS  NMAX,   INTERV,   NCM,   EMMAX,
     1 XIMAX,     ACCUR,     NTIME)
       WRITE(6,443) NMAX,INTERV,NCM,EMMAX,XIMAX,ACCUR,NTIME
  443  FORMAT(1H0,19X,I6,2X,2I8,2F9.2,F13.7,I7)
       EMCCK=EMMAX-SPIN(1)+0.001
       WRITE(6,444)
  444  FORMAT(49H0OUTPUT CONTROLS        OUXI, OUPSI, OUAMP, OUPROW)
       WRITE(6,445) OUXI,OUPSI,OUAMP,OUPROW
  445  FORMAT(1H0,17X3I7,I8)
C
C      RANGE AND STEP WIDTH OF THE INTEGRATION
C
       WRITE(6,781) THETA
  781  FORMAT(55H0CM SCATTERING ANGLE USED FOR INTEGRATION IS TCMDG(NCM)
     13H = F7.2,8H DEGREES)
  446  TRAD=THETA/57.295779
       STR = SIN(TRAD/2.0)
       EPS = 1.0/STR
       UP=ALOG(1.0/(EPS*SQRT(ACCUR)))
       COT1 = COS(TRAD/2.0)*EPS
       COT2 = COT1*COT1
       ACC10=ACCUR/10.0
       DW=40.0*(ACCUR**0.2)/(10.0+48.0*XIM+16.0*XIM*EPS)
       IF((5.0*DW).GT.UP) DW=0.4*UP
       ISTEP=UP/DW
       IF(SWITCH)980,981,980
  981  WRITE(6,202)EPS,UP,ISTEP
  202  FORMAT(7H0EPS = F7.3,/
     128H0RANGE OF INTEGRATION, UP = F6.2 /
     236H0ESTIMATED NUMBER OF STEPS, ISTEP = I4)
  980  D2W = DW + DW
       IF(SWITCH)984,983,984
  983  WRITE(6,251)D2W
  251  FORMAT(27H0INITIAL STEP WIDTH, D2W = F8.5)
C
C      CATALOGUE OF MAGNETIC SUBSTATES
C
  984  IS = 1
       DO 18 N= 1,NMAX
       QUAN = SPIN(N)
       IF(QUAN.GT.EMMAX)QUAN = EMMAX
       MSTOP = 2.0*QUAN + 1.0
       QUAN = -QUAN
       DO 15 I = 1,MSTOP
       CAT(IS,1) = N
       CAT(IS,2)= SPIN(N)
       CAT(IS,3) = QUAN
       QUAN = QUAN +1.0
       IS = IS + 1
   15  CONTINUE
   18  CONTINUE
```

```
      ISMAX = IS -1
      IF(SWITCH)254,986,254
  986 WRITE(6,250)ISMAX
  250 FORMAT(45H0TOTAL NUMBER OF MAGNETIC SUBSTATES, ISMAX = I3)
      IF(ISMAX-90)254,254,252
  252 WRITE(6,253)
  253 FORMAT(24H0 ERROR ISMAX EXCEEDS 90)
      GO TO 500
  254 CONTINUE
C
C     COMPUTATION OF ZETA MATRIX
C
      AA2 =2.0
      DO 29 IS = 1,ISMAX
      IEX = CAT(IS,2)-CAT(IS,3) + 0.0001
      PHZ = (-1.0)**IEX
      JP = CAT(IS,1) + 0.001
      B1 = -CAT(IS,3)
      AA1 = CAT(IS,2)
      DO 20 IR = 1,ISMAX
      B2 = CAT(IS,3)-CAT(IR,3)
      IF(ABS(B2).GT.2.001)GO TO 815
      A3 = CAT(IR,2)
      B3 = CAT(IR,3)
      IP = CAT(IR,1) + 0.001
      ZETA(IR,IS)=PHZ*PSI(IP,JP)*2.236068*THREEJ(AA1,B1,AA2,B2,A3,B3)
      GO TO 20
  815 ZETA(IR,IS)=0.0
   20 CONTINUE
   29 CONTINUE
C
C     INTEGRATION OF THE DIFFERENTIAL EQUATIONS STARTS HERE
C
C     INITIAL CONDITIONS FOR INTEGRATION
C
      ISTEPS=0
C     ISTEPS COUNTS ACTUAL NUMBER OF STEPS
      KAST=0
      LMAX =  SPIN(1) + 1.001
      IZMAX = ISMAX+ISMAX
      W = -UP
      DO 80 L = 1,LMAX
      DO 81 IZR = 1,IZMAX
      AMP(IZR,L)=1.0 E-30
      IF(L.EQ.IZR)AMP(IZR,L)=1.0
   81 CONTINUE
   80 CONTINUE
C
C     INTEGRATION ROUTINE
C
C     CONSTANTS USED IN RUNGE-KUTTA EQUATIONS
      RB1=0.5857864
      C1=0.1213204
      RB2=3.4142136
      C2=-4.1213204
C
C     HEADING FOR PROW (VARIABLE FORMAT)
      IF(OUPROW.EQ.0) GO TO 399
      FMT(3)=XNUM(NMAX)
      WRITE(6,FMT)(N,N=1,NMAX)
      P(1)=1.00
      PTOT=1.00
      DO 70 N=2,NMAX
   70 P(N)=0.00
      FT1(4)=XNUM(IJ)
      WRITE(6,FT1) W,(P(N),N=1,NMAX),PTOT
C
C     THE RUNGE-KUTTA-GILL INTEGRATION PROCEDURE
```

```
  399 CONTINUE
      CALL Q(W,EPS,XIMAX,XI,NMAX,QU)
      CALL AMPDER(CAT,ZETA,AMP,QU,LMAX,ISMAX,AMPDOT)
      DO 400 L = 1,LMAX
      DO 400 IZR = 1,IZMAX
  400 F(IZR,L,1) = AMPDOT(IZR,L)
      DO 401 NAM = 2,4
      DO 90 L = 1,LMAX
      DO 91 IZR = 1, IZMAX
      Q1(IZR,L) = DW*AMPDOT(IZR,L)
      AMP(IZR,L)=AMP(IZR,L)+Q1(IZR,L)
   91 CONTINUE
   90 CONTINUE
      W = W + DW
      CALL Q(W,EPS,XIMAX,XI,NMAX,QU)
      CALL AMPDER(CAT,ZETA,AMP,QU,LMAX,ISMAX,AMPDOT)
      DO 96 L = 1,LMAX
      DO 97 IZR = 1,IZMAX
      RK1 = DW*AMPDOT(IZR,L)
      AMP(IZR,L) = AMP(IZR,L) + RB1*(RK1 - Q1(IZR,L) )
      Q1(IZR,L) = RB1*RK1 + C1*Q1(IZR,L)
   97 CONTINUE
   96 CONTINUE
      CALL AMPDER(CAT,ZETA,AMP,QU,LMAX,ISMAX,AMPDOT)
      DO 98 L = 1,LMAX
      DO 99 IZR = 1,IZMAX
      RK2 = DW*AMPDOT (IZR,L)
      AMP(IZR,L) = AMP(IZR,L) + RB2*(RK2 - Q1(IZR,L))
      Q1(IZR,L) = RB2*RK2 + C2*Q1(IZR,L)
   99 CONTINUE
   98 CONTINUE
      W = W + DW
      CALL Q(W,EPS,XIMAX,XI,NMAX,QU)
      CALL AMPDER(CAT,ZETA,AMP,QU,LMAX,ISMAX,AMPDOT)
      DO 110 L = 1,LMAX
      DO 111 IZR = 1,IZMAX
      RK3 = DW*AMPDOT(IZR,L)
      AMP(IZR,L) = AMP(IZR,L) + RK3/3.0 - 2.0*Q1(IZR,L)/3.0
  111 CONTINUE
  110 CONTINUE
      CALL AMPDER(CAT,ZETA,AMP,QU,LMAX,ISMAX,AMPDOT)
      DO 402 L = 1,LMAX
      DO 402 IZR = 1,IZMAX
  402 F(IZR,L,NAM) = AMPDOT(IZR,L)
      ISTEPS=ISTEPS+1
      KAST=KAST+1
  401 CONTINUE
C     WE NOW HAVE THE 4 STARTING VALUES OF THE DERIVATIVES AND CAN
C     PROCEED BY THE ADAMS-MOULTON METHOD
C
C     THE ADAMS-MOULTON ROUTINE
C
   95 CONTINUE
      DO 403 L = 1,LMAX
      DO 403 IZR = 1,IZMAX
      AMPP(IZR,L) = AMP(IZR,L) + DW/12. *(55.*F(IZR,L,4)
     1-59.*F(IZR,L,3) + 37.*F(IZR,L,2) - 9.*F(IZR,L,1) )
  403 CONTINUE
      W = W + DW + DW
      KAST = KAST + 1
      ISTEPS=ISTEPS+1
      CALL Q(W,EPS,XIMAX,XI,NMAX,QU)
      CALL AMPDER(CAT,ZETA,AMPP,QU,LMAX,ISMAX,AMPDOT)
      DO 404  L = 1,LMAX
      DO 404 IZR = 1,IZMAX
      AMP(IZR,L) = AMP(IZR,L) + DW/12. * (9.*AMPDOT(IZR,L)
     1+ 19.0*F(IZR,L,4) - 5.*F(IZR,L,3) + F(IZR,L,2))
  404 CONTINUE
```

```
      CALL AMPDER(CAT,ZETA,AMP,QU,LMAX,ISMAX,AMPDOT)
      DO 405 L = 1,LMAX
      DO 405 IZR = 1,IZMAX
      F(IZR,L,1) = F(IZR,L,2)
      F(IZR,L,2) = F(IZR,L,3)
      F(IZR,L,3) = F(IZR,L,4)
      F(IZR,L,4) = AMPDOT(IZR,L)
  405 CONTINUE
  579 IF(W.GT.UP) GO TO 571
C
C     ACCURACY CONTROL
C
      FF=0.0
C     FIND LARGEST AMPP - AMP
      DO 573 L=1,LMAX
      DO 574 IR=1,ISMAX
      IMAG = IR + ISMAX
      FZR = AMPP(IR,L) - AMP(IR,L) +1.0 E-30
      FZI=AMPP(IMAG,L)-AMP(IMAG,L) + 1.0 E-30
      FZ=(SQRT(FZR*FZR+FZI*FZI))/14.0
      IF(FZ-FF)574,574,21
   21 FF=FZ
  574 CONTINUE
  573 CONTINUE
      ACC050 = ACCUR/ 50.0
      IF(FF.LT.ACC050) GO TO 575
      IF(FF.GT.ACCUR) GO TO 577
      IF(KAST-INTERV)95,571,571
  575 DW=2.0*DW
      D2W=DW+DW
      WRITE(6,576) W,D2W
  576 FORMAT(8H0AT W = F7.3,36H, STEP WIDTH WAS DOUBLED TO BE D2W =F8.5)
      GO TO 399
  577 DW=DW/2.0
      D2W=DW+DW
      WRITE(6,578) W,D2W
  578 FORMAT(8H0AT W = F7.3,36H, STEP WIDTH WAS HALVED TO BE D2W = F8.5)
      GO TO 399
C
C     THE EXCITATION PROBABILITIES DURING INTEGRATION
C
  571 LLMAX = 2.0*(SPIN(1) + 1.001)
      DO 52 IR = 1,ISMAX
      IMAG = IR+ISMAX
      PROB(IR)=0.0
      L = 1
      DO 54 LL =  2,LLMAX,2
C     LL IS INDEX COUNTER ONLY
      IF(LL-LLMAX)50,51,52
   50 FAC = 2.0
      GO TO 53
   51 FAC = 1.0
   53 CONTINUE
      PROB(IR)=PROB(IR)+(FAC/(2.0*SPIN(1)+1.0))*(AMP(IR,L)*AMP(IR,L)+
     1AMP(IMAG,L)*AMP(IMAG,L))
      L=L+1
   54 CONTINUE
   52 CONTINUE
      IR=1
      DO 61 N = 1,NMAX
      P(N) = 0.0
   60 P(N) = P(N) + PROB(IR)
      IR = IR + 1
      IF(IR.GT.ISMAX) GO TO 62
      ICAT = CAT(IR,1) + .01
      IF(ICAT-N) 60,60,61
   61 CONTINUE
   62 CONTINUE
```

```
      PTOT=0.0
      DO 410 N = 1,NMAX
  410 PTOT = PTOT + P(N)
      IF(W.GT.UP) GO TO 93
C
C     PTOT CHECK
      ABW = ABS(PTOT - 1.0)/20.0
      IF(ABW.LT.ACCUR) GO TO 93
      FT(10)=XNUM(IJ)
      WRITE(6,FT) W,PTOT
      GO TO 500
   93 IF(OUPROW)801,802,801
  801 WRITE(6,FT1) W,(P(N),N=1,NMAX),PTOT
  802 KAST=0
      IF(W-UP)95,92,92
   92 CONTINUE
      WRITE(6,790) ISTEPS
  790 FORMAT(34HOACTUAL NUMBER OF STEPS, ISTEPS = I4)
C
C     INTEGRATION COMPLETED
C
C     PRINT-OUT OF THE FINAL AMPLITUDES AMP(W=+UP)
  572 IF(OUAMP)350,122,350
  350 DO 120 L=1,LMAX
      WRITE(6,313) CAT(L,3)
  313 FORMAT(13H1INITIAL M = F4.1 )
      WRITE(6,314)
  314 FORMAT(1H0,1X4HSPIN5X12HMAG.QUAN.NO.6X14HREAL AMPLITUDE7X
     114HIMAG AMPLITUDE/)
      VAL = CAT(1,1)
      DO 120 IZR = 1,ISMAX
      IMAG = IZR + ISMAX
      IF(CAT(IZR,1) - VAL) 842,842,840
  840 VAL = CAT(IZR,1)
      WRITE(6,841)
  841 FORMAT(1H0)
  842 FT2(5)=XNUM(IJ)
      WRITE(6,FT2)(CAT(IZR,LC),LC=2,3),AMP(IZR,L),AMP(IMAG,L)
  120 CONTINUE
  122 CONTINUE
C
C     COMPUTATION OF THE DIFFERENTIAL CROSS-SECTIONS
C
C     HEADING FOR CM CROSS SECTIONS
  298 WRITE(6,510)
  510 FORMAT(1H0,12H LEVEL INDEX10X10HEXCITATION11X16HCM CROSS SECTION/
     122X13HPROBABILITIES9X15HBARNS/STERADIAN//7X1HN18X4HP(N)18X
     211HDSIG(MEN,N))
      GO TO 297
  297 CDSIG1 = (1.0+A1/A2)
      CDSIG=SQRT(EP)*(CDSIG1*Z1*Z2/EP)**2
      DO 470 N = 1,NMAX
      DSIG(MEN,N)=.001296*CDSIG*SQRT(1./(EP-CDSIG1*EN(N)))
     1*P(N)*(EPS**4)
  295 FT3(4) = XNUM(IJ)
      FT3(7) = XNUM(IJ+1)
      WRITE(6,FT3) N,P(N),DSIG(MEN,N)
      SWITCH = SWITCH + 1.0
  470 CONTINUE
 1000 EP = EP - ESTEP
      RETURN
      END
$IBFTC BLKDTA  DECK
      BLOCK DATA
      COMMON /XX/NMAX,EN(10),SPIN(10),MATRIX(10,10),FMT4(6),XNUM(10)
      REAL FMT4,XNUM
      DATA FMT4(1)/33H(1H0,10X,2HM=           (I2,10X))/,(XNUM(I),I=1,10)
     1)/1H1,1H2,1H3,1H4,1H5,1H6,1H7,1H8,1H9,2H10/
      END
```

```
$IBFTC MATE    DECK
      SUBROUTINE MAT
C
C     READ IN AND PRINT OUT OF E2-MATRIX ELEMENTS
C
      REAL MATRIX
      COMMON /XX/NMAX,EN(10),SPIN(10),MATRIX(10,10),FMT4(6),XNUM(10)
      DO 36 N=1,NMAX
   36 READ(5,1)(MATRIX(N,M),M=1,NMAX)
    1 FORMAT(6F12.4)
      WRITE(6,441)
  441 FORMAT(53H0QUADRUPOLE MATRIX ELEMENTS IN BARNS, READ FROM DATA
     15HCARDS)
      FMT4(4) = XNUM(NMAX)
      WRITE(6,FMT4)(M,M=1,NMAX)
      DO 2 N=1,NMAX
    2 WRITE(6,207) N,(MATRIX(N,M),M=1,NMAX)
  207 FORMAT(4H0N =I2,10F12.4)
      RETURN
      END
$IBFTC FAC10F  DECK
      FUNCTION FAC10(N)
C
C     FAC10 GENERATES FACTORIAL(N)/10**N FOR INTEGERS N.LT.79
C
      IF(N)1,2,3
    1 WRITE(6,6)
    6 FORMAT(36H0ERROR- FACTORIAL OF NEGATIVE NUMBER)
      RETURN
    2 FAC10=1.0
      RETURN
    3 IF(N.GT.79) GO TO 5
      FAC10=1.0
      Q=1.0
      DO 4 K=1,N
C     K IS INDEX COUNTER ONLY
      FAC10=FAC10*Q/10.0
      Q=Q+1.0
    4 CONTINUE
      RETURN
    5 WRITE(6,7)
    7 FORMAT(33H0ERROR- FACTORIAL OF NUMBER.GT.79)
      RETURN
      END
$IBFTC THREE   DECK
      FUNCTION THREEJ(A1, B1, A2, B2, A3, B3)
C
C     A FUNCTION FOR THREE J SYMBOLS WITH ARBITRARY ARGUMENTS
C
C     ROTENBERG ET. AL. (1.5) PAGE 2 WITH (2.4) FROM PAGE 13
C     INPUT IS THREE-J(J1,M1,J2,M2,J3,M3) FLOATING POINT ARGUMENTS
C     ROUTINE REQUIRES FACTORIAL FUNCTION ROUTINE
C
      DIMENSION A(3), B(3)
      A(1) = A1
      A(2) = A2
      A(3) = A3
      DO 19 N=1,3
      IF(A(N)+0.001) 20,19,19
   20 WRITE(6,60)
   60 FORMAT(28H0ERROR- NEGATIVE J IN THREEJ)
      CALL EXIT
   19 CONTINUE
   21 LA1=A1+A2+A3+0.001
      LA2=A1+A2+A3+0.6
      IF(LA2-LA1) 22,23,22
   22 WRITE(6,61)
   61 FORMAT(39H0ERROR- HALF INTEGER SUM OF J IN THREEJ)
      CALL EXIT
```

```
   B(1) = B1
   B(2) = B2
   B(3) = B3
   LB1=ABS(B1+B2+B3)+0.001
   LB2=ABS(B1+B2+B3)+0.6
   IF(LB2-LB1) 24,16,24
24 WRITE(6,62)
62 FORMAT(39HOERROR- HALF INTEGER SUM OF M IN THREFJ)
   CALL EXIT
16 NBA1=ABS(B1)-A1-100.001
   NBA2=ABS(B1)-A1-100.6
   IF(NBA2-NBA1) 30,40,30
40 IF(NBA1.GT.(-100)) GO TO 26
   NBA1=ABS(B2)-A2-100.001
   NBA2=ABS(B2)-A2-100.6
   IF(NBA2-NBA1) 30,41,30
41 IF(NBA1.GT.(-100)) GO TO 26
   NBA1=ABS(B3)-A3-100.001
   NBA2=ABS(B3)-A3-100.6
   IF(NBA2-NBA1)30,42,30
42 IF(NBA1.GT.(-100)) GO TO 26
   GO TO 52
30 WRITE(6,63)
63 FORMAT(35HOERROR- J-M HALF INTEGER IN THREE J)
   CALL EXIT
26 WRITE(6,64)
64 FORMAT(33HOERROR- M LARGER THAN J IN THREEJ)
   CALL EXIT
52 IF(LB1) 1,2,1
 2 S1 = A1 + A2 - A3 +0.001
   IF(S1)1,12,12
12 S2 = A1 -A2 + A3  +0.001
   IF(S2)1,14,14
14 S3 = A2 + A3 - A1+0.001
   IF(S3)1,15,15
15 N=ABS(A1-A2-B3)+0.001
   PHZ = (-1.0)**N
   M = S1
   FS1=FAC10(M)
   M = S2
   FS2=FAC10(M)
   M = S3
   FS3=FAC10(M)
   FD=FAC10(LA1+1)
   DELTA=SQRT((FS1*FS2*FS3)/(FD*10.01))
   X=1.0
   DO 3 J = 1,3
   M=A(J)+B(J)+0.001
   FS=FAC10(M)
   X=X*FS
   M= A(J)-B(J)+0.001
   FSM=FAC10(M)
 3 X = X*FSM
   ROOT = SQRT(X)
   SUM = 0.0
   AK = 0.0
11 DS1 = AK+A3-A1-B2 +0.001
   IF(DS1)5,4,4
 4 M = DS1
   FDS1=FAC10(M)
   DS2 = AK + B1 + A3 - A2 +0.001
   IF(DS2)5,6,6
 6 M = DS2
   FDS2=FAC10(M)
   DS3 = A1 - B1 - AK +0.001
   IF(DS3)8,7,7
```

```
      7 M = DS3
        FDS3=FAC10(M)
        DS4 = A1 + A2 - A3 - AK+0.001
        IF(DS4)8,9,9
      9 M = DS4
        FDS4=FAC10(M)
        DS5 = A2 + B2 - AK +0.001
        IF(DS5)8,10,10
     10 M = DS5
        FDS5=FAC10(M)
        M = AK +0.001
        FAK=FAC10(M)
        TOP=(-1.0)**M
        DENOM = FAK*FDS1* FDS2* FDS3* FDS4* FDS5
        SUM = SUM + (TOP/DENOM)
      5 AK = AK + 1.0
        GO TO 11
      8 THREEJ=PHZ*DELTA*ROOT*SUM
        RETURN
      1 THREEJ = 0.0
        RETURN
        END
$IBFTC QR       DECK
        SUBROUTINE Q(W,EPS,XIMAX,XI,NMAX,QU)
C
C       GENERATES QU(N,M,NU) FOR A GIVEN W
C
        COMMON COT1,COT2
        REAL NOMW
        DIMENSION XI(10,10),QU(10,10,6)
        EW = EXP(W)
        COSHY= 0.5 * (EW+ 1.0/EW)
        SINHY= 0.5*(EW-1.0/EW)
        DW1 = EPS*COSHY + 1.0
        DWSQ = DW1*DW1
        DENW = DWSQ*DWSQ
        NOMW = COSHY + EPS
        PE1 = 0.75*(2.0*NOMW*NOMW - COT2*SINHY*SINHY)/DENW
        PE2 = 1.83711730 * COT1 * SINHY* NOMW/DENW
        PE3 = 0.91855865 * COT2 * SINHY*SINHY/DENW
        ALFA = EPS*SINHY+ W
        DO 36 N = 1,NMAX
        DO 34 M = 1,NMAX
        IF(ABS(XI(N,M)).GE.XIMAX)GO TO 30
        ALF=ALFA*XI(N,M)
        S = SIN(ALF)
        C= COS(ALF)
        QU(N,M,1) = PE1*C
        QU(N,M,2) = PE1*S
        QU(N,M,3) = PE2*S
        QU(N,M,4) = -PE2*C
        QU(N,M,5) = -PE3*C
        QU(N,M,6) = -PE3*S
        GO TO 34
     30 DO 35 I = 1,6
     35 QU(N,M,I) = 0.0
     34 CONTINUE
     36 CONTINUE
        RETURN
        END
$IBFTC AMDER    DECK
        SUBROUTINE AMPDER(CAT,ZETA,AMP,QU,LMAX,ISMAX,AMPDOT)
C
C       A SUBROUTINE TO GENERATE THE AMPDOT ARRAY
C
        COMMON/Y/ACC10
        DIMENSION CAT(90,3),ZETA(90,90),AMPDOT(180,4),AMP(180,4)
        DIMENSION QU(10,10,6)
        DO 43 IR = 1,ISMAX
```

```
      N = CAT(IR,1) + 0.001
      IMAG=IR+ISMAX
      DO 45 L = 1,LMAX
      AMPDOT(IR,L)=0.0
      AMPDOT(IMAG,L)=0.0
   45 CONTINUE
      DO 42 IS = 1,ISMAX
      M = CAT(IS,1) + 0.001
      IARG = IS+ISMAX
      MU = ABS(CAT(IR,3) - CAT(IS,3)) + 0.001
      IF(MU.GT.2) GO TO 42
      Z = ZETA(IR,IS)
      IF(ABS(Z).LE.ACC10) GO TO 42
      NU = MU+MU+2
      R1 = Z*QU(N,M,NU)
      NU = MU+MU+1
      R2 = Z*QU(N,M,NU)
      DO 41 L = 1,LMAX
      AMPDOT(IR,L)= AMPDOT(IR,L)-R1*AMP(IS,L)-R2*AMP(IARG,L)
      AMPDOT(IMAG,L)= AMPDOT(IMAG,L)-R1*AMP(IARG,L)+R2*AMP(IS,L)
   41 CONTINUE
   42 CONTINUE
   43 CONTINUF
      RETURN
      END
```

```
$DATA
  70.3        1.0      165.00     164.0        5.0      7
   8.00      16.00      76.0      188.00
   0.29317    0.00356    0.0
 57.10  57.15  57.35  57.40  57.55  57.55  57.65
   10    10     2 0.001
2.00       0.0             7
    0     0     0     1
   8.00      16.00      76.0      188.00
0.0         0.0
0.155       2.0
0.478       4.0
0.633       2.0
0.950       6.0
0.961       4.0
1.086       0.0
      0.0          -1.675        0.0          0.495        0.0          0.0
      0.0
     -1.675         1.7160      -2.670         0.9300       0.0          0.320
      0.175
      0.0          -2.670         2.1440       0.0         -2.240        1.21
      0.0
      0.495         0.9300        0.0         -1.7160       0.0         -2.120
      0.0
      0.0           0.0          -2.240         0.0          2.5920       0.0
      0.0
      0.0           0.320         1.21         -2.120        0.0          0.8440
      0.0
      0.0           0.175         0.0          -0.000        0.0          0.000
      0.0
```

IX. REFERENCES

1. S. T. Belyaev, Mat. Fys. Medd. Dan. Vid. Selsk. 31, No. 11 (1959)

2. An excellent reference that develops and compares several different approaches (e. g. , RPA, Hartree-Fock) and which includes detailed considerations of excitation spectra, matrix elements, spheroidal deformations and oscillations with specific emphasis on O^{16} is: S. Fallieros, thesis, University of Maryland, 1959, Technical Report No. 128. Related references are: R. Ferrell, Phys. Rev. 107, 1631 (1957) and S. Fallieros and R. Ferrell, Phys. Rev. 116, 660 (1959).

3. J. J. Griffin and M. Rich, Phys. Rev. 118, 850 (1960); S. G. Nilsson and O. Prior, Mat. Fys. Dan. Vid. Selsk. 32, No. 16 (1961).

4. C. J. Gallagher and V. G. Soloviev, Mat. Fys. Medd. Dan. Vid. Selsk. Skr. 2, No. 2 (1962).

5. M. Baranger, Phys. Rev. 120, 957 (1960).

6. See D. Bès, Mat. Fys. Medd. Dan. Vid. Selsk. 33, No. 2 (1961) for calculations of the properties of gamma vibrations and D. Bès, Nucl. Phys. 49, 544 (1963) for beta vibrations.

7. L. Kisslinger and R. A. Sorensen, Mat. Fys. Medd. Dan. Vid. Selsk. 32, No. 9 (1961). An extension of this work to non-single-closed shell nuclei is found in T. Tamura and T. Udagawa, Prog. in Theoret. Phys. 26, 947 (1961).

8. E. R. Marshalek and J. O. Rasmussen, Nucl. Phys. 43, 438 (1963).

9. See E. R. Marshalek, Phys. Rev. 139, B770 (1965) and E. R. Marshalek and J. B. Milazzo, Phys. Rev. Lett. 16, 190 (1966). For similar calculations reference may be made to: T. Udagawa and R. K. Sheline, Phys. Rev. Lett. 16, 325 (1966) and K. Y. Chan, Nucl. Phys. 85, 261 (1966).

10. A. Faessler, W. Greiner, and R. K. Sheline, Technical Report 372, Florida State University, April, 1964.

11. Much of the work in this field has been done by Brueckner and co-workers. See, for example: K. A. Brueckner, Phys. Rev. 96, 508 (1954) and K. A. Brueckner and C. A. Levinson, Phys. Rev. 97, 1344 (1955) as well as the review article by R. J. Eden in Nuclear Reactions, Vol. 1, ed. by P. M. Endt and M. Demeur, (North Holland Publishing Co., Amsterdam, 1959), p. 1.

12. G. Scharff-Goldhaber, in Proc. of the Univ. of Pittsburgh Conf. on Nuclear Structure. (Univ. of Pittsburgh and Office of Ordnance Research, U.S. Army, 1957).

13. There are several relevant publications by these authors. We cite the following: M. Baranger and K. Kumar, in Perspectives in Modern Physics, ed. by R. E. Marshak (Wiley, Interscience, New York, 1966), K. Kumar and M. Baranger, Nucl. Phys. A92, 608 (1967); K. Kumar and M. Baranger, Phys. Rev. Lett. 17, 1146 (1966) and K. Kumar, private communication.

14. J. Weneser, Lectures at Yale University, 1966-67 (unpublished). These successes are also referred to in the article cited in reference 57.

15. A. Bohr and B. R. Mottelson, Mat. Fys. Medd. Dan. Vid. Selsk. 27, No. 16 (1953).

16. A. Bohr, Mat. Fys. Medd. Dan. Vid. Selsk. 26, No. 14 (1952).

17. A. K. Kerman in Nuclear Reactions, ed. by P. M. Endt and M. Demeur (North Holland Publishing Co., Amsterdam, 1959), p. 427.

18. C. J. Gallagher in Selected Topics in Nuclear Spectroscopy, ed. by B. J. Verhaar (North Holland Publishing Co., Amsterdam, 1964), p. 133.

19. O. Nathan and S. G. Nilsson, Alpha-Beta-and Gamma-Ray Spectroscopy, ed. by K. Siegbahn, Vol. 1 (North Holland Publishing Co., Amsterdam, 1964) and J. P. Davidson, Rev. Mod. Phys. 37, 105 (1965).

20. M. A. Preston, Physics of the Nucleus (Addison-Wesley Pub. Co., Cambridge Mass., 1962).

21. K. T. Hecht in Selected Topics in Nuclear Spectroscopy, ed. by B. J. Verhaar (North Holland Publishing Co., Amsterdam, 1964), p. 1.

22. G. Scharff-Goldhaber and J. Weneser, Phys. Rev. 98, 212 (1955). See also, B. J. Raz, Phys. Rev. 114, 1116 (1959).

23. A. K. Kerman and C. M. Shakin, Phys. Lett. 1, 151 (1962). See also L. Wilets and M. Jean, Phys. Rev. 102, 788 (1956), T. Tamura and L. G. Komai, Phys. Rev. Lett. 3, 344 (1959) and B. Sørensen, Phys. Lett. 21, 683 (1966).

24. D. Mitra and M. K. Pal, Phys. Lett. 1, 153 (1962). Also see S. T. Belyaev and V. G. Zelevinsky for a slightly different approach. These authors obtain a formula for the $2^{+'}$ state branching ratio similar to one derived with the Davydov-Filippov model thus indicating the connection between anharmonicity and axial asymmetry. Also see ref. 122. The HRPA is also discussed by J. Sawicki, Phys. Rev. 126, 2231 (1962).

25. G. A. Burginyon, thesis, Yale University, 1967.

26. M. A. Preston and D. Kiang, Can. J. Phys. 41, 7421 (1963).

27. G. G. Seaman, thesis, Yale University, 1965.

28. G. Alaga, K. Alder, A. Bohr and B. R. Mottelson, Mat. Fys. Medd. Dan. Vid. Selsk. 29, No. 9 (1955).

29. P. O. Lipas, Nucl. Phys. 39, 468 (1962); J. Brude, M. Rakavy and G. Rakavy, Phys. Rev. 129, 2147 (1963).

30. O. B. Nielson, Proceedings of the Rutherford Jubilee International Conference, ed. by J. B. Birks (Heyward and Co., London, 1962), p. 317.

31. R. K. Sheline, Rev. Mod. Phys. 32, 1 (1960).

32. A. S. Davydov and G. F. Filippov, Nucl. Phys. 8, 237 (1958) and A. S. Davydov and G. F. Filippov, JETP (USSR) 35, 303 (1959).

33. A. S. Davydov and V. S. Rostovskii, JETP (USSR) 36, 1275 (1959); and A. S. Davydov and V. S. Rostovskii, Nucl. Phys. 12, 58 (1959).

34. A. S. Davydov and A. A. Chaban, Nucl. Phys. 20, 499 (1960).

35. A. S. Davydov, Nucl. Phys. 24, 682 (1961).

36. J. P. Davidson and M. G. Davidson, Phys. Rev. 138, B316 (1965).

37. C. A. Mallmann and A. K. Kerman, Nucl. Phys. 16, 105 (1960).

38. This is pointed out in many places. For example, see the following: Discussion by A. Bohr, Proceedings of the International Conference on Nuclear Structure, Kingston, Canada, ed. by D. A. Bromley and E. W. Vogt (Univ. of Toronto Press, Toronto, 1960), pp. 807-813; A. S. Davydov, V. S. Rostovskii and A. A. Chaban, Nucl. Phys. 27, 134 (1961); T. Tamura and T. Udagawa, Nucl. Phys. 16, 460 (1960); T. Yamazaki, Nucl. Phys. 49, 1 (1963).

39. T. Yamazaki, J. Sato, Y. Yokoyama, S. Baba, H. Ikegami and M. Sakai, Proceedings of the International Conference on Nuclear Physics, Gatlinburg, Tennessee, 1966.

40. D. M. Van Patter, Nucl. Phys. 14, 42 (1959).

41. A. Faessler, W. Greiner and R. K. Sheline, Phys. Rev. 135, B591 (1964) and Nucl. Phys. 70, 33 (1965).

42. A. Bohr, B. R. Mottelson and D. Pines, Phys. Rev. 110, 936 (1958).

43. J. Bardeen, L. N. Cooper and J. R. Schrieffer, Phys. Rev. 108, 1175 (1957).

44. A. M. Lane, Nuclear Theory (Benjamin, New York, 1964).

45. I. Kelson and C. A. Levinson, Phys. Rev. 134, B269 (1964).

46. I. Kelson, Phys. Rev. 132, 2189 (1963). See also J. Bar-Touv and I. Kelson, Phys. Rev. 138, B1035 (1965) and I. Kelson, preprint.

47. See, for example, I. Green and S. A. Moszkowski, Phys. Rev. 139, B790 (1965); A. Plastino, R. Arvieu and S. A. Moszkowski, Phys. Rev. 145, 837 (1966), R. Arvieu and S. A. Moszkowski, Phys. Rev. 145, 830 (1966); A. Plastino, A. Faessler and S. A. Moszkowski, Bull. Am. Phys. Soc. 12, 67 (1967).

48. An early article on the subject, frequently referred to in later work, is: H. A. Jahn, Proc. Roy. Soc. A 201, 516 (1949). Three articles that develop the theory in detail are: J. P. Elliott, Proc. Roy. Soc. A245, 128 (1958); J. P. Elliott, Proc. Roy. Soc. A245, 562 (1958) and J P. Elliott and M. Harvey, Proc. Roy. Soc. A272, 557 (1963). Two other articles that develop explicit formulas are: M. K. Banerjee and C. A. Levinson, Phys. Rev. 130, 1036 (1963) and M. K. Banerjee, C. A Levinson and S. Meshkov, Phys. Rev. 130, 1064 (1963). The latter contains applications in Mg^{24}. Detailed applications of the ideas of the previous papers, to the oxygen isotopes, are found in: D. M. Brink and G. F. Nash, Nucl. Phys. 40, 608 (1963), and T. Engleland, Nucl. Phys. 72, 68 (1965). An interesting review article is the one by Hecht, cited in reference 21.

49. See, for example, G. E. Brown, J. A Evans and D. J. Thoulese, Nucl. Phys. 24, 1 (1961); M. Baranger in 1962 Cargèse Lectures in Theoretical Physics, edited by M. Levy (Benjamin, New York, 1963), Ch. V. (This is, in general, an excellent review of the subject with particular emphasis on, and a clear presentation of, Hartree-Fock approaches)

50. N. Bogoliubov, JETP (USSR), 34, 58 and 73 (1958) and J. G. Valatin, Nuovo Cimento 7, 843 (1958).

51. S. Yoshida, Phys. Rev. 123, 2122 (1961) and B. L. Cohen and R. E. Price, Phys. Rev. 121, 1441 (1961).

52. R. Arvieu and M. Veneroni, Compt. Rend. 250, 992 (1960) and another article by these two authors is found in the same volume, p. 2155.

53. T. Marumori, Prog. in Theoret. Phys. 24, 331 (1960).

54. D. Bès, P. Federman, E. Maqueda and A. Zuker, Nucl. Phys. 65, 1 (1965).

55. D. Inglis, Phys. Rev. 96, 1059 (1954); D. Inglis, Phys. Rev. 103, 1786 (1956). See also H. J. Lipkin, A. de-Shalit and I. Talmi, Phys. Rev. 103, 1773 (1956).

56. See, for example, R. G. Stokstad, I. Hall, G. D. Symons and J. de Boer, Nucl. Phys. A92, 319 (1967), J. Glenn and J. X. Saladin, Phys. Rev. Lett.

19, 33 (1967) and J. J. Simpson, D. Eccleshall, M. O. L. Yates, and N. J. Freeman, Nucl. Phys. A94, 319 (1967).

57. R. Casten, J. S. Greenberg, G. A. Burginyon, D. A. Bromley and G. Holland, Bull. Am. Phys. Soc. 12, 35 (1967).

58. W. T. Milner, F. K. McGowan, R. L. Robinson and P. H. Stelson, Bull. Am. Phys. Soc. 12, 35 (1967).

59. L. C. Biedenham and P. J. Brussard, Coulomb Excitation (Clarendon Press, Oxford, 1965).

60. K. Alder, A. Bohr, T. Huus, B. Mottelson and A. Winther, Rev. Mod. Phys. 28, 432 (1956).

61. A. Winther and J. de Boer, "A Computer Program for Multiple Coulomb Excitation", Technical Report, November 18, 1965, Calif. Inst. of Technology. Also reprinted in: Coulomb Excitation, ed. by K. Alder and A. Winther, (Academic Press, New York, 1966). Many of the other important Coulomb excitation references (e.g., refs. 60, 70) are likewise collected in this book.

62. A. C. Douglas, Nucl. Phys. 42, 428 (1963) and A. W. R. E. Report No. NR/P-2/62, Aldermaston.

63. K. Alder and A. Winther, Mat. Fys. Medd. Dan. Vid. Selsk. 32, No. 8 (1961).

64. K. Alder, Proceedings of the Third Conference on Reactions Between Complex Nuclei, Asilomar, 1963, ed. by A. Ghiorso, R. M. Diamond and H E. Conzett (Univ. of Calif. Press, Berkeley, 1963). See also reference 107.

65. H. Lutken and A. Winther, Matt. Fys. Medd. Dan. Vid. Selsk. Skr. 2, No. 6 (1964).

66. A. E. Litherland and A. J. Ferguson, Can. J. Phys. 39, 788 (1961). A. R. Poletti and E. K. Warburton, Phys. Rev. 137, B595 (1965).

67. I. Berson, JETP (USSR), 1, 325 (1965).

68. See P. Henrici, Elements of Numerical Analysis (Wiley and Sons, New York, 1964).

69. L. Collaz, The Numerical Treatment of Differential Equations (Springer-Verlag, third ed., Berlin, 1960).

70. J. de Boer, G. Goldring and H. Winkler, Phys. Rev. 134, B1032 (1964).

71. F. K. McGowan and P. H. Stelson, Phys. Rev. 122, 1274 (1961).

72. B. Harmatz and T. H. Handley, Nucl. Phys. 56, 1 (1964).

73. G. T. Emery, W. R. Kane, M. McKeown, M. L. Perlman and G. Scharff-Goldhaber, Phys. Rev. 129, 2597 (1963).

74. F. R. Metzger and R. D. Nell, Phys. Rev. 82, 646 (1951).

75. W. J. King and M. W. Johns, Can. J. Phys. 37, 755 (1959).

76. J. Blachot, E. Monnand, A. Moussa, Compt. Rend. 261, 1835 (1965).

77. The isotopes and their spectographic analyses were obtained from Oak Ridge National Laboratory Isotopes Division.

78. See the Nuclear Data Sheets compiled by K. Way et al, Washington, D. C., and reference 72 as well. Also see the compilations by N. B. Gove and M. J. Martin in Nuclear Data, B1, 1 and B1, 53 (1966), respectively.

79. N. L. Lark and H. Morinaga, Nucl. Phys. 63, 466 (1965).

80. J. O. Newton, F. S. Stephens and R. M. Diamond, Nucl. Phys. A95, 377 (1967).

81. J. P. Hurley and P. S. Jastram, Phys. Rev. 95, 627 (1954).

82. D. H. Rester, M. S. Moore, F. E. Durham and C. M. Class, Nucl. Phys. 27, 104 (1961).

83. F. K. McGowan, Phys. Rev. 81, 1066 (1951).

84. E. E. Berlovich, JETP (USSR) 6, 1176 (1958).

85. D. B. Fosson and B. Herskind, Nucl. Phys. 40, 24 (1963).

86. E. Bashandy and M. S. El- esr, Nucl. Phys. 34, 483 (1962).

87. E. Bashandy and S. G. Hanna, Nucl. Phys. 84, 577 (1966).

88. T. Yamazaki, Nucl. Phys. 44, 353 (1963).

89. W. R. Kane, thesis, Harvard University, 1959.

90. L. B. Warner and R. K. Sheline, Nucl. Phys. 36, 207 (1962).

91. F. K. McGowan and P. A. Stelson, Phys. Rev. 109, 901 (1958).

92. R. Barloutaud, P. Lehman and A. Levêque, Compt. Rend 245, 523 (1957).

93. F. K. McGowan, P. A. Stelson and R. L. Robinson, Proceedings of the

Conference on Electromagnetic Lifetimes and Properties of Nuclear States, NAS-NRC Pub. No. 974, (1962), p. 119.

94. A level is known in Os^{188} at 790 kev but this is a 3^+ level and no known decay branch to the ground state exists. Since the 3^+ state is also of unnatural parity it would be very negligibly excited in these experiments and so cannot be the source of the 780 kev transition we observe.

95. W. R. Kane, G. T. Emery, G. Scharff-Goldhaber and M. McKeown, Phys. Rev. 119, 1953 (1960).

96. B. Nielson, N. D. Poulsen, R. K. Sheline and B. J. Jensen, Nucl. Phys. 10, 475 (1959).

97. A. W. Sunyar, Proc. of the Second United Nations International Conference on the Peaceful Uses of Atomic Energy, 1958, United Nations, Geneva.

98. L. L. Baggerly, P. Meunier, F. Boehm, and J. S DuMond, Phys. Rev. 100, 1364 (1955).

99. D. K. Butt and B. C. Dutta, Nucl. Phys. 39, 517 (1962).

100. G. A. Burginyon, J. S. Greenberg, D. A. Bromley and R. F. Casten, Bull. Am. Phys. Soc. 12, 36 (1967). G. A. Burginyon, J. S. Greenberg, R. F. Casten and D. A. Bromley, contribution to the International Conference on Nuclear Structure, Tokyo, 1967.

101. N. K. Glendenning, Nucl. Phys. 29, 109 (1962); N. K. Glendenning, Phys. Rev. 137, B102 (1965) and N. K. Glendenning in Annual Reviews of Nuclear Science, ed. by E. Segrè (Annual Reviews,Inc., Palo Alto, Calif. 1963), Vol. 13.

102. R. L. Heath, Scintillation Spectrometry: Gamma-Ray Spectrum Catalogue IDO-16880-1, TID-4500, Aug. 1964.

103. L. A. Sliv and I. M. Band, Report 57, ICC, (Physics Dept., Univ. of Illinois, Urbana, Illinois).

104. S. C. Pancholi, Nucl. Phys. 67, 203 (1965).

105. A. A. Wapstra, G. J. Nijgh and R. Van Lieshout, Nuclear Spectroscopy Tables (North Holland Publ. Co., Amsterdam, 1959).

106. Obtained from the International Atomic Energy Agency, Division of Research and Laboratory Physics Section, December 1966.

107. M. Simonius, W. Bierter, A. Zwicky and K. Alder, Helv. Phys. Acta 38, 699 (1965). See K. Alder, W. Bierter, M. Simonius and A. Zwicky, Numerical

Results of Multiple Coulomb Excitation (Univ. of Basel, Basel, Switzerland, 1965) for related tabulations.

108. Tabulated in Alpha-Beta-and Gamma-Ray Spectroscopy, ed. by Kai Siegbahm (North Holland Pub. Co., Amsterdam, 1965), Vol. 2, appendix.

109. M. J. Yates, Nucl. Inst. and Meth. 23, 152 (1963).

110. L. C. Northcliffe, Pub. 1133 (National Academy of Sciences, National Research Council, Washington, D. C.).

111. A. C. Worthing, J. Geffner, Treatment of Experimental Data (Wiley and Sons, New York, 1943).

112. Materials Research Corporation Instruction Manual for MRC V4-200 Electron Vapor Deposition Gun (Orangeburg, New York).

113. Metals Handbook (American Society for Metals, Cleveland, Ohio, 1966). It may also be noted that evaporation of osmium is rendered even more difficult since its vapor pressure is quite low, and in fact is the lowest of any of the "platinum group" of metals.

114. Handbook of Chemistry and Physics, 43rd Edition, 1961-62, ed. by Charles D. Hodgman (The Chemical Rubber Pub. Co., Cleveland, Ohio, 1961).

115. Drs. Carl Nelson and Lance Davis, private communication.

116. P. H. Stelson and L. Grodzins, Nuclear Data, AI, 21 (1965).

117. G. G. Seaman, J. S. Greenberg, D. A. Bromley and F. K. McGowan, Phys. Rev. 149, 925 (1966).

118. G. A. Burginyon, J. S. Greenberg, D. A. Bromley and R. F. Casten, Contribution to the International Conference on Heavy Ion Physics, Dubna, USSR, 1966.

119. R. F. Casten, J. S. Greenberg, G. A. Burginyon and D. A. Bromley, Contribution to the International Conference on Nuclear Structure, Tokyo, 1967.

120. J. S. Greenberg, G. G. Seaman, E. V. Bishop and D. A. Bromley, Phys. Rev. Lett. 11, 211 (1963).

121. Some calculations of a somewhat less microscopic sort by one of these authors on Sm nuclei are already available. These are discussed in K. Kumar, Nucl. Phys. A92, 653 (1967). The results cited in this article may be compared with the experimental results contained in references 117, 118, 120 and in reference 27 in which other relevant articles on Sm are cited.

122. Several other attempts to account for finite quadrupole moments in nearly spherical nuclei exist. Relevant references are: T. Tamura and T. Udagawa, Phys. Rev. Lett. 19, 765 (1965); G. Do Dang, R. Dreszler, A. Klein and C. S. Wu, Phys. Rev. Lett 17, 709 (1966); B. Sørensen, Phys. Lett. 21, 683 (1966); B. Sørensen, Phys. Lett. 23, 274 (1966). Related background material is afforded especially by the articles by Mitra and Pal and by Belyaev and Zelevinsky cited in reference 24.

123. This figure is reproduced with appreciation from the article cited in reference 117.

124. K. Sawada, Phys. Rev. 106, 372 (1957).